Protein-protein interactions of the BCL-2 family

Philip Lee Rowell

Submitted in accordance with the requirements for the degree of
Doctor of Philosophy

The University of Leeds
Astbury Centre for Structural and Molecular Biology

February 2018

Intellectual Property and Publication Statements

The candidate confirms that the work submitted is his/her own and that appropriate credit has been given where reference has been made to the work of others.

This copy has been supplied on the understanding that it is copyright material and that no quotation from the thesis may be published without proper acknowledgement.

The right of Philip Lee Rowell to be identified as Author of this work has been asserted by him in accordance with the Copyright, Designs and Patents Act 1988.

Acknowledgements

I would like to start by thanking my supervisor, Dr Thomas Edwards, for help, support and guidance throughout the project. Your advice was always good, and on the occasions where I chose to ignore it, my decision invariably came back to bite me on the bum. Thanks also for (your attempts at) schooling me, an inveterate lager drinker, on the joys of real ale. I apologise for defacing the pictures on your office door and for laughing at you when you came limping in after suffering one of your frequent cricketing injuries.

Thanks also to my co-supervisor, Professor Andy Wilson, the truest advocate for a career in science I have met. Your passion and enthusiasm for all things chemistry is a great example to all. Thanks for all your help and suggestions along the way. If purification of some of my proteins had been a bit easier, I promise I would have spent more time up in the Chemistry department!

Past and present members of the Edwards group have given me a huge amount of support and encouragement over the last three years. Thanks first of all to Dr Jennifer Miles, who introduced me to the intricacies of recombinant protein expression and purification. Your patience and good humour were greatly appreciated. Thanks particularly to Dr Hannah Kyle, who taught me how to set up crystal plates at the start of my PhD, supervised my SPR experiments in the final months of my PhD, and helped me out with many other science problems in the intervening period. Thanks to Dr Selvaraj Muniyandi for helping me out with viewing EM grids before I was trained up and allowed to drive the electron microscope by myself. Thanks to Dr Fruzsina Hobor for doing some of the later batches of protein purification when it got to the stage I could delay thesis writing no longer and had to start getting out of the lab. Thanks to Georgia Pangratiou for being a cheerful presence and organising influence in the lab, especially in the last few months as I have become more and more neurotic!

I would also like to thank Dr Brian Jackson for use of the facilities in the PPF for analytical SEC, to Dr Christian Tiede for supervision during phage

display experiments, to Dr Rebecca Thompson for help and supervision in the EM facility, and to Dr Shaun Rawson for showing me how to use the RELION software.

Thanks to Professor Jane Clarke for allowing me to visit her lab at the University of Cambridge to carry out BAX expression trials, and thanks to all members of the Clarke group, especially Basile Wicky and Tristan Kwan, for looking after me and making me welcome during my time there. Thanks also to Basile for providing protein samples for crystal trials and EM studies.

And finally, thanks to my fantastic wife Annette, who supported me in my ambition to leave the lucrative world of banking and become a 40 year old undergraduate, and who has since done a fantastic job keeping my feet on the ground when I had delusions of being the next Einstein, and cheering me up when the science was just not working!

Abstract

The BCL-2 family of proteins are important regulators of mitochondrial apoptosis, comprising both pro- and anti-apoptotic members that interact with one another at the mitochondrial outer membrane to determine cellular fate. Dysregulation of their activities in the cell is implicated in many forms of cancer; the development of molecules able to mimic and modulate their interactions is thus highly desirable and has been the subject of a great deal of research effort. The use of techniques including structure based design and peptidomimetic approaches has produced some notable successes in this area, but few have successfully transitioned from laboratory to clinic, and the search for more and better ways to develop such molecules continues.

In this thesis, I present a novel approach to identifying binding partners for BCL-2 proteins, which uses phage display experiments and the production of non-antibody scaffold proteins called Affimers. Five BCL-2 family proteins were selected as targets for study, comprising a good cross section of pro- and anti-apoptotic members. In the following chapters, I first describe the work undertaken to purify and characterise these target proteins, then detail the work done to identify and purify Affimer binding partners for each of them. Finally, I report on structural studies carried out to explore the mechanism by which BAX, a pro-apoptotic family member, forms death inducing oligomers.

Taken together, the results of this project lay the foundations for further structural studies of BAX oligomerisation, and demonstrate that the use of phage display to generate selectively binding non-antibody scaffold proteins can provide useful additions to the existing array of BCL2 family interacting molecules.

Table of Contents

List of Tables

List of Figures

Abbreviations

AML	Acute myeloid leukemia
ARF	ADP Ribosylation Factor
BAD	BCL-2 Associated Death promoter protein
BAK	BCL-2 Associated Killer protein
BAX	BCL-2 Asoociated X protein
BC groove	BCL-2 family C-terminal groove
BCL-2	B-cell Lymphoma 2 protein
BCL-X_L	B-cell Lymphoma Extra Large protein
BH domain	BCL-2 Homology domain
BID	BH3 Interacting Domain Death Agonist
BSA	Bovine Serum Albumin
BSTG	BioScreening Technology Group
CBD	Chitin binding domain
CD	Circular Dichroism
CLL	Chronic lymphocytic leukemia
CMC	Critical micelle concentration
DMSO	Dimethyl sulfoxide
DNA	Deoxyribonucleic acid
dNTP	Deoxynucleotide
DTT	Dithiothreitol
EDTA	Ethylenediaminetetraacetic acid
FA	Fluorescence Anisotropy
FITC	Fluorescein isothiocyanate
FOSL1	FOS like 1 protein
GST	Glutathione S-transferase
hDM2	Human Double Minute 2 protein
HEPES	4-(2-hydroxyethyl)-1-piperazineethanesulfonic acid
HMGA2	High-mobility group AT-hook 2
HRMS	High Resolution Mass Spectrometry
HRP	Horse Radish Peroxidase
INrf2	Inhibitor of NF-E2-related factor 2
IPTG	Isopropyl β-D-1-thiogalactopyranoside
MCL1	Myeloid Cell Leukaemia-1 protein
MEF	Mouse Embryonic Fibroblast
MOM	Mitochondrial Outer Membrane
MOMP	Mitochondrial Outer Membrane Permeabilisation

MRE	Mean Residue Ellipticity
OD	Optical Density
PBS	Phosphate Buffered Saline buffer
PBST	Phosphate Buffered Saline buffer + Tween 20
PCR	Polymerase Chain Reaction
PUMA	P53 Upregulated Modulator of Apoptosis
RE	Restriction Enzyme
RNA	Ribonucleic acid
SAHB	Stabilised α-Helices of BCL-2 domains
SCLC	Small Cell Lung Cancer
SDS-PAGE	Sodium dodecyl sulfate polyacrylamide gel electrophoresis
SEC	Size Exclusion Chromatography
TBE	Tris/Borate/EDTA buffer
TM domain	Trans-Membrane domain
TMB	3,3',5,5'-Tetramethylbenzidine
TNFα	Tumour Necrosis Factor α
TRAIL	TNF-related apoptosis-inducing ligand
WEHI	Walter and Eliza Hall Institute of Medical Research

Chapter 1 - Introduction

1.1 Apoptosis

Apoptosis, or programmed cell death, carries out many essential functions in multicellular organisms [1]. It is characterised by distinct morphological and biochemical changes to the cell, including cell shrinkage; membrane blebbing; chromatin condensation; DNA degradation; nuclear fragmentation and exposure of phosphatidylserine on the outside of the plasma membrane. These changes lead to the formation of apoptotic bodies, which are removed *in vivo* by endogenous phagocytes, preventing the escape into tissues of potentially damaging cellular constituents [2]. During embryonic development, apoptosis is responsible for hollowing out ducts and removing superfluous cells, for example the interdigital cells lost during the formation of limbs. In the adult, it acts as a balance to mitosis in maintaining a steady level of healthy cells, especially in high turnover tissues such as the intestinal epithelium. Apoptosis also eliminates potentially dangerous immune cells with self recognizing antigen receptors that could cause auto-immune disease [3], and limits pathogenic spread by forcing the suicide of infected cells [4].

Apoptosis is initiated by a variety of stimuli, leading to the downstream activation of caspases, a family of cysteine proteases that carry out nucleophilic attack on substrate proteins, cleaving peptide bonds on the carboxyl side of aspartic acid (Asp) residues [5]. Caspases are initially synthesized as inactive zymogens called pro-caspases, and become active through hetero-dimerisation, followed by cleavage into small and large subunits to form active hetero-tetramers (Figure 1-1) . Caspases involved in apoptosis consist of two sub-groups: the upstream initiators (caspases 2, 8, 9 and 10) and the downstream ‘executioners’ (caspases 3, 6 and 7). Activated initiator caspases will cleave and activate the executioners, which

in turn act to degrade cellular components, resulting in the morphological changes associated with apoptosis, with each executioner caspase targeting many hundreds of components within the cell [6].

Apoptosis may be triggered extrinsically following ligation of Death Receptors (e.g. Fas, TNFα, TRAIL-R1), leading to formation of the Death Inducing Signaling Complex (DISC) and subsequent activation of initiator caspases [7, 8]. Less commonly, cytotoxic T cells and natural killer (NK) cells may release molecules onto the cell surface, including perforin and granzyme B, which respectively form pores in the membrane, and enter the newly formed pore to activate initiator caspases [9]. Alternatively, and of significance to this study, apoptosis can be triggered intrinsically (Figure 1-1). This involves apoptotic stimuli that modulate interactions between endogenous proteins of the BCL-2 family, leading to the permeabilisation of the mitochondrial outer membrane (MOM) and escape of caspase activating factors, including cytochrome c, from the mitochondrial intermembrane space to the cytosol. The consequences of cytochrome c release are twofold: the disabling of energy production within mitochondria, and initiation of the caspase cascade that leads to apoptotic cell death [10].

Dysregulated apoptosis is linked to a variety of pathologies. Increased apoptosis is associated with atherosclerosis [11]; infertility; diabetes [12]; AIDS; renal failure; and neurodegenerative diseases including multiple sclerosis [13] and Parkinson’s, Huntington’s and Alzheimer’s diseases [14]. Excessive apoptosis also contributes to damage caused during chronic inflammation, myocardial infarction and stroke [15-17]. Conversely, impaired apoptosis is associated with many forms of cancer and autoimmune disease [18]. The ability to modulate and control apoptosis within the cell is therefore highly desirable.

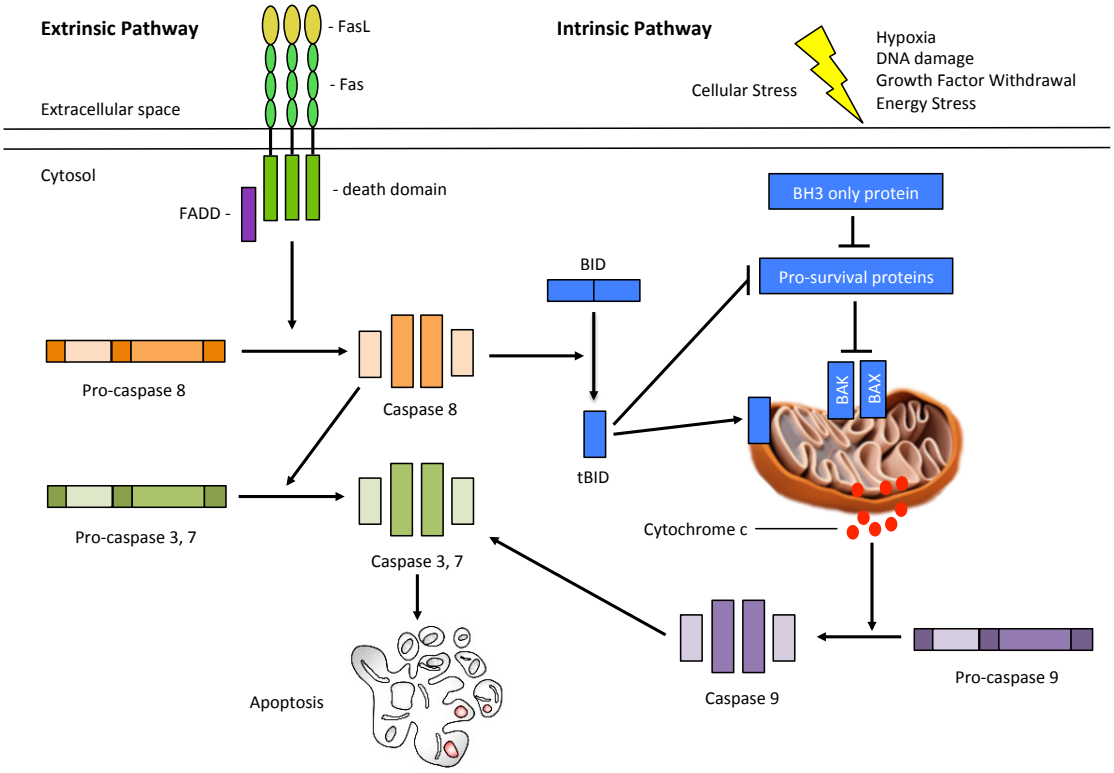

Figure 1-1 – Alternative pathways to apoptosis. The extrinsic (death receptor mediated) pathway involves the binding of ligands to death receptors such as Fas. Alternatively, the intrinsic (mitochondrial) pathway is initiated by different forms of cellular stress, including DNA damage and hypoxia. Such stresses lead to an increase in pro-apoptotic members of the BCL-2 protein family, causing permeabilisation of the mitochondrial outer membrane (MOMP). The release of cytochrome c to the cytosol as a result of MOMP leads to a cascade of caspase activation, culminating in the break down of cellular components and apoptotic cell death.

1.2 Mitochondrial Apoptosis and the BCL-2 family

In mitochondrial, or intrinsic apoptosis, cell death is dependent on the apoptotic threshold, which is determined by interactions at the mitochondrial outer membrane between three distinct sub-groups of the BCL-2 family of proteins. Family members are classified as pro-apoptotic or anti-apoptotic (pro-survival) depending on whether they promote or inhibit mitochondrial outer membrane permeabilisation (MOMP), a process seen as the 'point of no return' of cellular fate in mitochondrial apoptosis. In simple terms, the

decision to induce apoptotic cell death depends on the balance of pro- and anti-apoptotic BCL-2 proteins present and functional in the cell.

Members of the BCL-2 family are thus important regulators of intrinsic mitochondrial apoptosis. BCL-2, the prototype of this evolutionarily conserved family of proteins, was first identified from the break point of a chromosomal translocation frequently seen in follicular and large B-cell lymphomas [19], and the first evidence of its anti-apoptotic function came from its ability to prevent cell death in cytokine deprived haematopoietic cells [20]. Subsequently, over 25 sequence homology sharing family members have been identified in the genome of higher eukaryotes [21, 22]. Members of the BCL-2 family are present in all somatic cells, though with tissue specific patterns of expression.

Three distinct sub-families exist (Figure 1-2). The pro-apoptotic effectors BAX and BAK are the mitochondrial pore forming members of the BCL-2 family; on activation, they oligomerise and form pores in the MOM. This activity is inhibited by the anti-apoptotic / pro-survival family members (for the remainder of this thesis, the terms pro-survival and anti-apoptotic will be used interchangeably when referring to BCL-2 proteins), which sequester BAX and BAK in the MOM and, in the case of BAX, also in the cytoplasm [23]. Six anti-apoptotic family members have been identified: BCL-2, BCL-X_L, MCL1, BFL1, BCL-W and BCL-B. Finally, BH3 only members act as sensors of cellular stress, relaying pro apoptotic signals to multi-domain members to modulate MOM permeability [24, 25]. They are further divided into ‘direct activators’ and ‘sensitisers’, based on the nature of their interactions with BAX and BAK, as described later in this section.

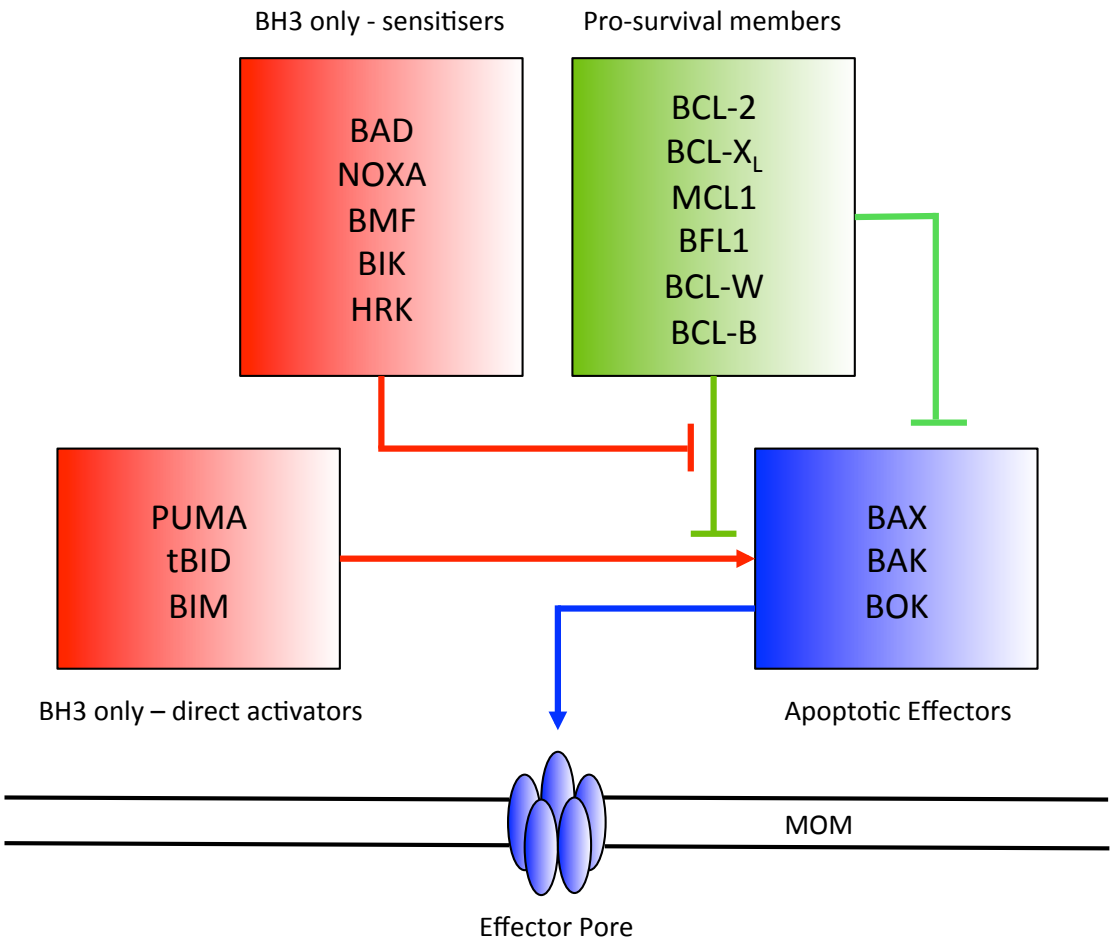

Figure 1-2 – The BCL-2 family. The family as a whole comprises members with pro-apoptotic and anti-apoptotic (pro-survival) functions. The pro-apoptotic effectors, principally BAX and BAK (blue) form the mitochondrial pores responsible for MOMP. In order to do this, they need to oligomerise in the mitochondrial outer membrane (MOM) and are prevented from doing this when bound and sequestered by the anti-apoptotic family members (shown in green). BH3 only family members (so named because they have only the third of the four identified family BH homology domains - see main body text for details) are either upregulated or become active as a result of cytotoxic stress. They bind and sequester the anti-apoptotic family members, freeing up BAX and BAK to oligomerise. A subset of BH3 only proteins (direct activators), also have a more active role in BAX and BAK activity.

BCL-2 family members share sequence homology in a number of BCL-2 homology (BH) domains, named BH1, 2, 3 and 4 (Figure 1-3). In addition to the BH domains, all BCL-2 family members have C terminal transmembrane domain, which is used to govern their cellular location at internal (mainly mitochondrial) membranes [21, 26]. Not all members share all BH domains: BH3 only members, such as BIM, BID and BAD, live up to their name by

sharing only the eponymous BH3 domain; anti-apoptotic family members have all four BH domains, and though it was initially thought that BAX and BAK shared only the first three of the four BH homology domains [27], later analyses clearly show they also share the BH4 domain [28]. BAX, BAK and the anti-apoptotic members are collectively referred to as the multi-domain members.

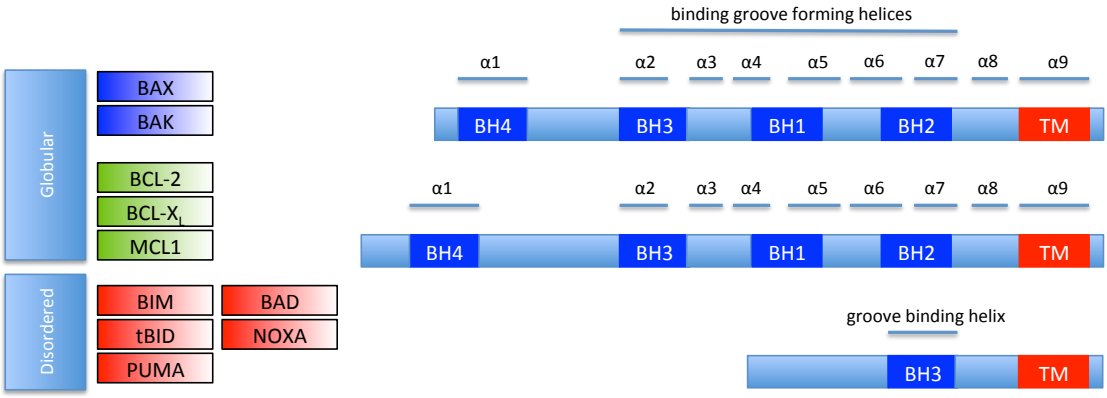

Figure 1-3 – BCL-2 sub-families and BCL-2 homology (BH) domains. BH3 only family members share only one BH homology domain and are intrinsically disordered. BAX, BAK and the pro-survival members contain 4 BH domains and share a large degree of globular structural homology. BH domains are numbered according to the chronology of their discovery, rather than their sequential position in the protein. Helical segments on the multi-BH domain members are shown. TM – transmembrane domain, common to all BCL-2 family members.

Multi-domain members are α-helix rich and, despite significant divergence in their primary amino acid sequence, share a large degree of structural homology, forming globular folds comprising two central hydrophobic helices, surrounded by multiple amphipathic helices [29] [30], in a structure referred to as the BCL-2 core. (Figure 1-4). Though BAX and BAK are pro-apoptotic and carry out opposing functions to the like of BCL-2 and BCL-X_L, structural studies have revealed that their globular fold is remarkably similar to that found in their pro-survival counterparts [30-34]. In all of these structures, the BH1, 2 and 3 domains combine to form the top of a C-terminal, solvent exposed, hydrophobic groove (the BC groove) that is crucial for interacting with the BH3 domain of pro-apoptotic BH3 only family members such as tBID and BIM (Figure 1-5a).

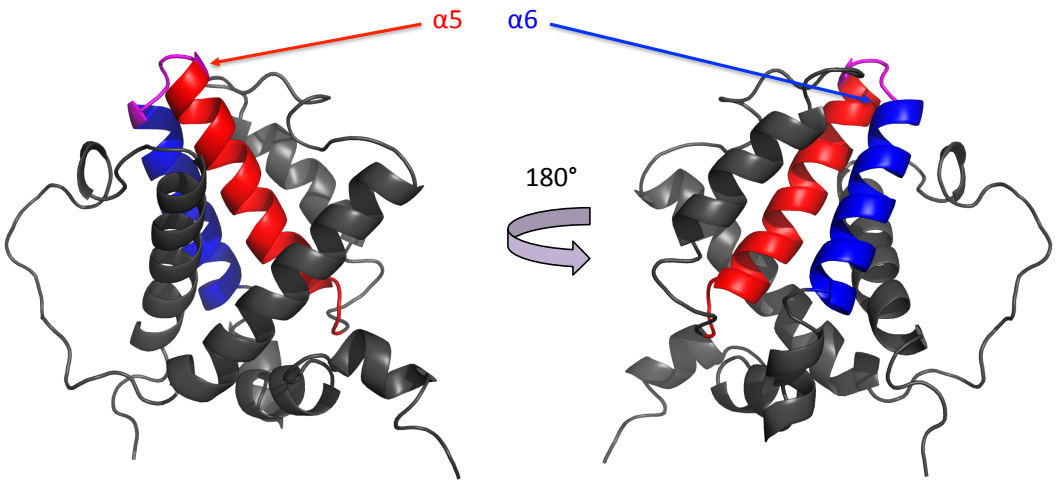

Figure 1-4 - The 'BCL-2 core'. All multi-domain members of the BCL-2 family (anti-apoptotic members plus BAX and BAK) share a common globular fold, in which a pair of hydrophobic helices, α5 and α6 (shown in red and blue respectively), are surrounded by a further 6 amphipathic helices. The above figure shows the BCL-2 core of the anti-apoptotic family member BCL-X_L (PDB 1BXL).

Unlike the multi-domain members, BH3 only proteins are intrinsically disordered, though their BH3 domain adopts an α-helical conformation on interaction with a binding partner. There is one exception to this: BID is considered a member of the BH3 only subfamily, due to the fact that it shares only one region of BH homology with multi-domain family members, but it is unusual in that, rather than being intrinsically disordered, it forms a putative BCL-2 core and adopts a similar fold to the pro-survival family members, albeit with a shorter and flatter BC groove, which does not form a cleft into which the BH3 domain of other family members can bind [35, 36]. When cleaved by caspase 8, it forms the active truncation tBID in which its own BH3 domain is exposed, and is able to carry out its pro-apoptotic function.

BH3 only proteins are upregulated in response to cytotoxic or genotoxic stress and exert their effects by two distinct mechanisms [37-39]: sequestration and neutralization of pro-survival BCL-2 family members [40-42], and / or direct activation of BAX and BAK [25, 43-45].

tBID, BIM and PUMA are able to directly bind BAX and BAK, inducing their oligomerisation [44-47]; they are collectively known as direct activator BH3 only proteins (Figure 1-2). Though all three are able to activate both BAX and BAK, there is evidence for relative levels of selectivity, for instance tBID has been shown to preferentially activate BAK, while BIM preferentially activates BAX [48]. There have been claims that NOXA is able to directly activate BAK [46, 49], but this is disputed [50-52]. Studies using $BAX^{-/-}$ $BAK^{-/-}$ double negative mouse models have shown that direct activators act upstream of BAX and BAK, and are unable to initiate MOMP and apoptosis by themselves [53-55].

BH3 only proteins that are not direct activators are called ‘sensitizers’ or ‘de-repressors’; they bind and inhibit pro-survival family members (Figure 1-2). Sensitizer BH3 only proteins exert no direct apoptotic activity: instead, indirect induction of MOMP occurs through the freeing up of sequestered BAX and BAK, and also the dissociation of direct activator BH3 only proteins from pro-survival heterodimers, allowing them to bind and activate quiescent BAX and BAK. Direct activators also partially act as sensitizers when bound to pro-survival partners.

1.2.1 The Canonical Binding Interaction

The canonical interaction between BCL-2 family proteins is for the BH3 domain of a pro-apoptotic member (BAX, BAK, or a BH3 only) to bind the BC groove of a multi-domain member (Figure 1-5b). Most commonly, this BH3 in BC groove interaction occurs between the BH3 domain of a BH3 only member and the BC groove of a pro-survival member, with each effectively cancelling out the pro- or anti-apoptotic effects of the other. However, conformational changes occurring during the activation of BAX and BAK result in the transient exposure of their respective BH3 domains. The exposed BH3 domains may then bind the BC groove of another activated molecule of BAX or BAK to form a pro-apoptotic homo-dimer, or be bound and sequestered by the BC groove of pro-survival members to form inactive

hetero-dimers, in which the pro-survival member acts as a dominant negative partner, preventing MOMP and inhibiting pro-apoptotic activity [22, 23, 56, 57].

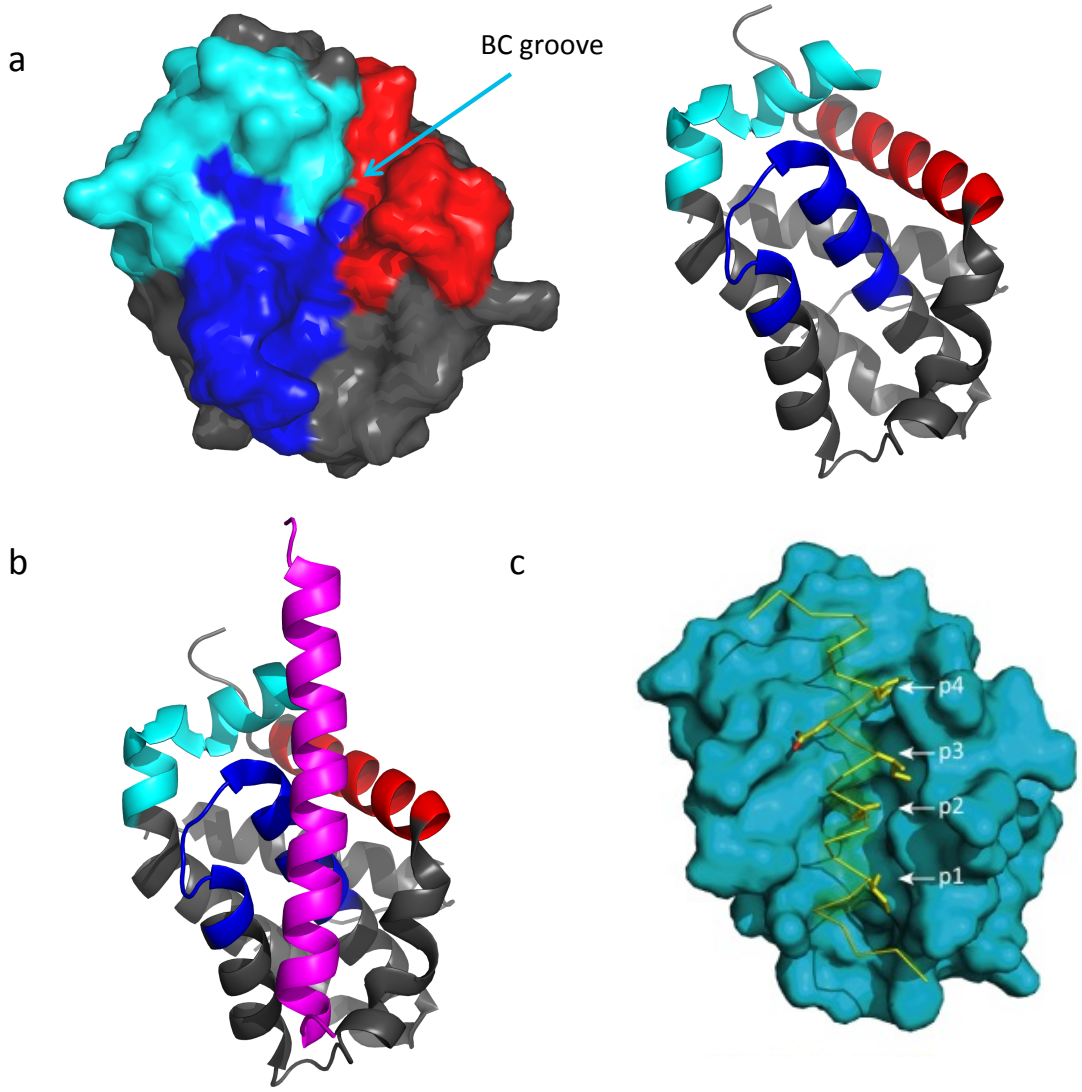

Figure 1-5 - The BCL-2 family canonical binding interaction. This involves the binding of the BH3 domain from a pro-apoptotic family member (BAX, BAK or a BH3 only) to the BC groove of a multi-domain member (BAX, BAK, or an anti-apoptotic). This most often results in the formation of an anti-apoptotic heterodimer consisting of a pro-apoptotic member bound to an anti-apoptotic partner, but can also result in pro-apoptotic homo-dimers of BAX or BAK. a) the C-terminal binding (BC) groove of multi domain members is formed by the conjunction of the BH1, 2 and 3 domains (shown in blue, cyan and red respectively). Figure shown is of BCL-X_L (PDB 1PQ1) in both surface and ribbon format; b) shows the structure from a) with the BH3 domain of BAD (magenta) bound. c) Basis for BH3 domain to BC groove binding: hydrophobic residues on one face of the BH3 domain helix bind to four hydrophobic pockets (P1 – P4) in the BC groove. Figure adapted from [58].

BAX and BAK activation also involves a canonical binding event, with the BH3 domain of a direct activator binding the BC groove of BAX or BAK. However, while BH3 only proteins form stable heterodimers with pro-survival family members, the interactions of direct activators with BAX and BAK are thought to be of a transient 'hit and run' nature. This is likely due to direct activator binding causing the conformational changes in BAX and BAK described above, with exposure of the BAX / BAK BH3 domain causing dissociation of the activating BH3 only protein [59]. There is a wealth of structural and biochemical data to support direct activation of BAX and BAK [38, 47, 50, 52], but other factors are also likely to play a part [41, 57]. Post translational modifications of BAX and BAK [60-62] and changes to the intra-cellular environment [63-66] have been implicated, and the MOM itself is likely to play a significant role; it has been shown, for instance, that BAX and tBID do not interact unless there is a membrane present [67-69].

In each of the above instances, the BH3 domain of the pro-apoptotic member acts as the endogenous ligand to the BC groove of the multi-domain member. BH3 domains have a central, homologous segment with between three and four α-helical turns containing conserved Leu and Asp residues, and in all known structures of this BH3 in groove interaction, four conserved hydrophobic residues (including the aforementioned Leu residue) on a single face of the α-helical BH3 domain (H1-H4) interact with 4 hydrophobic pockets (labelled P1-P4) in the BC groove [70-72] (Figure 1-5c). When BH3 only proteins bind multi-domain pro-survival members, this interaction is augmented by a salt bridge formed between the conserved aspartate residue on the BH3 domain of the pro-apoptotic family member and a conserved arginine residue on the BH1 domain of the pro-survival protein [70, 72, 73].

The molecular basis by which the BC groove of a multi domain family member recognises the BH3 domain of pro-apoptotic members is remarkably similar for all BCL-2 family canonical interactions [50, 52, 74, 75]. Notwithstanding this, individual family members display preferences for

which of their pro-apoptotic counterparts they bind to [40, 76]. Such variances in binding affinity can be accounted for by differences in the primary amino acid sequence of different proteins, which change the electrostatic and hydrophobic contacts between individual binding pairs in the groove, and also alter the potential for steric clashes. This helps explain differences seen in specificity and selectivity, for example why BAD demonstrates strong affinity for BCL-X_L and weak affinity for MCL1, while NOXA has strong affinity for MCL1, yet little or no affinity for BCL-X_L [71, 77], and also why some BH3 onlys act as direct activators of BAX and BAK, while others act only as apoptotic sensitizers [50, 52, 78].

1.2.2 Downstream effects

The anti-apoptotic family member BCL-X_L was the first to have a high resolution structure published. Similarities between the structure of BCL-X_L and the membrane insertion domains of the colicins and diphtheria toxin were observed [30], suggesting that BCL-2 family proteins may exert their apoptotic effects through pore formation in membranes. This has subsequently proved to be the case: MOMP involves the formation of pores, allowing the escape of pro-apoptotic molecules including cytochrome c from the intra-membrane space into the cytosol. As previously stated, this is considered to be the 'point of no return', the instant at which the cell becomes committed to undergoing apoptotic cell death. MOMP is the primary means of inducing cancer cell death in response to both radiotherapy and chemotherapy [79], as well as stresses incurred by the cell during tumour progression [80]. Downstream of MOMP, cytosolic cytochrome c binds the protein Apaf-1 (apoptotic protease activating factor 1) [81], leading to Apaf-1 oligomerisation [82]. Procaspase 9 molecules then bind to each of the Apaf-1 monomers in the oligomeric structure to form a heptameric assembly known as the apoptosome, a high molecular weight complex that promotes caspase 9 activation [83] [84-86]. This causes a subsequent proteolytic cascade of executioner caspases, leading to cleavage of cellular components, apoptosis, and clearance of cellular debris [87, 88] (Figure 1-6).

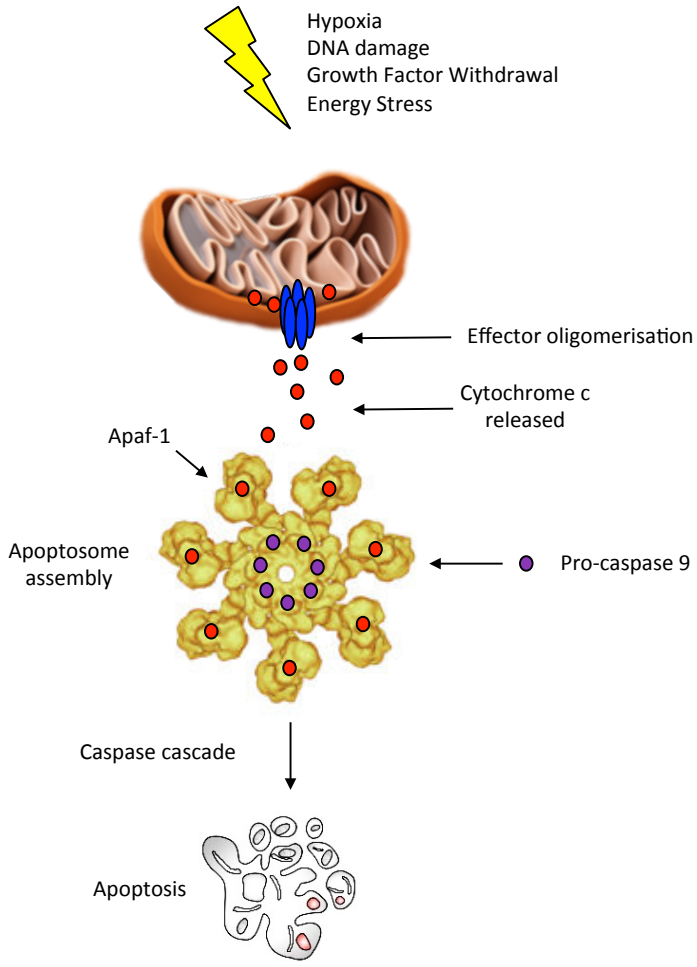

Figure 1-6 – Apoptotic activity downstream of MOMP in mitochondrial apoptosis. Cytosolic cytochrome c molecules bind monomers of Apaf-1, which oligomerise to form a heptamer. Pro-caspase 9 molecules bind to each Apaf-1 monomer in the heptameric assembly, forming a high molecular weight assembly called the apoptosome, which promotes caspase 9 activation and initiates the caspase cascade.

1.2.3 Non-canonical interactions

It should be noted that the canonical BH3 in BC binding groove interaction is not the only binding event occurring between BCL-2 family members; other, non-canonical binding events occur, which act allosterically outside of the binding groove. They cause the activation or inhibition of BAX and BAK and induce their oligomerisation, regulate the affinity of BH3 only proteins for their pro-survival binding partners, and modulate binding activity with non BCL-2 family members[89].

Pro-survival members also interact with downstream proteins in the apoptotic cascade, including some caspases. BCL-2 interactions hold pro-caspase 8 in its inactive form, preventing it from cleaving BID to its active, truncated tBID variant and stalling the caspase cascade of extrinsic apoptosis in some cases of neuroblastoma. Also, BCL-X_L has been shown to interact with both Apaf-1 and caspase 9, preventing the formation of the apoptosome downstream of MOMP in mammalian cell systems [90, 91].

Proteins from outside the BCL-2 family bind and regulate the activity of family members. They may do this through increasing [92], or decreasing [93, 94] the interactions of pro-survival family members with the MOM, doing so by way of direct protein to protein interactions, or through post translation modifications [95-97]. Other proteins interact with pro-survival members to regulate their stability in the cell [98, 99].

1.3 BCL-2 family dysregulation

From the first use of the term apoptosis almost 50 years ago, predictions were made that its dysregulation was likely to underlie a number of diseased states [100]. This is true for many types of cancer; indeed, the ability to evade apoptosis is one of the hallmarks of cancer identified by Hanahan and Weinberg in their landmark Cell paper [17] (Figure 1-7).

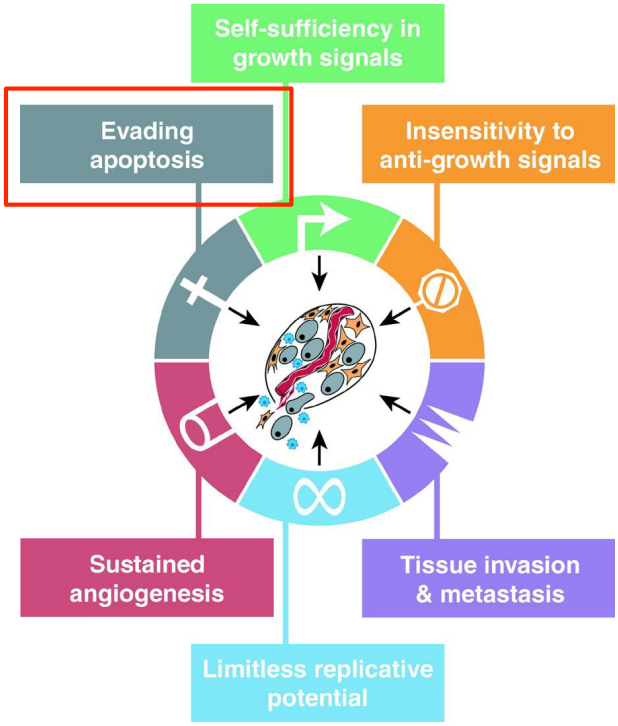

Figure 1-7 – Evading apoptosis as a hallmark of cancer. Figure adapted from [17]

It is thought that the mutations to cancer cells that result in dysregulation of apoptosis occur early in tumour progression: this allows the cells to survive and accumulate other oncogenic mutations that drive further tumour development. Cancer cells hijack the same BCL-2 intra-family interactions that occur in healthy cells under normal physiological conditions, but alter the balance between pro- and anti-apoptotic members to increase the apoptotic threshold (Figure 1-8). This means that in many cancers, despite high levels of cellular stress, the balance is pushed towards cell survival, often due to increases in the levels of functional pro-survival members. Genomic changes leading to the over expression of anti-apoptotic members have been detected in many cancers [19, 101], likewise genetic deletions or mutations to pro-apoptotic members are also seen [102, 103]. Increased expression of pro-survival members such as BCL-2, BCL-X_L or MCL1 provides competitive and selective advantage to cancer cells; such cells are described as being ‘addicted’ to these anti-apoptotic members, as without them, they cannot survive in the face of the death inducing signals that persist during tumour progression.

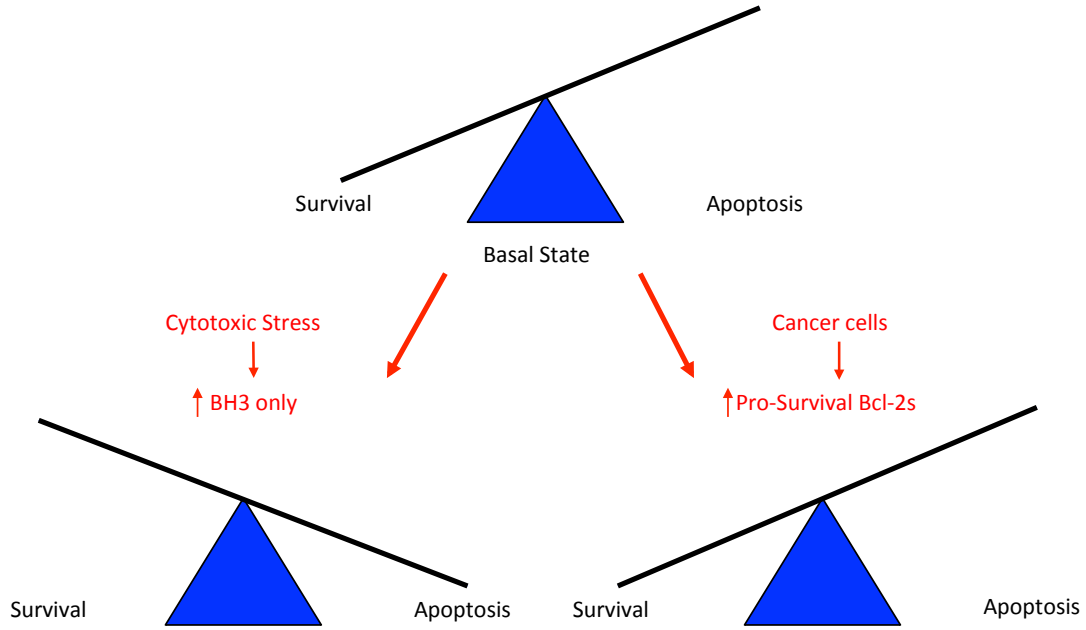

Figure 1-8 – 'BCL-2 family addiction' in cancer. Healthy cells in the Basal State have an excess of anti-apoptotic BCL-2 family proteins, and the apoptotic threshold is balanced in favour of cell survival. When cells are subjected to cytotoxic stress, they upregulate levels of BH3 only proteins, and the balance moves in favour of apoptosis. However, cancer cells often circumvent this process by upregulating pro-survival BCL-2 family members, setting the balance back in favour of cell survival. Such cancer clones are said to be 'addicted' to the BCL-2 family protein they over express.

Some of these death signals are induced by the very oncogenes that promote tumour growth: during tumour progression, c-MYC activity promotes both cellular proliferation and apoptosis [80, 104], and is thereby self limiting in its ability to transform cells (Figure 1-9); to overcome this, BCL-2 or BCL-X_L may be overexpressed as a compensatory measure to promote cell survival [20, 105, 106].

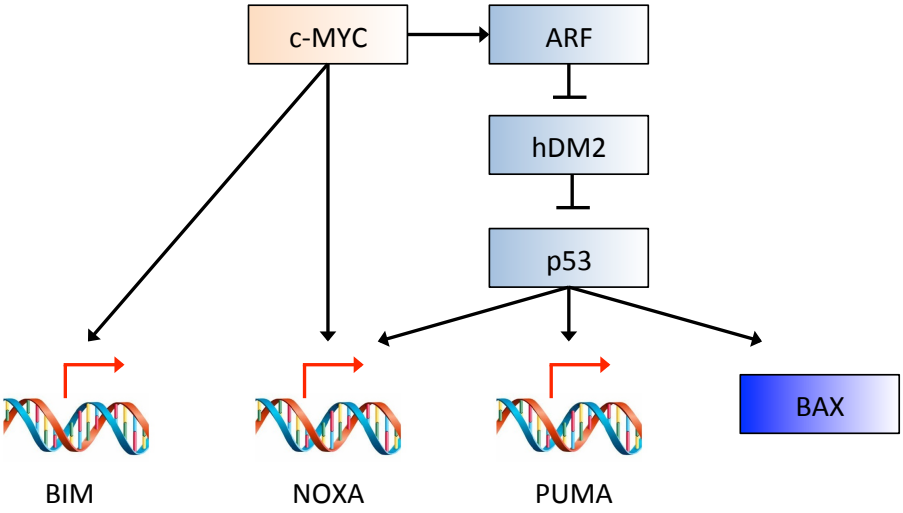

Figure 1-9 – The oncogene c-MYC also promotes apoptosis. Illustrative of the complex network of protein to protein interactions that underpin tumour progression. c-MYC directly regulates the transcription of BIM and NOXA, and activates the p53 pathway of tumour suppression, which involves transcription of NOXA and PUMA, and activation of BAX. Upregulation of pro-survival proteins often occurs as a compensatory measure, leading to BCL-2 or BCL-X_L addiction.

Defects in the mitochondrial apoptotic pathway are also common features of chemo-resistant cancers [104, 107]. This is usually due to deficiencies in the expression of, or failure to up-regulate, specific BH3 only proteins. Take BIM as an example: this BH3 only member is required for the action of therapeutics including paclitaxel [108], glucocorticoids [109], and kinase inhibitors including imatinib, erlotinib and gefitinib [110-113].

1.4 BCL-2 family proteins and cancer

1.4.1 BCL-2

More than thirty years ago, a number of groups began to report a novel t(14;18) translocation between chromosomes 14 and 18, resulting in the fusion of the immunoglobin heavy chain and *BCL2* (B cell leukaemia locus 2), in acute B cell leukaemia and follicular lymphoma cells. This caused overexpression of the BCL-2 protein [114-118], a phenomenon that was subsequently shown to enhance the survival of cells under apoptotic stress

[20, 119-121]. BCL-2 was therefore identified as an anti-apoptotic protein and became the ‘founding member’ of the BCL-2 family.

Elevated levels of BCL-2 are seen in numerous solid and blood borne tumours. In addition to the t(14;18) related increase seen in follicular and large B cell lymphomas, BCL-2 is also overexpressed in melanoma, neuroblastoma, and in breast, prostate, colorectal and small cell lung cancers [122-128]. The causes of overexpression are varied. In lymphomas, the aforementioned t(14:18) translocation places the *Bcl-2* gene adjacent to immunoglobulin heavy chain enhancer elements, leading to increased levels of BCL-2 transcription [19, 114, 116]. The half life of BCL-2 in the cell is regulated by the ubiquitin-proteosomal system [129-131], and mutations in proteins involved in this process such as INrf2 reduce the level of ubiquitin tagging of BCL-2, reduce turnover rates, and stabilise levels of BCL-2 under conditions of apoptotic stress [131]. BCL-2 levels are also indirectly increased due to genetic mutations resulting in the loss of miR-15a and miR-16, which would normally target BCL-2 mRNA: such mutations are seen in over 50% of CLL patients [132].

BCL-2 is also able to promote tumour progression by means outside its canonical role as an apoptotic inhibitor. It is implicated in promoting the epithelial-mesenchymal transition, and in elevating levels of invasiveness and enhanced metastatic potential in multiple cancer cell lines, including breast carcinoma, glioma, squamous carcinoma and neuroblastoma cells [133-137]. It is also implicated in angiogenesis in multiple tumour types [138-141]: its overexpression is often seen in tandem with hypoxia in cancer cells, where it promotes the release of VEGF, a potent pro-angiogenic factor [142-144].

1.4.2 BCL-X_L

BCL-2 overexpression is seen in many blood borne malignancies, but BCL-X_L is thought to have a more important pro-survival role than BCL-2 in many solid tumours. Evidence also points to BCL-X_L being more potent in its anti-

apoptotic activity, due to the broad range of pro-apoptotic partners it interacts with. Its overexpression also leads to chemo-resistance in multiple cancer cell lines [145].

BCL-X_L has been found to be over-expressed in prostate and breast cancer patients [146, 147]. Increased copy number of the *BCL-XL* gene has also been found in multiple solid tumours [148]. Levels of BCL-X_L activity may also be elevated in cancer cells in which certain miRNAs are deficient: for example, reductions in levels of miR-let7c have been seen in lung cancers, hepatocellular carcinomas and AML [149-151], and reduced levels of miR-491-5P in ovarian, colorectal and pancreatic cancers [152, 153].

BCL-X_L exerts other tumour promoting effects outside of its canonical role in mitochondrial apoptosis. Studies have reported its ability to induce EMT, a pre-requisite for metastatic activity, in lung, breast and pancreatic cell lines [154, 155], and to promote invasive behavior in breast carcinoma, glioma, and colon cancer cells [154, 156-158]. It has been shown to directly interact with the RAS oncogene in a BH4 dependent manner, modulating RAS's downstream activity to induce production of the proteins HMGA2 and FOSL1, which promote a non-differentiated, stem like phenotype in cancer cells [159].

Worthy of specific comment in the context of apoptotic dysregulation are the interactions between BCL-X_L and the pro-apoptotic effector BAX. BCL-X_L is recruited to the MOM bound to tBID. Once at the membrane, it behaves in the same way as other pro-survival family members, binding BAX, preventing its oligomerisation and MOMP, thus aiding cell survival, even in the presence of BAX activating stimuli [67]. But BCL-X_L has also been shown to retrotranslocate BAX away from the MOM and back to the cytosol, abrogating BAX insertion in the membrane and preventing its subsequent activation by pro-apoptotic factors [160, 161]. As only around 100 molecules of BAX are required per mitochondria to induce MOMP [162], retro-translocation by BCL-X_L may prove to be an extremely important protective

function. Over expression of BCL-X_L therefore benefits tumour progression by a variety of mechanisms.

1.4.3 MCL1

While MCL1 shares many features with other pro-survival family members, it also has a number of unique differences. Compared to BCL-2 and BCL-X_L, its transcription, translation and proteosomal degradation in the cell are very tightly controlled [163], hence it has a much shorter cellular half life, of up to 4 hours, but often much less, depending on cell type and intra-cellular conditions [164]. MCL1 also has an extended N-terminus, which is thought to be involved in regulating MCL1 turnover rates and localisation in the cell.

MCL1 is considered an important target in cancer therapy, as its over-expression is one of the most common genetic abnormalities seen in multiple tumour types [101, 145]. MCL1 has been found over-expressed in CLL and multiple myeloma samples [165-168], also in solid tumours including breast, ovarian, gastric and hepatocellular carcinomas, and in liver metastases from colorectal cancer patients [169-173]. Additionally, MCL1 over-expression is a major resistance factor in many chemo-resistant cell lines [174-176]. It also confers resistance to tumours treated with drugs that are selective for other pro-survival members, including BCL-2 and BCL-X_L.

To date, the development of binders / inhibitors for MCL1 has proven difficult in comparison to other pro-survival members, possibly due to the fact that the hydrophobic BC binding groove of MCL1 is more rigid than that on either BCL-2 or BCL-X_L [73].

1.4.4 BAX and BAK

Much of the research carried out on the role of BAX in tumour progression has been done using cellular systems [177, 178] or mouse models [179-182]. Inactivating BAX mutations in tumour samples are relatively

uncommon, compared to mutations that cause upregulation of pro-survival family members. However, frameshift mutations of BAX have been detected in colon cancers of patients suffering from defects in DNA mismatch repair, known as the microsatellite mutator phenotype [102, 183]. BAX mutations were also found in 21% of human haematopoietic malignancies sampled, especially in samples of acute lymphoblastic leukaemias [184]. These mutations led to alterations in BAX dimerization and inhibition of its pro-apoptotic function. Epigenetic silencing of BAX, through hyper-methylation of the 5'UTR near the TATA box of the *Bax* gene, has also been found in glioblastoma patients [185].

Inactivating BAK mutations are encountered even less frequently, but have been seen in gastric and colorectal cancers [186].

1.5 BAX / BAK Oligomerisation

BAX and BAK are the pro-apoptotic effector members of the BCL-2 family, oligomerising at the mitochondrial outer membrane to cause MOMP, which effectively commits the cell to undergo apoptotic cell death. As such, BAX and BAK are essential to the apoptotic process, but their activity must be tightly regulated to prevent damage to healthy cells.

Monomeric BAX and BAK molecules are dormant, and must be activated before they are able to oligomerise, form pores at the MOM, and trigger their apoptotic effects. In their inactive, monomeric states, BAX and BAK reside in different parts of the cell. Unique among the multi domain family members, BAX sequesters its own C terminal transmembrane TM domain (α9) in its own BC binding groove (Figure 1-10b). This not only covers the hydrophobic residues of the BC groove, but also conceals the hydrophobic residues of the α9 helix, hence BAX is predominantly cytosolic rather than membrane bound in healthy cells. The α9 TM domain of BAK contains more hydrophobic residues than that on BAX; it appears to prefer the overtly hydrophobic membrane environment to the more amphipathic environment

of its own BC groove, and is therefore found constitutively membrane bound in the MOM (Figure 1-10a).

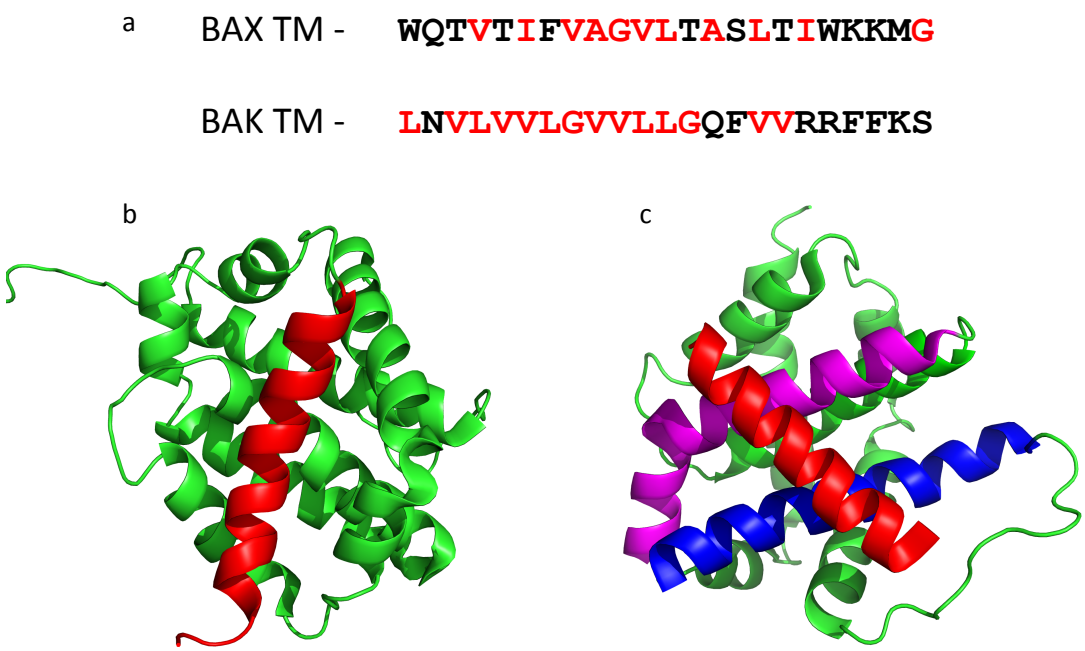

Figure 1-10 - BAX and BAK localisation at the Mitochondrial Outer Membrane. a) BAX and BAK transmembrane domain sequences. Hydrophobic residues are shown in red. The higher proportion of hydrophobic residues in the BAK TM may explain why BAK is constitutively located at the MOM, while cytosolic BAX sequesters its own TM domain in its amphipathic BC groove. b) Structure showing the C terminal TM domain of BAX (red) bound in the BC groove (PDB 1F16). c) BAX requires a pre-activation step before it translocates to the mitochondrial membrane. This is thought to be triggered by the transient binding of a BH3 family member to a rear pocket at the conjunction of the α1 and α6 helices, which is on the opposite side of BAX to the BC groove. Figure shows the BH3 domain of BIM (red) bound to the rear pocket. α1 helix shown in blue, α6 helix in magenta (PDB 2K7W).

BAX requires a pre-activation step before translocating to the mitochondrial outer membrane. This pre-activation step is thought to involve a transient interaction with an activator BH3 only protein at a non-canonical, N-terminal binding site on BAX, which acts allosterically to cause a conformational change that displaces the TM domain from the BC groove [45, 187, 188]. The binding site is located on the rear side of BAX (opposite the BC groove), is partially masked by the unstructured loop region between α1 and α2, and has a similar distribution of charged and hydrophobic residues to the canonical BC groove [45, 189] (Figure 1-10c). Displacement of the TM

domain facilitates the translocation of BAX from the cytosol to the MOM. Interestingly, BAX may be subject to an additional level of regulation: work carried out by the same group that initially discovered the BAX N terminal binding site also identified the presence of an autoinhibited dimeric form of BAX in the cytosol, in which the N-terminal activation site of one protomer binds the C terminal, TM domain containing surface of another [190]. Interactions with BH3 only proteins disrupt these dimers, causing them to dissociate to monomers, which can then translocate to the mitochondria and become active.

Activation of BAX and BAK is required at the MOM as a pre-requisite to the formation of higher order oligomers. Complexes of the BCL-2 core of BAK bound to the BH3 domain of BID studied using solution NMR [50], and crystal structures of BAX bound to BID BH3 [52] indicate that the activation step involves low affinity binding of a BH3 only direct activator at the BC groove of BAX or BAK, with subsequent conformational changes in the BCL-2 core that exposes their respective BH3 domains.

Exposure of the BH3 domain uncovers hydrophobic regions on BAX and BAK that need embedding into membranes, or alternative hydrophobic protein interfaces; this leads to oligomerisation. The nature and method of formation of these oligomers remains to be elucidated. It is also unknown whether BAX and BAK oligomers form proteinaceous or lipidic pores, and whether the pores are closed, linear assemblies, or unstructured aggregates [191, 192]. A number of models exist, competing to explain the means of activation, and subsequent oligomerisation and pore formation. Each model has biochemical evidence backing its claims, but a relative dearth of supporting structural data.

Initially, a single interface ‘daisy chain’ model of oligomerisation was proposed for BAX, with the BH3 domain of one BAX monomer engaging a groove formed by the intersection of α1 and α6 helices on another [193]. A similar model was also proposed for BAK [194]. However, there is now a body of evidence to support the formation of symmetric BH3 in groove

homodimers as the basic oligomeric unit for both BAX and BAK [52, 195-199]. Various methods have been used to confirm this mechanism *in vitro*, including stabilization of complexes with antibodies recognizing BH3 domains and N-terminal sequences, limited proteolysis assays to identify stable and exposed fragments during conformational changes, and supporting mutagenesis studies [39, 195, 200, 201]. High resolution structural data for these complexes in the mitochondrial outer membrane have yet to be obtained. How and whether these dimers go on to form higher order oligomers is a subject of ongoing debate and study. Biochemical studies suggest that the α6 helix, on the opposite side of BAX and BAK to the BC groove, may mediate a non-canonical binding interaction, but no structural data exist to support this claim [202, 203]. Structural studies of the BAX BH3 in groove dimer have raised another possible mechanism for the induction of MOMP, which abrogates the requirement for formation of a structured pore in the MOM: dimer formation results in exposure of a high concentration of lipophilic residues, which may penetrate the mitochondrial membrane, displacing phospholipid headgroups and inducing membrane curvature that would eventually cause the membrane to tear. Should this prove to be the case under physiological conditions, oligomerisation of BAX dimers into unstructured aggregates could cause MOMP, without the need for a structured proteinaceous or lipidic pore. This would be analogous to the ‘carpet’ model of membrane permeabilisation employed by anti-bacterial toxins such as the melittins [204, 205].

The structural mechanics of how BAK and BAX insert into the MOM to cause MOMP is also an open question. The core α5-α6 helices of both effector proteins are able to insert as hairpins into the MOM, where they bear striking similarity to the pore forming domains of bacterial toxins such as colicin A and diphtheria toxin [30, 206] (Figure 1-11). Synthetic peptides based on this α5-α6 combination also have pore forming abilities [207-209]. However, structural studies on BAX carried out by Czabotar and co-workers provide compelling evidence that the α5 and α6 helices dissociate on membrane binding [52], separating BAX into α1-α5 ‘core’ and α6-α8 ‘latch’ domains, and that this is an essential step in the ability of BAX to form domain

swapped dimers. Recent work by the same group has uncovered a similar mechanism for BAK [51].

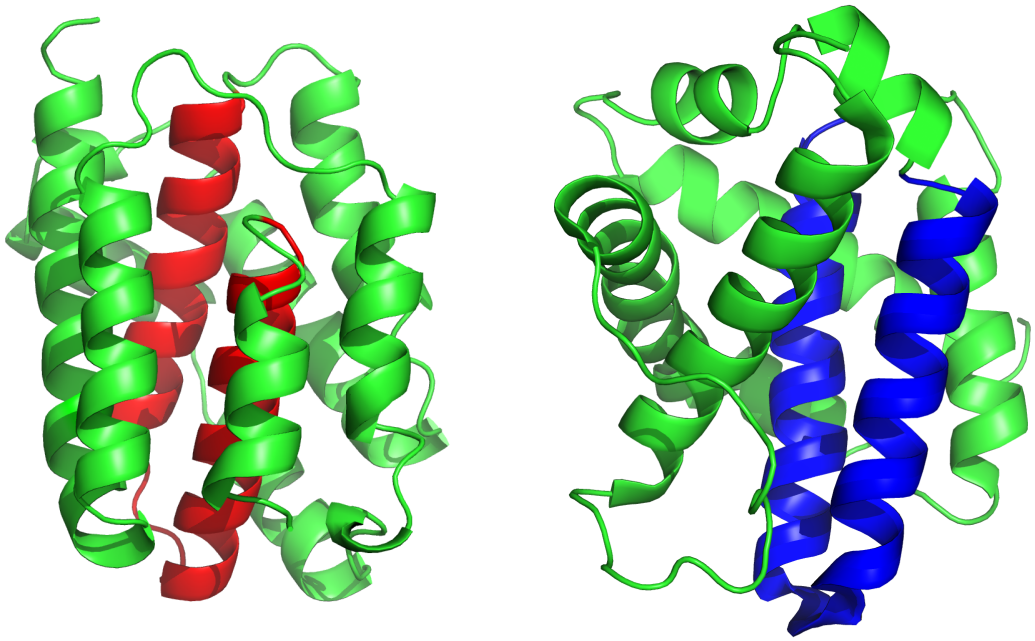

Figure 1-11 – Comparison of the pore forming domains of Colicin A in red (PDB 1COL, left) and BAX in blue (PDB F16, right). Both comprise a pair of alpha helices, able to insert as hairpins in cellular membranes.

1.6 BCL-2 family therapeutics

As the dysregulation of BCL-2 family proteins is implicated in human disease, the family is considered a worthwhile target for the development of novel therapies [210, 211], particularly those targeting cancer. A strange paradox exists for cancer cells: although they are able to circumvent apoptosis, most of them are closer to their apoptotic threshold, and therefore more 'primed to die', than their normal, cellular counterparts. Evidence points to this being due to elevated levels of BH3 only proteins [43, 212, 213]. Tumour cells should therefore be more responsive than normal, healthy cells to therapeutics targeting the mitochondrial apoptotic pathway, specifically those able to tip the balance of BCL-2 family activity back in favour of apoptosis. Such therapies would include molecules that mimic the pro-apoptotic function of the BH3 domain, so called BH3 mimetics.

1.6.1 BH3 mimetics

Much research effort has gone into the development of BH3 mimetics, molecules able to mimic the canonical BH3 in BC binding groove interaction described earlier in this chapter. Targeting this interaction with novel inhibitors is difficult, because the BC groove is shallow.

For a small molecule, peptide, or other binder to truly be considered a BH3 mimetic, it must meet certain criteria: it must have high affinity for at least one anti-apoptotic BCL-2 family member, and its cytotoxic effects must be BAX and / or BAK dependent [214]. Many molecules first thought to act as BH3 mimetics had only moderate affinity for their targets and have since been found to act through off target effects, independent of BAX or BAK [214-216].

It is also important to consider the size of the therapeutic window available for such molecules, given the important physiological roles carried out by many pro-survival proteins outside of their canonical roles in mitochondrial apoptosis. Gene deletion experiments have demonstrated the consequences of losing individual pro-survival members: BCL-2 ablation causes the death of renal epithelial progenitor cells, leading to polycystic kidney disease [217], while loss of BCL-X_L is linked to reduced platelet counts and cirrhosis of the liver [218, 219]. Loss of MCL1 causes the greatest level of physiological damage, as it is crucial for the ongoing survival of several cell types, including lymphocytes, haematopoietic stem and progenitor cells, and cardiomyocytes [220-225]. Unless they can be selectively targeted to cancer cells, very strong binders that may permanently sequester their targets could have negative consequences in healthy cells.

Notwithstanding the difficulties outlined above, efforts to develop small molecule inhibitors of pro-survival members have been underway since the turn of the millennium. Early breakthroughs were made using computer based screening and docking strategies, yielding binders to BCL-2 with low

micromolar affinities [226, 227]. Soon after, high throughput screens were used to identify low micromolar affinity binders of BCL-X_L [228, 229]. These molecules were shown to be effective in anti-proliferation assays, and were able to induce apoptosis in cellular systems.

1.6.2 BH3 peptidomimetics

A strategy that has proved successful is the use of peptidomimetics, small, protein like chains that mimic peptides, and usually arise from the modification of an existing peptide. An early development in this field was the design of terphenyl derivatives mimicking the amphipathic BH3 helix of BAK, which bound to the BC groove of BCL-X_L with sub-micromolar affinity [230, 231].

In general, unmodified peptides are not good drug candidates, as they suffer a number of pharmacological drawbacks, including limited membrane penetration and a lack of proteolytic stability once inside the cell. Organic chemists have been creative in devising strategies to overcome these issues. The incorporation of β-amino acids into peptides to create α/β foldamers has been shown to increase proteolytic stability, while maintaining the essential α-helical nature of the peptide [232]. This approach has been used in the design and synthesis of BIM and PUMA BH3 α/β peptides, which have been tested successfully in cellular assays using mouse embryonic fibroblast (MEF) cells [232-234].

Constrained peptides (also known as stapled peptides or SAHBs) have been shown to demonstrate improved cell penetration and stability [235, 236]. These modified peptides incorporate a constraint between two amino acids on the opposite side of the peptide α-helix to the H1-H4 binding residues, which stabilises the peptide in a helical conformation. The constraint is usually achieved through use of a ring closing olefin cross-metathesis reaction, as shown in Figure 1-12, but can also be achieved using amide or ‘click’ triazole linkages [237-240]. The peptide staple / constraint itself has proved to be a far from passive molecular addition: it has been found to

impact binding affinity in both positive and negative ways, and must therefore be considered when designing and testing such molecules [241-243].

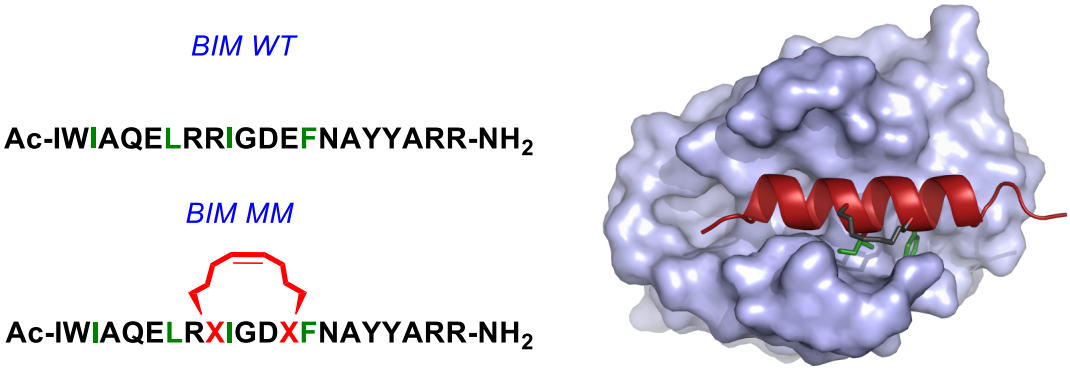

Figure 1-12 – BH3 mimetics - constrained peptides. Comparison of sequences of peptides for the BH3 domain of wild type BIM (BIM WT) and a mono-metathasised variant (BIM MM,) synthesised at the University of Leeds, in which monosubstituted α-alkenyl amino acids are substituted at *i* and *i+4* positions, then metathesized to create a covalent cross-link on one side of the peptide. The cross-link 'constrains' the peptide in a helical structure, affording improved helicity and proteolytic stability. The structure on the right of the figure shows the BIM MM peptide bound to BCL-X_L (PDB 5C3G). BIM MM was shown to inhibit interactions between BCL-X_L and BAK BH3 with much greater potency than BIM WT (IC50 11.9 ± 3.8μM for BIM MM, compared to IC50 320 ± 70μM for BIM WT) [244].

1.6.3 Small molecule inhibitors

The use of small molecule inhibitors of pro-survival BCL-2s, typified by the acyl-sulfonamides pioneered by Abbott laboratories, has been a notable success story in the field of BH3 mimetics. ABT-737 (Figure 1-13a) was the first such molecule developed, demonstrating high affinity (K_d <1nM) for BCL-2, BCL-X_L and BCL-W [245], and able to kill cells in a BAX / BAK dependent manner [215, 246]. The fact that ABT-737 exhibits poor aqueous solubility and oral bioavailability precluded its clinical development, but it is still widely used as a molecular probe. ABT-263 (navitoclax) was subsequently developed as an orally available analogue of ABT-737 (Figure 1-13a).

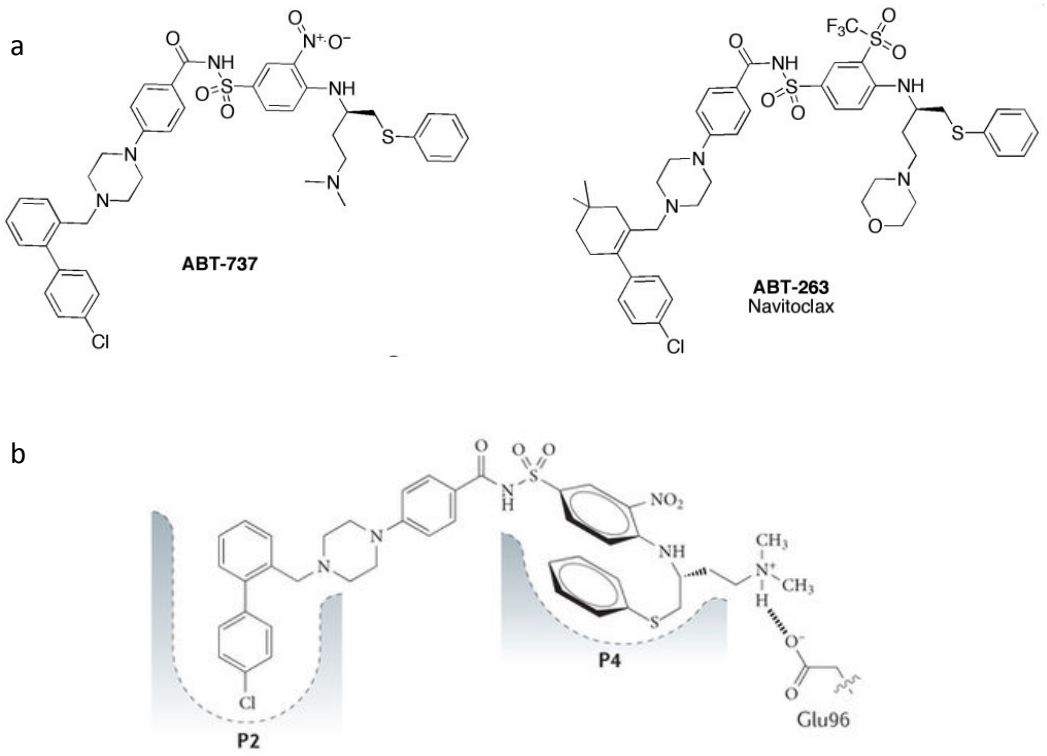

Figure 1-13 – BH3 mimetic small molecules - acyl sulphonamides. a) ABT-737 and its orally available analogue ABT-263 (navitoclax). b) ABT-737 and ABT-263 share a similar mechanism of action, binding strongly to the P2 and P4 pockets in the BC groove of their target proteins. Shown here is ABT-737 bound to BCL-X_L. Figure adapted from [247].

ABT -737 and navitoclax share a similar mechanism of action: both are seen to bind the P2 and P4 pockets in the BC groove of their target proteins, with evidence of substantial remodelling of the P2 pocket on binding [248, 249] (Figure 1-13b). Navitoclax has undergone clinical trials for treatment of haematological tumours, both as a single agent and in combination, and demonstrated early promise in patients suffering from CLL [212, 250-254]. Unfortunately, navitoclax also induced acute thrombocytopaenia (a sudden drop in platelet levels) in these patients, highlighting the important role carried out by BCL-X_L in platelet survival [251, 255], and resulting in a limited therapeutic window for the treatment of lymphoid malignancies.

The limited therapeutic window of multi-target small molecules such as ABT-263 has driven the search for single target inhibitors. Abbott laboratories designed ABT-199 (venetoclax), a selective inhibitor of BCL-2, specifically to

avoid the thrombocytopaenia caused by BCL-X_L inhibition [249] (Figure 1-14). To date, venetoclax is the only BH3 mimetic to attain FDA approval, for use in the treatment of CLL patients with an identified chromosomal 17p deletion, where it has been shown to act without inducing thrombocytopaenia.

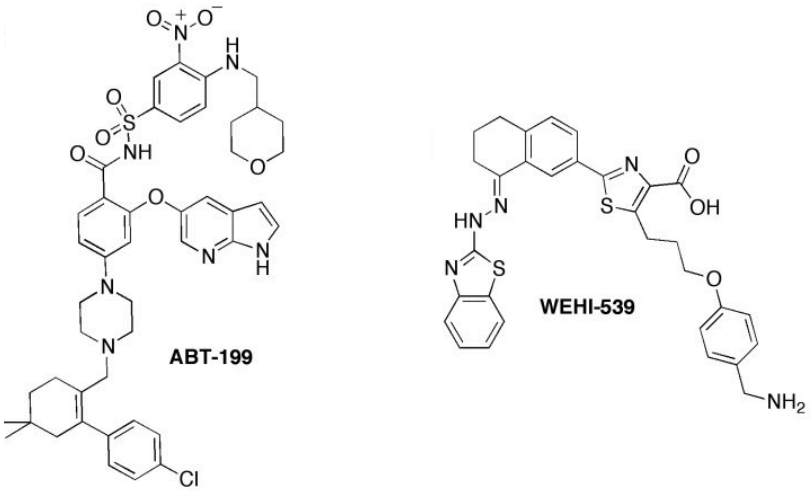

Figure 1-14 - Single target inhibitors. ABT-199 selectively targets BCL-2. WEHI-539 is a selective inhibitor of BCL-X_L.

Many solid tumours are addicted to BCL-X_L, hence selective inhibitors of this protein are an attractive proposition. Researchers at WEHI, in collaboration with a team from Genentech, used high throughput screening, combined with structure guided design and classical medicinal chemistry techniques, to develop WEHI-539, which binds BCL-X_L with sub nanomolar affinity, and high selectivity over other pro-survival members (more than 400 fold compared to BCL-2) [256, 257] (Figure 1-14). WEHI-539 does appear to be a genuine and selective BH3 mimetic acting against BCL-X_L, as do its recently synthesised analogues A-1155463 and A-1331852 [257-259]. WEHI-539 has shown synergistic anti-tumour activity in combination with doxorubicin in osteosarcoma samples, and when combined with carboplatin against ovarian cancer cells [260, 261], and A-1155463 inhibits SCLC xenograft growth in mouse models [259]. However, due to the role of BCL-X_L in platelet survival, the ongoing issue of thromobcytopaenia means that the clinical application of any BCL-X_L inhibitor remains an issue.

Some BH3 mimetics have reached the clinical trials stage, but almost all have failed to be approved for use in the clinic due to their lack of efficacy as single agents, or the rapid appearance of resistant clones [262]. Therapeutic resistance to mimetics such as navitoclax and venetoclax is most commonly caused by increased levels of cellular MCL1 [175, 215, 263-266]. The search for MCL1 inhibitors has therefore been an active area of research, though many of the putative BH3 mimetics discovered that apparently target MCL1 appear to exert their effects indirectly through NOXA upregulation. An exception to this is A-1210477, a recently discovered indole-2-carboxylic acid molecule, which disrupts MCL1:BIM complexes in the cell, has been shown to induce apoptosis in MCL1 dependent cells as a single agent, and enhances ABT-263 activity in other cells lines [265]. Strangely, the effect of treatment with A-1210477 is an *accumulation* of MCL1 in cells prior to apoptosis: this is thought to be due to MCL1 being sequestered and held inactive, and therefore being unavailable to bind to HUWE1 (MULE), an E3 ligase that ubiquitylates MCL1, tagging it for degradation at the proteasome.

For the apoptotic effectors, there is interest in developing direct activators of BAX and BAK as potential cancer treatments [267], and conversely for inhibitors of BAX and BAK to be used in diseases such as amyotrophic lateral sclerosis, or for patients suffering ischaemic reperfusion injury, where excessive acute levels of apoptosis occur [268-270]. In principle, molecules could be developed to directly activate BAX and BAK, by mimicking the actions of direct activator BH3s, in instances where, for instance, direct activators have been downregulated by tumours [101, 271]. The ability to directly target BAX and BAK in this manner would also provide a means of avoiding the cytotoxic side effects of targeting anti-apoptotic family members. Conversely, the ability to dampen the activity of effector proteins could also be put to good use in limiting the levels of ischaemic cell death in patients suffering heart attack or stroke [272].

The ability to develop molecules that target individual BCL-2 family members not only provides the basis for the development of therapeutics, but also

allows for the development of molecular tools to uncover the physiological activities of their target proteins, in both normal and pathological states, and to help unravel the interactions of BCL-2 protein family members, both within and without the family. The search for more and better ways to identify and synthesize such molecules continues.

1.7 Use of Phage Display and Affimers to identify novel binders for target proteins

Phage display has proven to be a useful tool in drug discovery, providing a relatively fast and cost effective means of identifying ligands for targeted proteins. It is dependent on the ability of bacteriophages to display protein fragments, peptides and other structures on their coat proteins, achieved by insertion of the nucleotides encoding the sequence of interest into the coat protein gene [273]. Based on this ability, simple molecular biology methods can be used to develop large libraries of clones, which are screened against target proteins to identify novel binding partners [274].

A typical phage display experiment begins with immobilisation of the target protein, followed by a series of ‘panning rounds’, in which the target is incubated with the phage library, non-bound phage is washed off, then bound phage is eluted and amplified by transfecting a phage display competent strain of bacterial cell. The use of multiple panning rounds results in the selection of high affinity binders for the target protein [274], which can then be sequenced to establish the genotype and phenotype of the binding residues (Figure 1-15).

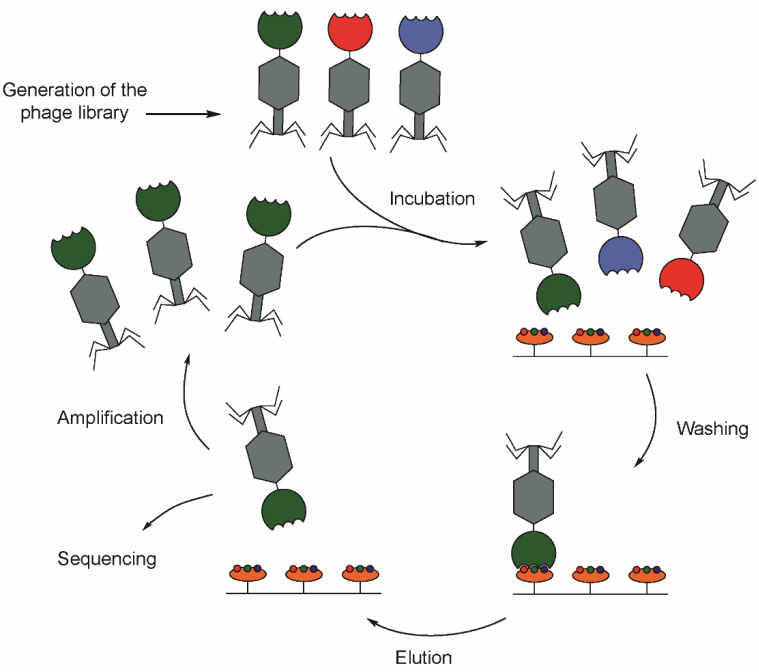

Figure 1-15 - Typical phage display experiment. A phage library (> 10^{10} clones) is generated. This library is incubated with an immobilised target protein in the first of a series of 'panning rounds'. Unbound phage is washed off, then bound phage is eluted and amplified by transfecting a phage competent strain of *E.coli*. Amplified phage is used in future panning rounds and the process is repeated, leading to the selection of high affinity binders, which can be sequenced to establish genotype, and subcloned into appropriate vectors for recombinant protein expression. Adapted from [275]

High affinity binding sequences can be sub-cloned into suitable vectors and recombinantly expressed as binding proteins, for further structural and biophysical analysis. Such proteins may mimic natural ligands for the target proteins, or they may display completely novel epitopes, which none the less still bind potently, and may affect endogenous interactions or induce conformational changes by allosteric mechnisms. Such epitopes may be transferable to small molecule scaffolds, which can be used to develop new drug targets.

Historically, antibodies have been the most commonly used binding proteins [276], but they are not without limitations. Being reliant on animals and mammalian cell culture systems for their production, they are both costly and time consuming to produce. They cannot be recombinantly expressed in bacterial systems, and are not always thermally stable. Protein engineering

methods have therefore been used to develop alternative non-antibody binding proteins, which mimic the positive molecular recognition properties of antibodies, but overcome their drawbacks. These include reagents such as DARPins [277], Monobodies [278] and Affibodies [279].

Affimers (adhirons) are another such class of novel non-antibody scaffold proteins, developed at the University of Leeds [280]. They are based on a phytocystatin consensus sequence, derived by identifying the most common amino acid residues at each position in an alignment of 57 individual phytocystatin sequences. Phytocystatins are small, plant derived cysteine protease inhibitors [281]. An Affimer comprises four β-strands, one α-helix, and two loops connecting each pair of β-strands and displays all the desirable properties of an ideal non-antibody binding protein: small, monomeric, high solubility, thermal stability, with a lack of disulphide bonds and glycosylation sites, and is therefore ideal for peptide presentation. The Affimer scaffold has been used to construct a phage display library containing over ten billion clones in which the inhibitory sequences on the phytocystatin scaffold have been replaced with a pair of nine residue variable peptide loops, which can be used to ‘pan’ against target proteins to identify novel binders for those proteins (Figure 1-16).

Affimers have proved useful in a variety of ways. They have been raised against a large number of individual proteins, and are able to distinguish different isoforms [280, 282]. In the last couple of years, Affimers have been developed for use in the production of biosensors [283], with practical applications targeting molecules such as interleukin 8 (IL-8), which is associated with chronic inflammatory diseases. Such biosensors can be used to track disease progression [284]. Affimers have also been tagged with gandolinium(III) complexes for potential use as contrast agents in MRI [285], and have been used to probe the surface of molecules such as p300, to help inform future inhibitor design to antagonise the HIF-1α : p300 interaction [286], which is thought to be involved in tumour growth, vascularization and metastatic potential [287, 288]. Most recently, they have

been shown to inhibit protein to protein interactions, both by direct binding, and by allosteric actions [289].

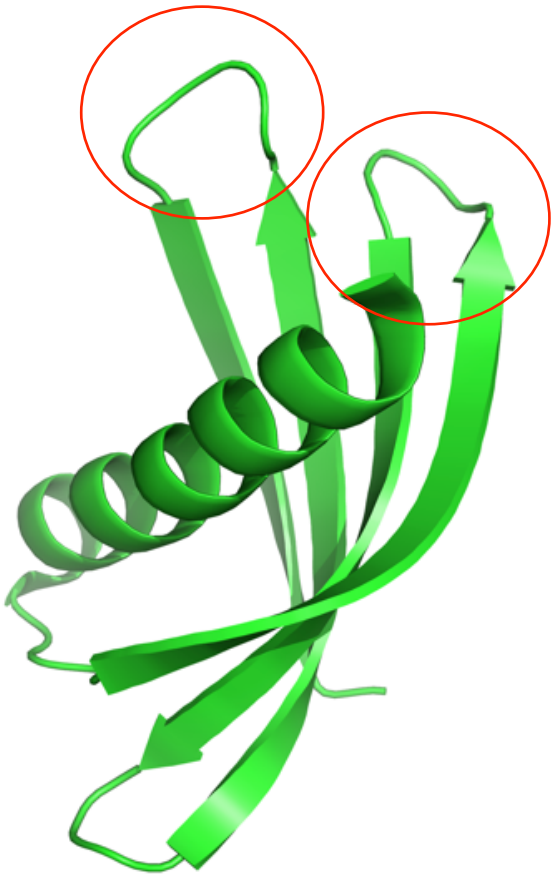

Figure 1-16 – Affimers are non-antibody scaffold proteins based on a highly stable phytocystatin concensus sequence. The scaffold structure comprises four β-strands, one α-helix, and two loops connecting each pair of β-strands. The Affimer scaffold has been used to construct a phage display library containing over ten billion clones in which each of the connecting loops (circled in red) contain nine randomly assigned residues, which can be used to 'pan' against target proteins to identify novel binders for those proteins (PDB 4N6T).

1.8 Project Aims

In recent years, great progress has been made in elucidating the interactions between different BCL-2 family members, and in the design and synthesis of molecules to mimic or antagonise those interactions. Much effort in this field has been directed towards the development of inhibitors of the pro-survival BCL-2 family members, with a view to directing the design of drug candidates to negate any survival advantage gained by cancer cells that avoid apoptosis through overexpressing these proteins. Though success in the clinic has so far been limited, molecules that selectively engage different BCL-2 family members have proved to have other benefits, such as helping to elucidate the activities of individual family members using *in vitro* and *in cellulo* assays. Efforts to develop mimetics targeting the pro-apoptotic effectors BAX and BAK have proved more difficult, though recent breakthroughs providing structural details of these proteins and their likely mode of activation have provided renewed impetus in this area. There has also been a growth in interest in non-canonical interactions occurring outside the BC groove, which may regulate apoptotic activity through allosteric mechanisms.

In its original form, this research project was focussed entirely on BAX, with the aim of using cellular systems and proteomic methods to characterise the BAX interactome at different stages of apoptotic induction. The hypothesis behind this work was that as yet undiscovered endogenous binding partners exist for BAX, and that discovering them and studying the nature of their interactions would help elucidate the mechanism of BAX activation in the cell.

Initial experiments aimed to capture BAX at various time-points between the application of an apoptotic stimulus and the appearance of apoptotic features in a panel of Mouse Embryonic Fibroblast (MEF) knock out cell lines, but issues were encountered in setting up a credible, working cellular system: the BAX $^{-/-}$ BAK $^{-/-}$ double knock out cell line responded to apoptotic stimuli in the same manner as the BAX $^{-/-}$ and BAK $^{-/-}$ single knock out lines.

This, combined with difficulties in obtaining anti-BAX antibodies sensitive enough to detect small amounts of BAX in extracts from sub-cellular cytosolic and mitochondrial fractions, led to a change in direction for the project at the transfer stage.

The revised project continued to involve study of protein-protein interactions of BAX, but also expanded its remit to include other members of the BCL-2 family. The primary aim of this project was to expand the toolbox of molecules able to bind (and hopefully regulate the activity of) BCL-2 family members, using the Affimer scaffold developed at the university of Leeds. It was hypothesised that the use of phage display experiments to probe the entire surface of target BCL-2 proteins would identify Affimers with the ability to bind the BC groove using novel binding motifs, and also identify binding sequences targeting novel sites on the protein surface that may moderate interactions through allosteric mechanisms. The use of multiple panning rounds would also allow for 'cross-panning' against multiple BCL-2 family members, with the view of identifying cross-reacting binding sequences that are able to target more than one family member at once. Within this context, the project aimed to raise Affimers as detailed below, and to characterise, as far as possible, their interactions with target proteins: -

- Raise Affimers selectively against the pro-apoptotic effectors BAX and BAK.
- Raise Affimers selectively against the pro-survival proteins BCL-2, BCL-X_L and MCL1.
- Cross pan to raise Affimers able to act against multiple pro-survival proteins.

The lack of structural evidence relating to higher order oligomers of BAX and BAK remains an issue in resolving outstanding questions relating to the apoptotic activity of these proteins. From *in vitro* studies, it has long been known that detergents are able to induce complex formation in BAX [290]. Titration of BAX with BOG is seen to trigger oligomerisation, and the same is true of other non-ionic detergents, though the nature of such oligomers has

not previously been characterised. A secondary aim of this project was to use structural techniques, specifically negative stain electron microscopy, to investigate the nature of the oligomers formed when BAX and BAK were treated with Tween 20. Though not replicating physiological membrane conditions, it was hypothesised that any data obtained could inform future research into higher order oligomerisation of these proteins, and help determine whether a structured pore is required to induce MOMP.

Chapter 2
Materials and Methods

2.1 Materials

2.1.1 DNA Constructs Used

BCL-X_L ^{ML} (1-26, 83-209 'Missing-Loop')
MCL1$^{172-327}$
BCL-2 $^{1-205}$
BAK $^{16-185\ C-S}$ (C166S)
BAX $^{1-171\ C-S}$ (C62S C126S)

2.1.2 Bacterial Strains Used

Competent DH5α *E. coli* cells (Invitrogen, genotype *F- endAI hsdRJ7 (r-k, Mk+) supE44 thi-I λ- recAI gyrA96 relAI deoR Δ(lacZYA-argF)-U169 Φ80dlacZΔM15)* were used to amplify plasmid vectors containing insert DNA.

E. coli expression strain BL21 (DE3) Rosetta 2 (Novagen, genotype F- *ompT hsdS*B(rB- mB-) *gal dcm* pRARE2 (Cam^R)) encoding T7 RNA polymerase and chloramphenicol resistance was used for over expression of protein from plasmid DNA in all cases except those noted immediately below.

Chemically competent C41 (DE3) *E. coli* cells (Lucigen, genotype F – *ompT hsdSB (rB- mB-) gal dcm* (DE3)) were used to express protein from plasmid DNA encoding BAX $^{1-171\ C-S}$ and BAK $^{16-185\ C-S}$ constructs.

E. coli ER2738 cells (NEB, genotype F *´proA+B+ lacIq Δ(lacZ)M15 zzf::Tn*10(TetR)*/ fhuA2 glnV Δ(lac-proAB) thi-1 Δ(hsdS-mcrB)5*) were used for the amplification of phage during affimer panning.

All strains were stored at -80°C, with the addition of 20% glycerol.

2.1.3 Plasmid Vectors Used

pET-28a (Novagen), with kanamycin resistance and the addition of a SUMO fusion tag (pET-28a-SUMO), was used to clone DNA for all constructs except those noted immediately below.

pGEX-6p-1 (GE Healthcare), with ampicillin resistance, was used to clone DNA for the BCL-2 $^{1-205}$ construct.

pTXB1 (NEB), with ampicillin resistance, was used to clone DNA for BAX $^{1-171\ C-S}$ and BAK $^{16-185\ C-S}$ constructs.

pET-11a (Novagen), with ampicillin resistance, was used to clone DNA for all affimers.

2.1.4 Media

Cultures were grown in either LB or 2xYT media, autoclaved and supplemented with the appropriate antibiotic.

LB media was made with 10g tryptone soya broth, 5g yeast extract and 10g sodium chloride per 1L ddH_2O.

2xYT media was made with 16g tryptone soya broth, 10g yeast extract and 10g sodium chloride per 1L dd H_2O.

Agar plates were made with 10g Tryptone, 5g Yeast Extract, 10g NaCl, 20g Agar per 1L dd H_2O.

Stock solutions of antibiotics were stored at -20°C, and added to media at a ratio of 1:1000. Stock concentration of Kanamycin was 50mg/mL, stock concentration of Ampicillin 100mg/mL, giving working concentrations of 50µg/mL and 100µg/mL respectively.

2.1.5 Buffers

Buffers used throughout this study are summarized in Table 2-1below.

Table 2-1 – Buffers used in this study

Procedure / Assay	Buffer
BAX / BAK column buffer	20mM HEPES pH 7.0 100mM NaCl 1mM EDTA
BAX / BAK size exclusion buffer	50mM Sodium Phosphate pH 7.0
BCL-2 lysis buffer	50mM Tris pH 8.0 200mM NaCl 5mM DTT 1mM EDTA 0.1% Triton X-100
BCL-2 high salt wash buffer	50mM Tris pH 8.0 500mM NaCl 1mM DTT 1mM EDTA 10% glycerol 0.01% Triton X-100
BCL-2 low salt wash buffer	50mM Tris pH 8.0 200mM NaCl 1mM DTT 1mM EDTA 10% glycerol 0.01% Triton X-100
BCL-2 size exclusion buffer	20mM Tris pH 8.0 200mM NaCl 0.5mM DTT 5% glycerol
Bcl_{XL} / MCL1 column buffer	50mM Tris pH 8.0 500mM NaCl 15mM imidazole (wash / elute with increased concentration of imidazole: 50mM, 100mM, 300mM)
Bcl_{XL} / MCL1 dialysis buffer	50mM Tris pH 8.0 250mM NaCl
Bcl_{XL} / MCL1 size exclusion buffer	50mM Tris pH 8.0 250mM NaCl 0.5mM DTT 2.5% glycerol
Affimer lysis buffer	50mM Tris pH 8.0 500mM NaCl 15mM imidazole
FA binding buffer (MCL1, Bcl_{XL}, BCL-2)	20mM Tris pH8.0 150mM NaCl 0.01% Triton x100
FA binding buffer (BAX, BAK)	50mM Sodium Phosphate pH 7.0

	0.02% v/v BSA
SDS running buffer	25mM Tris pH6.8 190mM Glycine 0.1% w/v SDS
WB transfer buffer	25mM Tris pH6.8 190mM Glycine 20% MeOH
CD Buffer	50mM Sodium Phosphate pH 7.0

2.1.6 Reagents

All reagents were supplied by Sigma Aldrich, unless otherwise specified.

2.2 Methods

2.2.1 Recombinant DNA methods

2.2.1.1 PCR

Affimer PCR subcloning experiments were conducted in 0.2 mL thin-walled dome capped tubes (Alpha Laboratories). The total reaction mixture was 25 µL containing 5µL 5x Phusion polymerase buffer (New England Biolabs), 0.75 µL DMSO, 1µL dNTP stock solution (2.5 mM of each dNTP, Invitrogen), 2 µL each of 10 µM forward and reverse primers, 1 µL PCR DNA template, 0.25 µL Phusion DNA polymerase (New England Biolabs) and 13 µL water. PCR was conducted in a Prime thermocycler (Techne). The PCR protocol is detailed in Table 2-2 below.

Table 2-2 – Affimer PCR subcloning protocol

Step	Temp (°C)	Time	# of cycles
1	98	30 sec	1
2	98	20 sec	30
	54	20 sec	
	72	20 sec	
3	72	10 min	1
4	4		

PCR amplified samples were digested with 0.5 µL Dpn1 for 1 hour at 37°C, analysed by agarose gel electrophoresis and purified using the QIAquick gel extraction kit (QIAGEN), following the manufacturer's recommended

protocol.

All other PCR experiments were conducted in 0.2 mL thin-walled dome capped tubes (Alpha Laboratories). The total reaction mixture was 50 µL containing 10µL 5x Phusion polymerase buffer (New England Biolabs), 1µL dNTP stock solution (2.5 mM of each dNTP, Invitrogen), 1 µL each of 10 µM forward and reverse primers, 1 µL PCR DNA template, 0.5 µL Phusion DNA polymerase (New England Biolabs) and 35.5 µL water. PCR was conducted in a Prime thermocycler (Techne). The PCR protocol is detailed in Table 2-3 below.

Table 2-3 – General PCR protocol

Step	Temp (°C)	Time	# of cycles
1	98	30 sec	1
2	98	30 sec	30
	68	30 sec	
	72	30 sec	
3	72	5 min	1
4	4		

PCR samples were analysed by agarose gel electrophoresis and purified using the QIAquick gel extraction kit (QIAGEN), following the manufacturer's recommended protocol.

2.2.1.2 Vector Digests and Ligations

Destination vectors used in sub-cloning experiments were cut using restriction endonucleases. 1 µg of vector DNA was mixed with 1 µL of each restriction endonuclease, 10 µL of appropriate RE buffer (e.g. Cutsmart® (New England Biolabs)), and the addition of ddH_2O to a total reaction volume of 50 µL. Reactions were incubated at 37°C for 3 hours, or at 25°C overnight. Cut vector DNA was analysed by agarose gel electrophoresis, then extracted and purified using the QIAquick gel extraction kit (QIAGEN), following the manufacturer's recommended protocol.

Ligation reactions were set up using 3 molar equivalents DNA insert to 1 molar equivalent cut vector, 1uL 10x ligation buffer and 1uL T4 ligase (New England Biolabs) and the addition of ddH_2O to a total reaction volume of 10 µL. Reactions were incubated at 25°C for 30 minutes., after which ligated product was stored at -20°C, ready to be used in transformation experiments.

2.2.1.3 Agarose gel electrophoresis

Agarose gels were prepared using 0.5x TBE buffer containing 10,000 x SYBR Safe DNA gel stain (Invitrogen). Samples were mixed with 6x DNA loading dye (New England Biolabs) prior to loading onto gels. Gels were run at 100 V in 0.5x TBE buffer until bands were sufficiently separated. Band size was measured by inclusion of a DNA ladder (100 bp or 1kbp)(New England Biolabs) alongside the samples.

2.2.1.4 Gibson Assembly

PCR amplified DNA samples were inserted into cut vectors using Gibson Assembly® (New England Biolabs) following the manufacturer's recommended protocol. On ice, 50 – 100ng of cut vector was mixed with a 2-3 x molar excess of DNA insert, made up to 10 µL with dd H_2O, and added to 10 µL 2x Gibson Assembly® or HiFi® master mix (New England Biolabs) for a total reaction volume of 20 µL. Reactions were incubated at 50°C for 20 minutes on a Prime thermocycler (Techne).

2.2.1.5 Competent cell transformation

50 µL competent *E.coli* DH5α, BL21 (DE3) or C41 (DE3) cells were transformed by addition of 1 µL assembled DNA vector product in ice chilled 1.5ml Eppendorf tubes, with gentle mixing. Cells were then incubated for 30 minutes on ice, heat shocked at 42°C for 45 seconds and returned to ice for 2 minutes. 450 µL of LB was added and the transformation mixture was then incubated at 37°C for 1 hour with shaking at 180rpm. 100 µL of transformed

cells were spread onto agar plates inoculated with the appropriate antibiotic.

2.2.1.6 Plasmid extraction

Plasmid DNA was extracted from 5 mL of overnight culture using QIAprep spin miniprep kit (QIAGEN) as per the manufacturers handbook. The extracted DNA samples were stored at -20 °C. Each new plasmid obtained from positive colonies was transformed into both DH5α and BL21(DE3) or C41(DE3) *E. coli* strains and glycerol stocks of the resulting cells were produced by the addition of 0.6 mL sterile 50 % glycerol to 0.9 mL of overnight culture prior to storage at -80.

2.2.1.7 Sanger sequencing

15 µL of each purified recombinant plasmid was sent to Cogenics (Essex) to be sequenced prior to expression trials, to test for any mutations introduced during PCR.

2.2.2 Protein preparation and purification

2.2.2.1 Protein expression – general and small scale

2.2.2.1.1 OD_{600} Measurement

The Optical Density (OD) of cell cultures was read with a spectrophotometer (Helious β) set to 600 nm by using 1 mL of culture in a plastic cuvette (brand) after the spectrophotometer was blanked against a 1mL sample of un-inoculated media.

2.2.2.1.2 Size Exclusion Chromatography

Size exclusion chromatography was performed on a Superdex 75 (26/600) column (GE healthcare) attached to an Akta prime system at 4 °C. The column, stored in 20% ethanol, was washed with water and equilibrated with

appropriate SEC buffer. 5 mL of filtered protein sample (after affinity chromatography) was loaded onto the column using a 5 mL injection loop. The absorbance of the sample was monitored at 280 nm throughout. Upon completion of the method, the column was washed with water and stored in 20% ethanol. Fractions from within the peak of the UV trace were analysed by SDS-PAGE.

2.2.2.1.3 Protein Concentration Measurement

Approximate protein concentration was determined using a protein assay reagent dye (Bio-Rad). 200 µL of dye was added to 800 µL of water and 20 µL of protein. The sample was placed in a plastic cuvette (Brand) and absorbance measured at 595 nm in a UV/visible spectrophotometer (Spectronic). The spectrophotometer was first blanked against a sample in which 20 µL of appropriate buffer was substituted for protein. In the assay an absorbance of 1 signifies a concentration of 1 mg/mL for readings between 0.2-0.8; if outside this range the volume of protein sample added is adjusted.

Accurate protein concentration was determined by measuring absorbance at 280nm. The sample was placed in a high precision quartz cuvette (Hellma Analytics), with a 10mm light path, and absorbance measured at 280 nm in a UV/visible spectrophotometer (Spectronic). The spectrophotometer was first blanked against appropriate buffer.

2.2.2.2 Chitin Affinity Chromatography

Mxe intein / chitin binding domain (CBD) tagged fusion protein constructs were over-expressed in *E.coli* C41 (DE3) cells, and purified using a protocol adapted from ref[291]. 2 ml of overnight starter culture was used to inoculate 1 L LB containing 100 µg/ml Ampicillin. Cultures were grown at 37°C plus shaking at 180rpm until OD_{600} reached 0.6 – 0.8. For BAX $^{1\text{-}171\ C\text{-}S}$ protein expression was induced by adding 0.1mM IPTG. Induced cultures were grown at 28°C plus shaking at 180rpm overnight. For BAK $^{16\text{-}185\ C\text{-}S}$ protein expression was induced by adding 1mM IPTG, and induced cultures were grown at 37°C plus shaking at 180rpm for 4 hours. Cells were harvested by

centrifugation (Beckmann JLS 8.1, 5000rpm, 15minutes, 8°C). Cell pellets were resuspended in lysis buffer (20mM HEPES pH7.0, 100mM NaCl, 1mM EDTA)) and lysed by sonication. Cell lysate was clarified (Sorvall SS34 rotor, 18,000 rpm, 45 min, 8°C), the supernatant was filtered (0.22 µM Minisart, Sartorius). Clarified cell lysate was added to approximately 20 mL Chitin Resin (New England Biolabs) packed in a free-flow gravity column, equilibriated with 20 column volumes of lysis buffer. The lysate was then added to the column and eluted from the column at a flow rate of 1mL/min, then the resin was washed with 10 column volumes of lysis buffer. The column was quickly equilibriated with 3 column volumes of lysis buffer supplemented with 50mM DTT. The resin was then resuspended in 1 column volume of lysis buffer supplemented with 50mM DTT. Following overnight incubation on an analogue roller mixer (SKS science) at 25°C, cleaved protein was obtained by collecting the flow through from the column. To collect all cleaved protein, the resin was washed with 50ml of lysis buffer, then a further 100ml of lysis buffer. All wash fractions were collected and analysed by SDS-PAGE. Columns were stored in 20% ethanol.

Cleaved protein was concentrated (Amicon, MWCO 10,000) to 10 ml, filtered (0.22 µM Minisart, Sartorius) and further purified by Size Exclusion Chromatography. Purified protein was stored at 4°C, for a maximum of 42 days, without further concentration.

2.2.2.3 Nickel Affinity Chromatography

His-SUMO tagged MCL1$^{172\text{-}327}$ and BCL-X_L ^{ML} fusion protein constructs were over-expressed in *E.coli* BL21 (DE3) Rosetta 2, and purified using a protocol adapted from ref[292]. 10 ml of overnight starter culture was used to inoculate 1 L 2 xYT containing 50 µg/ml Kanamycin. Cultures were grown at 37 °C plus shaking at 180rpm until OD_{600} reached 0.6 – 0.8. The temperature was reduced to 18 °C and protein expression induced by adding 0.5mM IPTG. Induced cultures were grown at 18°C plus shaking at 180rpm overnight before harvesting by centrifugation (Beckmann JLS 8.1, 5000rpm, 15minutes, 4°C). Cell pellets were resuspended in column buffer

(50 mM TRIS pH 8.0, 500 mM NaCl, 15 mM imidazole) and lysed by sonication in the presence of 10 µL of 1 U/ml^{-1} DNase I per litre of over-expression culture. Cell lysate was clarified (Sorvall SS34 rotor, 18,000 rpm, 45 min, 4°C), the supernatant was filtered (0.45 µM Minisart, Sartorius). Clarified cell lysate was applied to a 5 mL Ni^{2+} sepharose HisTrap HP column (GE Healthcare) charged with 0.1 M $NiSO_4$ and equilibrated with column buffer, using a peristaltic pump to maintain a flow rate of 1mL/min. The HisTrap was then washed with 10 volumes of column buffer, followed by 10 volumes of column buffer supplemented with 50 mM imidazole, and 10 volumes of column buffer supplemented with 100 mM imidazole. Fusion proteins were then eluted from the HisTrap with column buffer supplemented with 300 mM imidazole. The His-SUMO tag was cleaved from fusion protein in dialysis buffer (50 mM TRIS pH 8.0, 250 mM NaCl in the presence of Smt3 protease, Ulp1), overnight at 4°C. The dialysed sample was reapplied to a 5mL HisTrap and the flow through containing cleaved protein collected.

Cleaved protein was concentrated (Amicon, MWCO 10,000) to 5 ml, filtered (0.22 µM Minisart, Sartorius) and further purified by Size Exclusion Chromatography. Purified protein was concentrated and stored at -80°C, with the addition of 5% glycerol to aid long term stability.

2.2.2.4 Glutathione affinity chromatography

Glutathione S-transferase (GST) tagged BCL-2 $^{1\text{-}205}$ fusion protein constructs were over-expressed in *E.coli* BL21 (DE3) Rosetta 2, and purified using a protocol adapted from ref[293]. 10 ml of overnight starter culture was used to inoculate 1 L 2 xYT containing 100 µg/ml Ampicillin. Cultures were grown at 37 °C plus shaking at 180rpm until OD_{600} reached 0.6 – 0.8. The temperature was reduced to 18 °C and protein expression induced by adding 0.3mM IPTG. Induced cultures were grown at 18°C plus shaking at 180rpm overnight before harvesting by centrifugation (Beckmann JLS 8.1, 5000rpm, 15minutes, 4°C). Cell pellets were resuspended in lysis buffer (50mM TRIS pH 8.0, 200mM NaCl, 5mM DTT, 1mM EDTA) and lysed by sonication in the presence of 10 µL of 1 U.ml-1 DNase I per litre of over-

expression culture. Cell lysate was clarified (Sorvall SS34 rotor, 18,000 rpm, 45 min, 4°C), the supernatant was filtered (0.45 µM Minisart, Sartorius). Clarified cell lysate was added to approximately 10 mL Glutathione Superflow Resin (Generon) packed in a free-flow gravity column. The column was washed with 5 column volumes of water and equilibrated with 5 column volumes of lysis buffer. The lysate was then added to the column and and placed on an analogue roller mixer (SKS science) at 4°C for 1-3 hours. Lysate was then eluted from the column under gravity, and the resin was washed first with 100ml high salt wash buffer (50mM Tris pH8, 1mM DTT, 1mM EDTA, 500mM NaCl, 10% glycerol, 0.01% Triton), then 100mL low salt wash buffer (50mM Tris pH8, 1mM DTT, 1mM EDTA, 200mM NaCl, 10% glycerol, 0.01% Triton). The resin was re-suspended in 20mL of low salt wash buffer, supplemented with 400µL Prescission protease to cleave the GST tag from the fusion protein. Following overnight incubation on an analogue roller mixer (SKS science) at 4°C, cleaved protein was obtained by collecting the flow through from the column. To collect all cleaved protein, the resin was washed with 50ml of low salt wash buffer, and the flow through collected. All wash fractions were collected and analysed by SDS-PAGE. Columns were stored in 20% ethanol.

Cleaved protein was concentrated (Amicon, MWCO 10,000) to 5 ml, filtered (0.22 µM Minisart, Sartorius) and further purified by Size Exclusion Chromatography. Purified protein was concentrated and stored at -80°C, with the addition of 5% glycerol to aid long term stability.

2.2.3 Protein characterisation

2.2.3.1 SDS PAGE

Sodium dodecyl sulphate polyacrylamide (SDS-PAGE) gel electrophoresis was performed based on the method described by Laemmli [294]. 12%, 15 % and 17% gels were prepared. Protein samples were mixed with 4x loading buffer in a 3:1 ratio, heated at 95°C for 6 minutes, and electrophoresed through SDS PAGE gels in SDS running buffer at 120V-150V. Proteins were

visualized using coomassie blue stain (45% (v/v) methanol, 10% (v/v) acetic acid, 0.25% (w/v) coomassie brilliant blue R-250), then destained in 30% (v/v) methanol, 10% (v/v) acetic acid. A broad range molecular marker was included in the first lane of each gel to ascertain the M_r of proteins.

2.2.3.2 Western Blot

Samples from different stages of protein purification were separated by SDS-PAGE and immunoblotted. Samples were boiled for 6 minutes in 2 x SDS sample buffer (100mM Tris pH6.8, 4% SDS, 20% glycerol, 0.2% bromophenol blue, 200mM DTT), submitted to polyacrylamide gel electrophoresis in 1% SDS running buffer and immunoblotted with anti-BAX (Abcam ab 7977).

2.2.3.3 Mass Spectrometry

High Resolution Mass Spectrometry (HRMS) was used to confirm the correct M_w of proteins and affimers. Samples at 1mg / mL were analysed using a Bruker Maxis impact mass spectrometer, using Electro-spray Ionisation (ESI), with values reported as a ratio of mass to charge.

2.2.3.4 Circular Dichroism (CD)

CD was performed using Applied Photophysics ChiraScan apparatus and software. Secondary structure was determined using standard CD scans in the ultraviolet range. For each CD scan, the following parameters were used: 190-260 nm range; time per point 1.0 s; step = 1 nm; bandwidth = 2.5 nm; path length = 10 mm. Scans were carried out in duplicate and averaged. Samples were prepared in the appropriate buffer (described in results for individual experiments). The raw circular dichroism data obtained for the peptides was processed by the subtraction of the solvent signal and converted into a mean residue ellipticity.

$$[\theta] = \theta / (10 \times c \times l) \qquad \textbf{Equation 1}$$

$$[\theta]_{MRE} = [\theta] / (R - 1) \qquad \textbf{Equation 2}$$

Where θ = raw circular dichroism, c = protein molar concentration, l = pathlength (in cm), R = number of residues in protein construct.

2.2.3.5 Analytical SEC

Analytical SEC was performed on a Superdex 200 (5/150) column (GE healthcare) attached to an Akta pure system at 25°C. The column, stored in 20% ethanol, was washed with water and equilibrated with appropriate SEC buffer. 100 µL of filtered protein sample was loaded onto the column using a 100 µL injection loop. The absorbance of the sample was monitored at 280 nm throughout.

2.2.3.6 Direct Binding Fluorescence Anisotropy (FA)

Protein binding assays were performed in 384 well plates. Experiments were carried out in triplicate. 20 µL binding buffer was added to all experimental and control wells. 40 µL of protein was added to the first column well of each row, then serially diluted across the plate. 20 µL FITC labelled tracer peptide diluted to 20nM in binding buffer was added to all experimental wells (giving a final concentration of 10nM), and 20 µL binding buffer added to control wells. The plate was incubated under foil for 1 hour, then read on a Tecan Spark 10M plate reader at 25.0°C with excitation at 485 (20) nm and emission at 535 (25) nm. The intensity was calculated for each point using Equation 3 and used to calculated anisotropy using Equation 4. The data were then fitted using Equation 5 in OriginPro 9 to determine the dissociation constant, K_d.

$$I = (2PG) + S \qquad \textbf{Equation 3}$$

$$R = (S - PG) / I \qquad \textbf{Equation 4}$$

$$y = ((Kd + x + [FL]) - \sqrt{((Kd + x + [FL])2 - 4x[FL]))}/2 \qquad \textbf{Equation 5}$$

Where R= anisotropy, I= total intensity, P=perpendicular intensity, S= parallel intensity, G = an instrument factor set to 1, [FL] = concentration of fluorescent peptide, Kd = dissociation constant, x = protein concentration

2.2.3.7 SPR

0.5 nM affimer was isolated on to one flow cell of a CM5 chip (GE Healthcare), at a flow rate of 5 uL/min, while the other flow cell was left unfunctionalised. A series of concentrations of target protein were tested. Each concentration was flowed over both the functionalised and the unfunctionalised flow cells at 40 µL/min and the on- and off-rates were calculated using the Biacore software. The on- and off-rates were used to calculate the K_d.

2.2.3.8 Crystallography

Factorial screens were set up using 384 unique buffer conditions, and carried out using a Douglas Instruments Oryx 6 plate loader with NT8 robotics software. Drops of 0.2 µL of protein in a 1:1 drop ratio with mother liquor were used in 96 well MRC 3-drop sitting drop plates (Molecular Dimensions). Wells were filled with 25 µL mother liquor, sealed with pressure adhesive clear seals (Viewseal) and incubated at 4°C. Initial hits from the factorial screens were optimised in 24 well hanging drop plates, with 1 µL protein added to 1 µL mother liquor. Optimisations centred on the variation of precipitant and pH. Crystals were picked using a nylon loop mounded on a cryo pin (Hampton Research) and submerged in to 1 µL of mother liquor + appropriate cryo protectant. Crystals were then immediately immersed in liquid nitrogen for storage and transport. All data was collected at Diamond light source, using various beamlines.

2.2.3.9 Negative Stain Electron Microscopy (EM)

Samples were added to glow-discharged carbon-coated EM copper grids, stained with 1% uranyl acetate, and then imaged on a FEI Tecnai-F20 microscope using low-dose protocols and a dose of ~40 e-/Å2. Micrographs were recorded with a Gatan US4000 CCD camera at a calibrated magnification of ×25,500, giving a final object sampling of 3.51 Å/pixel. Class averages were collected and analysed using RELION software (MRC-LMB).

2.2.3.10 Detergent Treatment

All detergents were dissolved at 10x desired final concentration in 50mM Sodium Phosphate pH 7.0. 50µL of 10x detergent solution was then added to 450µL of protein.

2.2.4 Affimer Identification, Expression and Purification

2.2.4.1 Affimer Phage display

Target BCL-2 family proteins were biotinylated using EZ-link NHS-SS-biotin (Pierce), then desalted to remove any remaining biotin using Zeba Spin Desalting Columns, 7K MWCO (Thermo Scientific) according to the manufacturer's instructions. Biotinylation was confirmed using streptavidin conjugated to horseradish peroxidase (HRP). Biotinylated target protein was bound to streptavidin-coated wells (Pierce) for 1-2 hours, then 10^{12} cfu pre-panned phage were added for 2 hours with shaking. Panning wells were washed 27 times with PBST and bound phage eluted with 50 mM glycine–HCl (pH 2.2) for 10 min, neutralised with 1 M Tris–HCL (pH 9.1), further eluted with triethylamine 100 mM for 6 min, and neutralized with 1M Tris–HCl (pH 7). Eluted phage were used to infect ER2738 cells for 1 hour at 37° C and 90 rpm then plated onto LB agar plates with 100 mg/ml carbenicillin and grown overnight. Colonies were scraped into 5 ml of 2TY medium, inoculated in 25 ml of 2TY medium with carbenicillin (100 m g/ml) and

infected with ca. 1 x 10^9 M13K07 helper phage. After 1 hour at 90 rpm, kanamycin was added to 25 mg/ml for overnight incubation at 25° C and 170 rpm. Phage were precipitated with 4% polyethylene glycol 8000, 0.3 M NaCl and resuspended in 1 ml of 10 mM Tris, pH 8.0, 1 mM EDTA (TE buffer). A 2 ml aliquot of phage suspension was used for the second round of selection using streptavidin magnetic beads (Invitrogen). Beads labeled with target protein were washed and incubated with pre-panned phage for 1 hour then washed five times using a KingFisher robotic platform (ThermoFisher), then eluted and amplified as above. The final pan used neutravidin high binding capacity plates (Pierce), as previously described for panning round one, with phage eluted as described above. Eluted phage were recovered from wells containing target protein and control wells, then used to infect ER2738 cells for 1 hour at 37° C and 90 rpm. A range of volumes (0.1µL to 100µL) of culture from target wells were plated onto LB agar plates with 100 mg/ml carbenicillin and grown overnight. 10µL of culture from control wells was also plated to determine the level of amplification in target wells.

2.2.4.2 Phage ELISA

Individual ER2738 colonies were grown in 200 µl of 2TY with 100 m g/ml of carbenicillin in a 96-deep well plate at 37° C (900 rpm) for 6 hours. A 25 µl aliquot of the culture was added to 200 µl of 2TY containing carbenicillin and grown at 37° C (900 rpm) for 1 h. Helper phage (10 µl of 10^{11} /ml) was added for 30 minutes (450 rpm), followed by kanamycin to 25 mg/ml with overnight incubation at 25° C (450 rpm). Streptavidin-coated plates (Pierce) were blocked with 2 x casein blocking buffer (Sigma) overnight at 37° C. The plates were incubated with biotinylated target protein or blocking buffer (control) for 1 hour, and 45 µl of growth medium containing the phage was added and incubated for 1 hour. Following washing, phage were detected by a 1:1000 dilution of HRP-conjugated anti-phage antibody (Seramun) for 1 hour, visualised with 3,3',5,5' -tetramethylbenzidine (TMB) (Seramun) and measured at 610 nm.

2.2.4.3 Affimer synthesis and purification

The DNA coding sequences of affimers were amplified by PCR, restriction digested with NheI and PstI and cloned into pET11a containing the affimer scaffold similarly digested. Plasmid DNA was purified (Qiagen) from transformant colonies and sequenced to confirm the correct insert. Following transformation into BL21 (DE3) Rosetta 2 cells, affimers were purified using the Nickel Affinity Chromatography protocol described above.

2.2.4.4 Affimer binding ELISA

100µL of target protein diluted to 2µg/mL in PBS was added to each well of a F96 Maxisorp Nunc-Immuno Plate (Thermo Scientific). After overnight incubation at 4°C, all wells were washed in PBST, then blocked by the addition of 100µL PBST with 2% BSA (Sigma) for 1 hour at 25°C. All wells were washed with PBST, then 200µL affimer diluted to 20µg/mL in PBS was added to the first column well of each row. 100µL PBS was added to all remaining wells, and serial dilutions made down each row. Plates were incubated a further 1 hour at 25°C, then washed with PBST. 100µL of poly-Histidine−Peroxidase conjugated monoclonal antibody (Sigma) diluted 1:4000 in PBS was added to each well, with incubation at 25°C for 1 hour. After a final wash with PBST, all wells were developed by adding 50µL 3,3',5,5'-Tetramethylbenzidine (TMB) (Thermo Fisher). Reactions were stopped by adding 50µL 2M H_2SO_4. Absorbances were read using a Powerwave XS2 plate reader (Biotek).

Chapter 3 - Expression, purification and characterisation of Bcl-2 family proteins

3.1 Selecting BCL-2 family members for study

The work described in this chapter was undertaken to produce and quality control the reagents (BCL-2 family proteins) required to pursue the thesis aims as described in the introduction.

The mitochondrial apoptotic pathway is initiated through the transcriptional and/or post-transcriptional activation of BH3-only proteins in response to various upstream signaling events (e.g. hypoxia, withdrawal of growth signals). However, BH3 only family members, with the notable exception of BID, are intrinsically disordered proteins, which makes them unsuitable targets for recombinant expression.

By contrast, all pro-survival members, and the pro-apoptotic effectors BAX and BAK have a high degree of structural homology, including the presence of a hydrophobic BC binding groove. BAX, BAK, BCL-2, BCL-X_L and MCL1 were therefore chosen for use in this study, providing a good representative selection of pro- and anti-apoptotic family members.

3.2 Protein Purification

All target proteins were over expressed in competent *E.coli* cells, but a variety of vectors, cell strains, and protein purification methods were used to purify individual family members (fully detailed in Materials and Methods).

BCL-2 was previously sub-cloned into the pGEX-6P-1 plasmid by the Edwards group, creating a GST fusion, which both enhances solubility and allows for single step purification on glutathione conjugated sepharose resin. The fusion vector was transformed into BL21 (DE3) Rosetta 2 *E. coli* cells. During expression trials against other BL21 (DE3) strains, Rosetta 2 was

found to produce the greatest yield of fusion protein with minimal bacterial protein contamination, better facilitating further purification.

BCL-X_L and MCL1 were both previously sub-cloned into the pET-28a-SUMO plasmid by the Edwards group, creating a hexa-His-SUMO fusion. The hexa His tag allows for purification by metal affinity chromatography, while the SUMO tag enhances solubility of the fusion product. These fusion vectors were also transformed into BL21 (DE3) Rosetta 2 *E. coli* cells, after expression trials showed that this strain gave the best and cleanest yield of fusion protein for both MCL-X_L and MCL1.

BAX and BAK were both previously sub-cloned into the pTXB1 plasmid by the group of Jane Clarke (Dept. of Chemistry, Cambridge), creating an intein-chitin binding domain (CBD) fusion, allowing for single step purification. The fusion vector was transformed into C41 (DE3) *E. coli* cells. C41 cells were used in this instance as they are particularly suitable for use with difficult to express and / or toxic proteins.

The methods used for subsequent protein expression and purification are summarised in Figure 3-1.

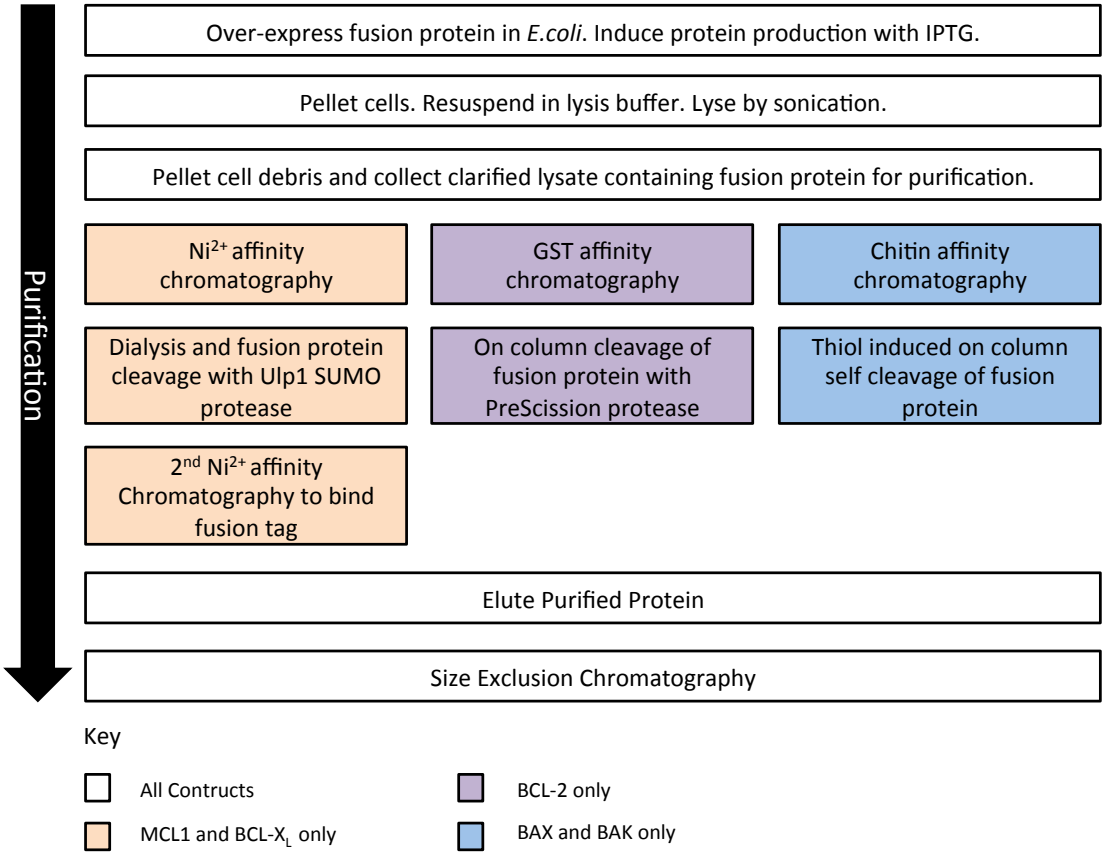

Figure 3-1– Summary of expression and purification protocols used for target BCL-2 family proteins.

3.3 Protein Characterisation

A variety of biophysical methods were used to characterise and quality control purified proteins, ensuring protein purity, determining whether proteins expressed as monomers or higher order oligomers, and checking for correct secondary and tertiary folded structures.

3.3.1 Size Exclusion Chromatography

Size Exclusion Chromatography (SEC) is used primarily as a final 'polishing' step in protein purification, to provide as clean and homogenous a protein sample as possible (Figure 3-2). It is also useful in determining the oligomerisation state of proteins in solution, and can be used to detect

protein aggregation. SEC works by filtering a homogenous molecular mix through a sepharose resin of spherical beads that contain pores with a defined size distribution. Molecules of different sizes are either able to enter, or are excluded from the pores: small molecules diffuse into the pores, hence their flow through the column is retarded; larger molecules do not enter the pores and flow through the column more freely. Consequently, molecules are separated based on their size as they pass through the column and are eluted in order of decreasing molecular weight, with large aggregates eluting in the void volume.

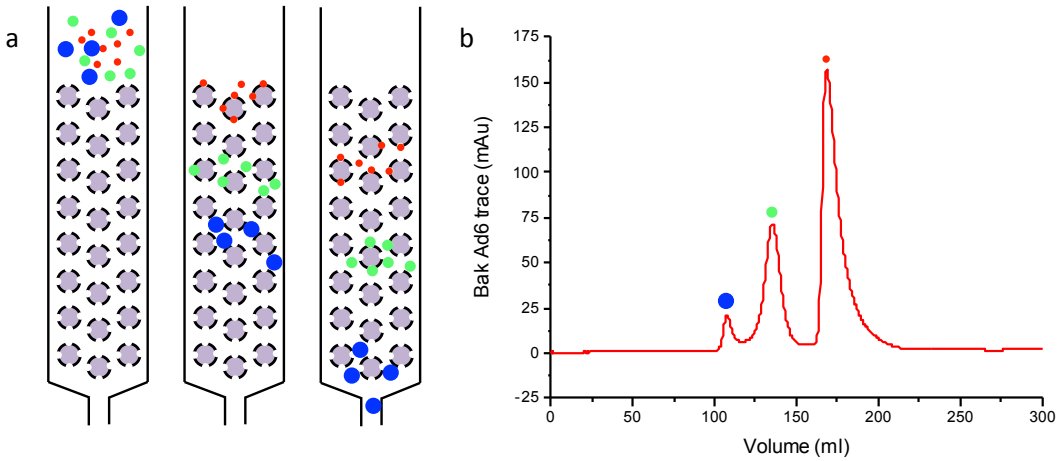

Figure 3-2 - Size Exclusion Chromatography (SEC). a) Filtering through a sepharose resin enables a homogenous molecular mix to be sorted by size. Beads in the resin have pores with a defined size distribution. Smaller molecules are able to enter the pores and their progress through the column is thereby retarded, so that homogenous species will be eluted from the column in order of decreasing size. b) A standard SEC chromatograph, showing individual protein peaks, is useful for enhancing protein purity, and can also be used to determine the oligomerisation state of an eluted protein by comparing its peak elution volume against the elution volumes of a panel of protein standards.

3.3.1.1 Use of Protein Standards for Column Calibration in SEC

All SEC experiments described in this chapter were carried out using a HiLoad 26/60 Superdex 75 pg column (GE healthcare). Prior to assaying target proteins, the column was calibrated by running the protein standards detailed in Table 3-1. Blue Dextran was loaded to the column to determine the void volume.

Table 3-1 – SEC column calibration. Details of protein standards used to calibrate the HiLoad 26/60 Superdex S75 pg column, including molecular weight and observed elution volume.

Protein standard	Molecular weight (kDa)	Source	Observed elution volume (mL)
Aprotinin	6.5	Bovine lung	246
Ribonuclease A	13.7	Bovine pancreas	213
Carbonic anhydrase	29.0	Bovine erythrocytes	183
Ovalbumin	43.0	Chicken egg white	159
Conalbumin	75.0	Chicken egg white	141
Blue dextran	2,000	N/A	111 (void volume)

The chromatogram showing all protein standard elution peaks is shown in Figure 3-3.

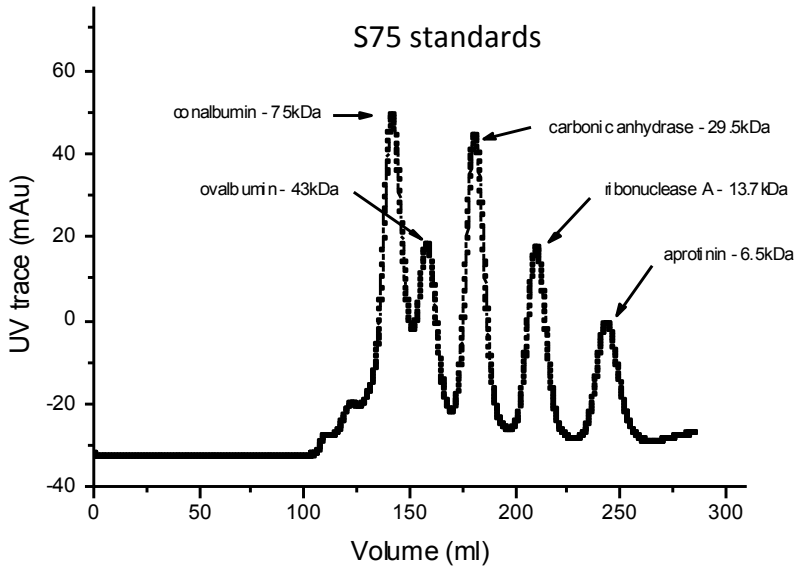

Figure 3-3 – Chromatogram of elution peaks for protein standards used in HiLoad 26/60 Superdex S75 pg column calibration.

The determination of molecular weight (M_w) by SEC is achieved by comparing the partition coefficient (K_{av}) of the target protein with the K_{av} values obtained for the calibration standards. The M_w (and oligomerisation state) of the target protein can then be determined by plotting K_{av} against $\log_{10} M_w$. K_{av} is calculated using the following equation: -

$$K_{av} = (V_e - V_o) / (V_t - V_o)$$

where V_e is the target protein elution volume, V_t is the total volume of the column used, and V_o is the column void volume. The HiLoad 26/60 Superdex S75 pg column has a V_t of 320mL, and a void volume, established using blue dextran, of 111mL. Using the known molecular weights and observed elution volumes for protein standards from Table 3-1, $\log_{10} M_w$ and K_{av} values were calculated (Table 3-2), and the calibration curve in Figure 3-4 was produced.

Table 3-2 – Calculated $\log_{10} M_w$ and K_{av} values for protein standards.

Protein standard	M_w (kDa)	$\log_{10} M_w$	V_e (mL)	K_{av}
Conalbumin	75	1.9	141	0.144
Ovalbumin	43	1.6	159	0.230
Carbonic Anhydrase	29	1.5	183	0.344
Ribonuclease A	13.7	1.1	213	0.488
Aprotinin	6.5	0.8	246	0.646

A line plotting the best fit of all data points on the calibration curve was calculated to have gradient - 0.48018 and intercept 1.03568 intercept, giving the equation

$$y = -0.48018x + 1.03568$$

which was used to calculate expected elution volumes for the target proteins, and subsequently to determine oligomeric states based on the actual elution volumes seen.

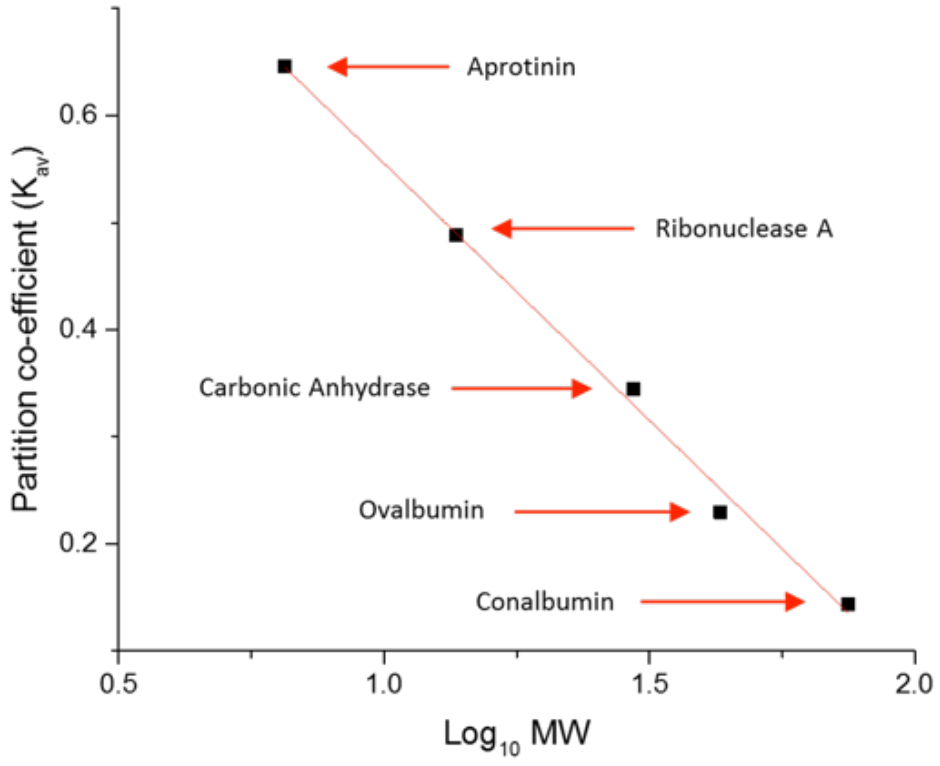

Figure 3-4 – HiLoad 26/60 Superdex S75 pg column calibration curve for protein standards

3.3.2 Fluorescence Anisotropy

Fluorescence anisotropy (FA) assays measure the tumbling rate (rotational diffusion) of fluorescently tagged molecules. Rotational diffusion is a function of molecular size: the larger the molecule, the slower the tumbling rate, which is measured in FA as a ratio of plane polarized light within the total light intensity. Plane polarized light is applied to a group of randomly oriented fluorophores. Only those fluorophores oriented within a narrow range of angles to the applied polarisation will become excited and emit light. If these fluorophores have low rotational diffusion (i.e. are larger molecules), their orientation will change slowly, emitted light will remain in the same plane of polarisation, and there will be high anisotropy. If the fluorophores are small and have a high rate of rotational diffusion, they will rapidly change orientation and much more of the emitted light will be in a different plane from the excitation light, resulting in low anisotropy. FA can therefore be used to measure the potency of binding events between

molecules as follows: one molecule (the smaller of the two) is fluorescently labelled; upon binding to its larger binding partner, the rotational diffusion is reduced, and the level of observed anisotropy increases. Plotting the fluorescence anisotropy against protein concentration of the larger, unlabelled protein partner allows a K_d to be calculated. This direct binding assay can be adapted into a competition binding assay to measure the potency of molecular inhibitors. Starting with a pre-bound complex of fluorophore and binding partner, the rotational diffusion of the fluorophore will be low and anisotropy will be high. When an inhibitor disrupts this complex, the fluorophore will be released from the complex, and its rotational diffusion will increase, resulting in a decrease in anisotropy (Figure 3-5).

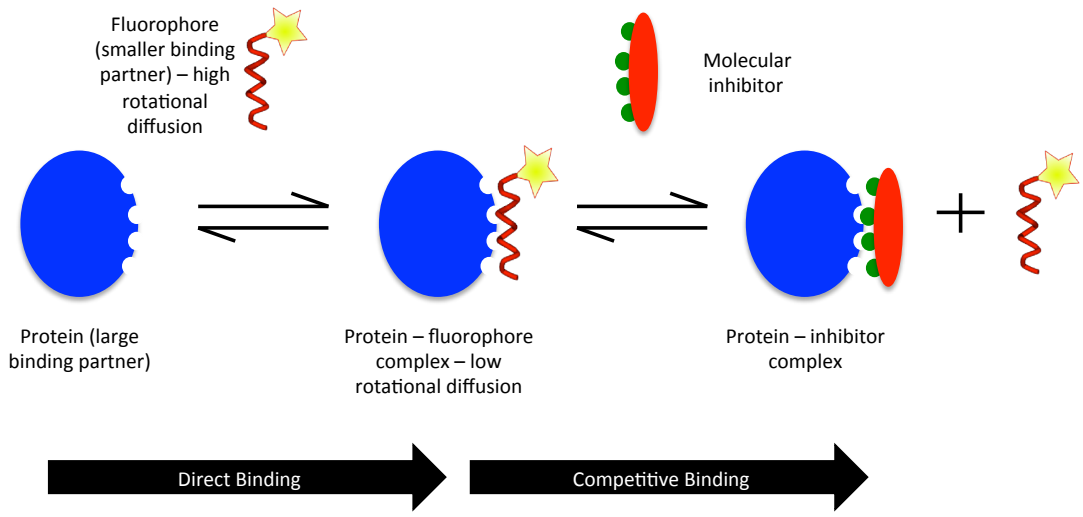

Figure 3-5 - Fluorescence Anisotropy (FA). FA uses the rotational diffusion (tumbling rate) of fluorescently tagged molecules to investigate binding events between molecules. Binding interactions decrease the tumbling rate and increase the anisotropy of polarised light emitted by the fluorophore. This assay can be used to measure direct binding, and also to measure the ability of molecular inhibitors to disrupt complexes, in competition binding mode.

3.3.3 Circular Dichroism

Secondary structure can be determined by Circular Dichroism (CD) spectroscopy in the 'far-UV' spectral region (190-250 nm). CD functions through the interaction of circularly polarized light with chiral molecules, such

as proteins. Circular polarised light has a “handedness”; it is either rotating left or right. Bonds around a chiral centre act as chromophores, absorbing left and right polarised light differently and this difference is measured by a spectrapolarimeter (CD spectrometer). The spectrapolarimeter lamp switches between left and right polarized light and compares the relative absorbance of each by the sample; the difference between the two signals is known as the ellipticity (θ). This measurement is combined with the mean residue molar concentration of the sample to calculate a mean residue ellipticity (MRE).

At ‘far UV’ wavelengths, the chromophore in a protein sample is the peptide bond. Distinct CD signals arise when these bonds are arranged in regular, folded patterns, so that different distinct secondary structures have characteristic CD signatures (Figure 3-6).

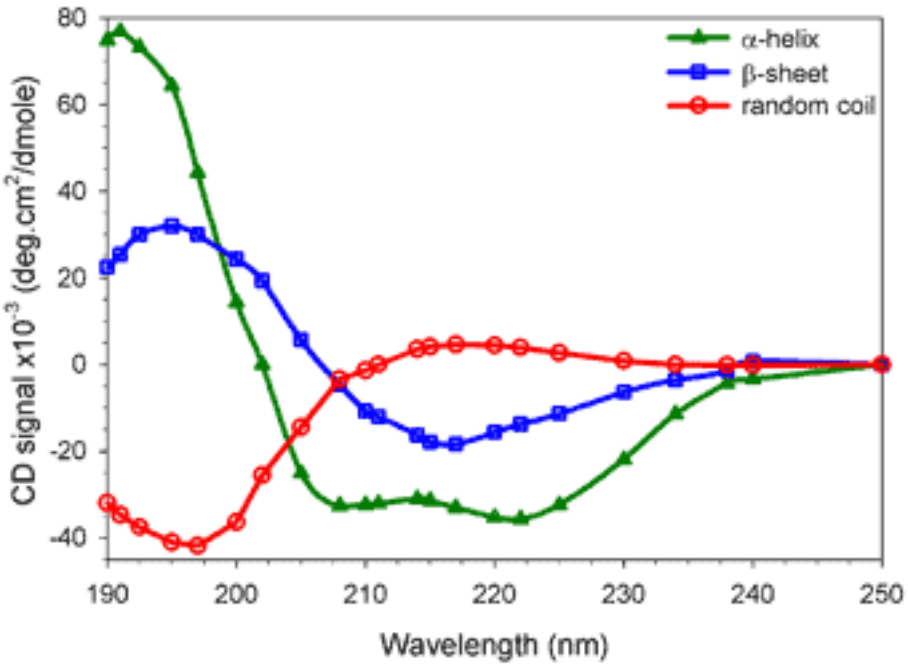

Figure 3-6 - Circular Dichroism secondary structure profiles. Of interest to this study is the standard alpha-helical profile (shown in green) with local absorption minima at 208 and 222nm.

The spectrum relating to α-helix secondary structure, pertinent to all BCL-2 family protein proteins used in this study, has MRE absorption minima at 208

nm and 222nm [295], while proteins with well defined anti-parallel β-sheets have absorption minima around 218nm [296].

3.4 Expression, Purification and Characterisation of Pro-survival family members

The following sections describe the purification and characterization of the pro-survival targets selected for this study (BCL-2, BCL-X_L and MCL1). All proteins were expressed with a C terminal truncation, corresponding to the removal of the transmembrane domain, which is used *in vivo* to tether BCL-2 family members to the mitochondrial membrane, where the majority of intra-family interactions take place. Removal of the transmembrane domain greatly reduces the risk of protein aggregation during purification but does not affect residual protein structure or function [30, 52].

3.4.1 BCL-2

The BCL-2$^{1-205}$ protein, incorporating a 34 residue C terminal deletion was over-expressed as a GST tagged fusion protein in BL21 (DE3) Rosetta 2 competent *E.coli* cells and purified by glutathione affinity chromatography. The GST tag was cleaved by overnight incubation with Prescission protease, allowing for single step purification of tag free recombinant protein (Figure 3-7).

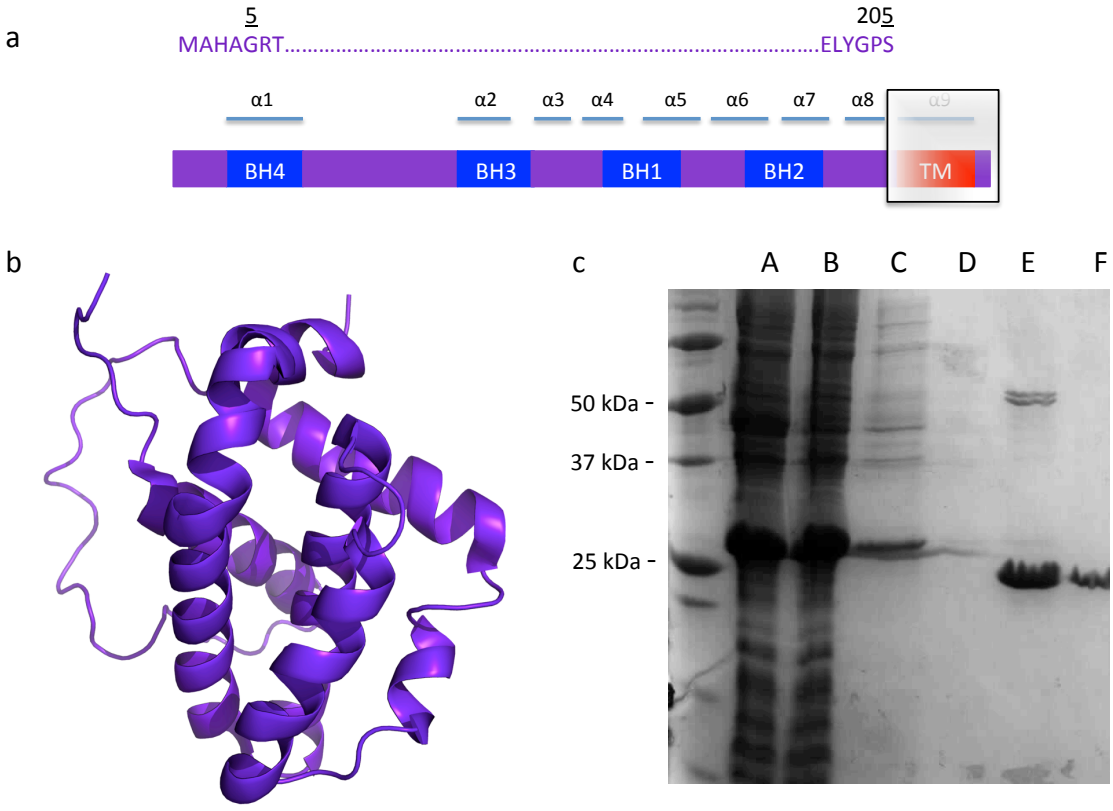

Figure 3-7 - BCL-2 expression and purification. a) schematic of the BCL-2 $^{1-205}$ protein used in this study. A 34 residue truncation at the C terminal equates to removal of the transmembrane (TM domain). b) Cartoon representation of the crystal structure of BCL-2, showing alpha-helical secondary structure (PDB 1G5M). c) SDS-PAGE analysis of BCL-2 $^{1-205}$ expression. The 49.8kDa GST tagged fusion protein band can be seen between 37kDa and 50kDa markers. The large band just above the 25kDa marker in A and B is free GST. Cleaved protein at 23.4kDa can be seen in columns E and F. Key A: clarified lysate, B: column flow through, C: high salt wash, D: low salt wash, E: elute, F: post elute low salt wash.

The cleaved and eluted protein was concentrated and further purified by SEC, producing a main A_{280} peak at 162mL, with a further small peak at

136mL (Figure 3-8). With reference to Figure 3-4, these correspond to dimer and tetramer peaks respectively. This result is not unexpected, as BCL-2 is known to homo-dimerise through different and extensive binding interfaces [297].

Good initial protein yields per litre of media were seen for BCL-2, and recovery of protein at each stage of purification was also favourable, as detailed in Table 3-3.

Table 3-3 – BCL-2 yield and recovery for each stage of protein purification. All protein concentrations were measured using the Biorad assay.

Purification stage	mg / L media	Yield (%)
Column elute of BCL-2	18.15	100
Concentrated and loaded to SEC column	17	93
Recovered from SEC	12	66

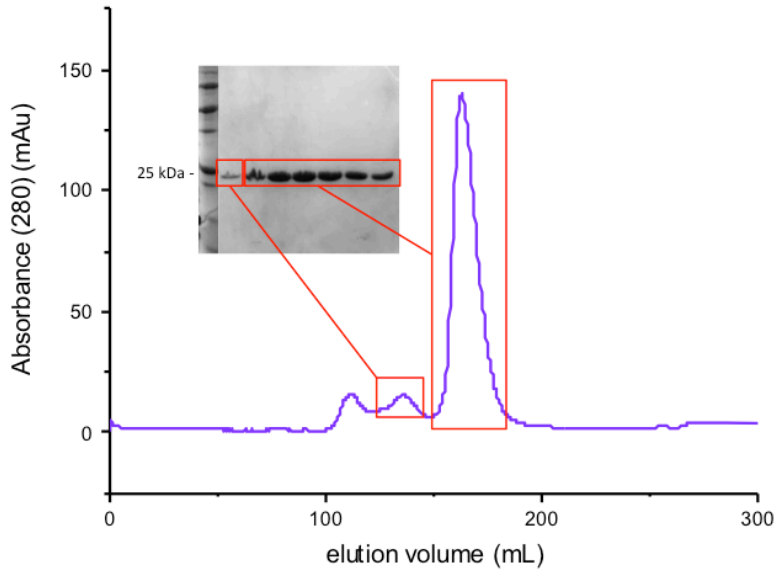

Figure 3-8 – Size exclusion chromatography of eluted BCL-2 $^{1-205}$. The main peak at 162mL corresponds to a dimer.

Fractions from the dimer peak were pooled, transferred to 50mM sodium phosphate buffer pH7, and analysed by CD to check for correct secondary structure. Figure 3-9a shows the expected α-helical spectrum. Local MRE

minima of -26923 and -24810 are seen at 208nm and 222nm respectively. Further analysis for correct, active tertiary structure was carried out by means of a FA direct binding assay against a FITC labelled BAX BH3 peptide, which gave a binding curve with predicted K_d of 33.2 ± 4.4nM (Figure 3-9b).

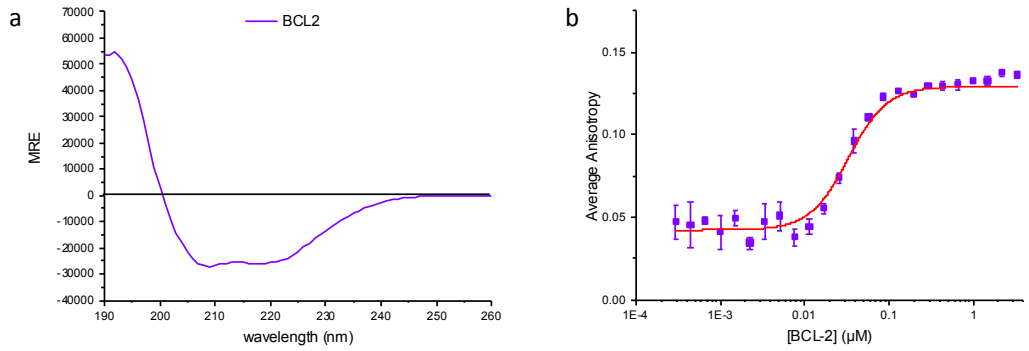

Figure 3-9 - BCL-2 characterisation. a) far UV circular dichroism (CD) shows the expected alpha-helical profile (trace shown is representative of multiple experiments). b) Direct binding fluorescence anisotropy assay of BCL-2 against FITC-BAX-BH3 produces a binding curve with K_d of 33.2 ± 4.4nM, indicative of correctly folded, active tertiary structure.

3.4.2 BCL-X_L

The BCL-X_L ^{ML} (1-26, 83-209 'Missing-Loop') protein, incorporating a C terminal 23 residue TM domain truncation, was over-expressed in BL21 (DE3) Rosetta 2 competent *E.coli* cells and purified by nickel affinity chromatography (Figure 3-10). Initial expression was of a hexa-His-SUMO tagged fusion protein; the tag was cleaved by overnight dialysis in the presence of Sumo protease, and tag free protein purified with a second round of nickel affinity chromatography.

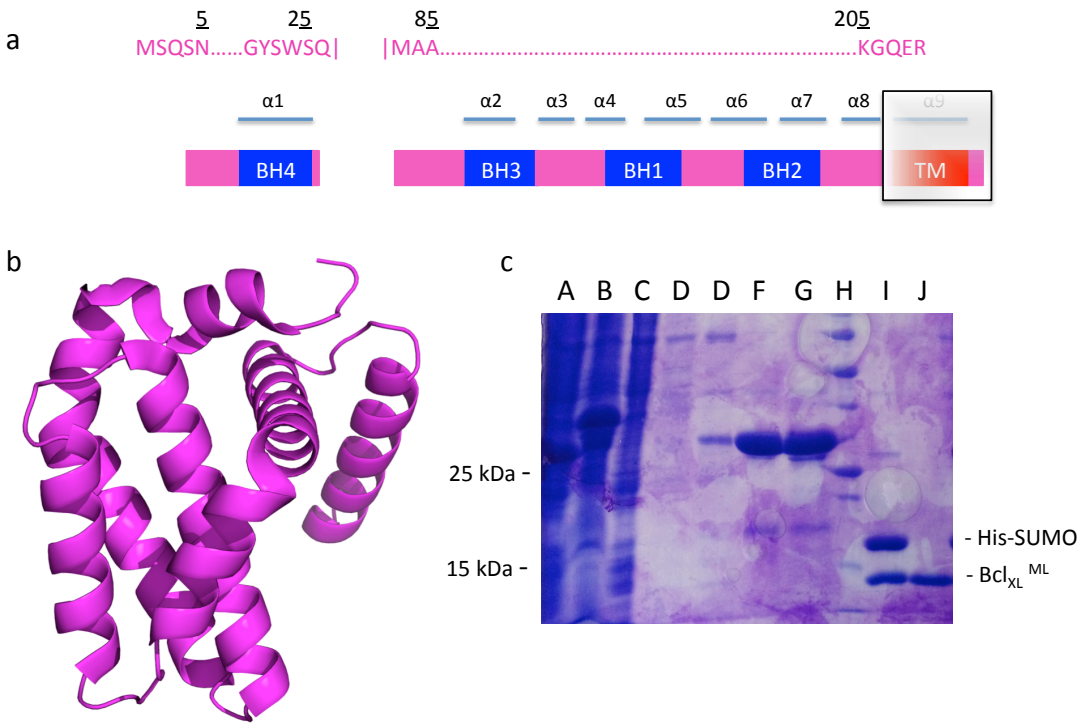

Figure 3-10 - BCL-X_L expression and purification. a) schematic of the BCL-X_L ML (1-26, 83-209 'Missing-Loop') protein used in this study. An unstructured loop, corresponding to residues 27 – 82 inclusive, has been removed from the main body of the protein, and a further 23 residue truncation, corresponding to removal of the TM domain, made at the C terminal. b) cartoon representation of the crystal structure of BCL-X_L ML, showing alpha-helical secondary structure (PDB 5B1Z). c) SDS-PAGE analysis of BCL-X_L ML expression. The 30.9kDa His-SUMO-Bcl$_{XL}$ ML fusion protein can be seen in columns F and G. Overnight dialysis in the presence of Ulp1 SUMO protease removes the fusion tag, allowing for purification of the 17.5kDa cleaved protein, shown as the lower band in columns I and J. Confusingly, the cleaved His-SUMO tag (13.4kDa) runs on the SDS-PAGE gel at approximately 17kDa, while the 17.5kDa BCL-X_L ML protein runs at approximately 14kDa, effectively reversing their expected positions on the gel. Key A: clarified lysate, B: insoluble pellet fraction, C: flow through, D-F: column buffer washes with increasing imidazole concentration, 15mM, 50mM, 100mM, G: elute, containing fusion protein, H: marker, I: cleaved elute, J: His trap column flow through of cleaved elute.

Eluted protein was concentrated and further purified by SEC, producing a main A_{280} peak on the chromatogram at an elution volume of 179mL, which, with reference to Figure 3-4, corresponds to a dimer (Figure 3-11). As with BCL-2, this result is not unexpected, as BCL-X_L is known to homo-dimerise by a variety of mechanisms [298-300].

Good initial yields per litre of media were seen for the His-SUMO-BCL-X_L fusion protein. Overnight dialysis with SUMO protease resulted in small amounts of precipitation, causing a small loss in yield prior to a second round of nickel affinity chromatography. Good recovery of protein at each subsequent stage of purification was seen, as detailed in Table 3-4 below.

Table 3-4 – BCL-X_L yield and recovery for each stage of protein purification. All protein concentrations were measured using the Biorad assay.

Purification stage	mg / L media	Yield (%)
Fusion protein elute of His-SUMO-BCL-X_L	36	100 (fusion protein)
Cleaved His-SUMO-BCL-X_L post dialysis	32	89 (fusion protein)
Tag free BCL-X_L	19.25	100
Concentrated and loaded to SEC column	18.75	97
Recovered from SEC	12.75	66

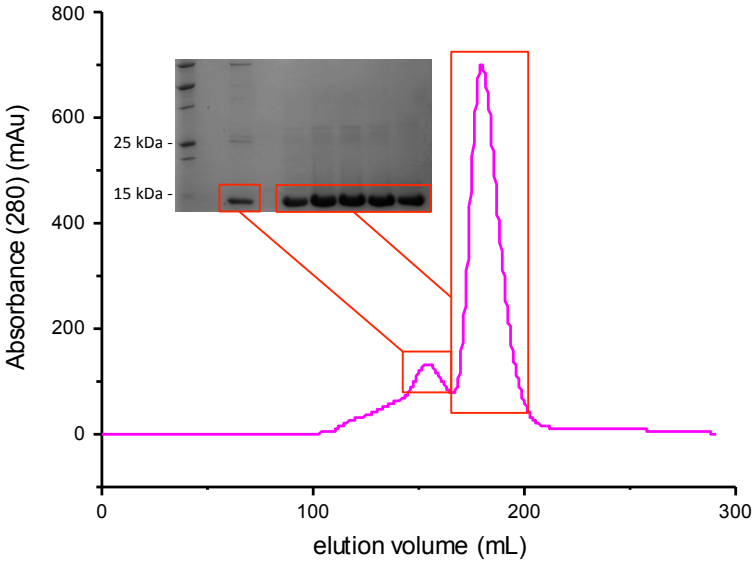

Figure 3-11 - Size exclusion chromatography of BCL-X_L ^{ML}. The main peak at 179mL corresponds to a protein dimer.

Protein was buffer exchanged to 50mM sodium phosphate buffer, pH 7. Biophysical analysis using far UV CD revealed the expected alpha helical profile with local MRE absorption minima of -25207 and -22721 seen at 222

and 208nm respectively. Direct binding FA of BCL-X_L^{ML} titrated against a FITC labeled BAX-BH3 peptide gave a binding curve with predicted K_d of 40.8 ± 6.2nM, indicative of correctly folded, active tertiary structure (Figure 3-12).

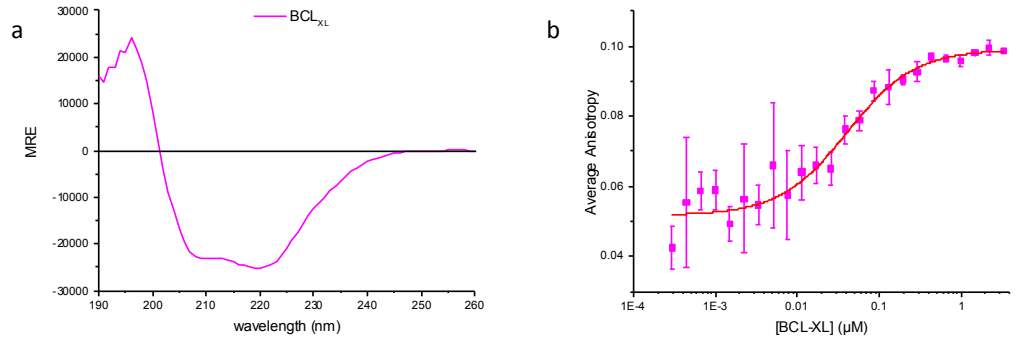

Figure 3-12 - BCL-X_L characterisation. a) Far UV CD shows expected alpha-helical secondary structure (trace shown is representative of multiple experiments). b) Direct binding FA produces a binding curve with predicted K_d of 40.8 ± 6.2nM, indicative of correctly folded, active tertiary structure.

3.4.3 MCL1

The MCL1$^{172-327}$ protein, incorporating an N terminal 171 residue deletion, and a C terminal 23 residue (TM domain) deletion, was over-expressed as a hexa-His-SUMO tagged fusion protein in BL21 (DE3) Rosetta 2 competent *E.coli* cells and purified by nickel affinity chromatography (Figure 3-13). The His-SUMO tag was removed by overnight dialysis in the presence of Sumo protease, and untagged MCL1 purified with a second round of nickel affinity chromatography.

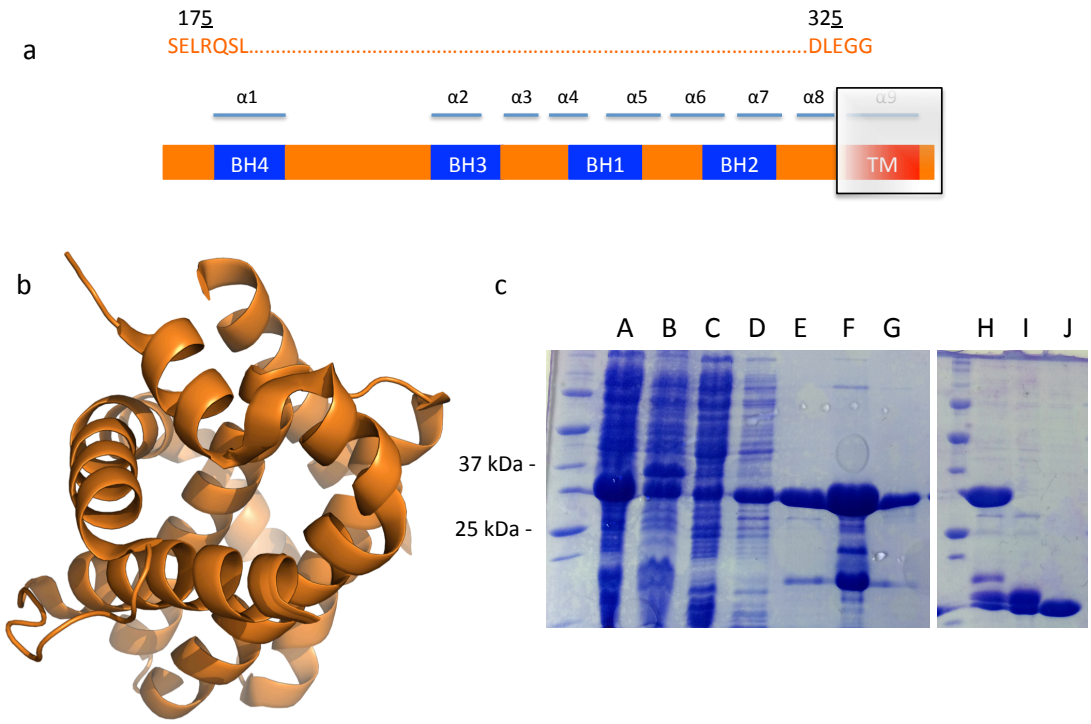

Figure 3-13 - MCL1 expression and purification. a) schematic of the MCL1$^{172-327}$ protein used. Truncations have been made at both N and C termini. b) cartoon representation of the crystal structure of MCL1$^{172-327}$ demonstrating a predominantly alpha helical secondary structure (PDB 5C3F). c) SDS-PAGE analysis of MCL1$^{172-327}$ expression. The 31.1kDa His-SUMO fusion protein can be seen midway between the 25kDa and 37kDa markers in columns A-H inclusive. Overnight dialysis in the presence of Ulp1 SUMO protease removes the fusion tag, allowing for purification of the 17.7kDa cleaved protein, shown as the lower band in columns I and J. Due to the previously mentioned anomaly with the His-SUMO tag running at above 17kDa, cleaved MCL1$^{172-327}$ appears in the lower band below the 25kDa marker in columns I and J. Key A: clarified lysate, B: insoluble pellet fraction, C: flow through, D-E: column buffer wash with 15mM and 50mM imidazole respectively, F-G: elutes with 400mM imidazole, H: sample to dialysis (from column E), I: cleaved elute, J: His trap column flow through.

Eluted protein was concentrated and further purified by SEC. On the chromatogram, an A_{280} monomer peak was observed at an elution volume of 208mL (Figure 3-14).

Good initial yields per litre of media were seen for the His-SUMO-MCL1 fusion protein. Overnight dialysis with SUMO protease resulted in small amounts of precipitation, causing a small loss in yield prior to a second

round of nickel affinity chromatography. Good recovery of protein at each subsequent stage of purification was seen, as detailed in Table 3-5.

Table 3-5 – MCL1 yield and recovery for each stage of protein purification. All protein concentrations were measured using the Biorad assay.

Purification stage	mg / L media	Yield (%)
Fusion protein elute of His-SUMO-MCL1	40.75	100 (fusion protein)
Cleaved MCL1 post dialysis	37.25	91 (fusion protein)
Tag free MCL1	21.5	100
Concentrated and loaded to SEC column	19.75	92
Recovered from SEC	17	79

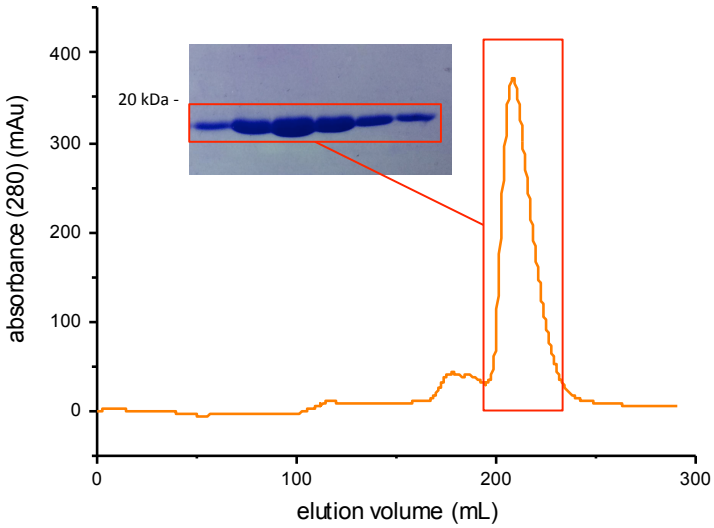

Figure 3-14 - Size exclusion chromatography of MCL1$^{172-327}$. The main peak at 208mL corresponds to a monomer.

The monomer peak was taken and buffer transferred into 50mM sodium phosphate pH7. Biophysical analysis using far UV CD revealed the expected alpha helical profile with local MRE minima of -21374 and -22510 seen at 222 and 208nm respectively. Direct binding FA of MCL1$^{172-327}$ titrated against a FITC labeled BAX-BH3 peptide gave a binding curve, indicative of correctly folded, active tertiary structure with predicted K_d of 7.5 ± 3.2nM.

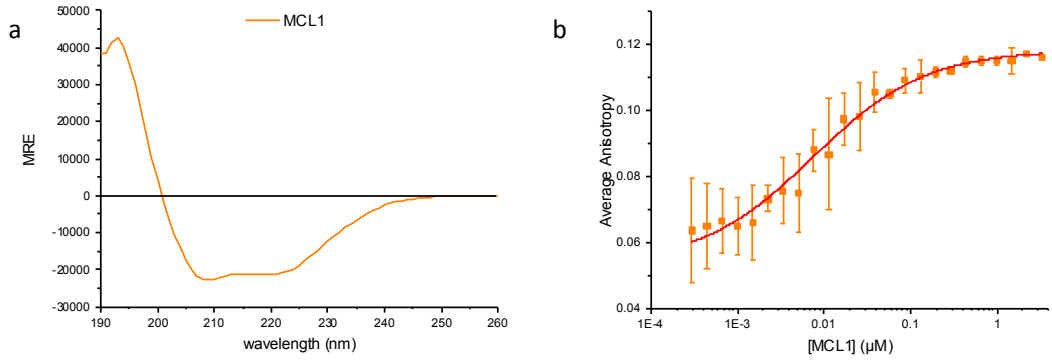

Figure 3-15 - MCL1 protein characterisation. a) Far UV CD shows expected alpha-helical secondary structure (trace shown is representative of multiple experiments). b) Direct binding FA for MCL1 titrated against FITC labelled BAX BH3 produces a binding curve with predicted K_d of 7.5nM, indicative of correctly folded, active tertiary structure.

3.5 Expression, Purification and Characterisation of Pro-apoptotic family members

3.5.1 BAX

BAX in solution should present as a monomer [52], but is notoriously unstable and prone to aggregation [301]. This tendency was encountered during this study, with BAX proving far more difficult to purify and characterize than other BCL-2 family members. Initial work involved the sub-cloning into pET-28a-SUMO of BAX $^{1\text{-}171\ C\text{-}S}$, containing a 21 residue C terminal truncation corresponding to the TM domain, and BAX $^{10\text{-}171\ C\text{-}S}$, containing a further 9 residue N terminal truncation (to aid in future planned future crystallography trials), using a synthetic gene optimised for recombinant expression in *E.coli.* In both proteins, cysteine residues at position 62 and 126 were mutated to serine to further reduce the risk of aggregation [52].

Sub-cloning was carried out using Gibson Assembly™ protocols. PCR amplified inserts for each BAX protein were combined with pET-28a-SUMO, cut with BamH1^{HF} and Xho1 restriction enzymes (Figure 3-16). The resulting product was used to transform DH5α cells. Plasmids were extracted from individual colonies and correctly subcloned inserts were confirmed by Sanger sequencing.

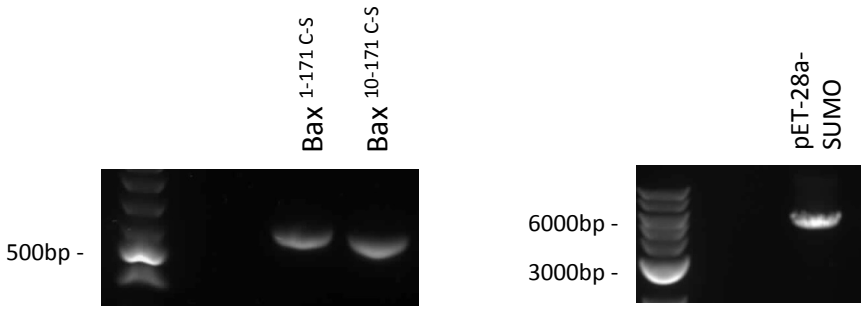

Figure 3-16 - BAX subcloning. BAX $^{1\text{-}171\ C\text{-}S}$ and BAX $^{10\text{-}171\ C\text{-}S}$ subcloned into pET-28a-SUMO vector using Gibson Assembly™ protocols. Bands are shown for both PCR amplified inserts (left) and BamH1^{HF} / Xho1 cut vector (right).

Recombinant plasmids containing BAX $^{1\text{-}171\ C\text{-}S}$ and BAX $^{10\text{-}171\ C\text{-}S}$ proteins respectively were used to transform *E.coli* BL21 (DE3) Star competent cells for protein expression trials. Recombinant fusion protein, incorporating a hexa-His SUMO tag, was extracted and purified using Nickel affinity chromatography using a 5ml His Trap column (GE), as detailed in Materials and Methods.

From 2L each of bacterial culture in Star, 12mg and 15mg total fusion protein was purified for BAX $^{1\text{-}171\ C\text{-}S}$ and BAX $^{10\text{-}171\ C\text{-}S}$ respectively, as measured using a Biorad colorimetric protein assay. Bands corresponding to SUMO fused BAX proteins were detected by SDS-PAGE followed by Coomassie Blue staining (Figure 3-17a), with confirmation by Western Blot, using the ab7977 anti-Bax antibody (Figure 3-17b).

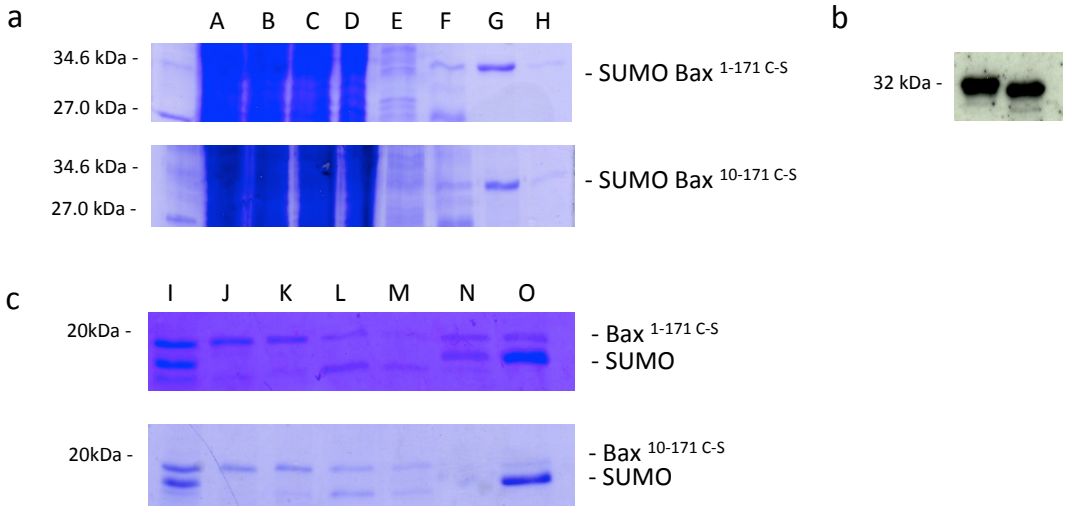

Figure 3-17 - BAX initial expression trials - SDS-PAGE and Western Blot analysis. a) BAX $^{1\text{-}171\ C\text{-}S}$ and BAX $^{10\text{-}171\ C\text{-}S}$. His-SUMO fusion proteins at 32.4kDa and 31.5kDa respectively can be seen for both proteins in column G, and confirmed in b) by Western Blot using an anti-Bax polyclonal antibody (ab7977). c) Overnight dialysis in the presence of Ulp1 SUMO protease removes the fusion tag, allowing for purification of the cleaved protein, shown as the upper bands in columns I to O. Key: A: Insoluble pellet, B: clarified lysate, C: filtered lysate, D: flow through, E: column buffer wash with 25mM imidazole, F: column buffer wash with 100mM imidazole, G: elute with 300mM imidazole, H: elute with 500mM imidazole, I: Cleaved sample, J: His trap column flow through, K-O: subsequent column washes with increasing imidazole concentration – 25mM, 50mM, 75mM, 100mM, 500mM.

BAX fusion proteins were dialysed overnight with SUMO protease, then subjected to a second round of metal affinity chromatography, with flow through and elutes collected and analysed by SDS-PAGE and Coomassie Blue staining (Figure 3-17c). 3.1mg of BAX $^{10\text{-}171\ C\text{-}S}$ and 4.7mg of BAX $^{1\text{-}171\ C\text{-}S}$ was collected from the flow through. Washes with increasing concentrations of imidazole contained decreasing, but significant, concentrations of the same BAX proteins, indicating issues with non-specific binding of protein to the Nickel His Trap column.

SUMO cleaved BAX proteins were buffer transferred to PBS and diluted to a concentration of 10μM. Analysis by far UV circular dichroism showed both proteins adopting an alpha helical secondary structure, with local absorbance minima at 208nm and 222nm as expected (Figure 3-18).

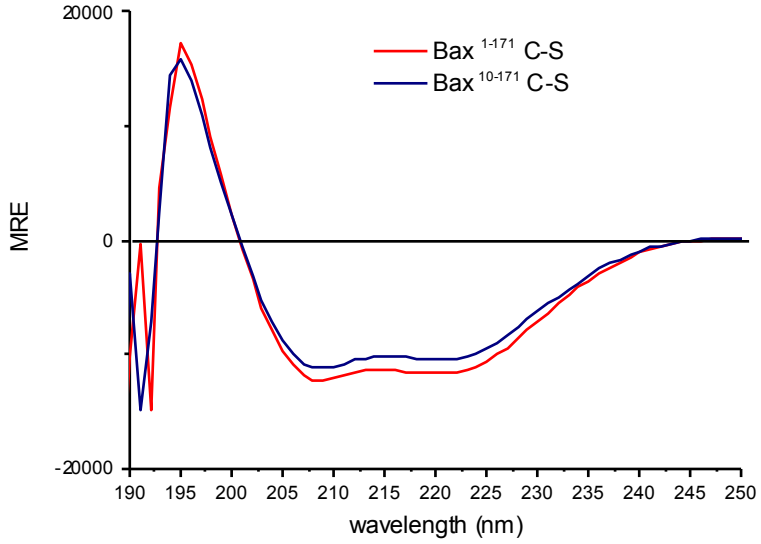

Figure 3-18 - CD analysis of BAX trial proteins. Both BAX $^{1\text{-}171\ C\text{-}S}$ and BAX $^{10\text{-}171\ C\text{-}S}$ show expected alpha-helical secondary structure, with local MRE absorption minima at 222nm and 208nm respectively.

Attempts to ascertain correct, active tertiary structure for both proteins, using direct binding fluorescence anisotropy failed to produce binding curves (data not shown). Further purification of proteins by SEC provided a potential

explanation for this result, as both proteins eluted in the void volume, indicating either high level oligomerisation, or likely aggregation of the protein (Figure 3-19a). To see if removal of the SUMO tag had an adverse effect on protein aggregation, a further round of SEC was carried out, this time without cleavage of the hexa-His-SUMO tag. Once again, both fusion proteins eluted in the void volume (Figure 3-19b).

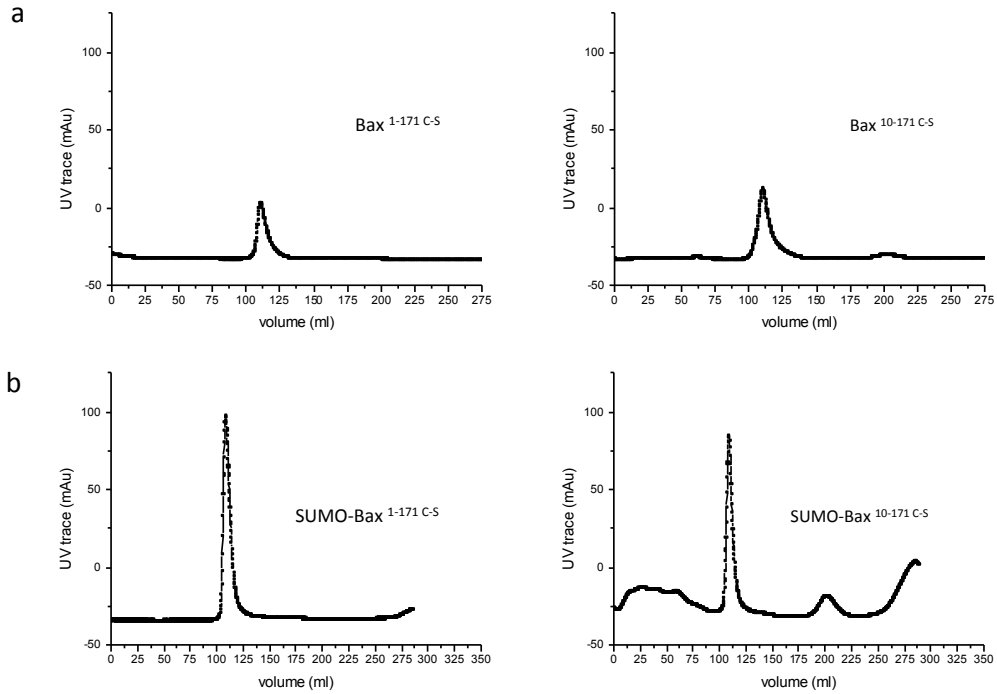

Figure 3-19 – SEC of BAX trial proteins. All proteins, both (a) tag cleaved and (b) His-SUMO fusion proteins elute in the column void volume, indicative of protein aggregation.

There are many variables that may affect protein solubility and oligomeric state during the purification process. To ascertain whether protein expression from the pET-28a-SUMO vector was incompatible with the synthesis of monomeric BAX, the BAX $^{1\text{-}171\ C\text{-}S}$ protein was subcloned into pGEX-6P-2, an expression vector used previously by the group to good effect in the expression of recombinant protein, including BCL-2. A PCR amplified insert was combined with pGEX-6P-2, cut with BamH1^{HF} and Xho1 restriction enzymes, using Gibson Assembly™ protocols (Figure 3-20a). The resulting product was used to transform DH5α cells with subcloned inserts confirmed by Sanger sequencing. Small scale expression trials using multiple strains of BL21 (DE3) competent cells identified the Codon Plus

(CD+) strain giving the best results for expression of the 43kDa GST-BAX $^{1-171\ C-S}$ fusion protein, as assayed using SDS-PAGE and Coomassie Blue staining (Figure 3-20b).

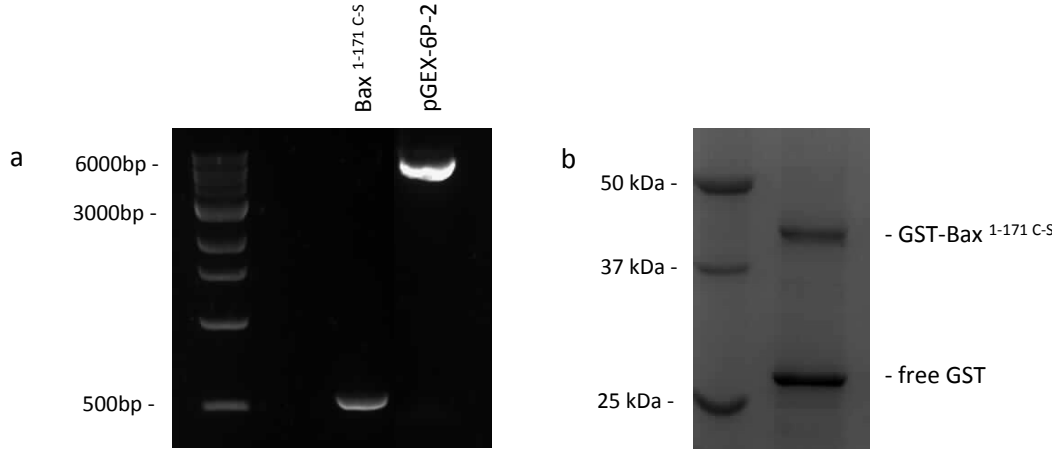

Figure 3-20 - BAX in pGEX-6P-2 subcloning and trial expression. BAX $^{1-171\ C-S}$ subcloned into pGEX-6P-2 vector using Gibson Assembly™ protocols. a) Bands are shown both PCR amplified inserts and BamH1^{HF} / Xho1 cut vector. b) Trial expression in BL21 (DE3) Codon Plus (CD+) competent cells shows a clear band at approximately 46kDa, corresponding to the GST- BAX $^{1-171\ C-S}$ fusion protein.

Large scale expression of GST-BAX $^{1-171\ C-S}$ in CD+ followed. The fusion protein expressed well, and was incubated overnight with glutathione conjugated beads in the presence of Prescission protease. Eluted volumes of cleaved protein were low, at 1.85mg / L media, as measured with a Biorad colorimetric protein assay. A Western Blot using an anti-Bax polyclonal antibody (Ab7977) detected bands for fusion and cleaved proteins (Figure 3-21a). Eluted fractions were combined, concentrated and analysed by SEC, but once again, protein eluted in the void volume, indicating aggregation of BAX during the purification process (Figure 3-21b).

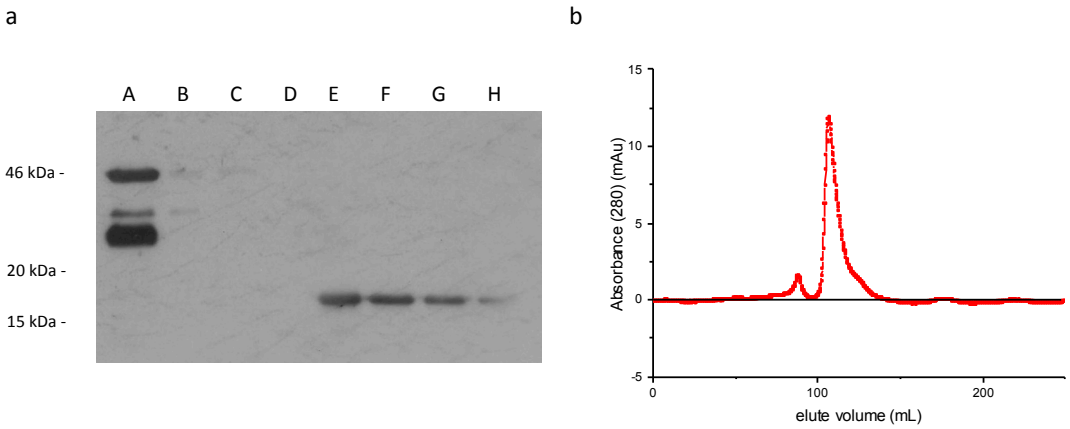

Figure 3-21 - BAX in pGEX-6P-2 large scale expression and characterisation. a) Both fusion protein at approximately 46kDa, and cleaved BAX at 19.3kDa detected by Western blot (ab7977). Key – A: clarified lysate, B: flow-through, C: high salt wash, D: low salt wash, E-G: sequential 5mL elutes following overnight incubation with Prescission protease, H: fraction from SEC peak in: b) Analysis by SEC showed cleaved protein eluting in the void volume, indicating protein aggregation during the purification process.

BAX was eventually expressed as a monomer using a protocol developed in the group of Jane Clarke at the University of Cambridge. BAX $^{1\text{-}171\ C\text{-}S}$ was cloned into the pTXB1 expression vector, and used to transform DH5α cells. The vector codes for a fusion protein with an intein CBD (chitin binding domain) tag, allowing for single step purification of BAX. The fusion protein was over-expressed in C41 (DE3) competent *E.coli* cells, and purified by means of chitin affinity chromatography (Figure 3-22). The intein-CBD tag was cleaved by overnight incubation at room temperature in the presence of 50mM DTT, and tag free protein eluted.

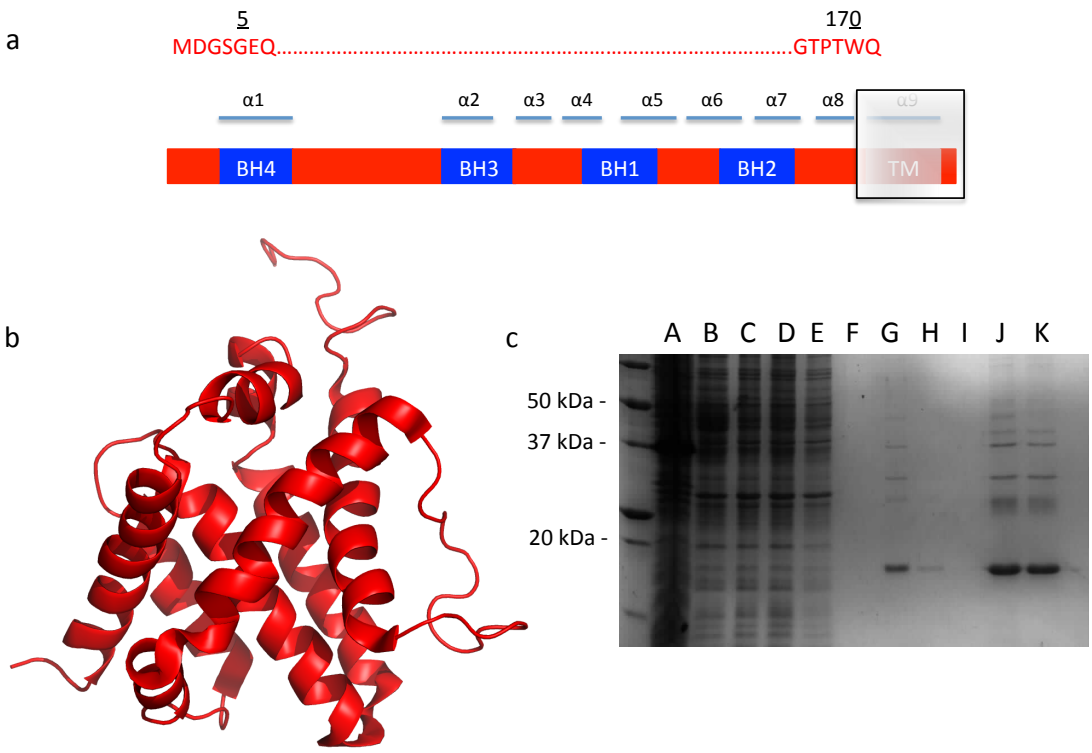

Figure 3-22 - Bax expression and purification. a) schematic of the BAX $^{1\text{-}171\ C\text{-}S}$ protein used in this study. A 21 residue truncation, corresponding to removal of the TM domain is made at the C terminal. b) cartoon representation of the crystal structure of BAX $^{1\text{-}171\ C\text{-}S}$, showing alpha-helical secondary structure (adapted from PDB 1F16). c) SDS-PAGE analysis of BAX $^{1\text{-}171\ C\text{-}S}$ expression. The protein initially expresses as a 46.8kDa intein-CBD (chitin binding domain) fusion. Overnight incubation in the presence of 50mM DTT causes the intein tag to self cleave, allowing for purification of the 18.9kDa cleaved protein, visible in columns G, J and K. Key – A: clarified lysate, B: filtered lysate (0.45µm), C: filtered lysate (0.22µm), D: flow-through, E: buffer wash, F: buffer + 50mM DTT 'flush', G: column elute, H-I: buffer elute / wash, J: concentrated sample, K: filtered conc. sample (0.22µm) for SEC.

Further purification by SEC yielded a monomer peak on the chromatogram at 187mL (Figure 3-23). A 'shoulder' on this peak corresponded to a band for the cleaved intein-CBD tag. Evidence of tag contamination in some monomer fractions was also seen. Only clean fractions were used for further analysis.

Compared to expression of anti-apoptotic family members, and in line with results from other groups [32, 52], protein yield for BAX was low, at approximately 1.8mg from 6L bacterial culture. The sudden drop off in yield following SEC purification caused in part by the removal of impurities seen in

the sample loaded to the column (Figure 3-22c, row K), but may also explained by the fact that the first two protein concentration measurements were made using the Biorad assay, but the sample recovered from SEC was measured using absorbance at UV_{280}, a more accurate method.

Table 3-6 - BAX yield and recovery for each stage of protein purification. Yield compared to pro-survival proteins is very low, but this is in line with the experience of other groups. The first two protein concentrations were measured using the Biorad assay, the measurement for BAX recovered from SEC was made using absorbance at UV_{280}.

Purification stage	mg / L media	Yield (%)
Column elute of BAX	1.6	100
Concentrated and loaded to SEC column	1.15	72
Recovered from SEC	0.3	19

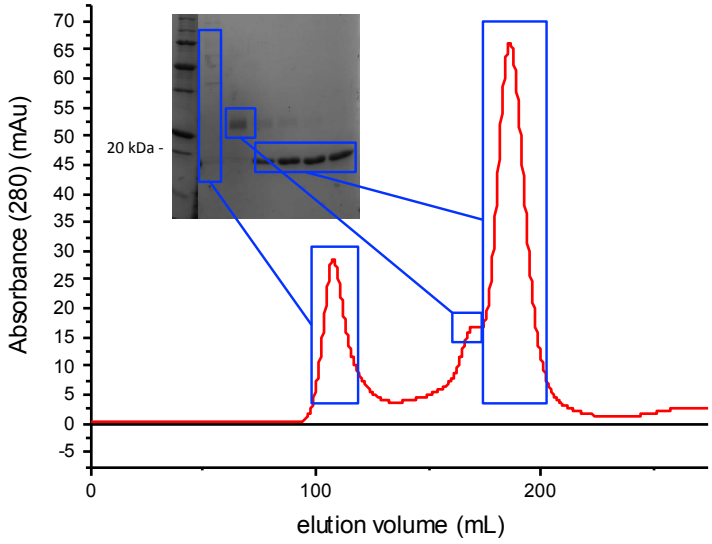

Figure 3-23 - Size exclusion chromatography of BAX $^{1\text{-}171\ C\text{-}S}$. The main peak at 187mL corresponds to a monomer. The adjacent shoulder corresponds to a band for cleaved intein-CBD.

3.5.2 BAK

BAK $^{16\text{-}185\ C\text{-}S}$ was over-expressed in C41 (DE3) cells and purified by chitin affinity chromatography, using an amended version of the protocol used to purify BAX $^{1\text{-}171\ C\text{-}S}$, which is fully detailed in the Materials and Methods section. The protein was first expressed as an intein-CBD tagged fusion, with the tag removed by intein self cleavage after overnight incubation in the presence of 50mM DTT (Figure 3-24).

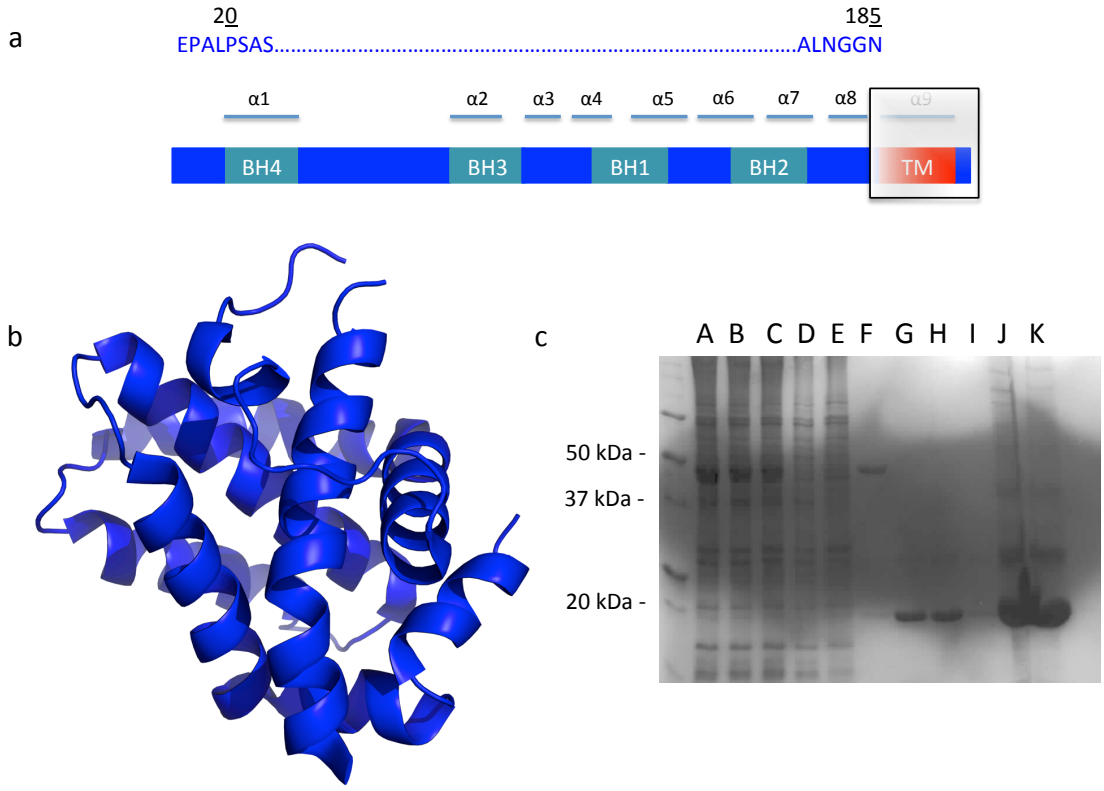

Figure 3-24 - BAK expression and purification. a) schematic of the BAK $^{16\text{-}185\ C\text{-}S}$ protein used in this study. A 21 residue truncation, corresponding to the TM domain is made at the C terminal, and a further 15 residue truncation made at the N terminus. b) cartoon representation of the crystal structure of BAK $^{16\text{-}185\ C\text{-}S}$, showing alpha-helical secondary structure (adapted from PDB 2YV6). c) SDS-PAGE analysis of BAK $^{16\text{-}185\ C\text{-}S}$ expression. The protein initially expresses as a 47kDa intein-CBD fusion. Overnight incubation in the presence of 50mM DTT causes the intein tag to self cleave, allowing for purification of the 19.2kDa cleaved protein, visible in columns E-H. Key – A: clarified lysate, B: filtered lysate (0.45µm), C: filtered lysate (0.22µm), D: flow-through, E: buffer wash, F: buffer + 50mM DTT 'flush', G: column elute, H-I: buffer elute / wash, J: concentrated sample, K: filtered conc. sample (0.22µm) for SEC.

Further purification by SEC yielded a monomer peak on the chromatogram at 187mL, with an adjacent dimer peak at 170mL (Figure 3-25).

Yield of cleaved protein was once again relatively low compared to anti-apoptotic family members, but good compared to BAX, with approximately 14mg BAK $^{16\text{-}185\ C\text{-}S}$ purified from 6L of bacterial culture.

Table 3-7 - BAK yield and recovery for each stage of protein purification. Yield compared to pro-survival proteins is low, but good in comparison to BAX. The first two protein concentrations were measured using the Biorad assay, the measurement for BAK recovered from SEC was made using absorbance at UV_{280}.

Purification stage	mg / L media	Yield (%)
Column elute of BAK	8	100
Concentrated and loaded to SEC column	6.5	81
Recovered from SEC	2.3	29

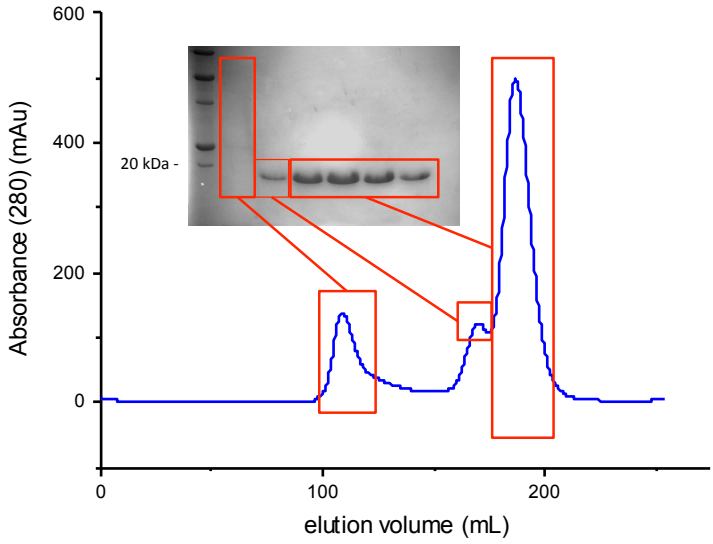

Figure 3-25 - Size exclusion chromatography of Bak $^{16\text{-}185\ C\text{-}S}$. The main peak at 187mL corresponds to a monomer. The adjacent shoulder at 170mL corresponds to a dimer.

Biophysical analysis on both BAX and BAK proteins using far UV CD revealed the expected alpha helical profile (Figure 3-26). For BAX, local MRE minima at 222 and 208nm were -16443 and -18451 respectively. For BAK, the minima were recorded as -21367 and -22563.

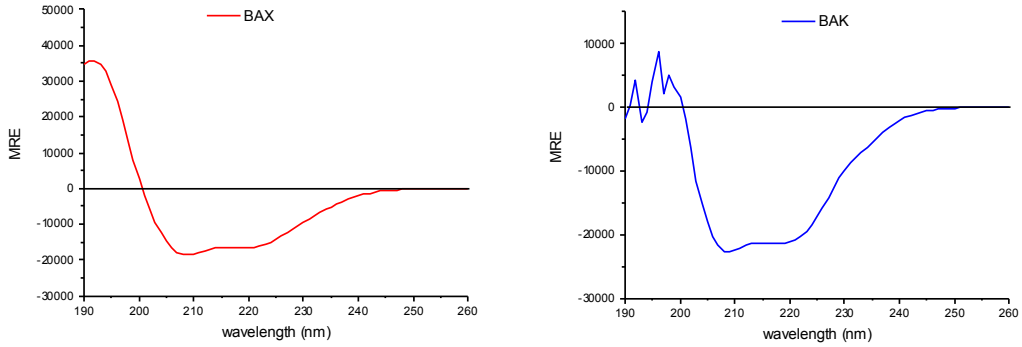

Figure 3-26 – BAX and BAK characterisation. Far UV CD shows the expected alpha helical profile for both proteins. BAX shows local absorption minima at 208nm and 222nm of -18451 and -16443 respectively. The corresponding figures for BAK are -22563 and -21367. Traces shown are representative of multiple experiments.

Both proteins were assayed for correct teriary structure using FA direct binding assays, with titration against FITC labelled BH3 peptides from the BH3 only activators BID and BIM. Unfortunately, I was unable to obtain binding curves for either BAX or BAK (Figure 3-27): the hypothesised 'hit and run' nature of interactions in the BC binding groove of BAX and BAK would explain why this result was likely, as does the absence of such data published in the literature.

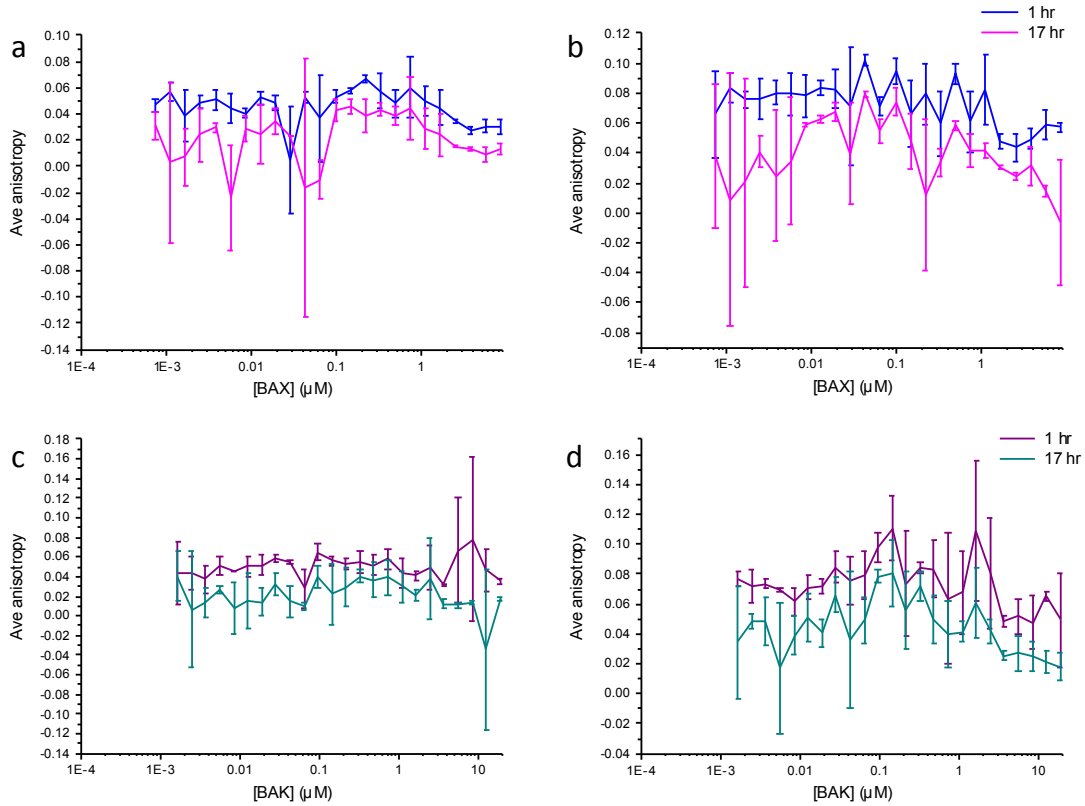

Figure 3-27 – Direct binding FA assays for BAX and BAK. a) BAX titrated against FITC-BID-BH3. b) BAX titrated against FITC-BIM-BH3. c) BAK titrated against FITC-BID-BH3. d) BAK titrated against FITC-BIM-BH3. Average anisotropy was measured for all reactions after 1 hour, and following overnight incubation at RT (17 hours). No binding curves were obtained.

3.6 Chapter Summary and Discussion

This chapter describes the work undertaken to select, synthesise, purify and characterise target proteins from the BCL-2 family for use in this study. As the interacting surfaces on proteins have historically proved difficult to target [302, 303], only multi-domain family members were selected, as these all present a well defined, globular tertiary structure, unlike the BH3 only family members, which are intrinsically disordered. Proteins selected covered both pro-survival and pro-apoptotic members.

All pro-survival family members, BCL-2, BCL-X_L and MCL1, expressed well as either dimers or monomers, and were easily characterised. BAX and BAK expressed as monomers, but at much lower yield than their pro-survival counterparts, and were not amenable to analysis by direct binding FA. This has been an issue for other groups working with BAX and BAK, and is most likely due to the transient 'hit and run' nature of binding events in their respective BC grooves. By contrast, the nanomolar binding affinities obtained in FA direct binding assays for pro-survival proteins titrated against FITC-BAX-BH3 were in line with previously published results [304]. α-helical secondary structure was confirmed for all target proteins, with expected levels of CD spectrum absorption minima seen at 208nm and 222nm in every case[1]. BCL-2, BCL-X_L, MCL1, BAX and BAK were taken forward as targets for Affimer panning in the next stage of this study.

---

[1] Using far UV CD, a hypothetical protein with 100% α-helical secondary structure would have MRE at 222nm of around -30,000 deg cm^2 $dmol^{-1}$ 305. Kelly, S.M., T.J. Jess, and N.C. Price, *How to study proteins by circular dichroism.* Biochim Biophys Acta, 2005. **1751**(2): p. 119-39., providing a theoretical maximum for MRE. However, other studies have measured spectra for recombinant BCL-2 family proteins with MRE readings between -15000 and -20,000 306. Wallgren, M., et al., *Reconstitution of the anti-apoptotic Bcl-2 protein into lipid membranes and biophysical evidence for its detergent-driven association with the pro-apoptotic Bax protein.* PLoS One, 2013. **8**(4): p. e61452, 307. Ivashyna, O., et al., *Detergent-activated BAX protein is a monomer.* J Biol Chem, 2009. **284**(36): p. 23935-46.

Chapter 4 – Identification and Characterisation of Affimers binding BCL-2 family proteins

The previous chapter detailed the work carried out to express, purify and characterise a selection of pro- and anti-apoptotic proteins from the BCL-2 family. This chapter describes the actions taken to raise Affimers, a class of engineered non-antibody binding protein, against these BCL-2 family members. It details the use of phage display experiments to isolate target binding clones from the Affimer phage display library, the subcloning and protein expression work carried out to purify these clones as Affimers, and the biophysical assays used to characterise individual Affimers and their interactions with target proteins.

4.1 Preliminary Work

Earlier work carried out in the Edwards group by Dr Jennifer Miles identified Affimers that selectively bound to MCL1 and BCL-X_L (Figure 4-1). Using fluorescence anisotropy competition binding assays, Affimers ADB10 and ADB13[2] were shown to bind BCL-X_L with sub-micromolar IC_{50} values (0.74 ± 0.08μM and 0.39 ± 0.05μM respectively) when titrated against a complex of BCL-X_L and BODIPY labelled BAK BH3 peptide. Similarly, Affimers ADM1 and ADM22 were shown to bind MCL1 with IC_{50} values of 3μM and 2μM respectively, when titrated against a complex of MCL1 and FITC labelled NOXA-B BH3 peptide (Figure 4-2 and Table 4-1). The ability of these Affimers to compete with peptides analogous to the BH3 domains of endogenous binding partners indicated that they were all interacting with the BC binding groove of their target protein.

[2] Affimers were previously known as adhirons, as reflected in the 'ADB' and 'ADM' prefixed nomenclature of binders raised against BCL-X_L and MCL1 in this preliminary work.

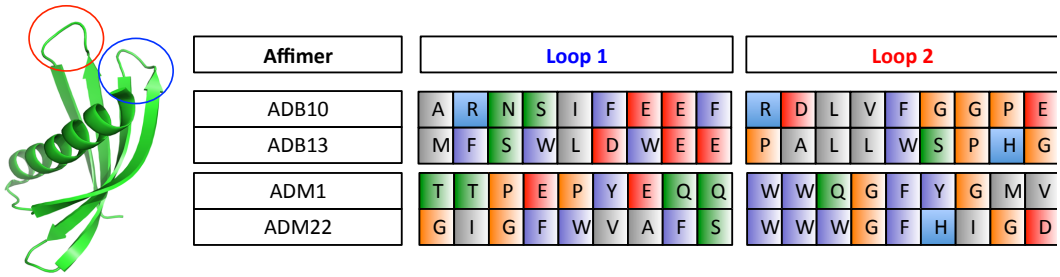

Figure 4-1 – Affimers targeting BCL-X_L and MCL1. Previous work in the group identified ADB10 and ADB13 as selective binders for BCL-X_L, and ADM1 and ADM22 as selective binders for MCL1. Details of residues in the two randomised Affimer loops are shown. Residues are coloured according to their side chain properties: Blue – polar, positive charge; red – polar, negative charge; green – polar, neutral; grey – non-polar, aliphatic; purple – non-polar, aromatic; orange – glycine and proline.

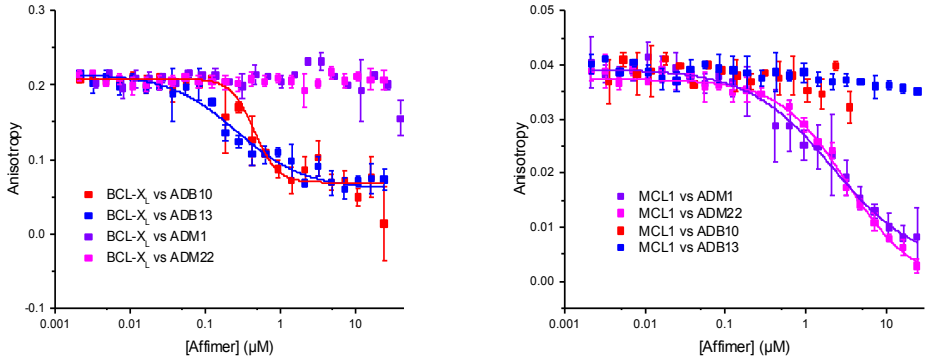

Figure 4-2 – Affimers selectively bind target proteins. Fluorescence anisotropy competition binding assays were used to demonstrate the ability of Affimers to selectively compete with endogenous binding partners of their target proteins. Left panel: ADB10 and ADB13 show competitive binding when titrated against a complex of BCL-X_L and BODIPY labelled BAK BH3 peptide, but no activity against a complex of MCL1 and FITC labelled NOXA-B BH3. Right panel: ADM1 and ADM22 show competitive binding when titrated against a complex of MCL1 and FITC labelled NOXA-B BH3 peptide, but no activity against a complex of BCL-X_L and BODIPY labelled BAK. The ability of these Affimers to compete off BH3 peptides mimicking binding domains of BH3 only family members indicates binding interactions in the BC groove. Data courtesy of Dr Jennifer Miles.

Table 4-1 – IC_{50} values for Affimers in competition binding assays. ADB10 and ADB13 bind BCL-X_L with IC_{50} values of 0.74 ± 0.08μM and 0.39 ± 0.05μM respectively when titrated against a complex of BCL-X_L and BODIPY labelled BAK BH3 peptide. ADM1 and ADM22 bind MCL1 with IC_{50} values of 3μM and 2μM respectively, when titrated against a complex of MCL1 and FITC labelled NOXA-B BH3 peptide. No competitive binding is seen against control protein in either case. Data courtesy of Dr Jennifer Miles.

	IC_{50} (μM)	
Affimer	**vs BCL-X_L : BODIPY-BAK BH3**	**vs MCL1 : FITC NOXA B**
ADB10	0.74 ± 0.08	-
ADB13	0.39 ± 0.05	-
ADM1	-	3
ADM22	-	2

Crystallisation trials undertaken by Dr Miles produced a low resolution (~ 3Å) structure for MCL1 bound to ADM22. These trials involved mixing protein and Affimer with overnight incubation and no further purification. To advance this study, SEC was used to see if ADM1 and ADM22 would co-purify with MCL1, and if so, whether the purified complexes would yield structural data for the MCL1:ADM1 complex, and higher resolution structural data for the MCL1:ADM22 complex. Affimers were mixed with MCL1 in a molar ratio of 1.2:1, incubated overnight at 4°C, then run on a HiLoad 26/60 Superdex S75 pg column. Results showed both ADM1 and ADM22 co-eluting in complex with MCL1 (Figure 4-3). The eluted complexes were used in crystallisation trials, with initial screening carried out against 384 unique buffer conditions. Unfortunately, the MCL1:ADM1 complex did not produce crystals in preliminary trials, and crystals produced and optimised for the MCL1:ADM22 complex failed to produce higher resolution data than that already obtained by Dr Miles.

Despite drawbacks in obtaining structural data, our group had established that Affimers can be raised to selectively target individual BCL-2 family proteins, namely the pro-survival members BCL-X_L and MCL1. The remainder of this chapter describes experiments designed to progress this work by raising selectively binding Affimers against BCL-2, and against the pro-apoptotic proteins BAX and BAK, as well as work to identify Affimers able to cross react with multiple pro-survival family members.

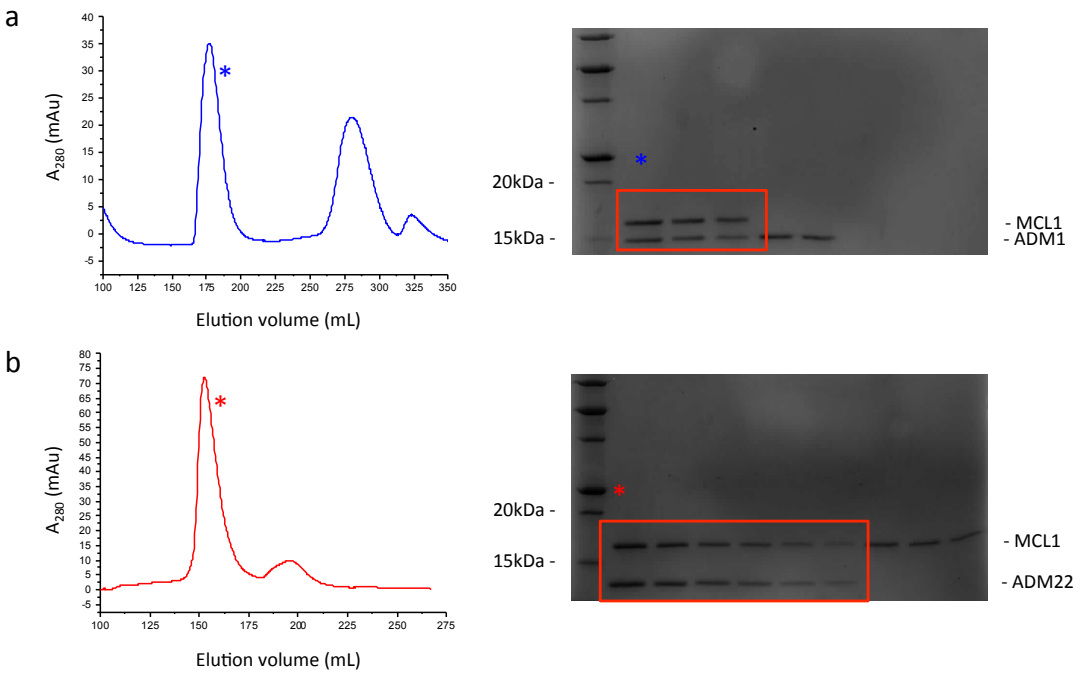

Figure 4-3 – Affimers co-purify with target proteins. ADM1 (a) and ADM22 (b) were mixed with MCL1 in a molar ratio of 1.2:1 and incubated overnight at 4°C. Left panels: Protein : Affimer complexes were purified by SEC using a HiLoad 26/60 Superdex S75 pg column. Asterisks denote elution peaks used for analysis by SDS-PAGE. Right panels: Coomassie staining of SDS-PAGE gels clearly shows band for both protein and Affimer in the SEC fractions collected.

4.2 Affimer Targeting of Pro-Survival BCL-2 Proteins

Work with the pro-survival BCL-2 family members comprised two major strands. Firstly, Affimers were raised against BCL-2, to augment the work already done with BCL-X_L and MCL1 and complete a library of selective binders against the pro-survival BCL-2 family members used in this study. Secondly, a comprehensive phage display 'cross-panning' exercise was carried out, with the aim of identifying cross-reacting Affimers able to bind combinations of BCL-2, BCL-X_L and MCL1.

To carry out phage display experiments, target proteins must first be immobilised. To this end, BCL-2, BCL-X_L and MCL1 were heterogeneously labelled using EZ-link NHS-SS-Biotin to biotinylate primary amines, and were then immobilised on Nunc-Immuno™ MaxiSorp™ strips. Biotinylation

was confirmed by ELISA, using streptavidin HRP and 3,3',5,5'-Tetramethylbenzidine (TMB) to develop the reaction. Absorbance was measured at 620nm, and successful biotinylation of all target proteins confirmed (Figure 4-4).

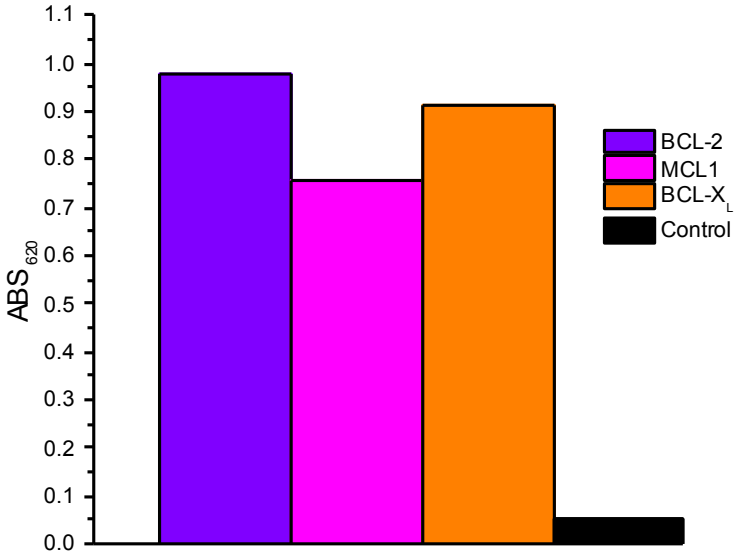

Figure 4-4 – ELISA confirms biotinylation of pro-survival BCL-2 family proteins for use in phage display experiments. Target proteins were diluted 1:50 in PBS and bound to wells in Nunc-Immuno™ MaxiSorp™ strips. The control well contained PBS with no target protein. Streptavidin HRP was added to all wells. Biotinylation was confirmed for all pro-survival target proteins by the subsequent addition of TMB as a HRP substrate, with absorbance read at 620nm.

4.2.1 BCL-2

Well established protocols for Affimer panning, developed and optimised by the BioScreening Technology Group (BSTG) at the University of Leeds, were followed. Three Affimer panning rounds were carried out as described in Chapter 2, with BCL-2 binding phage clones eluted at each step for use in the next panning round. In the first panning round, biotinylated BCL-2 was immobilised in streptavidin coated wells prior to incubation with the Affimer phage library. For the second panning round, immobilisation was carried out using streptavidin coated magnetic beads, followed by incubation with phage eluted from round 1. After the final panning round, phage were eluted from neutravidin coated target wells in which BCL-2 had been immobilised, and

from control wells containing buffer but no target protein (to detect non-specific binders). Target and control eluted phage were then used to infect ER2738 *E. coli* cells and grown in LB media. LB agar plates were subsequently inoculated with 10µL of culture from target wells, or 10µL of culture from control wells. Following overnight incubation at 37°C, the plate inoculated with target culture had >300 colonies; the plate inoculated with control culture had only seven colonies, confirming significant amplification of target binding phage in target wells, as opposed to non-specific binding phage in control wells.

a

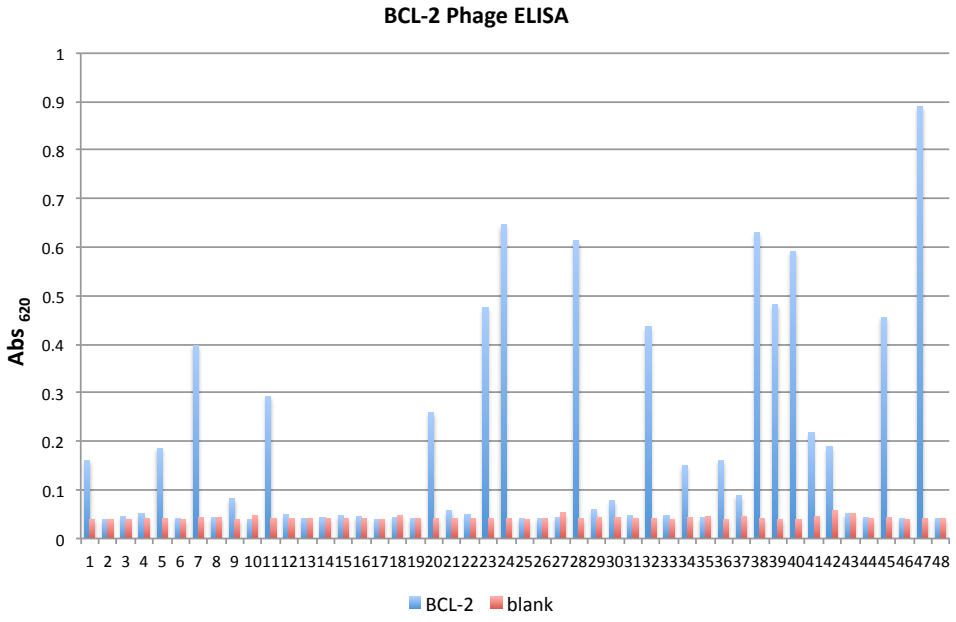

b

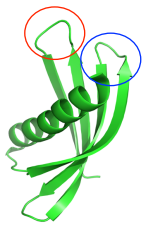

Affimer	Loop 1									Loop 2									#
B-2 Aff D4	S	A	F	S	W	W	E	R	I	D	H	S	Q	P	I	Q	M	R	9
B-2 Aff E5	G	I	G	F	W	V	A	F	S	S	S	K	P	N	Q	M	M	M	1
B-2 Aff E6	F	M	E	N	N	G	F	V	M	K	W	F	F	L	P	P	I	N	9
B-2 Aff F4	K	M	H	N	S	H	I	I	M	K	W	Y	L	F	P	I	G	A	1

Figure 4-5 – Identification of Affimers targeting BCL-2. a) Results of phage ELISA following three Affimer panning rounds against BCL-2. 48 phage transduced colonies were picked; 20 of these demonstrated increased binding activity against controls (results show differences in absorbance after incubation with Anti-Fd-Bacteriophage-HRP, addition of TMB and allowing HRP:TMB reaction to develop for 2 minutes). b) Sanger sequencing of extracted phagemid DNA identified four unique binders, B-2 Aff D4, E5, E6 and F4. Details of residues in the two randomised Affimer loops are shown. Residues are coloured according to their side chain properties (as described in Figure 4-1).

48 colonies were selected from the target plate and used in phage ELISA experiments (described in Chapter 2) to identify selectively binding clones for sequencing and further analysis (Figure 4-5a). Twenty clones were shown to demonstrate increased binding activity compared to blank controls. Phagemid DNA extracted from these clones was as sent for Sanger sequencing, and four unique binders, termed B-2 Aff D4, E5, E6 and F4, were identified (Figure 4-5b). Of these, D4 and E6 were each represented nine times in the pool of twenty, E5 and F4 each represented once only.

DNA for each of the unique binding sequences was sub-cloned from phagemid into pET-11a vectors, then used to transform BL21 (DE3) Rosetta 2 cells. Affimers were expressed as recombinant proteins with a hexa-His tag, and purified by Nickel affinity chromatography, providing good yields in all cases as detailed in Table 4-2.

Table 4-2 - BCL-2 Affimer expression and initial purification yields. All Affimers were purified using Nickel affinity chromatography. Yield is expressed as the amount of protein detected in the 300mM imidazole Nickel column elute, measured using a Biorad assay.

Affimer	Yield (mg/L media)
B-2 Aff D4	41
B-2 Aff E5	34
B-2 Aff E6	35
B-2 Aff F4	21

BCL-2 Affimers were further purified by size exclusion chromatography, then characterised using biophysical assays, the results of which are presented in Figure 4-6 - Figure 4-9, and described in the following paragraphs.

4.2.1.1 Size Exclusion Chromatography

Results of SEC are shown in Figure 4-6b - Figure 4-9b. The SEC chromatograms produced demonstrate a tendency for Affimers to elute late from the SEC column, an effect thought to be caused by Affimers interacting with the column itself, which makes it difficult to state with certainty whether

SEC peaks represent monomers or higher order structures. This is particularly apparent with the late elution peaks seen for E5 and E6, as detailed in Table 4-3 below.

Table 4-3 – Results of SEC purification of BCL-2 Affimers. Affimers were purified by SEC using a HiLoad 26/60 Superdex S75 pg column. Actual elution volumes are compared with expected elution volumes, determined by comparison against calibration standards. Late elution peaks for E5 and E6 demonstrate the tendency of Affimers to interact with the column during SEC purification. F4 elutes at 111mL, in the void volume, indicating aggregation during purification and precluding F4 from further study.

Affimer	M_w (Da)	Expected Elution Volume (mL)	Actual Elution Volume (mL)
B-2 Aff D4	13626	213	204
B-2 Aff E5	12247	218	256
B-2 Aff E6	12460	217	230
B-2 Aff F4	13539	214	111

Affimers may also demonstrate a tendency to oligomerise during purification. This effect has been witnessed in previous work carried out by the Edwards group with binders raised against p300 (unpublished data), and does not prevent such Affimers being used in further assays. In Figure 4-6 - Figure 4-9 higher order structures are seen for all Affimers, in addition to the void volume eluates at 111mL. Affimer F4 eluted almost exclusively in the void volume, having unfortunately aggregated on the SEC column (Figure 4-9), and was consequently excluded from further studies.

4.2.1.2 Far UV Circular Dichroism

The remaining Affimers, D4, E5 and E6, were buffer exchanged into PBS, and far UV CD was used to check for correct secondary structure. The Affimer backbone comprises two pairs of β-strands connected by loops and one α-helix, and the predominance of β-strands would dictate absorbance spectra with minima at around 218nm. This profile is indeed seen in all three cases (Figure 4-6c - Figure 4-8c), with MRE minima of -10,145, -8,665 and –10,713 for D4, E5 and E6 respectively.

4.2.1.3 Affimer target binding ELISA

Finally, as false positive results are frequently seen in phage display experiments, binding ELISAs were used to test that D4, E5 and E6 were all genuine and selective binders of BCL-2 (Figure 4-6d - Figure 4-8d), with BCL-X_L and BAK also assayed as controls. All proteins were diluted in PBS, and 200ng per well aliquoted to 96 well Nunc-Immuno™ MaxiSorp™ plates, with overnight incubation at 4°C. After washing and blocking with BSA, Affimers were applied to bound protein and serially diluted down the ELISA plate. Optimisation trials established an initial Affimer concentration of 1μg mL^{-1} and 1:3 dilutions as the conditions providing optimum results. As all Affimers are expressed from pET-11a with a hexa-His tag for purification, binding was assayed through the addition of a HRP conjugated anti poly-His antibody. TMB was added as HRP substrate, the reaction was allowed to develop, then was quenched by the addition of 2M sulphuric acid[3], with absorption read at 450nm. D4, E5 and E6 all presented as genuine and selective binders of BCL-2, with negligible binding to controls observed.

[3] Reaction quenching disrupts formation of the TMB radical cation dimer, resulting in a yellow colour in solution, the absorbance of which can be read at 450nm.

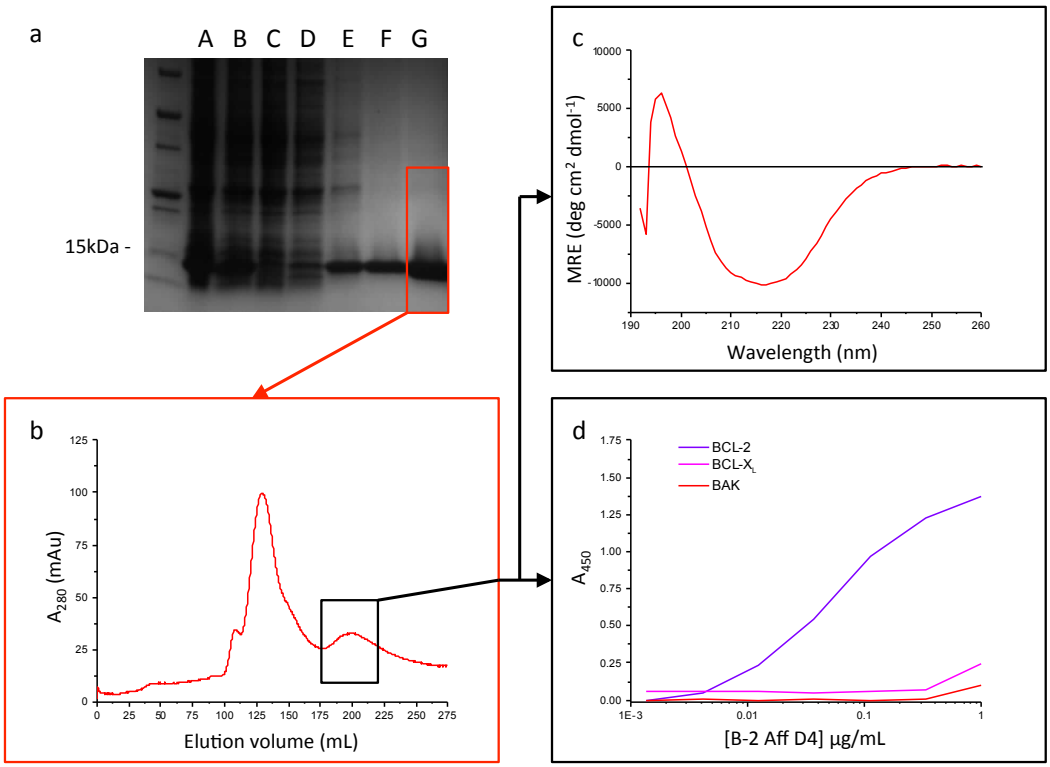

Figure 4-6 – Purification and Characterisation of B-2 Aff D4. a) Coomassie staining of SDS PAGE gel used to analyse D4 purification by Nickel affinity chromatography. Key: A = clarified lysate; B = filtered lysate; C = column flow through; D = column buffer (CB) wash; E = CB + 50mM imidazole wash; F = CB + 100mM imidazole wash; G = CB + 300mM imidazole elute. The 300mM imidazole elute was taken for further purification by SEC. b) Chromatogram of 300mM imidazole elute purified by SEC using a HiLoad 26/60 Superdex S75 pg column. The early peak shows high order oligomerisation. The late peak, eluting at 204mL, was taken for further biophysical analysis. c) Fractions collected from the selected Affimer peak were buffer exchanged into PBS and analysed by Far UV CD to check for correct secondary structure. The expected profile for predominantly β-sheet structures is seen, with an MRE absorption minima of – 10,145 seen at 217nm. d) ELISA results confirm selective binding of D4 for BCL-2 compared to BCL-X_L and BAK controls. Immobilised proteins were exposed to 1:3 serial dilutions of Affimer. Binding was assayed through the addition of a HRP conjugated anti poly-His antibody, which binds the hexa-His tag on purified Affimers. Reactions were developed with TMB and quenched by the addition of 2M sulphuric acid, with absorption measured at 450nm.

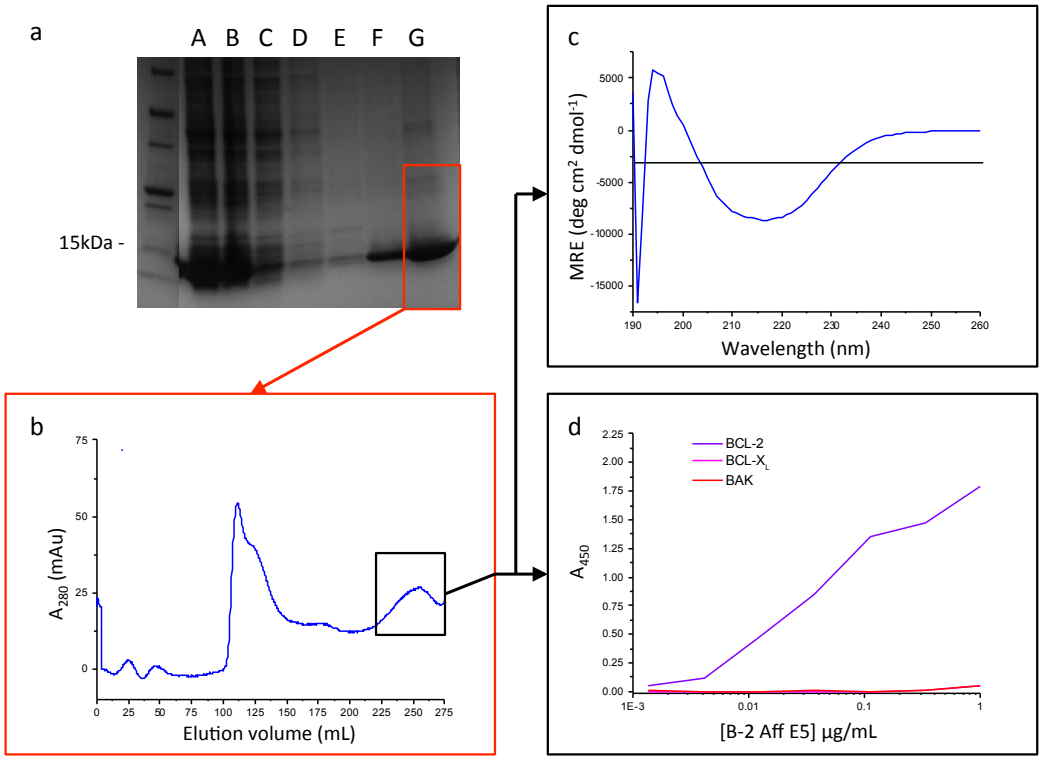

Figure 4-7 - Purification and Characterisation of B-2 Aff E5. a) Coomassie staining of SDS PAGE gel used to analyse E5 purification by Nickel affinity chromatography. Key as for Figure 4-6. The 300mM imidazole elute was taken for further purification by SEC. b) Chromatogram of 300mM imidazole elute purified by SEC using a HiLoad 26/60 Superdex S75 pg column. The early peak elutes in the void volume, with a shoulder of high order oligomers. The late peak elutes at 256mL, at a later volume than expected, a common artefact in Affimer purification. c) Fractions collected from the selected Affimer peak were buffer exchanged into PBS and analysed by Far UV CD to check for correct secondary structure. The expected profile for predominantly β-sheet structures is seen, with an MRE absorption minima of – 8,665 seen at 217nm. d) ELISA results confirm selective binding of E5 for BCL-2 compared to BCL-X_L and BAK controls. Assay as described in Figure 4-6.

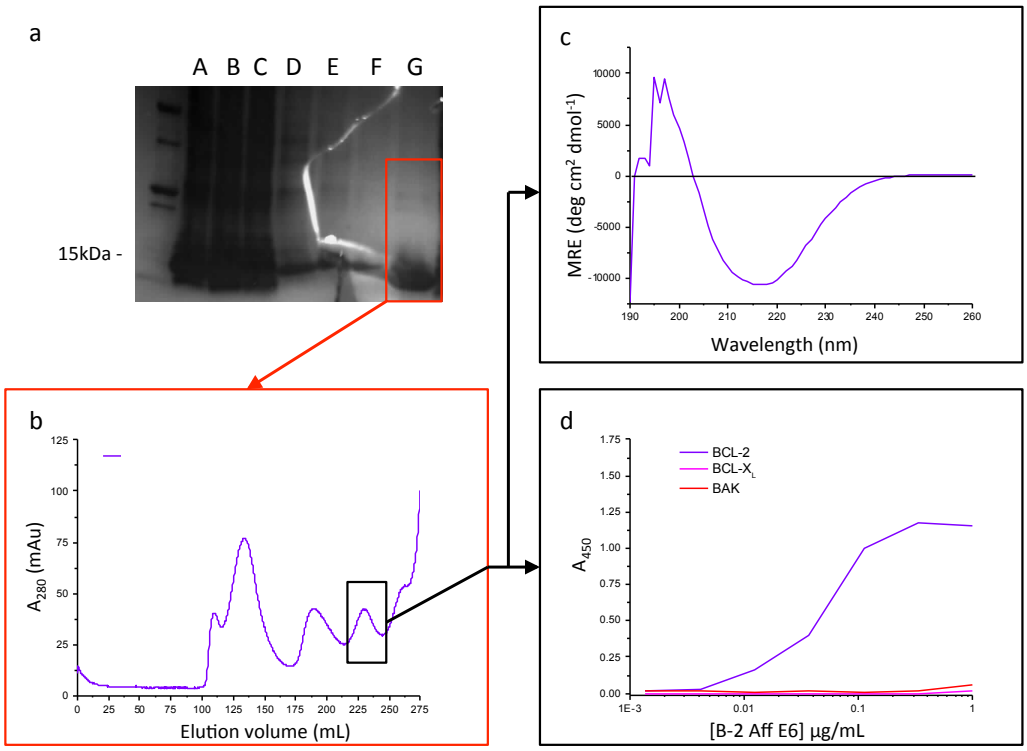

Figure 4-8 -- Purification and Characterisation of B-2 Aff E6. a) Coomassie staining of SDS PAGE gel used to analyse E6 purification by Nickel affinity chromatography. Key as for Figure 4-6. The 300mM imidazole elute was taken for further purification by SEC. b) Chromatogram of 300mM imidazole elute purified by SEC using a HiLoad 26/60 Superdex S75 pg column. The early peak elutes in the void volume, with an attached peak of high order oligomers. The late peak elutes at a later volume than expected, at 230mL. c) Fractions collected from the selected Affimer peak were buffer exchanged into PBS and analysed by Far UV CD to check for correct secondary structure. The expected profile for predominantly β-sheet structures is seen, with an MRE absorption minima of – 10,713 seen at 217nm. d) ELISA results confirm selective binding of E6 for BCL-2 compared to BCL-X_L and BAK controls. Assay as described in Figure 4-6.

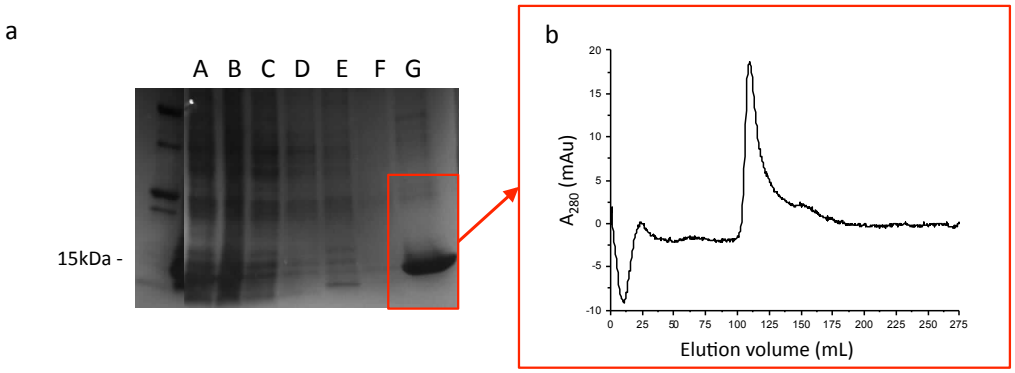

Figure 4-9 - Purification of B-2 Aff F4. a) Coomassie staining of SDS PAGE gel used to analyse F4 purification by Nickel affinity chromatography. Key as for Figure 4-6. The 300mM imidazole elute was taken for further purification by SEC. b) Chromatogram of 300mM imidazole elute purified by SEC using a HiLoad 26/60 Superdex S75 pg column, showing evidence of aggregation, with Affimer eluting predominantly in the void volume at 111mL, and no monomer peak.

4.2.2 Cross-reactive Affimers to bind multiple pro-survival members

Affimers for each of the pro-survival BCL-2 proteins used in this study had now been identified. All such Affimers demonstrated selectivity in binding their target proteins, with no evidence of cross-reactivity to other pro-survival proteins seen (Figure 4-2, Figure 4-6 - Figure 4-8).

The next set of experiments were carried out to determine if it was possible to raise cross-reacting Affimers with binding affinity for multiple pro-survival family members. If feasible, such Affimers could help guide the design of small molecules able to bind and neutralise combinations of pro-survival proteins, which would prove useful in cellular assays to investigate physiological activities of individual family members, or test clones of cancer cells for BCL-2 addiction[4].

---

[4] The concept of BCL-2 'addiction' of specific cancers with regard to pro-survival family members was introduced in Chapter 1. To reiterate, cancer cells with elevated levels of BCL-2, BCL-X_L or MCL1 gain a competitive and selective advantage and are described as

The EMBL-ESI Pairwise Sequence Alignment tool was used to compare the sequence identify of our three pro-survival proteins (Table 4-4). The most promising two way combination for cross-reactivity was BCL-2 with BCL-X_L, having 40.3% identity. The likelihood of MCL1 being included in any cross-reactivity was much lower, MCL1 having only 20.4% and 24.7% sequence identity with BCL-2 and BCL-X_L respectively.

Table 4-4 - Comparison of sequence identity for pro-survival BCL-2 proteins. Comparative data was obtained using the EMBL-ESI Pairwise Sequence Alignment tool.

% identity	BCL-2	BCL-X_L	MCL1
BCL-2	100.0	40.3	20.4
BCL-X_L	40.3	100.0	24.7
MCL1	20.4	24.7	100.0

Dual inhibitors of BCL-2 and BCL-X_L already exist, for example ABT-737 and ABT-263, developed using structure based design, and enhanced using medicinal chemistry techniques [245]. Using phage display to identify dual inhibitors, or even three-way 'pan inhibitors', would be a more speculative exercise, but the ability of such experiments to probe the entire surface of target proteins opened up the possibility of identifying novel binding sites common to pro-survival members that might not be apparent from comparing their primary structures. With this in mind, a comprehensive phage display 'cross-panning' exercise was designed, where cross-reacting phage clones would be isolated using three panning rounds as usual, but with phage eluted from each panning round incubated in the next round with a different immobilised pro-survival target protein.

Six different cross panning sequences were designed; these are outlined in Table 4-5, with each given a unique cross-pan sequence identifier, from A to F. To illustrate the design, in cross-pan sequence A, the first panning round

---

being 'addicted' to the pro-survival member they over-express: without them, they would be unable to survive the harsh inter-cellular environment that persists during tumour progression.

is carried out against immobilised BCL-2, with eluted phage panned in the second and third rounds against immobilised MCL1. Any identified binding clones would potentially be BCL-2 : MCL1 cross-reactive binders. In sequence B, the first pan is carried out against BCL-2, the second against BCL-X_L, and the final pan against MCL1; any identified binding clones in this case would potentially be three-way 'pan inhibitors', with the ability to bind all three of our pro-survival target proteins.

Table 4-5 – Cross panning exercise for pro-survival proteins. Six different cross-pan sequences, labelled A-F, were carried out. Individual cells identify the pro-survival protein immobilised and incubated with phage at each panning round. Following the final panning round, eluates from the different sequences A-F will contain phage panned against a combination of either 2 or 3 different pro-survival proteins.

	Cross-pan sequence					
Pan #	**A**	**B**	**C**	**D**	**E**	**F**
1	BCL-2	BCL-2	MCL1	MCL1	BCL-X_L	BCL-X_L
2	MCL1	BCL-X_L	BCL-2	BCL-X_L	MCL1	BCL-2
3	MCL1	MCL1	BCL-X_L	BCL-X_L	BCL-2	BCL-2

Following completion of the final panning round for each of the six cross-pan sequences A-F, phage was eluted from neutravidin coated target wells in which final round target protein had been immobilised, and from control wells containing buffer but no target protein. Target and control eluted phage were then used to infect ER2738 *E. coli* cells and grown in LB media. LB agar plates were subsequently inoculated with 10μL of culture from target wells, or 10μL of culture from control wells. This was to check for phage clone amplification in target wells, compared to any non-specific binders in control wells, as described previously for the BCL-2 Affimer pan. A significant increase in the number of colonies seen on target plates compared to control plates would be evidence for the presence of cross-reactive binders. Following overnight incubation at 37°C, amplification was seen on all target plates, though to a much lower extent than would typically be seen when panning against a single target (Table 4-6). This is not surprising, given the levels of sequence identity between BCL-2, BCL-X_L and MCL1 detailed in Table 4-4.

Table 4-6 – Phage amplification on target plates compared to blank controls. Comparison of colony numbers on target and control plates after three panning rounds. Low levels of amplification are seen in all cases.

Cross-pan identifier	Cross pan detail	# colonies (target)	# colonies (control)
A	BCL-2 : MCL1 : MCL1	48	4
B	BCL-2 : BCL-X_L : MCL1	13	7
C	MCL1 : BCL-2 : BCL-X_L	10	2
D	MCL1 : BCL-X_L : BCL-X_L	17	4
E	BCL-X_L : MCL1 : BCL-2	48	7
F	BCL-X_L : BCL-2 : BCL-2	16	7

Target colonies were selected, and phage ELISA was used to determine if any colonies contained clones with expected cross-reacting binding characteristics, compared to blank controls. With reference to Table 4-6, cross-pan sequences B, C and D showed no measurable absorbance in ELISA plates, for either target or blank wells (data not shown). Figure 4-10 shows the results for the remaining sequences: A, E and F. For A and F (top and bottom panels respectively), no difference in binding activity was seen between target clones and blank controls, indicating false positive results. For cross-pan identifier E (middle panel), some clones showed potential binding to BCL-2 and BCL-X_L compared to controls. However, as identifier E was a 3 way cross pan, and there was no binding for MCL1, these were also deemed to be false positive results, and were not subjected to further study.

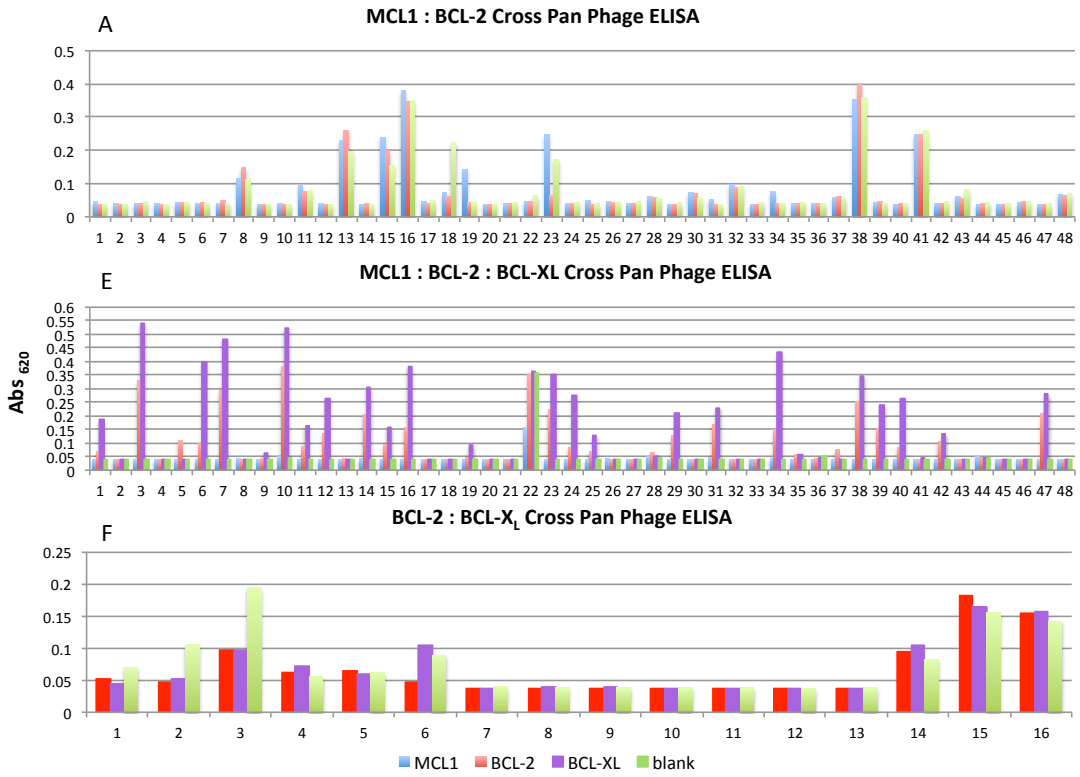

Figure 4-10 – Cross-panning to identify cross-reactive Affimers. Phage ELISA results from pro-survival protein cross-panning exercise. Results show differences in absorbance after incubation with Anti-Fd-Bacteriophage-HRP, addition of TMB and allowing HRP:TMB reaction to develop for >5 minutes. No genuine binding clones were identified.

4.3 Affimer Targeting of Pro-Apoptotic BCL-2 proteins

The pro-apoptotic proteins BAX and BAK were prepared for use as target proteins for Affimer panning. Both proteins were biotinylated using EZ-link NHS-SS-Biotin to tag primary amines, with biotinylation confirmed by ELISA. Absorbance was measured at 620nm, and successful biotinylation of both BAX and BAK confirmed as shown in Figure 4-11.

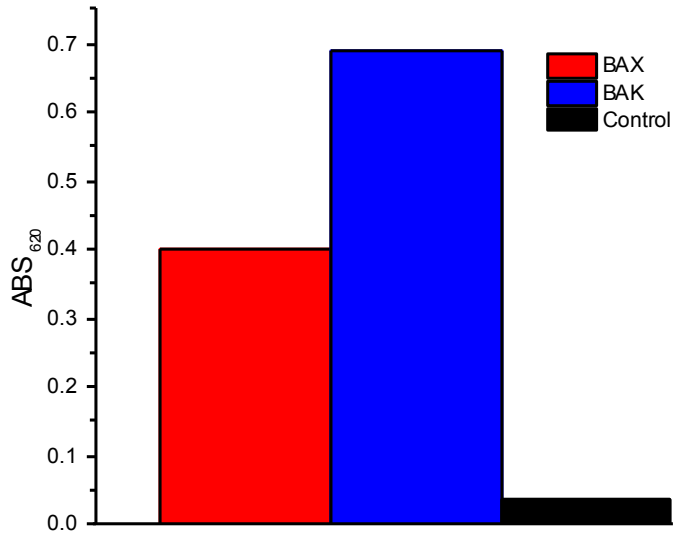

Figure 4-11 – ELISA confirms biotinylation of BAX and BAK for use in phage display experiments. Target proteins were diluted 1:50 in PBS and bound to wells in Nunc-Immuno™ MaxiSorp™ strips. The control well contained PBS with no target protein. Streptavidin HRP was added to all wells. Biotinylation was confirmed for BAX and BAK by the subsequent addition of TMB as a HRP substrate, with absorbance read at 620nm.

4.3.1 BAK

Three Affimer panning rounds were carried out, with amplification of BAK binding clones at each stage. Following completion of the final panning round, agar plates inoculated with media from target and control wells (as previously described for BCL-2) were compared for evidence of amplification in target wells. The target well plate had >200 colonies, with no colonies seen on the control plate.

24 colonies from the target plate were selected, and phage ELISA was used to detect binding clones for sequencing and further analysis (Figure 4-12a). All clones were shown to demonstrate increased binding activity compared to blank controls. Sanger sequencing carried out on phagemid DNA extracted from all 24 clones identified four unique binders, termed BAK Aff 1, 3, 6 and 15 (Figure 4-12b). Aff 1, Aff 3 and Aff 6 were represented multiple times from the pool of 24 clones.

a

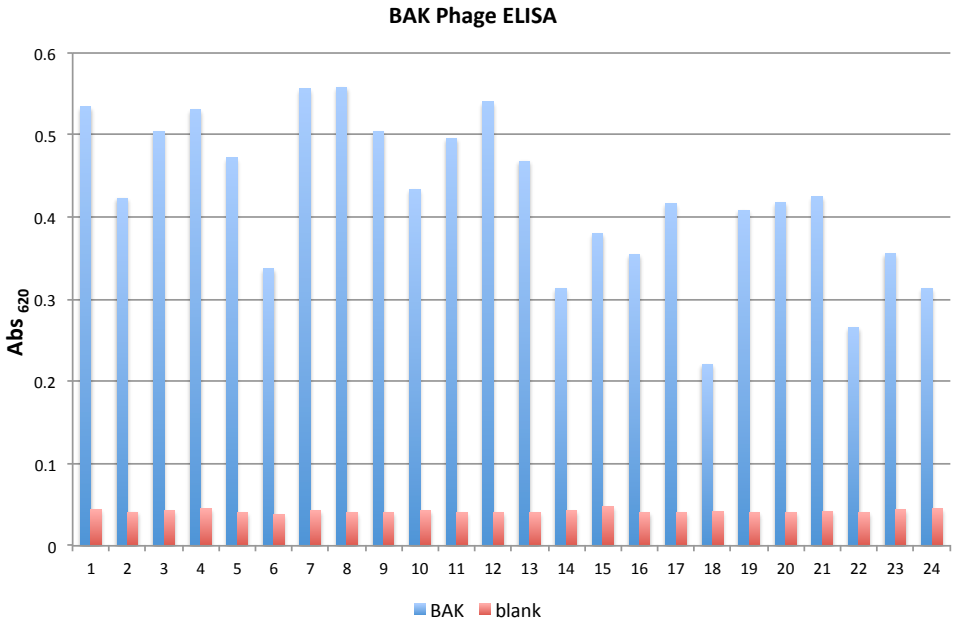

b

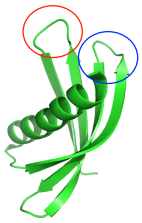

Affimer	Loop 1	Loop 2	#
BAK Aff 1	V G R H S D W A P	Y P I Q S H P P W	11
BAK Aff 3	F V F P H D Y F P	E I A Q W N G W F	2
BAK Aff 6	I M A R P P F E I	A Q L K K T L Y W	8
BAK Aff 15	I W N N S H Y I P	Y P L S L K P F I	1

Figure 4-12 - Identification of Affimers targeting BAK. a) Results of phage ELISA following three Affimer panning rounds against BAK. 24 phage transduced colonies were picked; all demonstrated increased binding activity against controls (results show differences in absorbance after incubation with Anti-Fd-Bacteriophage-HRP, addition of TMB and allowing HRP:TMB reaction to develop for 2 minutes). b) Sanger sequencing of extracted phagemid DNA identified four unique binders, BAK Aff 1, 3, 6 and 15. Details of residues in the two randomised Affimer loops are shown. Residues are coloured according to their side chain properties (as described in Figure 4-1).

DNA for each of the unique binding sequences was sub-cloned from phagemid into pET-11a vectors, then used to transform BL21 (DE3) Rosetta

2 cells. Affimers were expressed and purified by Nickel affinity chromatography, providing good yields for Aff 1, Aff 3 and Aff 15 (Table 4-7). Following growth in bacterial media and induction with IPTG, it had been noted that the culture for BAK Aff 6 produced a notably smaller bacterial pellet, and the comparatively low initial yield of BAK Aff 6 was attributed to this.

Table 4-7 - BAK Affimer expression and initial purification yields. All Affimers were purified using Nickel affinity chromatography. Yield is expressed as the amount of protein detected in the 300mM imidazole Nickel column elute, measured using a Biorad assay.

Affimer	Yield (mg/L media)
BAK Aff 1	48
BAK Aff 3	54
BAK Aff 6	11
BAK Aff15	45

Table 4-8 – SEC purification of BAK Affimers. Affimers were purified by SEC using a HiLoad 26/60 Superdex S75 pg column. Actual elution volumes are compared with expected monomer elution volumes (as determined by comparison against calibration standards described in Chapter 3). Aff 1 and Aff 15 elute as monomers. The late elution peak for Aff 3 demonstrates the tendency of Affimers to interact with the column during SEC purification. The main peak for Aff 6 elutes earlier than expected for a monomer peak, indicative of higher order oligomerisation.

Affimer	M_w (Da)	Expected Elution Volume (mL)	Actual Elution Volume (mL)
BAK Aff 1	12359	218	222
BAK Aff 3	13652	214	259
BAK Aff 6	13558	214	185
BAK Aff15	13554	214	212

BAK Affimers were further purified by SEC (Figure 4-13b – Figure 4-16b). BAK Aff1 and BAK Aff 15 eluted as monomers. BAK Aff 3 eluted later than expected, likely due to Affimer interaction with the SEC column, making it difficult to state with certainty whether the peak at 259mL represents a monomer or higher order structure. The main peak for BAK Aff 6 elutes in the correct position for a dimer (Table 4-8).

A considerable loss of Affimer yield following SEC of Aff 1 and Aff 3 was noted: only 1.6mg of Aff 1 and 3.4mg of Aff 3 were recovered, 3.3% and 6.3% respectively of the protein samples loaded to the column. Though there was sufficient protein remaining to to carry out further assays, this loss of protein Is still a concern. All BAK Affimers, purified by Nickel affinity chromatography as previously stated, had been eluted from the His trap column using Tris buffer containing 300mM imidazole, then concentrated down for SEC. However, SEC was carried out using 50mM sodium phosphate buffer, to better facilitate later assays between purified Affimers and their target protein BAK[5]. It was postulated that the change in buffer conditions was causing Affimers to precipitate on the SEC column. To test this theory, Aff 6 and Aff 15 were dialysed into 50mM sodium phosphate buffer overnight. In line with the hypothesis, BAK Aff 15 precipitated during dialysis, with approximately 40% of protein lost after precipitate had been filtered out; this still left 27mg for SEC. There was also a small amount of precipitation for Aff 6, with 10mg remaining to be loaded to the SEC column post filtration. Dialysis resulted in greatly improved Affimer yield following SEC: 4.3mg of Aff 6 and 12.3mg of Aff 15 were recovered, representing 43.0% and 45.6% respectively of protein loaded to the column. The large late peaks seen for Aff 1 and Aff 3 (Figure 4-13b and Figure 4-14b) were also absent on the Aff6 and Aff15 chromatograms. These peaks appeared just after the conductance spike, and were likely caused by imidazole present in the undialysed samples.

SEC fractions were collected and pooled, then BAK Affimers were assayed to check for correct secondary structure using far UV CD. In all cases, MRE absorbance minima were seen at around 218nm, as expected due to the predominance of β-sheet in the Affimer backbone (Figure 4-13c – Figure 4-16c).

Binding ELISAs were used to test that Aff 1, 3, 6 and 15 were all legitimate binders of BAK (Figure 4-13d - Figure 4-16d), with BAX also assayed as a

---

[5] SEC of BAK was carried out using 50mM sodium phosphate buffer, pH 7.0 (see Chapter 3).

negative control. The method used was an adaptation of that described for BCL-2 Affimers, though in this case, optimisation trials established an initial Affimer concentration of 20µg mL^{-1} and 1:2 serial dilutions as the conditions providing the best data. Reactions were developed with TMB, quenched after 2 minutes with 2M sulphuric acid, and absorbance read at 450nm. All four Affimers showed selectivity for BAK, with negligible binding to controls observed. Aff 6 and Aff 15 produced the best results over the dilution series, with Aff 1, and Aff 3 in particular, showing drop offs in absorbance at relatively high levels of Affimer concentration.

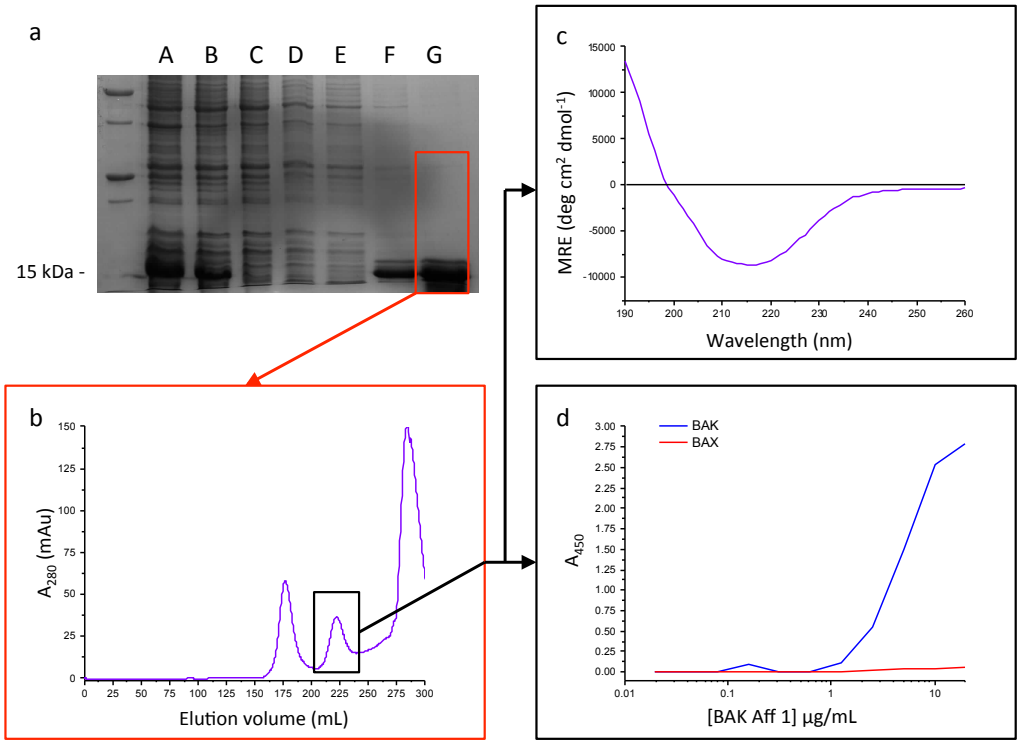

Figure 4-13 - Purification and Characterisation of BAK Aff 1. a) Coomassie staining of SDS PAGE gel used to analyse BAK Aff 1 purification by Nickel affinity chromatography. Key: A = clarified lysate; B = filtered lysate; C = column flow through; D = column buffer (CB) wash; E = CB + 50mM imidazole wash; F = CB + 100mM imidazole wash; G = CB + 300mM imidazole elute. The 300mM imidazole elute was taken for further purification by SEC. b) Chromatogram of 300mM imidazole elute purified by SEC using a HiLoad 26/60 Superdex S75 pg column. The early peak shows high order oligomerisation. The late peak occurs just after the conductivity spike and is caused by imidazole in the loaded sample. The middle peak, eluting at 222mL, was taken for further biophysical analysis. c) Fractions collected from the selected Affimer peak were buffer exchanged into PBS and analysed by Far UV CD to check for correct secondary structure. The expected profile for predominantly β-sheet structures is seen, with an MRE absorption minima of – 8,730 seen at 217nm. d) ELISA results confirm selective binding of BAK Aff 1 for BAK against BAX control. Immobilised proteins were exposed to 1:2 serial dilutions of Affimer. Binding was assayed through the addition of a HRP conjugated anti poly-His antibody, which binds the hexa-His tag on purified Affimers. Reactions were developed with TMB and quenched by the addition of 2M sulphuric acid, with absorption measured at 450nm.

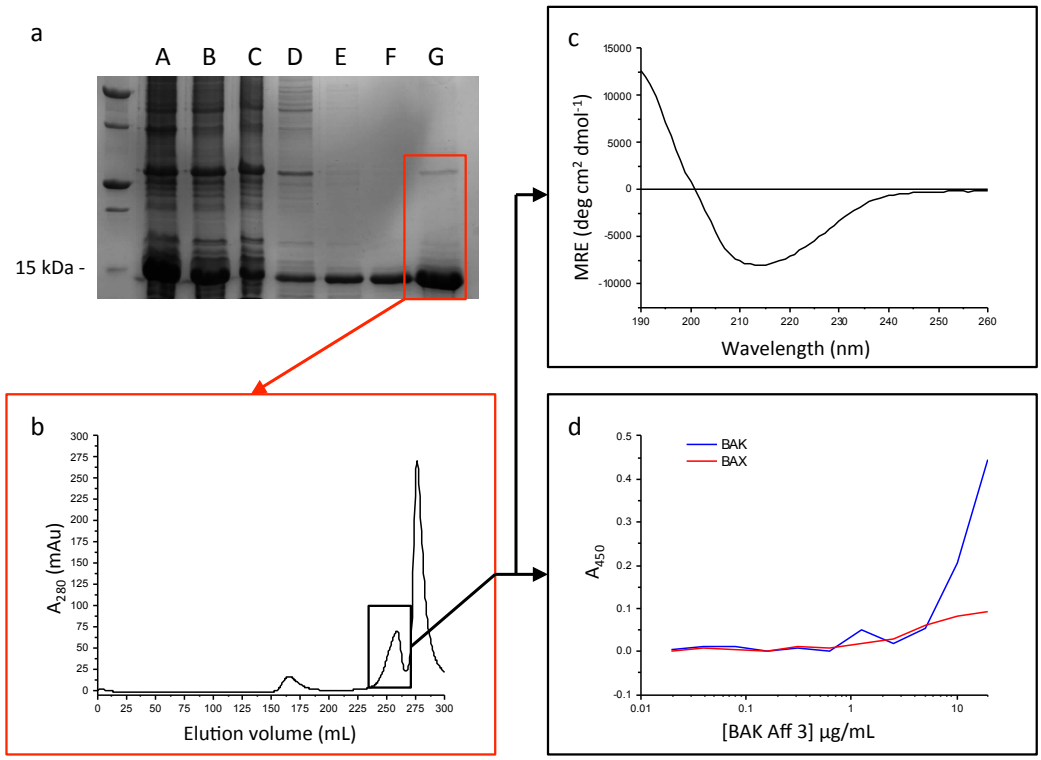

Figure 4-14 - Purification and Characterisation of BAK Aff 3. a) Coomassie staining of SDS PAGE gel used to analyse BAK Aff 3 purification by Nickel affinity chromatography. Key as for Figure 4-13. The 300mM imidazole elute was taken for further purification by SEC. b) Chromatogram of 300mM imidazole elute purified by SEC using a HiLoad 26/60 Superdex S75 pg column. The early peak shows a small amount of high order oligomerisation. The late peak occurs just after the conductivity spike and is caused by imidazole in the loaded sample. The middle peak, eluting at 259mL, was taken for further biophysical analysis. c) Fractions collected from the selected Affimer peak were buffer exchanged into PBS and analysed by Far UV CD to check for correct secondary structure. The expected profile for predominantly β-sheet structures is seen, with an MRE absorption minima of – 7,987 seen at 213nm. d) ELISA results show only low levels of selective binding of Aff3 for BAK against a BAX control. Assay as described in Figure 4-13.

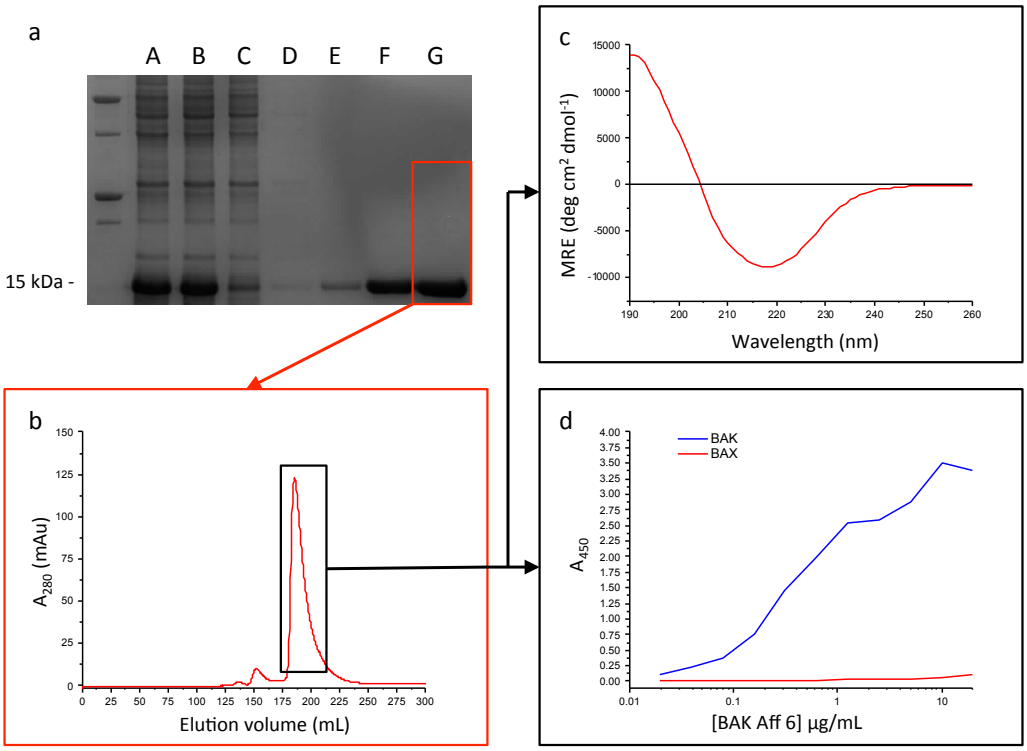

Figure 4-15 - Purification and Characterisation of BAK Aff 6. a) Coomassie staining of SDS PAGE gel used to analyse BAK Aff 6 purification by Nickel affinity chromatography. Key as for Figure 4-13. The 300mM imidazole elute was taken and buffer exchanged into 50mM sodium phosphate buffer prior to concentration and further purification by SEC. b) Chromatogram of 300mM imidazole elute purified by SEC using a HiLoad 26/60 Superdex S75 pg column. The early peak shows high order oligomerisation. The main peak, eluting at 185mL, was taken for further biophysical analysis. c) Fractions collected from the selected Affimer peak were buffer exchanged into PBS and analysed by Far UV CD to check for correct secondary structure. The expected profile for predominantly β-sheet structures is seen, with an MRE absorption minima of – 8,878 seen at 218nm. d) ELISA results confirm selective binding of BAK Aff 6 for BAK against BAX control. Assay as described in Figure 4-13.

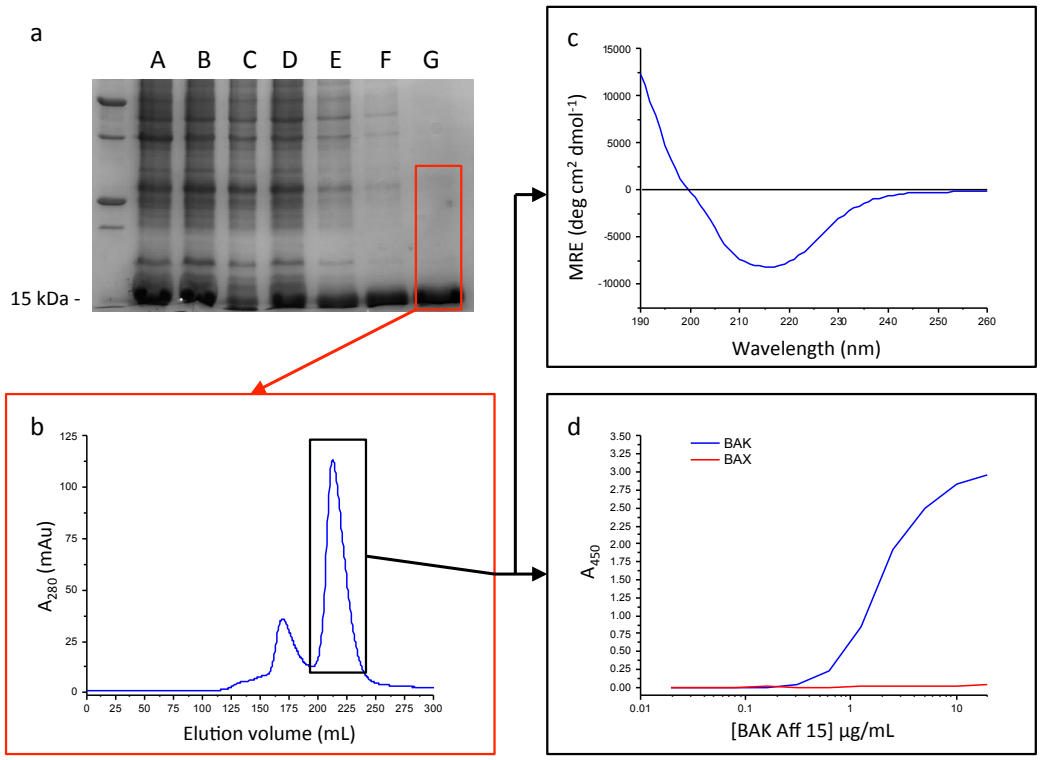

Figure 4-16 - Purification and Characterisation of BAK Aff 15. a) Coomassie staining of SDS PAGE gel used to analyse BAK Aff 15 purification by Nickel affinity chromatography. Key as for Figure 4-13. The 300mM imidazole elute was taken and buffer exchanged into 50mM sodium phosphate buffer prior to concentration and further purification by SEC. b) Chromatogram of 300mM imidazole elute purified by SEC using a HiLoad 26/60 Superdex S75 pg column. The early peak shows high order oligomerisation. The main peak, eluting at 212mL, was taken for further biophysical analysis. c) Fractions collected from the selected Affimer peak were buffer exchanged into PBS and analysed by Far UV CD to check for correct secondary structure. The expected profile for predominantly β-sheet structures is seen, with an MRE absorption minima of – 8,189 seen at 216nm. d) ELISA results confirm selective binding of BAK Aff 15 for BAK against BAX control. Assay as described in Figure 4-13.

Qualitative results from ELISA had established BAK Affimers as genuine binders of BAK. To progress the study, these results were augmented with quantitative binding data. Such data would usually be obtained by using a FA competition binding assay, with an IC_{50} value determined by the ability of each Affimer to compete against a fluorescently labelled tracer peptide for binding to the target protein (see Figure 4-2). To carry out such assays, the affinity of the fluorescent tracer for the target protein must first be determined; this is achieved using direct binding FA, with the target protein titrated against the tracer to establish a binding curve, which is used to

determine binding affinity. As detailed in the previous chapter, attempts to assay a number of FITC labelled peptides for binding to BAK failed to produce a binding curve. It was therefore decided to use Surface Plasmon Resonance (SPR) as an alternative means of establishing a K_d for the strongest BAK binding Affimers, Aff 6 and Aff 15.

SPR was carried out using the BIACORE 3000 system. BAK Aff 6 and Aff 15 were diluted to 5µg / mL in coupling buffer (10mM sodium acetate, pH5.0), and immobilised on a CM5 sensor chip (GE Healthcare). BAK was then flowed over the ligand surface and changes in refractive index were measured and plotted on the sensorgrams seen in Figure 4-17. Sensorgram curves were fitted using the Langmuir model [308], assuming a simple 1:1 binding relationship between protein and Affimer. Biacore software was used to determine association and dissociation constants (k_{on} and k_{off}), from which K_ds for BAK Aff 6 and BAK Aff 15 were calculated at 1.9µM and 8.7µM respectively (Table 4-9).

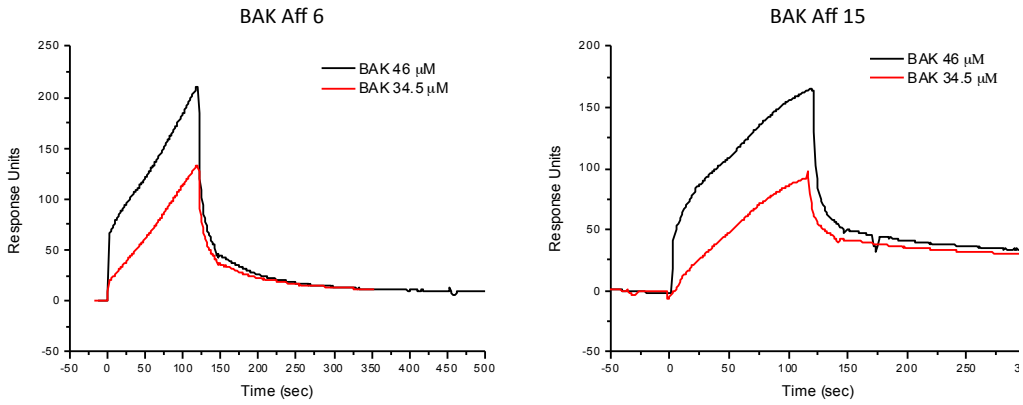

Figure 4-17 - BAK Affimer SPR. BAK Aff6 and BAK Aff15 were immobilised on a CM5 sensor chip (GE Healthcare). BAK at two different dilutions was then flowed over the chip surface, and changes in refractive index were measured over time and plotted in the sensorgrams shown. Biacore software was used to determine association and dissociation binding constants (k_{on} and k_{off}), from which K_ds for BAK binding to Aff 6 and Aff 15 were calculated to be 1.9µM and 8.7µM respectively.

Table 4-9 – Kinetics of Affimer binding to BAK

Interaction	Fitting Model	k_{on} ($M^{-1} s^{-1}$)	k_{off} (s^{-1})	K_d (μM)
BAK : Aff 6	Langmuir	9.98	1.9×10^{-5}	1.9μM
BAK : Aff 15	Langmuir	66.3	5.76×10^{-4}	8.7μM

4.3.2 BAX

Three Affimer panning rounds were carried out as described for BCL-2, with amplification of BAX binding clones at each stage. Following completion of the final panning round, agar plates inoculated with media from target and control wells were compared for evidence of amplification in target wells. The target well plate had >250 colonies, with only three colonies seen on the control plate.

72 colonies from the target plate were selected, and phage ELISA was used to detect binding clones for sequencing and further analysis (Figure 4-18a). 31 clones were shown to demonstrate increased binding activity. Sanger sequencing carried out on DNA extracted from these clones identified five unique binders, termed BAX Aff 1, 3, 6, 7 and 31 (Figure 4-18b). BAX Aff 1 was represented 22 times in this pool, other unique binders were all represented once only. Five clones failed to sequence.

DNA for each of the unique binding sequences was sub-cloned from phagemid into pET-11a vectors, then used to transform BL21 (DE3) Rosetta 2 cells as described for BCL-2. Affimers were expressed and purified by Nickel affinity chromatography, providing good yields in all cases (Table 4-10).

a

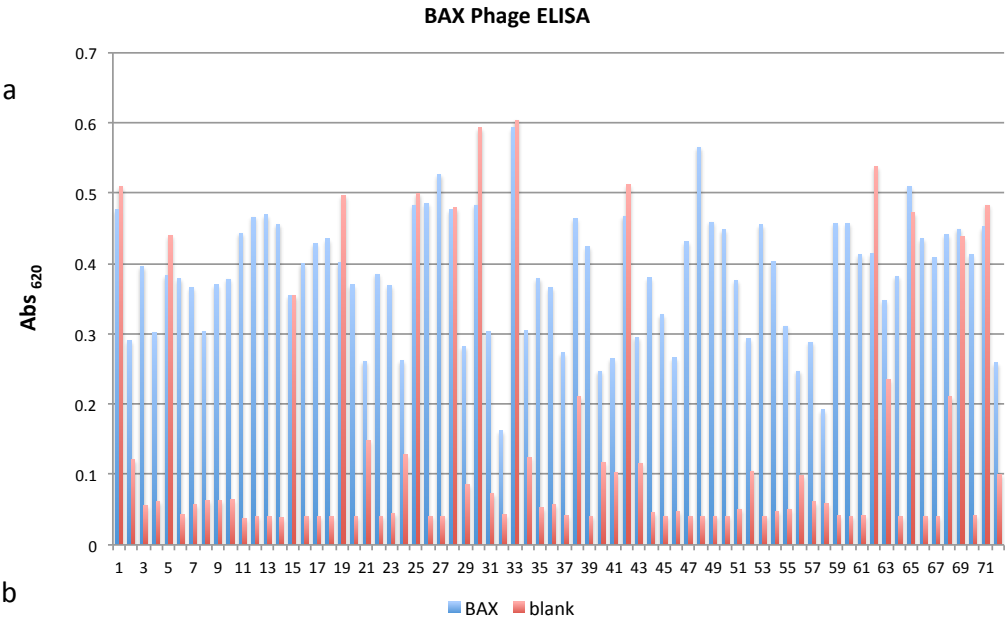

b

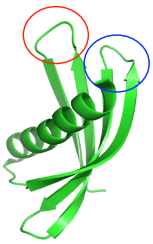

Affimer	Loop 1	Loop 2	#
BAX Aff 1	H V Q A H F W S I	P T E N I M G L K	22
BAX Aff 3	M Q L S S T R L W	T K Y T I Y N P I	1
BAX Aff 6	E E A V P W Y M P	N Y I K L K W H H	1
BAX Aff 7	Q V H M H W Y H A	H L K Q H P L I K	1
BAX Aff 31	N Q A P T F F Q Y	E T K W S N F I Q	1

Figure 4-18 - Identification of Affimers targeting BAX. a) Results of phage ELISA following three Affimer panning rounds against BAX. 72 phage transduced colonies were picked; 31 of these demonstrated increased binding activity against controls (results show differences in absorbance after incubation with Anti-Fd-Bacteriophage-HRP, addition of TMB and allowing HRP:TMB reaction to develop for 2 minutes). b) Sanger sequencing of extracted phagemid DNA identified five unique binders, BAX Aff 1, 3, 6, 7 and 31. Details of residues in the two randomised Affimer loops are shown. Residues are coloured according to their side chain properties (as described in Figure 4-1).

BAX Affimers were dialysed into 50mM sodium phosphate buffer prior to further purification by SEC. Dialysis resulted in some protein precipitation in all cases, with a consequent loss of protein yield prior to column loading (Table 4-10).

Table 4-10 - BAX Affimer expression and initial purification yields. All Affimers were purified using Nickel affinity chromatography. Yield is expressed as the amount of protein detected in the 300mM imidazole elute, measured using a Biorad assay. The final column details the yield after dialysing samples into 50mM sodium phosphate buffer prior to further purification by SEC, with recovered yield in brackets.

Affimer	Yield (mg/L media) - raw	Affimer yield loaded to SEC (mg)
BAX Aff 1	25	9.3 (37.2%)
BAX Aff 3	41	21.7 (52.9%)
BAX Aff 6	33	14.0 (43.8%)
BAX Aff 7	26	10.6 (40.8%)
BAX Aff 31	30	20.8 (69.3%)

Chromatograms of all BAX Affimer SEC elutions are shown in Figure 4-19 and Figure 4-20, with details of expected and actual elution volumes detailed below in Table 4-11.

Table 4-11 – SEC purification of BAX Affimers. Affimers were purified by SEC using a HiLoad 26/60 Superdex S75 pg column. Actual elution volumes are compared with expected monomer peak elution volumes (as determined by comparison against calibration standards described in Chapter 3). Late elution peaks for Aff 1 and Aff 6 demonstrate the tendency of Affimers to interact with the column during SEC purification. The main peaks of other BAX Affimers elute earlier than expected for monomer peaks, indicative of higher order oligomerisation.

Affimer	M_w (Da)	Expected Elution Volume (mL)	Actual Elution Volume (mL)
BAX Aff 1	13388	214	245
BAX Aff 3	12444	218	167
BAX Aff 6	13694	213	245
BAX Aff 7	13656	213	182
BAX Aff 31	12478	217	199

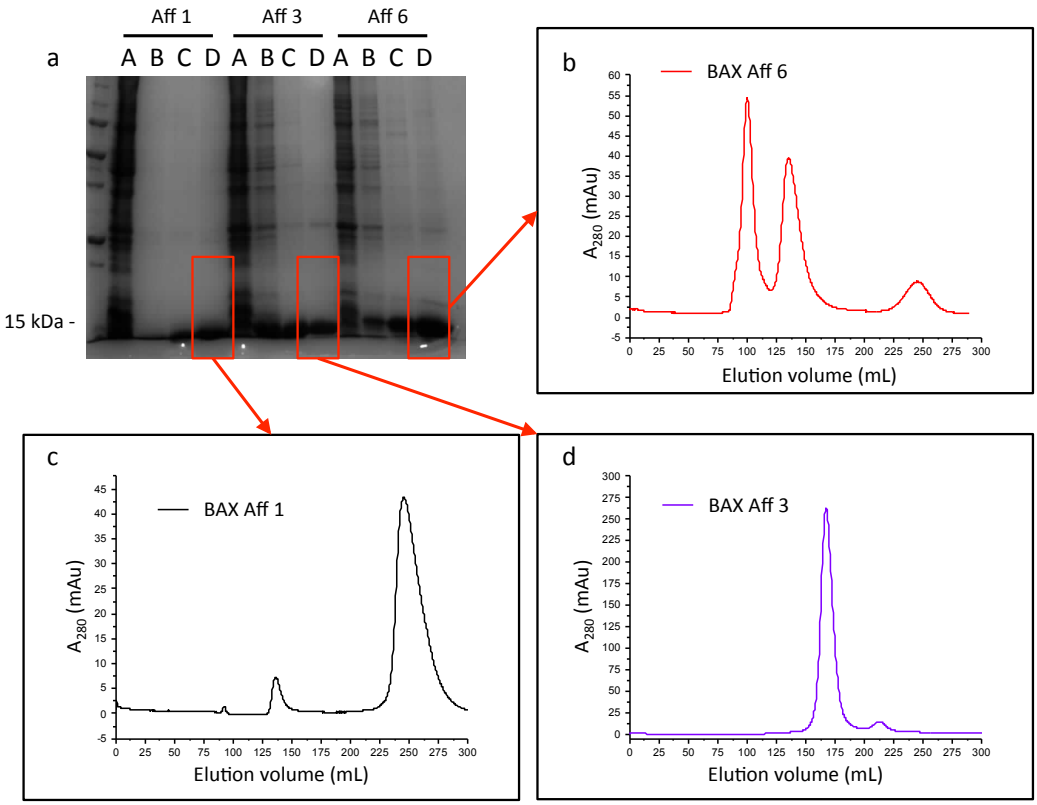

Figure 4-19 - Purification of BAX Aff 1, Aff 3 and Aff 6. a) Coomassie staining of SDS PAGE gel used to analyse Aff 1, Aff 3 and Aff 6 expression. Key: A = clarified lysate; B = CB + 50mM imidazole wash; C = CB + 100mM imidazole wash; D = CB + 300mM imidazole elute. b) – d) SEC chromatograms of Aff 6, Aff 1 and Aff3, with elution peaks at 245mL, 245mL and 167mL respectively.

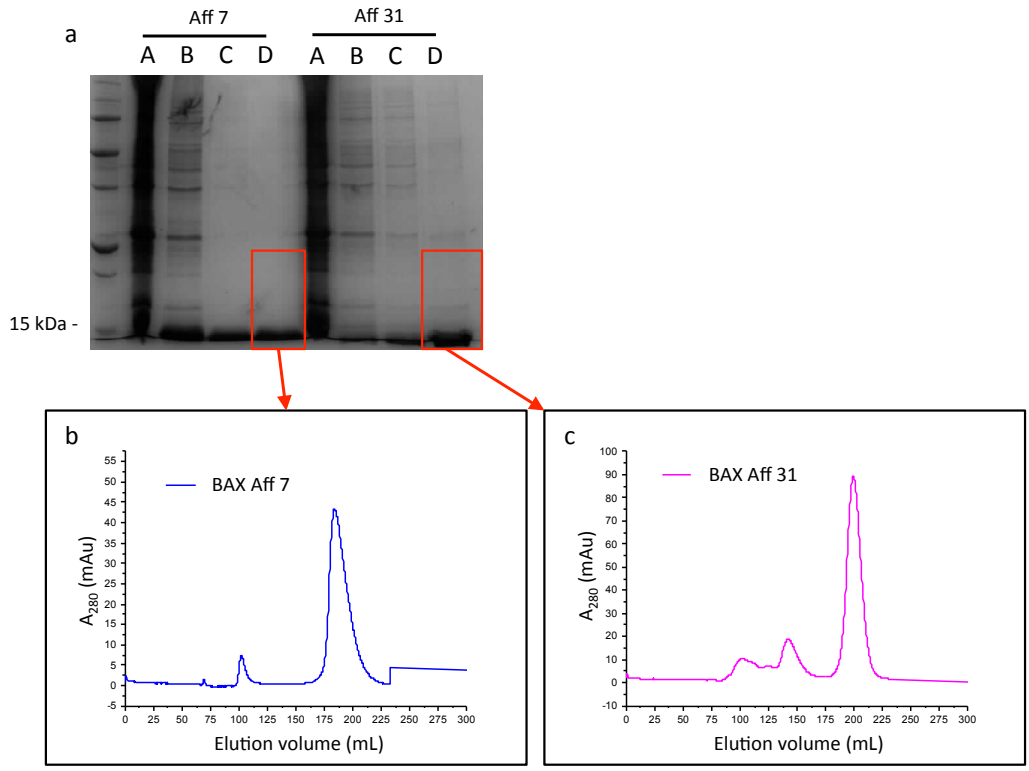

Figure 4-20 - Purification of BAX Aff 7 and Aff 31. a) Coomassie staining of SDS PAGE gel used to analyse Aff 7 and Aff 31 expression. Key as for Figure 4-19. b) – c) SEC chromatograms of Aff 7 and Aff 31, with elution peaks at 182mL and 199mL respectively.

The elution peaks detailed in Table 4-11 were used in binding ELISAs to test for genuine and selective binding, with BAK and MCL1 used as negative controls. The method used was as described previously for BAK Affimers, with initial Affimer concentration of 20μg mL^{-1} and 1:2 serial dilutions across wells in the ELISA plate. Reactions were developed with TMB, quenched after 2 minutes with 2M sulphuric acid, and absorbance read at 450nm. Unfortunately, no absorbance was measured for sample or control plates (data not shown), and no further studies were carried out on BAX Affimers.

4.4 Chapter Summary and Discussion

This chapter describes the results of Affimer panning undertaken against the recombinant BCL-2 family proteins purified and characterised in Chapter 3. The aim was to identify selective binders for the pro-apoptotic effectors BAX and BAK, to augment existing Affimers for MCL1 and BCL-X_L with Affimers selectively targeting BCL-2, and, through the completion of a comprehensive cross-panning exercise, to produce cross-reactive Affimers able to simultaneously target multiple pro-survival BCL-2 family proteins. The ideal outcome would be a 'toolkit' of Affimers, whose interactions with their target proteins could be structurally investigated to uncover novel interactions with known binding sites, potentially uncover previously unknown binding surfaces, and provide structural data to aid in the design of small molecules able to modulate apoptotic activity in cells.

Disappointingly, the cross-panning exercise for pro-survival BCL-2 family members failed to produce any usable binders, most likely due to limited levels of sequence homology between our recombinant target proteins. Cross-reactive small molecules able to inhibit multiple BCL-2 family members have already been developed: ABT-737 and ABT-263, as dual inhibitors of BCL-2 and BCL-X_L were mentioned previously. Additionally, the natural product Gossypol and some of its rationally designed derivatives have proven to be true pan-inhibitors of the main pro-survival BCL-2 family members, binding to all of BCL-2, BCL-X_L and MCL1 with sub micromolar affinities [214, 309]. Cross panning with Affimers to identify dual or triple inhibitors was always considered unlikely to yield better results than the rational, design based approaches undertaken to produce these small molecules. However, the chance that the phage display based approach might uncover novel cross-reactive binding sites on our target proteins meant that undertaking this work was still a worthwhile exercise.

It was also disappointing that all of the Affimers identified from the pan against BAX appeared to be false positives, with no genuine binding activity demonstrated in later assays. The presence of false positives is a common

artefact of phage display experiments. Phage may bind to other components in the experimental system, such as biotin, streptavidin, or potential contaminants in the sample. False positives may also occur from clones that simply benefit from a faster propagation rate, with increased replication giving them an advantage in the overall phage pool [310]. For this reason and as a more general point, there is no correlation between the frequency of appearance of a specific clone at the end of the panning process and its potential potency as a binder / inhibitor of its target protein.

Positive results were obtained from the Affimer pan against BCL-2: four unique Affimer sequences were identified that showed binding affinity for BCL-2, and were able to characterise three of these as legitimate and selective binders for the target protein. This means we now have a small library of Affimers shown to selectively bind our three pro-survival BCL-2 family members. Future work should include structural investigations into how these Affimers interact with their target proteins and whether novel binding sites are engaged, together with cell based assays to ascertain the ability or otherwise of these Affimers to modulate mitochondrial apoptosis *in cellulo*.

In the last decade, a great deal of research has been carried out to identify molecules that interact with the BCL-2 family. BH3 mimetics have been developed that have potential to act against various forms of cancer, but they are all targeted against pro-survival members [245, 249, 257, 311]. By comparison, relatively little progress has been made in developing molecules to modulate the activities of BAX and BAK. The fact that four Affimers were identified as selective binders of BAK is therefore potentially of great interest, especially as no cross reactivity was seen against BAX.

Notwithstanding the fact that BAK dysregulation is rarely employed as a survival mechanism by cancer cells, it remains true that molecules able to constitutively activate BAK could provide the basis for powerful new anti-cancer therapies; the use of such molecules would also avoid the deleterious side effects seen in the clinic when administering inhibitors of

pro-survival BCL-2 family members. Conversely, the ability to dampen or inhibit the activities of BAK may also be useful in limiting the levels of ischaemic cell death in patients suffering heart attack or stroke.

Until very recently, there were no reported specific inhibitors of BAK. Brouwer and co-workers have since described a BH3 derivative (BIM like peptide), incorporating a non-natural amino acid, which acted to inhibit BAK. Structural and biochemical data from this study provide evidence that ligands forming a stable complex with BAK at its activation site (BC groove) can block induction of apoptosis [312], thereby acting as inhibitors. There is also a body of evidence indicating that BAK activation involves *low* affinity binding of a BH3 only direct activator at the BAK BC groove, with subsequent conformational changes that expose the BAK BH3 domain [50], leading first to dimerisation, then higher order oligomerisation and apoptotic pore formation. On limited data obtained by SPR[6], our Affimers appear to bind BAK with low affinity and are therefore less likely to carry out an inhibitory role, but may have BAK activating features. Future work should include further assays to characterise the binding affinities of identified Affimers for BAK, structural studies to determine where and how binding is taking place, and cellular assays to determine whether our BAK binding affimers are able to modulate BAK activity *in cellulo*, in either activating or inhibitory roles.

---

[6] To generate a full kinetic profile by SPR for interaction of Affimer and target protein (or more generally analyte and ligand), and obtain the binding constants (k_{on}, k_{off}, K_d), the interaction should be measured using a broad range of protein concentrations that span a range from 10x greater to 10x lower than the expected K_d. Experiments established legitimate binding of Affimers to BAK, but a broader range of protein concentrations should be used to obtain a more accurate figure for binding affinity.

Chapter 5 - Investigations into mechanisms underpinning the oligomerisation of BAX

BAX acts as a pro-apoptotic effector, existing as a quiescent cytosolic monomer in healthy cells, but migrating to the mitochondrial outer membrane (MOM) under conditions of cytotoxic stress, where it oligomerises to cause mitochondrial outer membrane permeabilisation (MOMP). MOMP, which allows cytochrome c to escape to the cytosol, is considered the point of no return in mitochondrial apoptosis and effectively commits the cell to undergo apoptotic cell death. Despite intense levels of study, the molecular mechanisms underpinning oligomerisation and BAX induced MOMP remain unclear, though there is now a good body of evidence to suggest that BAX monomers initially form symmetric BH3 in groove homo-dimers (as described in the Introduction), and that these constitute the basic oligomerisation unit for BAX and its homologue BAK [52, 195-199]. However, due to an absence of high resolution structural data, the mechanism by which these dimers combine to form higher order oligomeric structures remains one of the key outstanding questions in the field of apoptosis research [52, 313, 314].

This chapter describes preliminary structural investigations undertaken with the aim of making progress towards answering this question.

5.1 BAX treatment with Tween20 induces oligomerisation

Early expression trials undertaken by the group of Professor Jane Clarke at the University of Cambridge failed to produce monomeric BAX. Instead, SEC results suggested BAX oligomerisation, with production of a single chromatogram peak thought to represent soluble hexameric species. These early trials purified BAX in the presence 0.2% Tween20, which is not unusual as moderate concentrations of nonionic detergents such as Tween are commonly used during protein purification for their ability to compromise the integrity of cell membranes, aid in the lysis of cells and help enable the

extraction of soluble protein. However, in the case of some BCL-2 family members, including BAX, it has also been shown that treatment with non-ionic detergents can cause protein dimerisation [52, 201], and higher order structures may also be formed under these conditions.

When a further series of purifications were carried out in the absence of Tween20, soluble protein was still produced, but in this case SEC showed no oligomer peak and BAX eluted from the column as a monomer. Interestingly though, subsequent incubation of purified BAX monomers with Tween20 (24 hours, room temperature) caused the formation of oligomers, with the same oligomeric peak reproduced on the SEC chromatogram.

5.2 Structural studies of BAX oligomers

The Tween20 induced BAX oligomers described above eluted from SEC in a single peak, representing an apparently homogenous species. It was questioned whether these oligomers might be forming regular structures, and whether these structures could provide data pertinent to understanding the mechanisms underpinning BAX oligomerisation at the MOM. Existing evidence supporting potential mechanisms for BAX dimerisation and subsequent oligomerisation is predominantly from biochemical studies [39, 52, 195-201] [202, 203]. To better investigate the nature of the oligomers formed, experiments were designed and carried out with the aim of augmenting this evidence using structural techniques.

5.2.1 Crystallisation trials

Preliminary crystallisation trials were carried out. Tween20 treated BAX, concentrated to 1mM[7] was screened for crystal production against 384 different buffer conditions. Unfortunately, the oligomerised protein failed to produce crystals under any of the tested conditions. This was possibly due

[7] Tween20 treated BAX for use in preliminary crystallisation trials was kindly provided by Basile Wicky, Jane Clarke group, University of Cambridge.

to the presence of residual Tween20 causing a fall in surface tension in the protein samples, which prevented drop formation on crystal plates.

5.2.2 Electron Microscopy

The apparent homogeneity of the BAX oligomer sample, which made it appropriate for use in crystal trials also signified its potential suitability for analysis by cryo-electron microscopy (cryo-EM). In recent years, cryo-EM has emerged as a powerful tool for solving structures at high resolution (<5Å) [315-318]. Many of these structures have been for proteins or complexes in the megadalton size range, which is the traditional domain of cryo-EM. Indeed, until very recently, there was thought to be a lower molecular size limit of around 300 kDa for use of this technique. In 2014, Lu and co-workers used cryo-EM to solve a 170kDa structure from the γ-secretase complex at 4.5Å resolution [319], and since then, continued advances in detector technology and software have combined to push the lower size limit further still, meaning that it *could* be possible to analyse BAX oligomers using cryo-EM. However, as recombinant BAX monomers are 19kDa, the reported hexameric oligomers would have a molecular weight of approximately 114kDa, still towards the extremes of the lower size limit, even at current capabilities.

While excellent results can be achieved using cryo-EM, it is a relatively high cost technique, both in terms of time and resources. Therefore, to visually check for levels of structural homogeneity, BAX samples were first analysed using negative stain transmission EM, a technique which benefits from being far cheaper than cryo-EM, with relatively easy sample preparation and loading procedures.

5.2.2.1 Sample preparation and analysis

A Superdex S200 5/15 GL column (GE Healthcare) was calibrated using a subset of the protein standards listed in Table 3.1. The peaks shown in Figure 5-1 then provided data points from which to plot a calibration curve for use in testing our samples of untreated and Tween20 treated BAX for evidence of oligomerisation (Figure 5-2).

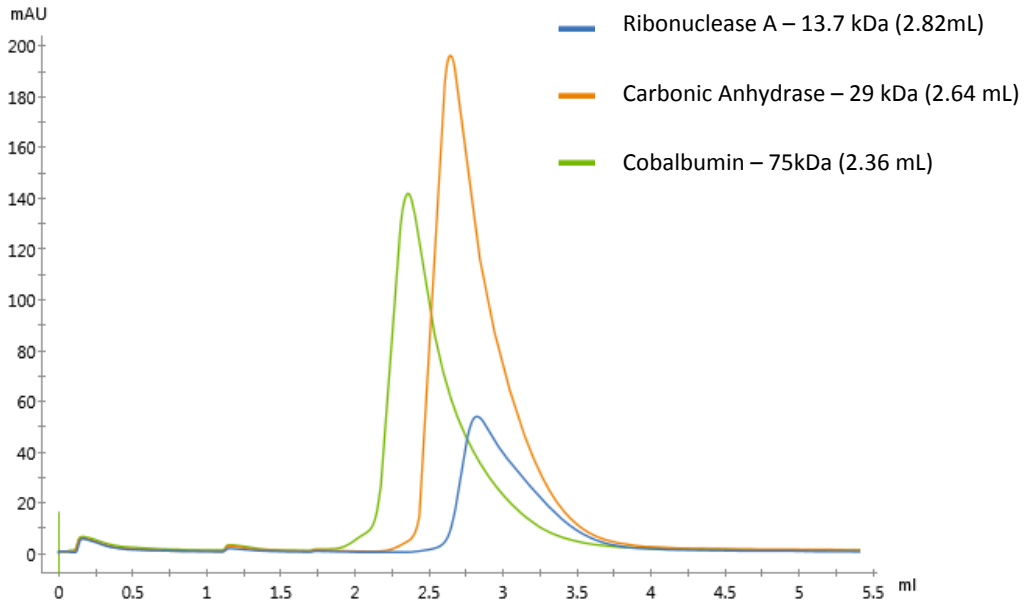

Figure 5-1 – Chromatogram of elution peaks for protein standards used in Superdex S200 5/150 GL column calibration.

Monomeric BAX was purified as described in Chapter 3 and concentrated to 50μM, then an aliquot was taken and incubated for 24 hours at room temperature with 0.2% Tween20. Untreated and Tween20 treated BAX samples were assayed for evidence of oligomerisation using analytical SEC. Untreated BAX eluted predominantly as a monomer, with a main elution peak at 2.79mL. A small shoulder of higher order species was also seen. By contrast, the Tween20 treated sample eluted at 2.35mL.The position of the elution peak is indicative of BAX tetramers, and not the putative hexameric species previously reported by the Clarke group in Cambridge, for which an elution peak at around 2.22mL would be expected according to our calibration calculations.

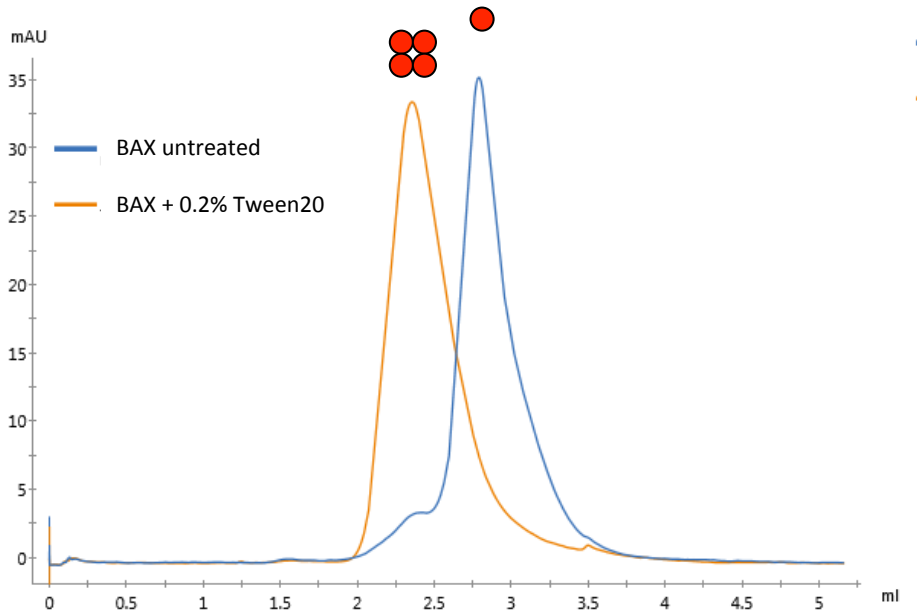

Figure 5-2 – Analytical SEC of BAX samples. The untreated sample (blue) elutes with a main monomer peak at 2.79mL, with a small shoulder of higher order oligomers. The Tween20 treated sample (orange) elutes at 2.35mL. This matches the elution peak for the 75kDa protein calibration standard Cobalbumin, and indicates a tetrameric species, conflicting with data previously reported by the Clarke group in Cambridge.

For comparison, analysis was carried out on a sample of BAX oligomer provided by the Clarke group: surprisingly, this also produced a peak at 2.35mL with an attached shoulder indicating some degradation, but no evidence of higher order oligomers larger than the tetramers indicated by our

column calibration (Figure 5-3). BAX oligomers had previously been shown to be stable at 4°C for over six weeks, so there was no question of wholesale degradation in the Cambridge sample, and the likelihood was that the same oligomeric species were being seen in both locations.

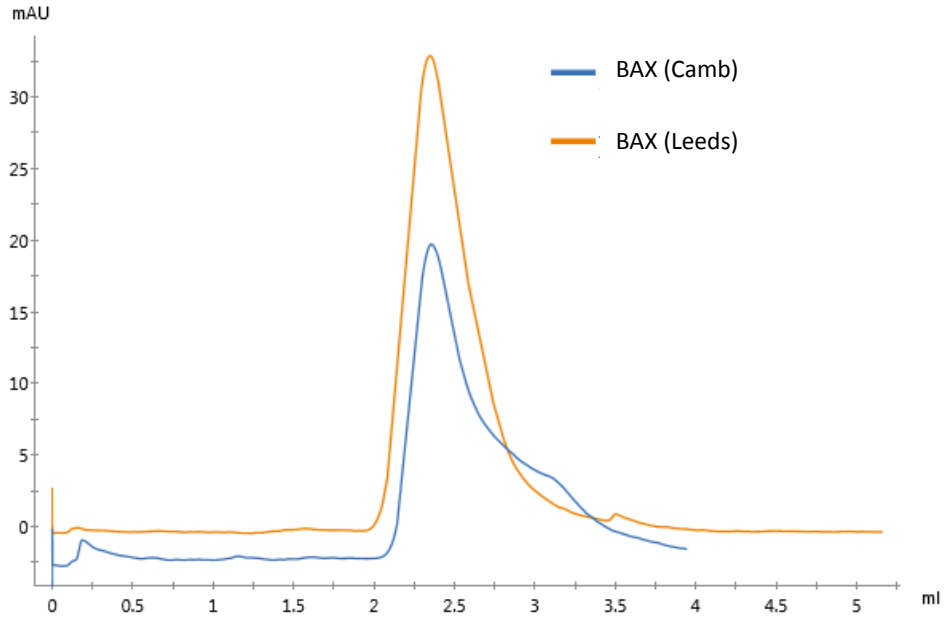

Figure 5-3 – Analytical SEC to compare Tween20 treated BAX samples purified at Leeds and Cambridge. Both samples produce elution peaks at 2.35mL. The shoulder on the peak for the Cambridge sample indicates some oligomer dissociation, but there is no evidence of higher order BAX species larger than tetramers.

SEC results indicated that incubating BAX with Tween20 for 24 hours allowed for full conversion of monomer to oligomer. Work carried out by Subburaj and co-workers to determine the kinetics of BAX oligomerisation at membranes reported monomers assembling into dimers and higher order structures very rapidly, in under one minute [314]. To test whether this was also true under our experimental conditions, we prepared a sample of BAX incubated with 0.2% Tween20 for five minutes, and tested it for presence of oligomerisation peaks using analytical SEC.

The results shown in Figure 5-4 appear to support the analysis carried out by Subburaj, with rapid oligomer formation seen. Though the largest

chromatogram peak is still monomeric, a significant secondary peak of oligomeric species is also seen.

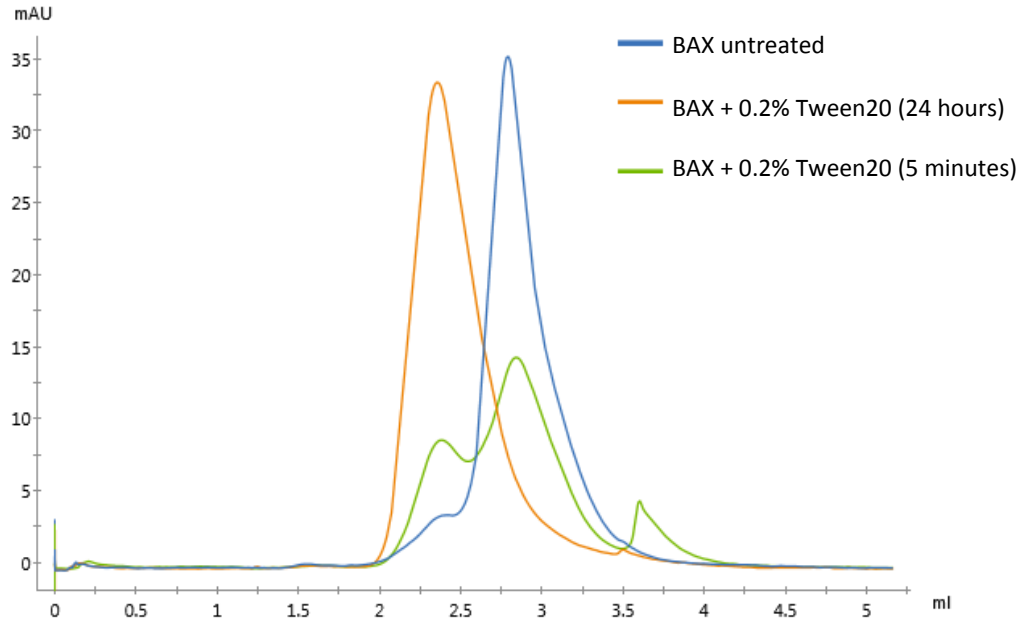

Figure 5-4 – Analytical SEC to compare effects of Tween20 treatment of BAX over time. BAX incubated at room temperature for 24 hours with 0.2% Tween20 results in full conversion of monomer to oligomer (orange peak). BAX incubated with Tween20 at room temperature for 5 minutes (green peak) shows evidence of rapid BAX oligomer formation on exposure to detergent.

5.2.2.2 Negative Stain EM analysis

To begin negative stain EM analysis, a sample dilution series of oligomerised species was tested to ascertain the optimum protein concentration for use, one at which high numbers of molecules were visible, but also sufficiently well dispersed to allow individual particle picking in later analysis. BAX at a concentration of 10μM was treated with 0.2% Tween20 and allowed to incubate for 24 hours at room temperature. The sample was subjected to a set of 10x serial dilutions, with each dilution loaded to a glow

discharged carbon coated copper grid[8], which was then stained with 1% uranyl acetate and viewed to check for levels of particle dispersal. Repeats of this process established an optimum protein concentration of 10nM.

Two 50µL samples of 10µM BAX were then prepared for analysis. One sample was treated with 0.2% Tween20, and 20µL aliquots were removed after 5 minutes and 24 hours. Both aliquots, together with a control sample of untreated BAX were quickly loaded to grids as described above; immediately prior to loading, all samples were diluted 1:1000 in 50mM sodium phosphate buffer to achieve the optimum 10nM protein concentration.

5.2.2.2.1 Untreated BAX

Samples were imaged at a calibrated magnification of 25,500x. Untreated BAX presented as extremely small, monomeric particles, with the presence of a small number of much larger heterogeneous aggregates (image not shown).

5.2.2.2.2 BAX incubated with Tween20 (5 minutes)

The sample treated with Tween20 for 5 minutes contained a large quantity of monomeric BAX, together with a heterogeneous mix of small oligomeric species and a very small number of larger protein aggregates (Figure 5-5).

[8] Prior to sample loading the grids were glow discharged; this process covers the carbon surface of the EM grid with negative ions, making it hydrophilic and more amenable to sample loading.

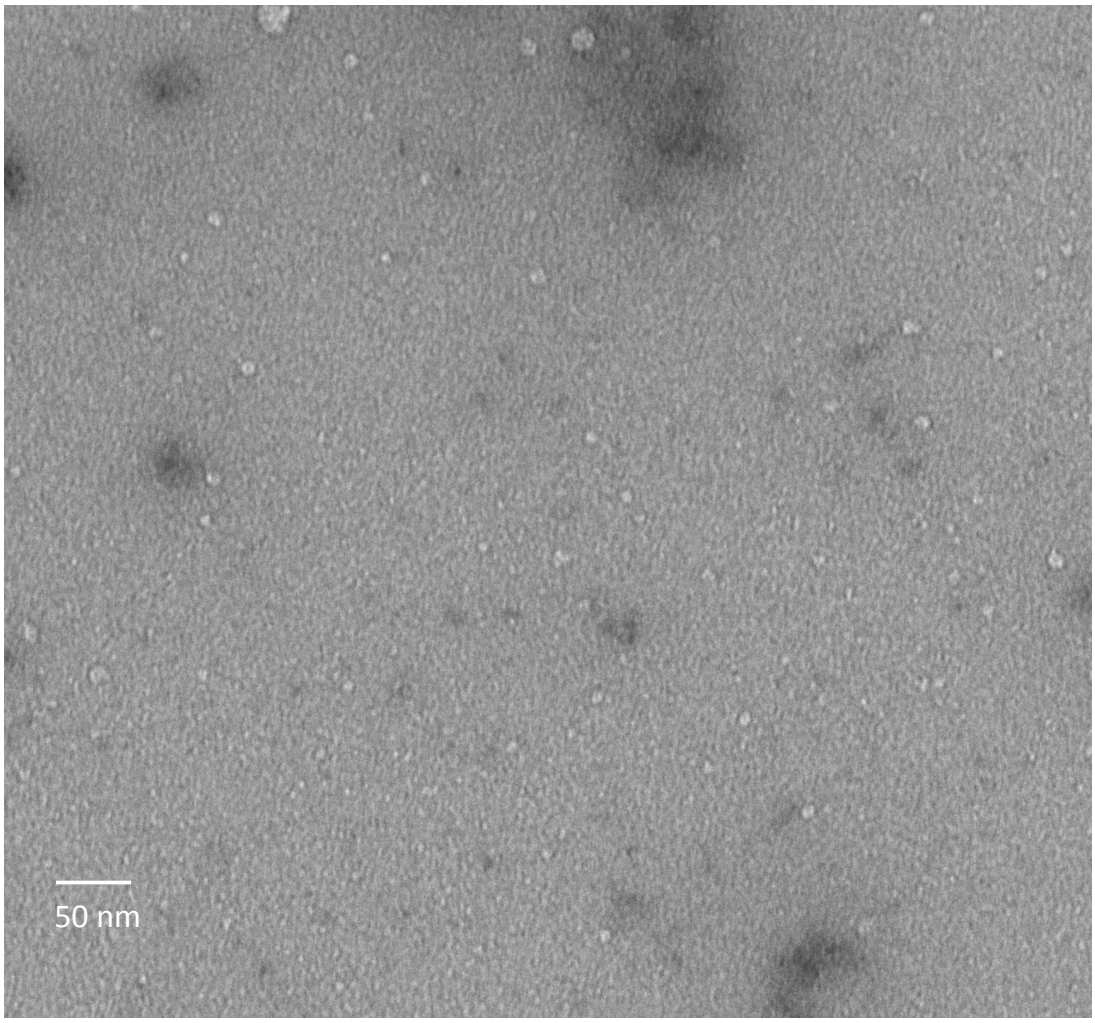

Figure 5-5 – Sample micrograph of BAX incubated with 0.2% Tween20 for 5 minutes

To better visualise the species present, a data set of images was taken and used to produce particle class averages. The data set used comprised 32 micrographs, from which 500 protein particles were manually picked as a representative sample of species present. Utilising RELION software, these were used as templates for an auto-picking exercise, which returned a total pool of 4736 particles. Three rounds of 2D image alignment and classification refined this pool down to 2810 particles, comprising the nine most common class averages, which are shown in Figure 5-6.

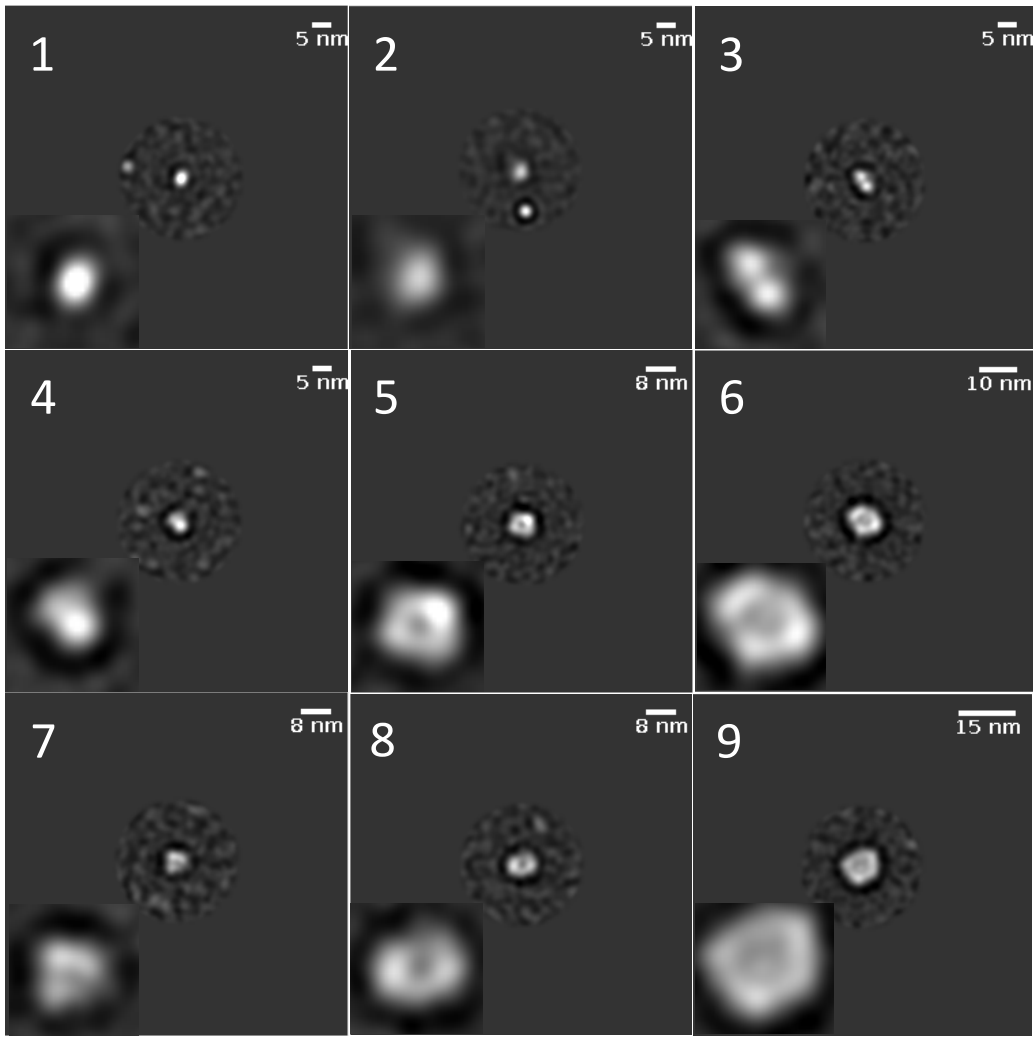

Figure 5-6 – Calculated particle class averages for BAX incubated with 0.2% Tween20 for 5 minutes. 32 micrographs were taken and RELION software was used to pick 4736 particles, which were then subjected to three rounds of 2D image alignment and classification. This refined the pool down to 2810 particles represented in nine class averages. Species 1-9 are shown in descending order of prevalence in the data set.

Images 1-9 are shown in descending order of their prevalence in the data set, though there is little discrepancy between the most and least commonly occurring, as seen in Table 5-1; 1 appears 391 times (13.91% of total data set), 9 appears 263 times (9.36%). Class averages other than those shown were either of indistinct images, or appeared with very low frequency in the data set. Though some images appear to show distinct species, for example monomeric (1), dimeric (3) or tetrameric (5), the resolution obtained for these class averages is insufficient for definite statements to be made about the oligomerisation state of BAX seen in all cases.

Table 5-1 – Numerical analysis of particle class averages for BAX incubated with 0.2% Tween20 for 5 minutes. Frequency of appearance, and percentage totals of the refined data set are shown.

Class #	Frequency	% Total		Class #	Frequency	% Total
1	391	13.91		6	274	9.75
2	346	12.31		7	274	9.75
3	336	11.96		8	271	9.64
4	333	11.85		9	263	9.36
5	322	11.46				
				TOTALS	**2810**	**100.00**

A better idea of the oligomerisation states seen may be achieved by measuring the apparent dimensions of the species in each image, then comparing them to the estimated size of a BAX monomer. Figure 5-7 shows monomeric recombinant BAX, with approximate dimensions determined using the Pymol measurement tool. Depending on its orientation on the EM grid, such a monomer should appear as a particle with dimensions between 3.3 and 4nm.

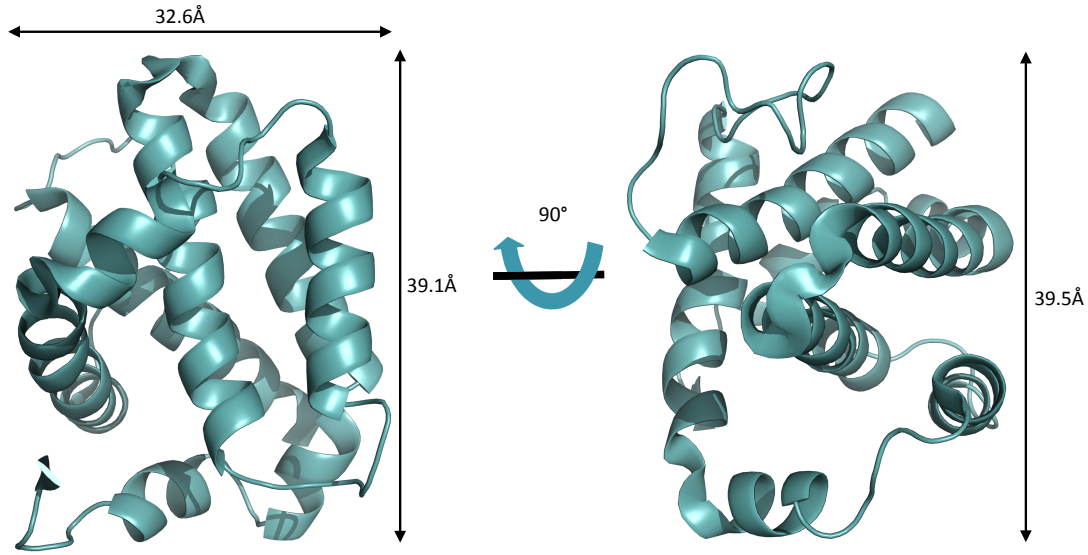

Figure 5-7 – Approximate dimensions of a BAX monomer. Molecular dimensions were determined using the Pymol measurement tool (PDB 1F16).

Using this information, it can be *speculated* that in Figure 5-6, monomeric species are seen in images 1 and 2, dimeric species in images 3 and 4,

trimers in image 7, tetramers in images 5 and 8, and hexamers in images 6 and 9. This represents a more heterogeneous mix of oligomeric states than would be suggested by the chromatogram in Figure 5-4. The presence of apparently hexameric species within this mix also casts doubt on whether this peak is, in fact, representative of tetramers.

5.2.2.2.3 BAX incubated with Tween20 (24 hours)

The 24 hour Tween20 treated sample contained a much reduced quantity of monomeric BAX, together with a heterogeneous mix of small oligomeric species (Figure 5-8), in significant contradiction to the single homogenous peak seen on the SEC chromatogram in Figure 5-2.

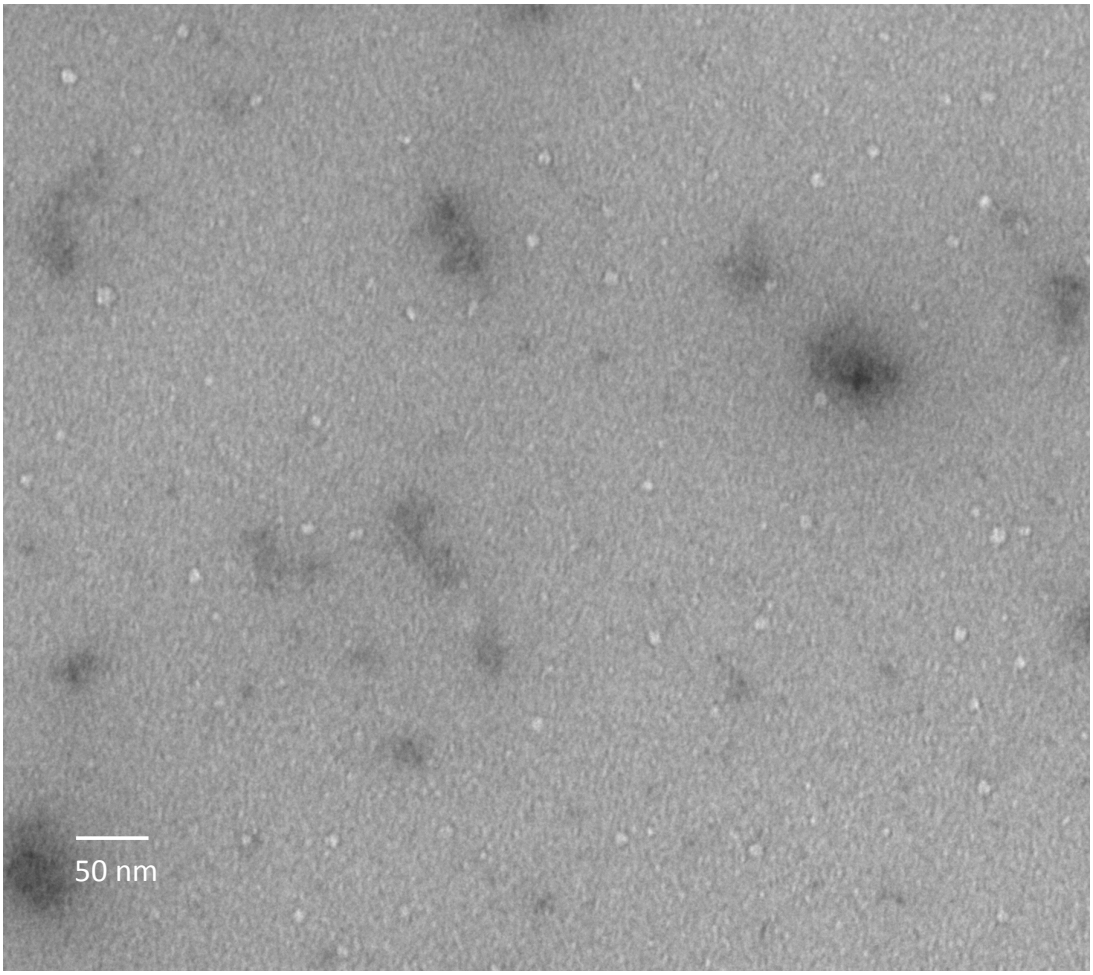

Figure 5-8 – Sample micrograph of BAX incubated with 0.2% Tween20 for 24 hours.

A data set of images was taken and used to produce particle class averages, as described previously. 500 protein particles were manually picked from 36 micrographs to act as templates for an auto-picking exercise, which returned a total of 6998 particles. Three rounds of 2D image alignment and classification were carried out, refining this pool down to 5150 particles. These comprise the nine most common class averages, shown in Figure 5-9.

As with the previous sample, images 1-9 are shown in descending order of their prevalence in the data set, and details of frequency of appearance together with the percentage of total pool comprised by each species are shown in Table 5-2. The images in this dataset are particularly difficult to interpret. Image 5 would appear to present a BAX monomer; 7 and 9 have similar features to the putative hexameric structures assigned to images 6 and 9 in Figure 5-6; the remainder do not even warrant speculation as to their oligomeric state, though it is interesting to note that images 3, 6 and 8 all appear to show the same species in different orientations.

The heterogeneity of species seen in this sample means that it is unsuitable for further analysis by cryo-EM at present. Optimisation of sample preparation protocols will be required to progress this work further.

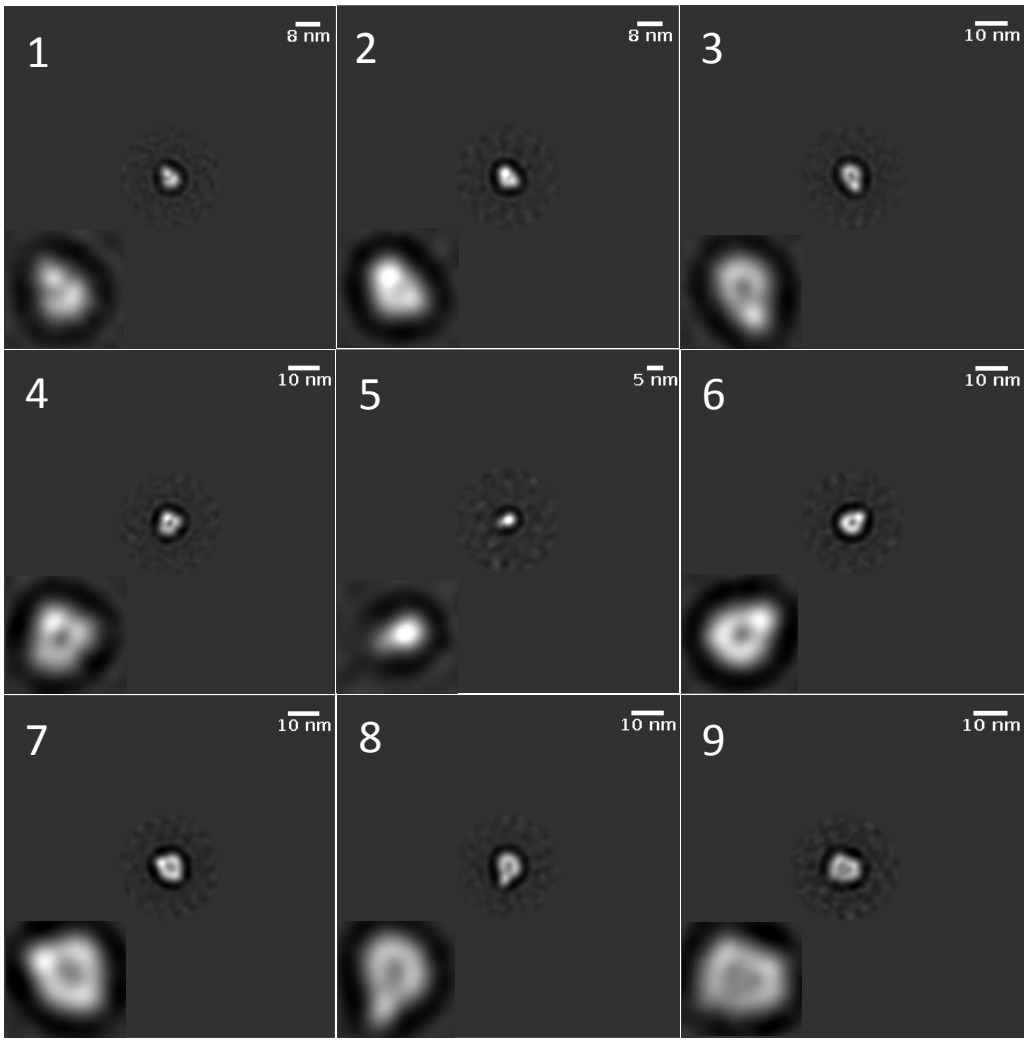

Figure 5-9 - Calculated particle class averages for BAX incubated with 0.2% Tween20 for 24 hours. 36 micrographs were taken and RELION software was used to pick 6998 particles, which were then subjected to three rounds of 2D image alignment and classification. This refined the pool down to 5150 particles represented in nine class averages. Species 1-9 are shown in descending order of prevalence in the data set.

Table 5-2 - Numerical analysis of particle class averages for BAX treated with 0.2% Tween20 for 24 hours. Frequency of appearance, and percentage totals of the refined data set are shown.

Class #	Frequency	% Total		Class #	Frequency	% Total
1	882	17.13		6	504	9.79
2	686	13.32		7	441	8.56
3	672	13.05		8	420	8.15
4	656	12.74		9	350	6.79
5	539	10.47				
				TOTALS	**5150**	**100.00**

5.3 Chapter Summary and Discussion

This chapter describes structural studies carried out with the aim of helping to elucidate the mechanisms underpinning BAX oligomerisation.

It was shown that adding 0.2% Tween20 to recombinant BAX monomers induced oligomerisation, with full conversion from monomer to oligomer within 24 hours of incubation at room temperature. A 0.2% concentration is over 20 times the critical micelle concentration (CMC) for this detergent, so this was by no means mimicking physiological conditions. The aim was to collect structural data on the oligomers formed: BAX dimerisation is generally accepted as the initiating action and it was hoped that our structural studies would provide evidence for how dimers then combine to form higher order oligomers.

Analytical SEC of Tween20 treated BAX produced a single chromatogram peak, eluting in the same place as cobalbumin, the 75kDa protein standard used in column calibration. This suggested a BAX tetramer, and not the hexameric species reported by the Clarke group at the University of Cambridge. A Tween20 treated sample provided by the Clarke group produced an identical peak when analysed on the same column. The stability of Tween20 induced BAX monomers precluded the chance of wholesale sample degradation, raising the possibility of an instrumental error relating to calibration of our column.

Structural studies were carried out using negative stain EM. Untreated BAX appeared monomeric, matching results from analytical SEC. Class averages calculated for BAX incubated with Tween20 for 5 minutes presented a heterogeneous mix of monomeric and oligomeric species. The SEC chromatogram suggested two major species (monomers and tetramers), but the particle class averages produced also appeared to include dimers, trimers and hexamers, with the presence of putative hexamers raising further doubt on the reliability of our SEC column calibration. Finally, BAX incubated with 0.2% Tween20 for 24 hours also presented a heterogeneous

mix of monomers and oligomeric species. Although class average image resolution made it difficult to identify each species with certainty, a reduction in monomers and an increase in higher order oligomers was apparent, as would be expected from the longer Tween20 incubation period.

As stated, image resolution of the class averages made it difficult to identify oligomeric species with certainty, but it is notable in both Tween20 treated samples that many of the oligomers appear to comprise monomers arranged in pore like structures (Figure 5-6, Figure 5-9). Mitochondrial apoptosis is initiated on induction of MOMP caused by BAX (or BAK) oligomerisation, allowing molecules including cytochrome c to escape to the cytosol from the mitochondrial. The molecular dimensions of cytochrome c are shown in Figure 5-10a below. Simple observational analysis of putative tetramers (Figure 5-10b) and hexamers (Figure 5-10c) indicates pore sizes of approximately 3nm and 5nm respectively, both of sufficient size to allow the passage of cytochrome c (it is worth iterating here, though, that the experimental conditions in no way mimic the physiological cellular environment in which BAX oligomerisation takes place).

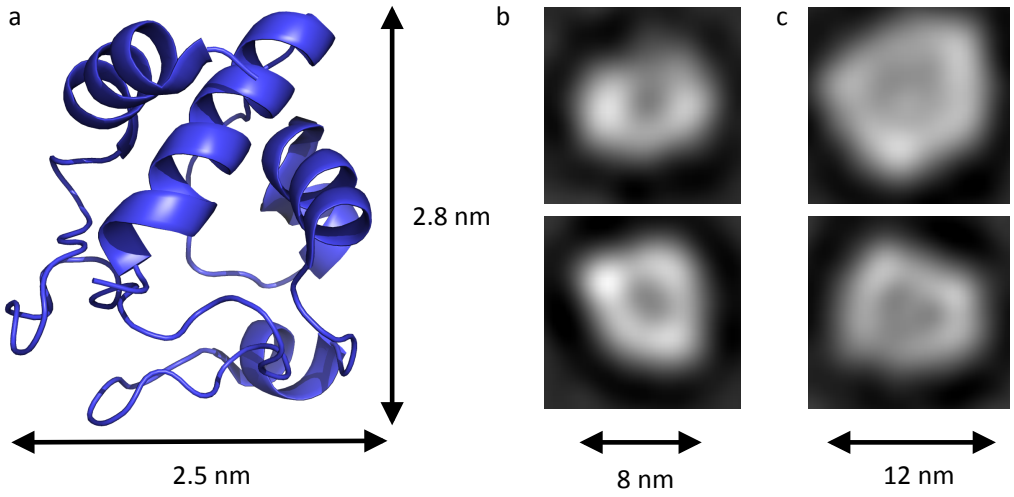

Figure 5-10 – Analysis of putative pore like structures in BAX oligomers. a) Approximate molecular dimensions of a cytochrome c monomer Molecular dimensions were determined using the Pymol measurement tool (PDB 3NWV). b) Putative BAX tetramers from Figure 5-6 (8) (top) and Figure 5-9 (7) (bottom) indicate a pore with approximate diameter of 3nm. c) Putative BAX hexamers from Figure 5-6 (9) (top) and 5-9 (9) (bottom) indicate a pore with approximate diameter of 5nm.

Notwithstanding the comments above, it was questioned why a heterogeneous mix of particles was being seen at all, when the single oligomeric peak seen on SEC suggested the presence of a single homogenous species. The discrepancy between the single species peak in the analytical SEC chromatogram and the mix of particles seen in EM may be explained in a number of ways. It may simply be due to artefacts caused during EM sample preparation, as production of a pure biological sample does not necessarily result in a homogenous sample when viewed by EM [315]. Another plausible explanation is that the heterogeneity seen was caused by the 1:1000 sample dilution carried out immediately prior to loading sample to EM grids, which reduces the Tween20 concentration in the sample to below its CMC. Incubating BAX with Tween20 had shown to induce a rapid rate of oligomer formation; it could also be the case that dilution of Tween20 to sub-CMC concentrations causes an equally rapid disintegration of BAX oligomers. Indeed, some of the class average images seen in Figure 5-9 could be interpreted as showing oligomeric species that have started to dissociate.

Regardless of the reason, the heterogeneity currently seen in our oligomer sample makes it unsuitable for study by cryo-EM. To progress this work, methods for isolating and stabilising BAX oligomers need to be developed and optimised, together with protocols for removing detergent without causing oligomer dissociation. A credible approach would be to use chemical cross-linking of Tween20 induced oligomers, followed by sample dialysis into detergent free buffer. If successful, this approach would also enable a fresh round of crystallisation trials to be carried out, using samples of detergent free BAX oligomers. Our recombinant BAX protein contains 7 lysine residues, 13 aspartates and 10 glutamates, which would facilitate cross linking via primary amines or carboxyl groups.

It will be interesting to obtain confirmation of whether the dominant oligomeric species is tetrameric, as indicated in our analytical SEC assays, or hexameric, as reported by the Clarke group and supported at least in part

by the presence of putative hexamers in our EM images. BAX tetramers would be 75kDa and hexamers 114kDa, neither at a size that would make them obvious candidates for structure determination by cryo-EM alone. It is worth noting, however, that the 66kDa structure of haemoglobin has recently been solved by this means [320].

Chapter 6 – Thesis Summary and Future Work

Apoptosis is an essential process during embryonic development, acts as a balance to mitosis in maintaining a steady level of healthy cells in adults, and provides a clean and efficient mechanism for the removal of old, diseased or infected cells before they become a risk to the health of surrounding tissues.

The BCL-2 family of proteins are important regulators of apoptosis; dysregulation of BCL-2 family activity in the cell is implicated in the progression of many forms of cancer, and is also a common feature in chemo-resistance [17]. The development of molecules able to bind and modulate BCL-2 family interactions as the basis for novel therapies is thus highly desirable, and has been the subject of a great deal of research effort. Techniques including structure based design and peptidomimetic approaches have been used to notable success in this area, but few of the synthesised molecules have successfully transitioned from laboratory to clinic, often due to their lacking potency as single agents, or the rapid appearance of resistant clones[262].

The first part of this project was designed to expand the existing library of BCL-2 family binding molecules. It employed a novel approach, combining the use of phage display to identify selective binding sequences by probing the surface of target proteins, with the subsequent expression of those binding sequences in purified non-antibody scaffold proteins called Affimers [280]. It aimed to develop a 'toolkit' of Affimers, whose interactions with their target proteins could be structurally investigated to uncover novel interactions with known binding sites, potentially uncover previously unknown binding surfaces, and provide structural data to aid in the design of small molecules able to modulate apoptotic activity in cells. Five BCL-2 family proteins, BCL-2, BCL-X_L, MCL1, BAX and BAK, were selected as targets for study, comprising a good cross section of pro- and anti-apoptotic members. Recombinant versions of each of these proteins were expressed in bacteria, purified, and characterised using biophysical assays.

Affimers that selectively bound to MCL1 and BCL-X_L had been produced in earlier work carried out by the Edwards group. The project was able to augment these with selective binders for BCL-2, thereby completing a set of Affimers able to selectively bind to the three chosen pro-survival targets.

Successful experiments were also carried out to identify, purify and characterise four Affimers that bound selectively to the pro-apoptotic effector BAK. As the majority of molecules developed to modulate the BCL-2 family have been targeted against pro-survival members, this result could potentially be of great interest [245, 249, 257, 311]. Though BAK dysregulation is rarely seen in cancer, molecules able to constitutively activate BAK could nonetheless provide the basis for powerful new anti-cancer therapies.

Though novel binders were identified for BCL-2 and BAK, further work is required to fully characterise the nature of their binding interactions with their target proteins. Time constraints also precluded any assays to test these Affimers for the induction of pro- or anti-apoptotic activity in cellular systems. To progress this part of the project, future work will include structural investigations into how BCL-2 and BAK binding Affimers interact with their target proteins and whether novel binding sites are engaged, together with cell based assays to ascertain the ability or otherwise of these Affimers to modulate mitochondrial apoptosis *in cellulo*.

In order to carry out its pro-apoptotic activities in the cell, BAX must first oligomerise at the mitochondrial outer membrane (MOM). A good body of evidence exists that suggests BAX monomers first form symmetric BH3 in groove homo-dimers, but the structural details for how these dimers combine to form higher order oligomeric structures remains unresolved [52, 313, 314]. The second part of this project was designed to shed some light on this mechanism, which remains one of the key outstanding questions in the field of apoptosis research. During BAX expression trials, it was shown that incubation of BAX monomers with Tween20 induced oligomerisation. As the Tween20 induced BAX oligomers eluted from SEC in a single peak, it was

postulated that these oligomers might be forming regular structures, and whether these structures could provide data pertinent to providing answers to this question.

The apparent homogeneity of the BAX oligomer sample meant that it might be suitable for analysis by cryo-electron microscopy (cryo-EM). Due to the high cost involved with this technique, samples were first analysed using negative stain EM. Disappointingly, the homogeneity seen in the SEC peak for oligomerised BAX was not recreated in the negative stain EM images; instead, a heterogeneous mix of species was seen, including a proportion of monomeric BAX. An optimum concentration of grid loading for BAX of 10nM was established (this to provide a good level of visible particles, sufficiently dispersed to allow particle picking for further analysis). This required a high level of dilution of our oligomerised samples before grid loading, taking the Tween20 concentration below CMC, which may result in the rapid breakdown of BAX oligomers.

The heterogeneity currently seen in the BAX oligomer sample makes it unsuitable for study by cryo-EM. To progress this part of the project, methods for isolating and stabilising BAX oligomers will be developed and optimised, together with protocols for removing detergent without causing oligomer dissociation. The recombinant BAX protein contains multiple lysine, aspartate and glutamate residues, which would facilitate chemical cross linking via primary amines or carboxyl groups. This approach, followed by sample dialysis into detergent free buffer, could be a credible approach to obtaining more homogenous, detergent free oligomers, which would be suitable for use in cryo-EM and in x-ray crystallography.

References

1. Jacobson, M.D., M. Weil, and M.C. Raff, *Programmed cell death in animal development.* Cell, 1997. **88**(3): p. 347-54.
2. Savill, J. and V. Fadok, *Corpse clearance defines the meaning of cell death.* Nature, 2000. **407**(6805): p. 784-8.
3. Goodnow, C.C., *Multistep pathogenesis of autoimmune disease.* Cell, 2007. **130**(1): p. 25-35.
4. Vaux, D.L., G. Haecker, and A. Strasser, *An evolutionary perspective on apoptosis.* Cell, 1994. **76**(5): p. 777-9.
5. Earnshaw, W.C., L.M. Martins, and S.H. Kaufmann, *Mammalian caspases: structure, activation, substrates, and functions during apoptosis.* Annu Rev Biochem, 1999. **68**: p. 383-424.
6. Julien, O. and J.A. Wells, *Caspases and their substrates.* Cell Death Differ, 2017. **24**(8): p. 1380-1389.
7. Nagata, S., *Apoptosis by death factor.* Cell, 1997. **88**(3): p. 355-65.
8. Ashkenazi, A. and V.M. Dixit, *Death receptors: signaling and modulation.* Science, 1998. **281**(5381): p. 1305-8.
9. Froelich, C.J., V.M. Dixit, and X. Yang, *Lymphocyte granule-mediated apoptosis: matters of viral mimicry and deadly proteases.* Immunol Today, 1998. **19**(1): p. 30-6.
10. Liu, X., et al., *Induction of apoptotic program in cell-free extracts: requirement for dATP and cytochrome c.* Cell, 1996. **86**(1): p. 147-57.
11. Kockx, M.M. and A.G. Herman, *Apoptosis in atherosclerosis: beneficial or detrimental?* Cardiovasc Res, 2000. **45**(3): p. 736-46.
12. Chandra, J., et al., *Role of apoptosis in pancreatic beta-cell death in diabetes.* Diabetes, 2001. **50 Suppl 1**: p. S44-7.
13. Kuhlmann, T., et al., *Bcl-2-expressing oligodendrocytes in multiple sclerosis lesions.* Glia, 1999. **28**(1): p. 34-9.
14. Yuan, J. and B.A. Yankner, *Apoptosis in the nervous system.* Nature, 2000. **407**(6805): p. 802-9.
15. Thompson, C.B., *Apoptosis in the pathogenesis and treatment of disease.* Science, 1995. **267**(5203): p. 1456-62.
16. Rutledge, S.E., J.W. Chin, and A. Schepartz, *A view to a kill: ligands for Bcl-2 family proteins.* Curr Opin Chem Biol, 2002. **6**(4): p. 479-85.
17. Hanahan, D. and R.A. Weinberg, *The hallmarks of cancer.* Cell, 2000. **100**(1): p. 57-70.
18. Krammer, P.H., *CD95's deadly mission in the immune system.* Nature, 2000. **407**(6805): p. 789-95.
19. Tsujimoto, Y., et al., *Involvement of the bcl-2 gene in human follicular lymphoma.* Science, 1985. **228**(4706): p. 1440-3.
20. Vaux, D.L., S. Cory, and J.M. Adams, *Bcl-2 gene promotes haemopoietic cell survival and cooperates with c-myc to immortalize pre-B cells.* Nature, 1988. **335**(6189): p. 440-2.
21. Adams, J.M. and S. Cory, *The Bcl-2 protein family: arbiters of cell survival.* Science, 1998. **281**(5381): p. 1322-6.
22. Reed, J.C., *Mechanisms of apoptosis.* Am J Pathol, 2000. **157**(5): p. 1415-30.

23. Oltvai, Z.N., C.L. Milliman, and S.J. Korsmeyer, *Bcl-2 heterodimerizes in vivo with a conserved homolog, Bax, that accelerates programmed cell death.* Cell, 1993. **74**(4): p. 609-19.
24. Edwards, A.L., et al., *Multimodal interaction with BCL-2 family proteins underlies the proapoptotic activity of PUMA BH3.* Chem Biol, 2013. **20**(7): p. 888-902.
25. Letai, A., et al., *Distinct BH3 domains either sensitize or activate mitochondrial apoptosis, serving as prototype cancer therapeutics.* Cancer Cell, 2002. **2**(3): p. 183-92.
26. Green, D.R. and J.C. Reed, *Mitochondria and apoptosis.* Science, 1998. **281**(5381): p. 1309-12.
27. Zha, H., et al., *Proapoptotic protein Bax heterodimerizes with Bcl-2 and homodimerizes with Bax via a novel domain (BH3) distinct from BH1 and BH2.* J Biol Chem, 1996. **271**(13): p. 7440-4.
28. Kvansakul, M., et al., *Vaccinia virus anti-apoptotic F1L is a novel Bcl-2-like domain-swapped dimer that binds a highly selective subset of BH3-containing death ligands.* Cell Death Differ, 2008. **15**(10): p. 1564-71.
29. Hinds, M.G., et al., *Bim, Bad and Bmf: intrinsically unstructured BH3-only proteins that undergo a localized conformational change upon binding to prosurvival Bcl-2 targets.* Cell Death Differ, 2007. **14**(1): p. 128-36.
30. Muchmore, S.W., et al., *X-ray and NMR structure of human Bcl-xL, an inhibitor of programmed cell death.* Nature, 1996. **381**(6580): p. 335-41.
31. Moldoveanu, T., et al., *The X-ray structure of a BAK homodimer reveals an inhibitory zinc binding site.* Mol Cell, 2006. **24**(5): p. 677-88.
32. Suzuki, M., R.J. Youle, and N. Tjandra, *Structure of Bax: coregulation of dimer formation and intracellular localization.* Cell, 2000. **103**(4): p. 645-54.
33. Wang, H., et al., *Novel dimerization mode of the human Bcl-2 family protein Bak, a mitochondrial apoptosis regulator.* J Struct Biol, 2009. **166**(1): p. 32-7.
34. Petros, A.M., et al., *Solution structure of the antiapoptotic protein bcl-2.* Proc Natl Acad Sci U S A, 2001. **98**(6): p. 3012-7.
35. Chou, J.J., et al., *Solution structure of BID, an intracellular amplifier of apoptotic signaling.* Cell, 1999. **96**(5): p. 615-24.
36. McDonnell, J.M., et al., *Solution structure of the proapoptotic molecule BID: a structural basis for apoptotic agonists and antagonists.* Cell, 1999. **96**(5): p. 625-34.
37. Kuwana, T., et al., *BH3 domains of BH3-only proteins differentially regulate Bax-mediated mitochondrial membrane permeabilization both directly and indirectly.* Mol Cell, 2005. **17**(4): p. 525-35.
38. Merino, D., et al., *The role of BH3-only protein Bim extends beyond inhibiting Bcl-2-like prosurvival proteins.* J Cell Biol, 2009. **186**(3): p. 355-62.
39. Llambi, F., et al., *A unified model of mammalian BCL-2 protein family interactions at the mitochondria.* Mol Cell, 2011. **44**(4): p. 517-31.

40. Chen, L., et al., *Differential targeting of prosurvival Bcl-2 proteins by their BH3-only ligands allows complementary apoptotic function.* Mol Cell, 2005. **17**(3): p. 393-403.
41. Willis, S.N., et al., *Apoptosis initiated when BH3 ligands engage multiple Bcl-2 homologs, not Bax or Bak.* Science, 2007. **315**(5813): p. 856-9.
42. Willis, S.N., et al., *Proapoptotic Bak is sequestered by Mcl-1 and Bcl-xL, but not Bcl-2, until displaced by BH3-only proteins.* Genes Dev, 2005. **19**(11): p. 1294-305.
43. Certo, M., et al., *Mitochondria primed by death signals determine cellular addiction to antiapoptotic BCL-2 family members.* Cancer Cell, 2006. **9**(5): p. 351-65.
44. Kim, H., et al., *Hierarchical regulation of mitochondrion-dependent apoptosis by BCL-2 subfamilies.* Nat Cell Biol, 2006. **8**(12): p. 1348-58.
45. Gavathiotis, E., et al., *BAX activation is initiated at a novel interaction site.* Nature, 2008. **455**(7216): p. 1076-81.
46. Dai, H., et al., *Evaluation of the BH3-only protein Puma as a direct Bak activator.* J Biol Chem, 2014. **289**(1): p. 89-99.
47. Ren, D., et al., *BID, BIM, and PUMA are essential for activation of the BAX- and BAK-dependent cell death program.* Science, 2010. **330**(6009): p. 1390-3.
48. Sarosiek, K.A., et al., *BID preferentially activates BAK while BIM preferentially activates BAX, affecting chemotherapy response.* Mol Cell, 2013. **51**(6): p. 751-65.
49. Du, H., et al., *BH3 domains other than Bim and Bid can directly activate Bax/Bak.* J Biol Chem, 2011. **286**(1): p. 491-501.
50. Moldoveanu, T., et al., *BID-induced structural changes in BAK promote apoptosis.* Nat Struct Mol Biol, 2013. **20**(5): p. 589-97.
51. Brouwer, J.M., et al., *Bak core and latch domains separate during activation, and freed core domains form symmetric homodimers.* Mol Cell, 2014. **55**(6): p. 938-946.
52. Czabotar, P.E., et al., *Bax crystal structures reveal how BH3 domains activate Bax and nucleate its oligomerization to induce apoptosis.* Cell, 2013. **152**(3): p. 519-31.
53. Lindsten, T., et al., *The combined functions of proapoptotic Bcl-2 family members bak and bax are essential for normal development of multiple tissues.* Mol Cell, 2000. **6**(6): p. 1389-99.
54. Zong, W.X., et al., *BH3-only proteins that bind pro-survival Bcl-2 family members fail to induce apoptosis in the absence of Bax and Bak.* Genes Dev, 2001. **15**(12): p. 1481-6.
55. Wei, M.C., et al., *Proapoptotic BAX and BAK: a requisite gateway to mitochondrial dysfunction and death.* Science, 2001. **292**(5517): p. 727-30.
56. Wang, K., et al., *Mutagenesis of the BH3 domain of BAX identifies residues critical for dimerization and killing.* Mol Cell Biol, 1998. **18**(10): p. 6083-9.
57. Fletcher, J.I., et al., *Apoptosis is triggered when prosurvival Bcl-2 proteins cannot restrain Bax.* Proc Natl Acad Sci U S A, 2008. **105**(47): p. 18081-7.

58. Cory, S., et al., *Targeting BCL-2-like Proteins to Kill Cancer Cells.* Trends Cancer, 2016. **2**(8): p. 443-460.
59. Wei, M.C., et al., *tBID, a membrane-targeted death ligand, oligomerizes BAK to release cytochrome c.* Genes Dev, 2000. **14**(16): p. 2060-71.
60. Azad, A., et al., *Blockade of the BAK hydrophobic groove by inhibitory phosphorylation regulates commitment to apoptosis.* PLoS One, 2012. **7**(11): p. e49601.
61. Fox, J.L., et al., *Tyrosine dephosphorylation is required for Bak activation in apoptosis.* EMBO J, 2010. **29**(22): p. 3853-68.
62. Xin, M. and X. Deng, *Nicotine inactivation of the proapoptotic function of Bax through phosphorylation.* J Biol Chem, 2005. **280**(11): p. 10781-9.
63. Cartron, P.F., et al., *Impact of pH on Bax alpha conformation, oligomerisation and mitochondrial integration.* FEBS Lett, 2004. **578**(1-2): p. 41-6.
64. Khaled, A.R., et al., *Withdrawal of IL-7 induces Bax translocation from cytosol to mitochondria through a rise in intracellular pH.* Proc Natl Acad Sci U S A, 1999. **96**(25): p. 14476-81.
65. Nie, C., et al., *Cysteine 62 of Bax is critical for its conformational activation and its proapoptotic activity in response to H2O2-induced apoptosis.* J Biol Chem, 2008. **283**(22): p. 15359-69.
66. Pagliari, L.J., et al., *The multidomain proapoptotic molecules Bax and Bak are directly activated by heat.* Proc Natl Acad Sci U S A, 2005. **102**(50): p. 17975-80.
67. Billen, L.P., et al., *Bcl-XL inhibits membrane permeabilization by competing with Bax.* PLoS Biol, 2008. **6**(6): p. e147.
68. Lovell, J.F., et al., *Membrane binding by tBid initiates an ordered series of events culminating in membrane permeabilization by Bax.* Cell, 2008. **135**(6): p. 1074-84.
69. Shamas-Din, A., et al., *tBid undergoes multiple conformational changes at the membrane required for Bax activation.* J Biol Chem, 2013. **288**(30): p. 22111-27.
70. Sattler, M., et al., *Structure of Bcl-xL-Bak peptide complex: recognition between regulators of apoptosis.* Science, 1997. **275**(5302): p. 983-6.
71. Petros, A.M., et al., *Rationale for Bcl-xL/Bad peptide complex formation from structure, mutagenesis, and biophysical studies.* Protein Sci, 2000. **9**(12): p. 2528-34.
72. Liu, X., et al., *The structure of a Bcl-xL/Bim fragment complex: implications for Bim function.* Immunity, 2003. **19**(3): p. 341-52.
73. Czabotar, P.E., et al., *Structural insights into the degradation of Mcl-1 induced by BH3 domains.* Proc Natl Acad Sci U S A, 2007. **104**(15): p. 6217-22.
74. Chipuk, J.E., et al., *The BCL-2 family reunion.* Mol Cell, 2010. **37**(3): p. 299-310.
75. Petros, A.M., et al., *Defining the p53 DNA-binding domain/Bcl-x(L)-binding interface using NMR.* FEBS Lett, 2004. **559**(1-3): p. 171-4.
76. Rautureau, G.J., et al., *The restricted binding repertoire of Bcl-B leaves Bim as the universal BH3-only prosurvival Bcl-2 protein antagonist.* Cell Death Dis, 2012. **3**: p. e443.

77. Day, C.L., et al., *Structure of the BH3 domains from the p53-inducible BH3-only proteins Noxa and Puma in complex with Mcl-1.* J Mol Biol, 2008. **380**(5): p. 958-71.
78. Liu, Q., et al., *Apoptotic regulation by MCL-1 through heterodimerization.* J Biol Chem, 2010. **285**(25): p. 19615-24.
79. Juin, P., et al., *c-Myc-induced sensitization to apoptosis is mediated through cytochrome c release.* Genes Dev, 1999. **13**(11): p. 1367-81.
80. Lowe, S.W., E. Cepero, and G. Evan, *Intrinsic tumour suppression.* Nature, 2004. **432**(7015): p. 307-15.
81. Li, P., et al., *Cytochrome c and dATP-dependent formation of Apaf-1/caspase-9 complex initiates an apoptotic protease cascade.* Cell, 1997. **91**(4): p. 479-89.
82. Acehan, D., et al., *Three-dimensional structure of the apoptosome: implications for assembly, procaspase-9 binding, and activation.* Mol Cell, 2002. **9**(2): p. 423-32.
83. Bratton, S.B. and G.S. Salvesen, *Regulation of the Apaf-1-caspase-9 apoptosome.* J Cell Sci, 2010. **123**(Pt 19): p. 3209-14.
84. Hengartner, M.O., *The biochemistry of apoptosis.* Nature, 2000. **407**(6805): p. 770-6.
85. Taylor, R.C., S.P. Cullen, and S.J. Martin, *Apoptosis: controlled demolition at the cellular level.* Nat Rev Mol Cell Biol, 2008. **9**(3): p. 231-41.
86. Jiang, X. and X. Wang, *Cytochrome C-mediated apoptosis.* Annu Rev Biochem, 2004. **73**: p. 87-106.
87. Enari, M., et al., *A caspase-activated DNase that degrades DNA during apoptosis, and its inhibitor ICAD.* Nature, 1998. **391**(6662): p. 43-50.
88. Suzuki, J., et al., *Xk-related protein 8 and CED-8 promote phosphatidylserine exposure in apoptotic cells.* Science, 2013. **341**(6144): p. 403-6.
89. Beverly, L.J., *Regulation of anti-apoptotic BCL2-proteins by non-canonical interactions: the next step forward or two steps back?* J Cell Biochem, 2012. **113**(1): p. 3-12.
90. Hu, Y., et al., *Bcl-XL interacts with Apaf-1 and inhibits Apaf-1-dependent caspase-9 activation.* Proc Natl Acad Sci U S A, 1998. **95**(8): p. 4386-91.
91. Poulaki, V., et al., *Fas-mediated apoptosis in neuroblastoma requires mitochondrial activation and is inhibited by FLICE inhibitor protein and Bcl-2.* Cancer Res, 2001. **61**(12): p. 4864-72.
92. Komatsu, K., et al., *Human homologue of S. pombe Rad9 interacts with BCL-2/BCL-xL and promotes apoptosis.* Nat Cell Biol, 2000. **2**(1): p. 1-6.
93. Iwahashi, H., et al., *Synergistic anti-apoptotic activity between Bcl-2 and SMN implicated in spinal muscular atrophy.* Nature, 1997. **390**(6658): p. 413-7.
94. Shirane, M. and K.I. Nakayama, *Inherent calcineurin inhibitor FKBP38 targets Bcl-2 to mitochondria and inhibits apoptosis.* Nat Cell Biol, 2003. **5**(1): p. 28-37.
95. Yamamoto, K., H. Ichijo, and S.J. Korsmeyer, *BCL-2 is phosphorylated and inactivated by an ASK1/Jun N-terminal protein*

kinase pathway normally activated at G(2)/M. Mol Cell Biol, 1999. **19**(12): p. 8469-78.
96. Tamura, Y., S. Simizu, and H. Osada, *The phosphorylation status and anti-apoptotic activity of Bcl-2 are regulated by ERK and protein phosphatase 2A on the mitochondria.* FEBS Lett, 2004. **569**(1-3): p. 249-55.
97. Schmitt, E., M. Beauchemin, and R. Bertrand, *Nuclear colocalization and interaction between bcl-xL and cdk1(cdc2) during G2/M cell-cycle checkpoint.* Oncogene, 2007. **26**(40): p. 5851-65.
98. Zhong, Q., et al., *Mule/ARF-BP1, a BH3-only E3 ubiquitin ligase, catalyzes the polyubiquitination of Mcl-1 and regulates apoptosis.* Cell, 2005. **121**(7): p. 1085-95.
99. Schwickart, M., et al., *Deubiquitinase USP9X stabilizes MCL1 and promotes tumour cell survival.* Nature, 2010. **463**(7277): p. 103-7.
100. Kerr, J.F., A.H. Wyllie, and A.R. Currie, *Apoptosis: a basic biological phenomenon with wide-ranging implications in tissue kinetics.* Br J Cancer, 1972. **26**(4): p. 239-57.
101. Beroukhim, R., et al., *The landscape of somatic copy-number alteration across human cancers.* Nature, 2010. **463**(7283): p. 899-905.
102. Rampino, N., et al., *Somatic frameshift mutations in the BAX gene in colon cancers of the microsatellite mutator phenotype.* Science, 1997. **275**(5302): p. 967-9.
103. Mestre-Escorihuela, C., et al., *Homozygous deletions localize novel tumor suppressor genes in B-cell lymphomas.* Blood, 2007. **109**(1): p. 271-80.
104. Gerl, R. and D.L. Vaux, *Apoptosis in the development and treatment of cancer.* Carcinogenesis, 2005. **26**(2): p. 263-70.
105. Strasser, A., et al., *Novel primitive lymphoid tumours induced in transgenic mice by cooperation between myc and bcl-2.* Nature, 1990. **348**(6299): p. 331-3.
106. Eischen, C.M., et al., *Apoptosis triggered by Myc-induced suppression of Bcl-X(L) or Bcl-2 is bypassed during lymphomagenesis.* Mol Cell Biol, 2001. **21**(15): p. 5063-70.
107. Reed, J.C., *Dysregulation of apoptosis in cancer.* J Clin Oncol, 1999. **17**(9): p. 2941-53.
108. Tan, T.T., et al., *Key roles of BIM-driven apoptosis in epithelial tumors and rational chemotherapy.* Cancer Cell, 2005. **7**(3): p. 227-38.
109. Bachmann, P.S., et al., *Epigenetic silencing of BIM in glucocorticoid poor-responsive pediatric acute lymphoblastic leukemia, and its reversal by histone deacetylase inhibition.* Blood, 2010. **116**(16): p. 3013-22.
110. Kuroda, J., et al., *Bim and Bad mediate imatinib-induced killing of Bcr/Abl+ leukemic cells, and resistance due to their loss is overcome by a BH3 mimetic.* Proc Natl Acad Sci U S A, 2006. **103**(40): p. 14907-12.
111. Cragg, M.S., et al., *Gefitinib-induced killing of NSCLC cell lines expressing mutant EGFR requires BIM and can be enhanced by BH3 mimetics.* PLoS Med, 2007. **4**(10): p. 1681-89; discussion 1690.

112. Costa, D.B., et al., *BIM mediates EGFR tyrosine kinase inhibitor-induced apoptosis in lung cancers with oncogenic EGFR mutations.* PLoS Med, 2007. **4**(10): p. 1669-79; discussion 1680.
113. Cragg, M.S., et al., *Treatment of B-RAF mutant human tumor cells with a MEK inhibitor requires Bim and is enhanced by a BH3 mimetic.* J Clin Invest, 2008. **118**(11): p. 3651-9.
114. Bakhshi, A., et al., *Cloning the chromosomal breakpoint of t(14;18) human lymphomas: clustering around JH on chromosome 14 and near a transcriptional unit on 18.* Cell, 1985. **41**(3): p. 899-906.
115. Cleary, M.L. and J. Sklar, *Nucleotide sequence of a t(14;18) chromosomal breakpoint in follicular lymphoma and demonstration of a breakpoint-cluster region near a transcriptionally active locus on chromosome 18.* Proc Natl Acad Sci U S A, 1985. **82**(21): p. 7439-43.
116. Cleary, M.L., S.D. Smith, and J. Sklar, *Cloning and structural analysis of cDNAs for bcl-2 and a hybrid bcl-2/immunoglobulin transcript resulting from the t(14;18) translocation.* Cell, 1986. **47**(1): p. 19-28.
117. Tsujimoto, Y., et al., *Cloning of the chromosome breakpoint of neoplastic B cells with the t(14;18) chromosome translocation.* Science, 1984. **226**(4678): p. 1097-9.
118. Tsujimoto, Y., et al., *Molecular cloning of the chromosomal breakpoint of B-cell lymphomas and leukemias with the t(11;14) chromosome translocation.* Science, 1984. **224**(4656): p. 1403-6.
119. Henderson, S., et al., *Induction of bcl-2 expression by Epstein-Barr virus latent membrane protein 1 protects infected B cells from programmed cell death.* Cell, 1991. **65**(7): p. 1107-15.
120. McDonnell, T.J., et al., *bcl-2-immunoglobulin transgenic mice demonstrate extended B cell survival and follicular lymphoproliferation.* Cell, 1989. **57**(1): p. 79-88.
121. McDonnell, T.J. and S.J. Korsmeyer, *Progression from lymphoid hyperplasia to high-grade malignant lymphoma in mice transgenic for the t(14; 18).* Nature, 1991. **349**(6306): p. 254-6.
122. Reed, J.C., *Bcl-2-family proteins and hematologic malignancies: history and future prospects.* Blood, 2008. **111**(7): p. 3322-30.
123. Scarfo, L. and P. Ghia, *Reprogramming cell death: BCL2 family inhibition in hematological malignancies.* Immunol Lett, 2013. **155**(1-2): p. 36-9.
124. Yip, K.W. and J.C. Reed, *Bcl-2 family proteins and cancer.* Oncogene, 2008. **27**(50): p. 6398-406.
125. Bhargava, V., et al., *Bcl-2 immunoreactivity in breast carcinoma correlates with hormone receptor positivity.* Am J Pathol, 1994. **145**(3): p. 535-40.
126. Callagy, G.M., et al., *Bcl-2 is a prognostic marker in breast cancer independently of the Nottingham Prognostic Index.* Clin Cancer Res, 2006. **12**(8): p. 2468-75.
127. Catz, S.D. and J.L. Johnson, *BCL-2 in prostate cancer: a minireview.* Apoptosis, 2003. **8**(1): p. 29-37.
128. Pepper, C., P. Bentley, and T. Hoy, *Regulation of clinical chemoresistance by bcl-2 and bax oncoproteins in B-cell chronic lymphocytic leukaemia.* Br J Haematol, 1996. **95**(3): p. 513-7.

129. Breitschopf, K., et al., *Posttranslational modification of Bcl-2 facilitates its proteasome-dependent degradation: molecular characterization of the involved signaling pathway.* Mol Cell Biol, 2000. **20**(5): p. 1886-96.
130. Niture, S.K. and A.K. Jaiswal, *Inhibitor of Nrf2 (INrf2 or Keap1) protein degrades Bcl-xL via phosphoglycerate mutase 5 and controls cellular apoptosis.* J Biol Chem, 2011. **286**(52): p. 44542-56.
131. Niture, S.K. and A.K. Jaiswal, *Nrf2 protein up-regulates antiapoptotic protein Bcl-2 and prevents cellular apoptosis.* J Biol Chem, 2012. **287**(13): p. 9873-86.
132. Cimmino, A., et al., *miR-15 and miR-16 induce apoptosis by targeting BCL2.* Proc Natl Acad Sci U S A, 2005. **102**(39): p. 13944-9.
133. Choi, J., et al., *Bcl-2 promotes invasion and lung metastasis by inducing matrix metalloproteinase-2.* Cancer Res, 2005. **65**(13): p. 5554-60.
134. Noujaim, D., et al., *N-Myc and Bcl-2 coexpression induces MMP-2 secretion and activation in human neuroblastoma cells.* Oncogene, 2002. **21**(29): p. 4549-57.
135. Wick, W., et al., *BCL-2 promotes migration and invasiveness of human glioma cells.* FEBS Lett, 1998. **440**(3): p. 419-24.
136. Wick, W., et al., *BCL-2-induced glioma cell invasiveness depends on furin-like proteases.* J Neurochem, 2004. **91**(6): p. 1275-83.
137. Zuo, J., et al., *Bcl-2 overexpression induces a partial epithelial to mesenchymal transition and promotes squamous carcinoma cell invasion and metastasis.* Mol Cancer Res, 2010. **8**(2): p. 170-82.
138. Biroccio, A., et al., *Bcl-2 overexpression and hypoxia synergistically act to modulate vascular endothelial growth factor expression and in vivo angiogenesis in a breast carcinoma line.* FASEB J, 2000. **14**(5): p. 652-60.
139. Diensthuber, M., et al., *Expression of bcl-2 is associated with microvessel density in olfactory neuroblastoma.* J Neurooncol, 2008. **89**(2): p. 131-9.
140. Fernandez, A., et al., *Angiogenic potential of prostate carcinoma cells overexpressing bcl-2.* J Natl Cancer Inst, 2001. **93**(3): p. 208-13.
141. Karl, E., et al., *Bcl-2 acts in a proangiogenic signaling pathway through nuclear factor-kappaB and CXC chemokines.* Cancer Res, 2005. **65**(12): p. 5063-9.
142. Iervolino, A., et al., *Bcl-2 overexpression in human melanoma cells increases angiogenesis through VEGF mRNA stabilization and HIF-1-mediated transcriptional activity.* FASEB J, 2002. **16**(11): p. 1453-5.
143. Trisciuoglio, D., et al., *Bcl-2 overexpression in melanoma cells increases tumor progression-associated properties and in vivo tumor growth.* J Cell Physiol, 2005. **205**(3): p. 414-21.
144. Trisciuoglio, D., et al., *Involvement of PI3K and MAPK signaling in bcl-2-induced vascular endothelial growth factor expression in melanoma cells.* Mol Biol Cell, 2005. **16**(9): p. 4153-62.
145. Wei, G., et al., *Chemical genomics identifies small-molecule MCL1 repressors and BCL-xL as a predictor of MCL1 dependency.* Cancer Cell, 2012. **21**(4): p. 547-62.
146. Castilla, C., et al., *Bcl-xL is overexpressed in hormone-resistant prostate cancer and promotes survival of LNCaP cells via interaction with proapoptotic Bak.* Endocrinology, 2006. **147**(10): p. 4960-7.

147. Keitel, U., et al., *Bcl-xL mediates therapeutic resistance of a mesenchymal breast cancer cell subpopulation.* Oncotarget, 2014. **5**(23): p. 11778-91.
148. Correia, C., et al., *Emerging understanding of Bcl-2 biology: Implications for neoplastic progression and treatment.* Biochim Biophys Acta, 2015. **1853**(7): p. 1658-71.
149. Chen, Y., et al., *CXCR4 downregulation of let-7a drives chemoresistance in acute myeloid leukemia.* J Clin Invest, 2013. **123**(6): p. 2395-407.
150. Shimizu, S., et al., *The let-7 family of microRNAs inhibits Bcl-xL expression and potentiates sorafenib-induced apoptosis in human hepatocellular carcinoma.* J Hepatol, 2010. **52**(5): p. 698-704.
151. Zhan, M., et al., *Let-7c sensitizes acquired cisplatin-resistant A549 cells by targeting ABCC2 and Bcl-XL.* Pharmazie, 2013. **68**(12): p. 955-61.
152. Guo, R., et al., *MicroRNA miR-491-5p targeting both TP53 and Bcl-XL induces cell apoptosis in SW1990 pancreatic cancer cells through mitochondria mediated pathway.* Molecules, 2012. **17**(12): p. 14733-47.
153. Nakano, H., et al., *Functional screening identifies a microRNA, miR-491 that induces apoptosis by targeting Bcl-X(L) in colorectal cancer cells.* Int J Cancer, 2010. **127**(5): p. 1072-80.
154. Choi, S., et al., *Bcl-xL promotes metastasis independent of its anti-apoptotic activity.* Nat Commun, 2016. **7**: p. 10384.
155. Ho, J.N., et al., *Bcl-XL and STAT3 mediate malignant actions of gamma-irradiation in lung cancer cells.* Cancer Sci, 2010. **101**(6): p. 1417-23.
156. Koehler, B.C., et al., *Beyond cell death - antiapoptotic Bcl-2 proteins regulate migration and invasion of colorectal cancer cells in vitro.* PLoS One, 2013. **8**(10): p. e76446.
157. Martin, S.S., et al., *A cytoskeleton-based functional genetic screen identifies Bcl-xL as an enhancer of metastasis, but not primary tumor growth.* Oncogene, 2004. **23**(26): p. 4641-5.
158. Weiler, M., et al., *BCL-xL: time-dependent dissociation between modulation of apoptosis and invasiveness in human malignant glioma cells.* Cell Death Differ, 2006. **13**(7): p. 1156-69.
159. Carne Trecesson, S., et al., *BCL-XL directly modulates RAS signalling to favour cancer cell stemness.* Nat Commun, 2017. **8**(1): p. 1123.
160. Edlich, F., et al., *Bcl-x(L) retrotranslocates Bax from the mitochondria into the cytosol.* Cell, 2011. **145**(1): p. 104-16.
161. Todt, F., et al., *The C-terminal helix of Bcl-x(L) mediates Bax retrotranslocation from the mitochondria.* Cell Death Differ, 2013. **20**(2): p. 333-42.
162. Dussmann, H., et al., *Single-cell quantification of Bax activation and mathematical modelling suggest pore formation on minimal mitochondrial Bax accumulation.* Cell Death Differ, 2010. **17**(2): p. 278-90.
163. Thomas, L.W., C. Lam, and S.W. Edwards, *Mcl-1; the molecular regulation of protein function.* FEBS Lett, 2010. **584**(14): p. 2981-9.

164. Yang-Yen, H.F., *Mcl-1: a highly regulated cell death and survival controller.* J Biomed Sci, 2006. **13**(2): p. 201-4.
165. Kitada, S., et al., *Expression of apoptosis-regulating proteins in chronic lymphocytic leukemia: correlations with In vitro and In vivo chemoresponses.* Blood, 1998. **91**(9): p. 3379-89.
166. Quinn, B.A., et al., *Targeting Mcl-1 for the therapy of cancer.* Expert Opin Investig Drugs, 2011. **20**(10): p. 1397-411.
167. Wuilleme-Toumi, S., et al., *Mcl-1 is overexpressed in multiple myeloma and associated with relapse and shorter survival.* Leukemia, 2005. **19**(7): p. 1248-52.
168. Zhuang, L., et al., *Mcl-1, Bcl-XL and Stat3 expression are associated with progression of melanoma whereas Bcl-2, AP-2 and MITF levels decrease during progression of melanoma.* Mod Pathol, 2007. **20**(4): p. 416-26.
169. Backus, H.H., et al., *Rb, mcl-1 and p53 expression correlate with clinical outcome in patients with liver metastases from colorectal cancer.* Ann Oncol, 2001. **12**(6): p. 779-85.
170. Ding, Q., et al., *Myeloid cell leukemia-1 inversely correlates with glycogen synthase kinase-3beta activity and associates with poor prognosis in human breast cancer.* Cancer Res, 2007. **67**(10): p. 4564-71.
171. Likui, W., et al., *Prognostic role of myeloid cell leukemia-1 protein (Mcl-1) expression in human gastric cancer.* J Surg Oncol, 2009. **100**(5): p. 396-400.
172. Shigemasa, K., et al., *Increased MCL-1 expression is associated with poor prognosis in ovarian carcinomas.* Jpn J Cancer Res, 2002. **93**(5): p. 542-50.
173. Sieghart, W., et al., *Mcl-1 overexpression in hepatocellular carcinoma: a potential target for antisense therapy.* J Hepatol, 2006. **44**(1): p. 151-7.
174. Lin, X., et al., *'Seed' analysis of off-target siRNAs reveals an essential role of Mcl-1 in resistance to the small-molecule Bcl-2/Bcl-XL inhibitor ABT-737.* Oncogene, 2007. **26**(27): p. 3972-9.
175. Meng, X.W., et al., *Mcl-1 as a buffer for proapoptotic Bcl-2 family members during TRAIL-induced apoptosis: a mechanistic basis for sorafenib (Bay 43-9006)-induced TRAIL sensitization.* J Biol Chem, 2007. **282**(41): p. 29831-46.
176. Taniai, M., et al., *Mcl-1 mediates tumor necrosis factor-related apoptosis-inducing ligand resistance in human cholangiocarcinoma cells.* Cancer Res, 2004. **64**(10): p. 3517-24.
177. Eischen, C.M., et al., *Bax loss impairs Myc-induced apoptosis and circumvents the selection of p53 mutations during Myc-mediated lymphomagenesis.* Mol Cell Biol, 2001. **21**(22): p. 7653-62.
178. Theodorakis, P., E. Lomonosova, and G. Chinnadurai, *Critical requirement of BAX for manifestation of apoptosis induced by multiple stimuli in human epithelial cancer cells.* Cancer Res, 2002. **62**(12): p. 3373-6.
179. Eischen, C.M., et al., *Loss of Bax alters tumor spectrum and tumor numbers in ARF-deficient mice.* Cancer Res, 2002. **62**(7): p. 2184-91.
180. Shibata, M.A., et al., *Haploid loss of bax leads to accelerated mammary tumor development in C3(1)/SV40-TAg transgenic mice:*

reduction in protective apoptotic response at the preneoplastic stage. EMBO J, 1999. **18**(10): p. 2692-701.
181. Yin, C., et al., *Bax suppresses tumorigenesis and stimulates apoptosis in vivo.* Nature, 1997. **385**(6617): p. 637-40.
182. Yin, X.M., et al., *Bid-deficient mice are resistant to Fas-induced hepatocellular apoptosis.* Nature, 1999. **400**(6747): p. 886-91.
183. Ionov, Y., et al., *Mutational inactivation of the proapoptotic gene BAX confers selective advantage during tumor clonal evolution.* Proc Natl Acad Sci U S A, 2000. **97**(20): p. 10872-7.
184. Meijerink, J.P., et al., *Hematopoietic malignancies demonstrate loss-of-function mutations of BAX.* Blood, 1998. **91**(8): p. 2991-7.
185. Cartron, P.F., et al., *Nonredundant role of Bax and Bak in Bid-mediated apoptosis.* Mol Cell Biol, 2003. **23**(13): p. 4701-12.
186. Kondo, S., et al., *Mutations of the bak gene in human gastric and colorectal cancers.* Cancer Res, 2000. **60**(16): p. 4328-30.
187. Cartron, P.F., et al., *The first alpha helix of Bax plays a necessary role in its ligand-induced activation by the BH3-only proteins Bid and PUMA.* Mol Cell, 2004. **16**(5): p. 807-18.
188. Gallenne, T., et al., *Bax activation by the BH3-only protein Puma promotes cell dependence on antiapoptotic Bcl-2 family members.* J Cell Biol, 2009. **185**(2): p. 279-90.
189. Gavathiotis, E., et al., *BH3-triggered structural reorganization drives the activation of proapoptotic BAX.* Mol Cell, 2010. **40**(3): p. 481-92.
190. Garner, T.P., et al., *An Autoinhibited Dimeric Form of BAX Regulates the BAX Activation Pathway.* Mol Cell, 2016. **63**(3): p. 485-97.
191. Garcia-Saez, A.J., *The secrets of the Bcl-2 family.* Cell Death Differ, 2012. **19**(11): p. 1733-40.
192. Terrones, O., et al., *Lipidic pore formation by the concerted action of proapoptotic BAX and tBID.* J Biol Chem, 2004. **279**(29): p. 30081-91.
193. Reed, J.C., *Proapoptotic multidomain Bcl-2/Bax-family proteins: mechanisms, physiological roles, and therapeutic opportunities.* Cell Death Differ, 2006. **13**(8): p. 1378-86.
194. Pang, Y.P., et al., *Bak Conformational Changes Induced by Ligand Binding: Insight into BH3 Domain Binding and Bak Homo-Oligomerization.* Sci Rep, 2012. **2**: p. 257.
195. Dewson, G., et al., *To trigger apoptosis, Bak exposes its BH3 domain and homodimerizes via BH3:groove interactions.* Mol Cell, 2008. **30**(3): p. 369-80.
196. Dewson, G., et al., *Bax dimerizes via a symmetric BH3:groove interface during apoptosis.* Cell Death Differ, 2012. **19**(4): p. 661-70.
197. Bleicken, S., et al., *Molecular details of Bax activation, oligomerization, and membrane insertion.* J Biol Chem, 2010. **285**(9): p. 6636-47.
198. Oh, K.J., et al., *Conformational changes in BAK, a pore-forming proapoptotic Bcl-2 family member, upon membrane insertion and direct evidence for the existence of BH3-BH3 contact interface in BAK homo-oligomers.* J Biol Chem, 2010. **285**(37): p. 28924-37.
199. Aluvila, S., et al., *Organization of the mitochondrial apoptotic BAK pore: oligomerization of the BAK homodimers.* J Biol Chem, 2014. **289**(5): p. 2537-51.

200. Griffiths, G.J., et al., *Cell damage-induced conformational changes of the pro-apoptotic protein Bak in vivo precede the onset of apoptosis.* J Cell Biol, 1999. **144**(5): p. 903-14.
201. Hsu, Y.T. and R.J. Youle, *Nonionic detergents induce dimerization among members of the Bcl-2 family.* J Biol Chem, 1997. **272**(21): p. 13829-34.
202. Dewson, G., et al., *Bak activation for apoptosis involves oligomerization of dimers via their alpha6 helices.* Mol Cell, 2009. **36**(4): p. 696-703.
203. Ma, S., et al., *Assembly of the Bak apoptotic pore: a critical role for the Bak protein alpha6 helix in the multimerization of homodimers during apoptosis.* J Biol Chem, 2013. **288**(36): p. 26027-38.
204. Ramamoorthy, A., et al., *Solid-state NMR investigation of the membrane-disrupting mechanism of antimicrobial peptides MSI-78 and MSI-594 derived from magainin 2 and melittin.* Biophys J, 2006. **91**(1): p. 206-16.
205. Brogden, K.A., *Antimicrobial peptides: pore formers or metabolic inhibitors in bacteria?* Nat Rev Microbiol, 2005. **3**(3): p. 238-50.
206. Wang, J. and E. London, *The membrane topography of the diphtheria toxin T domain linked to the a chain reveals a transient transmembrane hairpin and potential translocation mechanisms.* Biochemistry, 2009. **48**(43): p. 10446-56.
207. Garcia-Saez, A.J., et al., *Peptides derived from apoptotic Bax and Bid reproduce the poration activity of the parent full-length proteins.* Biophys J, 2005. **88**(6): p. 3976-90.
208. Garcia-Saez, A.J., et al., *Peptides corresponding to helices 5 and 6 of Bax can independently form large lipid pores.* FEBS J, 2006. **273**(5): p. 971-81.
209. Qian, S., et al., *Structure of transmembrane pore induced by Bax-derived peptide: evidence for lipidic pores.* Proc Natl Acad Sci U S A, 2008. **105**(45): p. 17379-83.
210. Strasser, A., S. Cory, and J.M. Adams, *Deciphering the rules of programmed cell death to improve therapy of cancer and other diseases.* EMBO J, 2011. **30**(18): p. 3667-83.
211. Green, D.R. and G. Kroemer, *Pharmacological manipulation of cell death: clinical applications in sight?* J Clin Invest, 2005. **115**(10): p. 2610-7.
212. Del Gaizo Moore, V., et al., *Chronic lymphocytic leukemia requires BCL2 to sequester prodeath BIM, explaining sensitivity to BCL2 antagonist ABT-737.* J Clin Invest, 2007. **117**(1): p. 112-21.
213. Letai, A.G., *Diagnosing and exploiting cancer's addiction to blocks in apoptosis.* Nat Rev Cancer, 2008. **8**(2): p. 121-32.
214. Lessene, G., P.E. Czabotar, and P.M. Colman, *BCL-2 family antagonists for cancer therapy.* Nat Rev Drug Discov, 2008. **7**(12): p. 989-1000.
215. van Delft, M.F., et al., *The BH3 mimetic ABT-737 targets selective Bcl-2 proteins and efficiently induces apoptosis via Bak/Bax if Mcl-1 is neutralized.* Cancer Cell, 2006. **10**(5): p. 389-99.
216. Baell, J.B. and D.C. Huang, *Prospects for targeting the Bcl-2 family of proteins to develop novel cytotoxic drugs.* Biochem Pharmacol, 2002. **64**(5-6): p. 851-63.

217. Veis, D.J., et al., *Bcl-2-deficient mice demonstrate fulminant lymphoid apoptosis, polycystic kidneys, and hypopigmented hair.* Cell, 1993. **75**(2): p. 229-40.
218. Mason, K.D., et al., *Programmed anuclear cell death delimits platelet life span.* Cell, 2007. **128**(6): p. 1173-86.
219. Takehara, T., et al., *Hepatocyte-specific disruption of Bcl-xL leads to continuous hepatocyte apoptosis and liver fibrotic responses.* Gastroenterology, 2004. **127**(4): p. 1189-97.
220. Opferman, J.T., et al., *Obligate role of anti-apoptotic MCL-1 in the survival of hematopoietic stem cells.* Science, 2005. **307**(5712): p. 1101-4.
221. Opferman, J.T., et al., *Development and maintenance of B and T lymphocytes requires antiapoptotic MCL-1.* Nature, 2003. **426**(6967): p. 671-6.
222. Vikstrom, I., et al., *Mcl-1 is essential for germinal center formation and B cell memory.* Science, 2010. **330**(6007): p. 1095-9.
223. Peperzak, V., et al., *Mcl-1 is essential for the survival of plasma cells.* Nat Immunol, 2013. **14**(3): p. 290-7.
224. Wang, X., et al., *Deletion of MCL-1 causes lethal cardiac failure and mitochondrial dysfunction.* Genes Dev, 2013. **27**(12): p. 1351-64.
225. Thomas, R.L., et al., *Loss of MCL-1 leads to impaired autophagy and rapid development of heart failure.* Genes Dev, 2013. **27**(12): p. 1365-77.
226. Wang, J.L., et al., *Structure-based discovery of an organic compound that binds Bcl-2 protein and induces apoptosis of tumor cells.* Proc Natl Acad Sci U S A, 2000. **97**(13): p. 7124-9.
227. Enyedy, I.J., et al., *Discovery of small-molecule inhibitors of Bcl-2 through structure-based computer screening.* J Med Chem, 2001. **44**(25): p. 4313-24.
228. Degterev, A., et al., *Identification of small-molecule inhibitors of interaction between the BH3 domain and Bcl-xL.* Nat Cell Biol, 2001. **3**(2): p. 173-82.
229. Lugovskoy, A.A., et al., *A novel approach for characterizing protein ligand complexes: molecular basis for specificity of small-molecule Bcl-2 inhibitors.* J Am Chem Soc, 2002. **124**(7): p. 1234-40.
230. Orner, B.P., J.T. Ernst, and A.D. Hamilton, *Toward proteomimetics: terphenyl derivatives as structural and functional mimics of extended regions of an alpha-helix.* J Am Chem Soc, 2001. **123**(22): p. 5382-3.
231. Kutzki, O., et al., *Development of a potent Bcl-x(L) antagonist based on alpha-helix mimicry.* J Am Chem Soc, 2002. **124**(40): p. 11838-9.
232. Boersma, M.D., et al., *Evaluation of diverse alpha/beta-backbone patterns for functional alpha-helix mimicry: analogues of the Bim BH3 domain.* J Am Chem Soc, 2012. **134**(1): p. 315-23.
233. Lee, E.F., et al., *Structural basis of Bcl-xL recognition by a BH3-mimetic alpha/beta-peptide generated by sequence-based design.* Chembiochem, 2011. **12**(13): p. 2025-32.
234. Smith, B.J., et al., *Structure-guided rational design of alpha/beta-peptide foldamers with high affinity for BCL-2 family prosurvival proteins.* Chembiochem, 2013. **14**(13): p. 1564-72.

235. Walensky, L.D., et al., *Activation of apoptosis in vivo by a hydrocarbon-stapled BH3 helix.* Science, 2004. **305**(5689): p. 1466-70.
236. Bird, G.H., et al., *Synthesis and biophysical characterization of stabilized alpha-helices of BCL-2 domains.* Methods Enzymol, 2008. **446**: p. 369-86.
237. Skelton, N.J., et al., *Structure-function analysis of a phage display-derived peptide that binds to insulin-like growth factor binding protein 1.* Biochemistry, 2001. **40**(29): p. 8487-98.
238. Yang, B., D. Liu, and Z. Huang, *Synthesis and helical structure of lactam bridged BH3 peptides derived from pro-apoptotic Bcl-2 family proteins.* Bioorg Med Chem Lett, 2004. **14**(6): p. 1403-6.
239. Cantel, S., et al., *Synthesis and conformational analysis of a cyclic peptide obtained via i to i+4 intramolecular side-chain to side-chain azide-alkyne 1,3-dipolar cycloaddition.* J Org Chem, 2008. **73**(15): p. 5663-74.
240. Kawamoto, S.A., et al., *Design of triazole-stapled BCL9 alpha-helical peptides to target the beta-catenin/B-cell CLL/lymphoma 9 (BCL9) protein-protein interaction.* J Med Chem, 2012. **55**(3): p. 1137-46.
241. Stewart, M.L., et al., *The MCL-1 BH3 helix is an exclusive MCL-1 inhibitor and apoptosis sensitizer.* Nat Chem Biol, 2010. **6**(8): p. 595-601.
242. Brown, C.J., et al., *Stapled peptides with improved potency and specificity that activate p53.* ACS Chem Biol, 2013. **8**(3): p. 506-12.
243. Okamoto, T., et al., *Stabilizing the pro-apoptotic BimBH3 helix (BimSAHB) does not necessarily enhance affinity or biological activity.* ACS Chem Biol, 2013. **8**(2): p. 297-302.
244. Miles, J.A., et al., *Hydrocarbon constrained peptides - understanding preorganisation and binding affinity.* Chem Sci, 2016. **7**(6): p. 3694-3702.
245. Oltersdorf, T., et al., *An inhibitor of Bcl-2 family proteins induces regression of solid tumours.* Nature, 2005. **435**(7042): p. 677-81.
246. Vogler, M., et al., *Different forms of cell death induced by putative BCL2 inhibitors.* Cell Death Differ, 2009. **16**(7): p. 1030-9.
247. Czabotar, P.E., et al., *Control of apoptosis by the BCL-2 protein family: implications for physiology and therapy.* Nat Rev Mol Cell Biol, 2014. **15**(1): p. 49-63.
248. Lee, E.F., et al., *Crystal structure of ABT-737 complexed with Bcl-xL: implications for selectivity of antagonists of the Bcl-2 family.* Cell Death Differ, 2007. **14**(9): p. 1711-3.
249. Souers, A.J., et al., *ABT-199, a potent and selective BCL-2 inhibitor, achieves antitumor activity while sparing platelets.* Nat Med, 2013. **19**(2): p. 202-8.
250. Gandhi, L., et al., *Phase I study of Navitoclax (ABT-263), a novel Bcl-2 family inhibitor, in patients with small-cell lung cancer and other solid tumors.* J Clin Oncol, 2011. **29**(7): p. 909-16.
251. Roberts, A.W., et al., *Substantial susceptibility of chronic lymphocytic leukemia to BCL2 inhibition: results of a phase I study of navitoclax in patients with relapsed or refractory disease.* J Clin Oncol, 2012. **30**(5): p. 488-96.

252. Rudin, C.M., et al., *Phase II study of single-agent navitoclax (ABT-263) and biomarker correlates in patients with relapsed small cell lung cancer.* Clin Cancer Res, 2012. **18**(11): p. 3163-9.
253. Campas, C., et al., *Bcl-2 inhibitors induce apoptosis in chronic lymphocytic leukemia cells.* Exp Hematol, 2006. **34**(12): p. 1663-9.
254. Wilson, W.H., et al., *Navitoclax, a targeted high-affinity inhibitor of BCL-2, in lymphoid malignancies: a phase 1 dose-escalation study of safety, pharmacokinetics, pharmacodynamics, and antitumour activity.* Lancet Oncol, 2010. **11**(12): p. 1149-59.
255. Zhang, H., et al., *Bcl-2 family proteins are essential for platelet survival.* Cell Death Differ, 2007. **14**(5): p. 943-51.
256. Sleebs, B.E., et al., *Discovery of potent and selective benzothiazole hydrazone inhibitors of Bcl-XL.* J Med Chem, 2013. **56**(13): p. 5514-40.
257. Lessene, G., et al., *Structure-guided design of a selective BCL-X(L) inhibitor.* Nat Chem Biol, 2013. **9**(6): p. 390-7.
258. Leverson, J.D., et al., *Exploiting selective BCL-2 family inhibitors to dissect cell survival dependencies and define improved strategies for cancer therapy.* Sci Transl Med, 2015. **7**(279): p. 279ra40.
259. Tao, Z.F., et al., *Discovery of a Potent and Selective BCL-XL Inhibitor with in Vivo Activity.* ACS Med Chem Lett, 2014. **5**(10): p. 1088-93.
260. Abed, M.N., M.I. Abdullah, and A. Richardson, *Antagonism of Bcl-XL is necessary for synergy between carboplatin and BH3 mimetics in ovarian cancer cells.* J Ovarian Res, 2016. **9**: p. 25.
261. Baranski, Z., et al., *Pharmacological inhibition of Bcl-xL sensitizes osteosarcoma to doxorubicin.* Oncotarget, 2015. **6**(34): p. 36113-25.
262. Liu, Z., et al., *BH4 domain of Bcl-2 as a novel target for cancer therapy.* Drug Discov Today, 2016. **21**(6): p. 989-96.
263. Konopleva, M., et al., *Mechanisms of apoptosis sensitivity and resistance to the BH3 mimetic ABT-737 in acute myeloid leukemia.* Cancer Cell, 2006. **10**(5): p. 375-88.
264. Chen, S., et al., *Mcl-1 down-regulation potentiates ABT-737 lethality by cooperatively inducing Bak activation and Bax translocation.* Cancer Res, 2007. **67**(2): p. 782-91.
265. Leverson, J.D., et al., *Potent and selective small-molecule MCL-1 inhibitors demonstrate on-target cancer cell killing activity as single agents and in combination with ABT-263 (navitoclax).* Cell Death Dis, 2015. **6**: p. e1590.
266. Yecies, D., et al., *Acquired resistance to ABT-737 in lymphoma cells that up-regulate MCL-1 and BFL-1.* Blood, 2010. **115**(16): p. 3304-13.
267. Gavathiotis, E., et al., *Direct and selective small-molecule activation of proapoptotic BAX.* Nat Chem Biol, 2012. **8**(7): p. 639-45.
268. Hochhauser, E., et al., *Bax deficiency reduces infarct size and improves long-term function after myocardial infarction.* Cell Biochem Biophys, 2007. **47**(1): p. 11-20.
269. Reyes, N.A., et al., *Blocking the mitochondrial apoptotic pathway preserves motor neuron viability and function in a mouse model of amyotrophic lateral sclerosis.* J Clin Invest, 2010. **120**(10): p. 3673-9.
270. Kudo, W., et al., *Inhibition of Bax protects neuronal cells from oligomeric Abeta neurotoxicity.* Cell Death Dis, 2012. **3**: p. e309.

271. Ng, K.P., et al., *A common BIM deletion polymorphism mediates intrinsic resistance and inferior responses to tyrosine kinase inhibitors in cancer.* Nat Med, 2012. **18**(4): p. 521-8.
272. Galluzzi, L., et al., *Targeting post-mitochondrial effectors of apoptosis for neuroprotection.* Biochim Biophys Acta, 2009. **1787**(5): p. 402-13.
273. Smith, G.P., *Filamentous fusion phage: novel expression vectors that display cloned antigens on the virion surface.* Science, 1985. **228**(4705): p. 1315-7.
274. Sidhu, S.S., et al., *Phage display for selection of novel binding peptides.* Methods Enzymol, 2000. **328**: p. 333-63.
275. Arrata, I., et al., *Interfacing native and non-native peptides: using Affimers to recognise alpha-helix mimicking foldamers.* Chem Commun (Camb), 2017. **53**(19): p. 2834-2837.
276. Reichert, J.M., *Antibodies to watch in 2010.* MAbs, 2010. **2**(1): p. 84-100.
277. Binz, H.K., et al., *Designing repeat proteins: well-expressed, soluble and stable proteins from combinatorial libraries of consensus ankyrin repeat proteins.* J Mol Biol, 2003. **332**(2): p. 489-503.
278. Koide, A., et al., *The fibronectin type III domain as a scaffold for novel binding proteins.* J Mol Biol, 1998. **284**(4): p. 1141-51.
279. Nord, K., et al., *A combinatorial library of an alpha-helical bacterial receptor domain.* Protein Eng, 1995. **8**(6): p. 601-8.
280. Tiede, C., et al., *Adhiron: a stable and versatile peptide display scaffold for molecular recognition applications.* Protein Eng Des Sel, 2014. **27**(5): p. 145-55.
281. Kondo, H., et al., *Gene organization of oryzacystatin-II, a new cystatin superfamily member of plant origin, is closely related to that of oryzacystatin-I but different from those of animal cystatins.* FEBS Lett, 1991. **278**(1): p. 87-90.
282. Tang, A.A., et al., *Isolation of isoform-specific binding proteins (Affimers) by phage display using negative selection.* Sci Signal, 2017. **10**(505).
283. Raina, M., et al., *Antibody mimetic receptor proteins for label-free biosensors.* Analyst, 2015. **140**(3): p. 803-10.
284. Sharma, R., et al., *Label-free electrochemical impedance biosensor to detect human interleukin-8 in serum with sub-pg/ml sensitivity.* Biosens Bioelectron, 2016. **80**: p. 607-613.
285. Fisher, M.J., et al., *Trivalent Gd-DOTA reagents for modification of proteins.* RSC Adv, 2015. **5**(116): p. 96194-96200.
286. Kyle, H.F., et al., *Exploration of the HIF-1alpha/p300 interface using peptide and Adhiron phage display technologies.* Mol Biosyst, 2015. **11**(10): p. 2738-49.
287. Selak, M.A., et al., *Succinate links TCA cycle dysfunction to oncogenesis by inhibiting HIF-alpha prolyl hydroxylase.* Cancer Cell, 2005. **7**(1): p. 77-85.
288. Semenza, G.L., *Hypoxia, clonal selection, and the role of HIF-1 in tumor progression.* Crit Rev Biochem Mol Biol, 2000. **35**(2): p. 71-103.
289. Robinson, J.I., et al., *Affimer proteins inhibit immune complex binding to FcgammaRIIIa with high specificity through competitive and allosteric modes of action.* Proc Natl Acad Sci U S A, 2018. **115**(1): p. E72-E81.

290. Wolter, K.G., et al., *Movement of Bax from the cytosol to mitochondria during apoptosis.* J Cell Biol, 1997. **139**(5): p. 1281-92.
291. Chong, S., et al., *Single-column purification of free recombinant proteins using a self-cleavable affinity tag derived from a protein splicing element.* Gene, 1997. **192**(2): p. 271-81.
292. Porath, J., et al., *Metal chelate affinity chromatography, a new approach to protein fractionation.* Nature, 1975. **258**(5536): p. 598-9.
293. Smith, D.B. and K.S. Johnson, *Single-step purification of polypeptides expressed in Escherichia coli as fusions with glutathione S-transferase.* Gene, 1988. **67**(1): p. 31-40.
294. Laemmli, U.K., *Cleavage of structural proteins during the assembly of the head of bacteriophage T4.* Nature, 1970. **227**(5259): p. 680-5.
295. Holzwarth, G. and P. Doty, *The Ultraviolet Circular Dichroism of Polypeptides.* J Am Chem Soc, 1965. **87**: p. 218-28.
296. Greenfield, N. and G.D. Fasman, *Computed circular dichroism spectra for the evaluation of protein conformation.* Biochemistry, 1969. **8**(10): p. 4108-16.
297. Zhang, Z., et al., *Bcl-2 homodimerization involves two distinct binding surfaces, a topographic arrangement that provides an effective mechanism for Bcl-2 to capture activated Bax.* J Biol Chem, 2004. **279**(42): p. 43920-8.
298. O'Neill, J.W., et al., *BCL-XL dimerization by three-dimensional domain swapping.* J Mol Biol, 2006. **356**(2): p. 367-81.
299. Denisov, A.Y., et al., *Heat-induced dimerization of BCL-xL through alpha-helix swapping.* Biochemistry, 2007. **46**(3): p. 734-40.
300. Feng, Y., et al., *Bcl-xL forms two distinct homodimers at non-ionic detergents: implications in the dimerization of Bcl-2 family proteins.* J Biochem, 2008. **143**(2): p. 243-52.
301. Pritz, J.R., et al., *Allosteric sensitization of proapoptotic BAX.* Nat Chem Biol, 2017. **13**(9): p. 961-967.
302. Jones, S. and J.M. Thornton, *Principles of protein-protein interactions.* Proc Natl Acad Sci U S A, 1996. **93**(1): p. 13-20.
303. Lo Conte, L., C. Chothia, and J. Janin, *The atomic structure of protein-protein recognition sites.* J Mol Biol, 1999. **285**(5): p. 2177-98.
304. Zhai, D., et al., *Differential regulation of Bax and Bak by anti-apoptotic Bcl-2 family proteins Bcl-B and Mcl-1.* J Biol Chem, 2008. **283**(15): p. 9580-6.
305. Kelly, S.M., T.J. Jess, and N.C. Price, *How to study proteins by circular dichroism.* Biochim Biophys Acta, 2005. **1751**(2): p. 119-39.
306. Wallgren, M., et al., *Reconstitution of the anti-apoptotic Bcl-2 protein into lipid membranes and biophysical evidence for its detergent-driven association with the pro-apoptotic Bax protein.* PLoS One, 2013. **8**(4): p. e61452.
307. Ivashyna, O., et al., *Detergent-activated BAX protein is a monomer.* J Biol Chem, 2009. **284**(36): p. 23935-46.
308. O'Shannessy, D.J., et al., *Determination of rate and equilibrium binding constants for macromolecular interactions using surface plasmon resonance: use of nonlinear least squares analysis methods.* Anal Biochem, 1993. **212**(2): p. 457-68.
309. Wei, J., et al., *Synthesis and biological evaluation of Apogossypolone derivatives as pan-active inhibitors of antiapoptotic B-cell*

lymphoma/leukemia-2 (Bcl-2) family proteins. J Med Chem, 2010. **53**(22): p. 8000-11.
310. Thomas, W.D., M. Golomb, and G.P. Smith, *Corruption of phage display libraries by target-unrelated clones: diagnosis and countermeasures.* Anal Biochem, 2010. **407**(2): p. 237-40.
311. Ashkenazi, A., et al., *From basic apoptosis discoveries to advanced selective BCL-2 family inhibitors.* Nat Rev Drug Discov, 2017. **16**(4): p. 273-284.
312. Brouwer, J.M., et al., *Conversion of Bim-BH3 from Activator to Inhibitor of Bak through Structure-Based Design.* Mol Cell, 2017. **68**(4): p. 659-672 e9.
313. Youle, R.J. and A. Strasser, *The BCL-2 protein family: opposing activities that mediate cell death.* Nat Rev Mol Cell Biol, 2008. **9**(1): p. 47-59.
314. Subburaj, Y., et al., *Bax monomers form dimer units in the membrane that further self-assemble into multiple oligomeric species.* Nat Commun, 2015. **6**: p. 8042.
315. Thompson, R.F., et al., *An introduction to sample preparation and imaging by cryo-electron microscopy for structural biology.* Methods, 2016. **100**: p. 3-15.
316. Wong, W., et al., *Cryo-EM structure of the Plasmodium falciparum 80S ribosome bound to the anti-protozoan drug emetine.* Elife, 2014. **3**.
317. Amunts, A., et al., *Structure of the yeast mitochondrial large ribosomal subunit.* Science, 2014. **343**(6178): p. 1485-1489.
318. Allegretti, M., et al., *Atomic model of the F420-reducing [NiFe] hydrogenase by electron cryo-microscopy using a direct electron detector.* Elife, 2014. **3**: p. e01963.
319. Lu, P., et al., *Three-dimensional structure of human gamma-secretase.* Nature, 2014. **512**(7513): p. 166-170.
320. Khoshouei, M., et al., *Cryo-EM structure of haemoglobin at 3.2 A determined with the Volta phase plate.* Nat Commun, 2017. **8**: p. 16099.

Appendix A Vectors used for Recombinant Protein Expression

A.1 pET-28a-SUMO

Used for the expression of $MCL1^{172-327}$ and $BCL\text{-}X_L^{ML}$. Both constructs were cloned into the MCS of vector cut with BamH1 and Xho1.

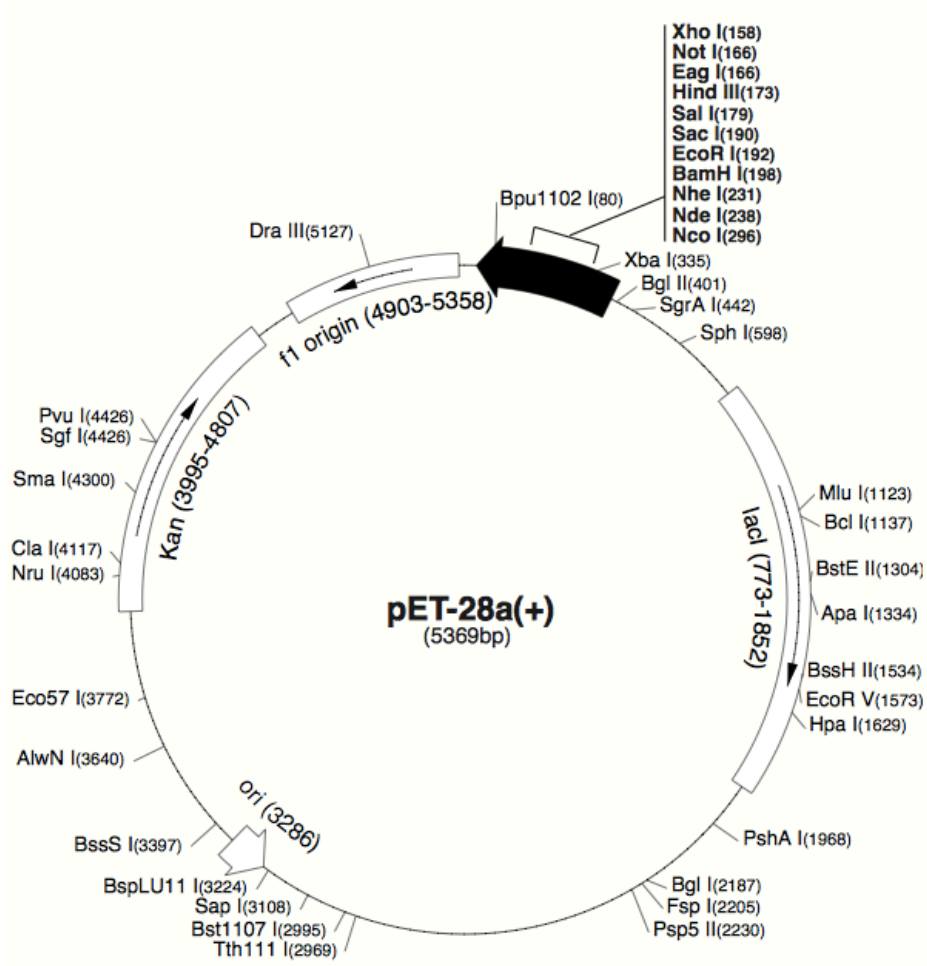

A.2 pGEX-6P-2

Used for the expression of BCL-2^{1-205}. This construct was cloned into the MCS of vector cut with BamH1 and Xho1.

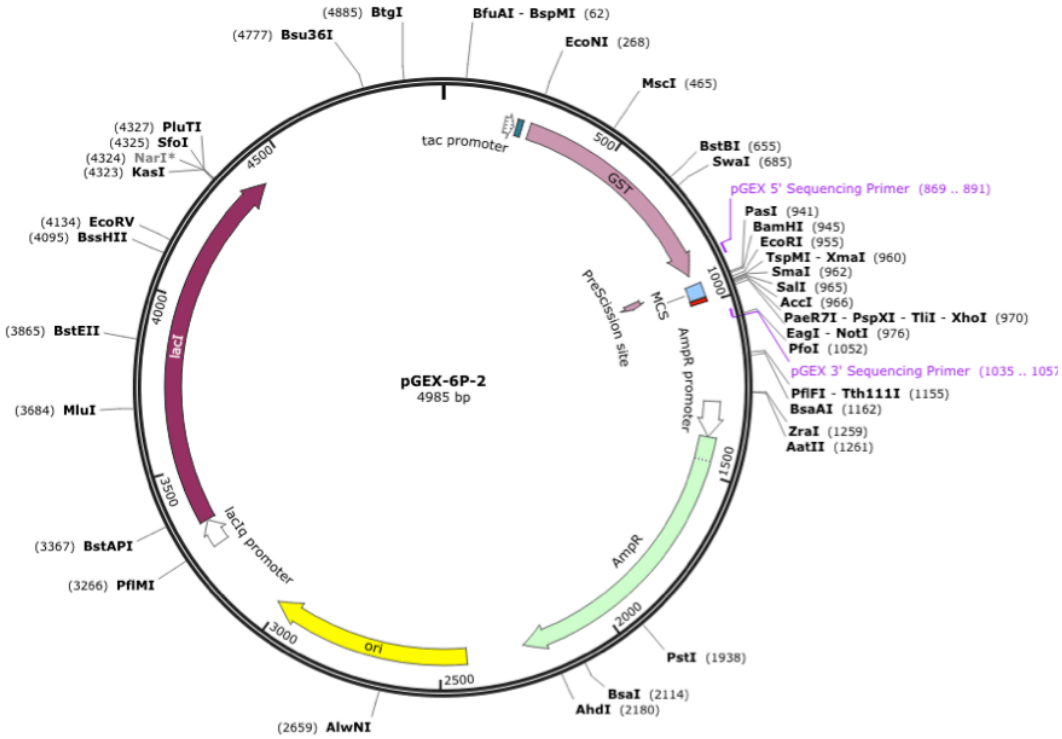

A.3 pTXB1

Used for the expression of BAX 1-171 C-S and BAK 16-185 C-S. Constructs were cloned into vector cut with Sap1 and Nde1.

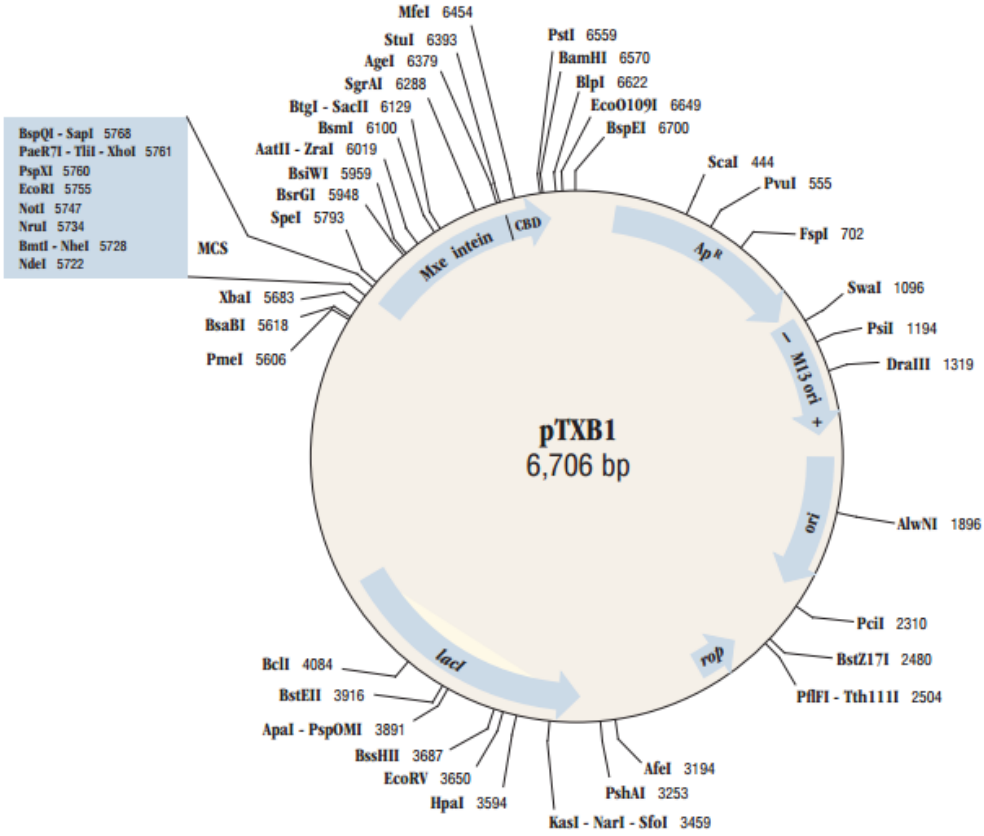

Appendix B Protein Sequences and Mass Spec Analysis

B.1 BAX

BAX$^{1\text{-}171\ C\text{-}S}$ – INTEIN-CBD fusion
Intein self cleaves at Sap1 site, leaving no linker residue
Molecular Weights: Fusion protein - 46773.97 Da, tag cleaved - 18933.56 Da

Sequence

MDGSGEQPRG GGPTSSEQIM KTGALLLQGF IQDRAGRMGG EAPELALDPV
PQDASTKKLS ESLKRIGDEL DSNMELQRMI AAVDTDSPRE VFFRVAADMF
SDGNFNWGRV VALFYFASKL VLKALSTKVP ELIRTIMGWT LDFLRERLLG
WIQDQGGWDG LLSYFGTPTW QCITGDALVA LPEGESVRIA DIVPGARPNS
DNAIDLKVLD RHGNPVLADR LFHSGEHPVY TVRTVEGLRV TGTANHPLLC
LVDVAGVPTL LWKLIDEIKP GDYAVIQRSA FSVDCAGFAR GKPEFAPTTY
TVGVPGLVRF LEAHHRDPDA QAIADELTDG RFYYAKVASV TDAGVQPVYS
LRVDTADHAF ITNGFVSHAT GLTGLNSGLT TNPGVSAWQV NTAYTAGQLV
TYNGKTYKCL QPHTSLAGWE PSNVPALWQL Q

Mass Spectrum

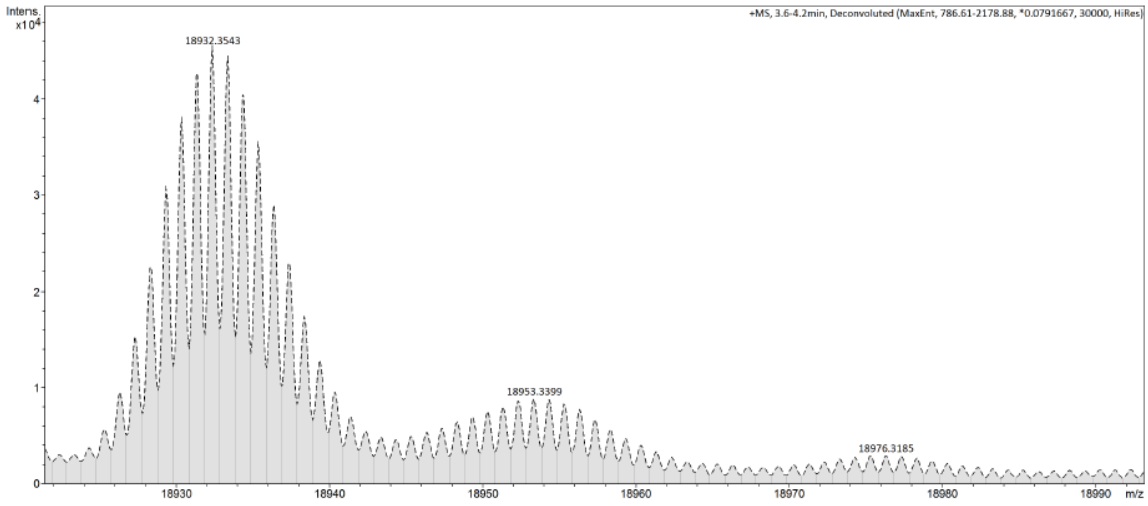

B.2 BAK

BAK $^{16\text{-}185\ C\text{-}S}$ – INTEIN-CBD fusion
Intein self cleaves at Sap1 site, leaving no linker residue
Molecular Weights: Fusion protein – 47058.05 Da, tag cleaved – 19217.64 Da

Sequence

MEPALPSASE EQVAQDTEEV FRSYVFYRHQ QEQEAEGVAA PADPEMVTLP
LQPSSTMGQV GRQLAIIGDD INRRYDSEFQ TMLQHLQPTA ENAYEYFTKI
ATSLFESGIN WGRVVALLGF GYRLALHVYQ HGLTGFLGQV TRFVVDFMLH
HSIARWIAQR GGWVAALNLG NCITGDALVA LPEGESVRIA DIVPGARPNS
DNAIDLKVLD RHGNPVLADR LFHSGEHPVY TVRTVEGLRV TGTANHPLLC
LVDVAGVPTL LWKLIDEIKP GDYAVIQRSA FSVDCAGFAR GKPEFAPTTY
TVGVPGLVRF LEAHHRDPDA QAIADELTDG RFYYAKVASV TDAGVQPVYS
LRVDTADHAF ITNGFVSHAT GLTGLNSGLT TNPGVSAWQV NTAYTAGQLV
TYNGKTYKCL QPHTSLAGWE PSNVPALWQL Q

Mass Spectrum

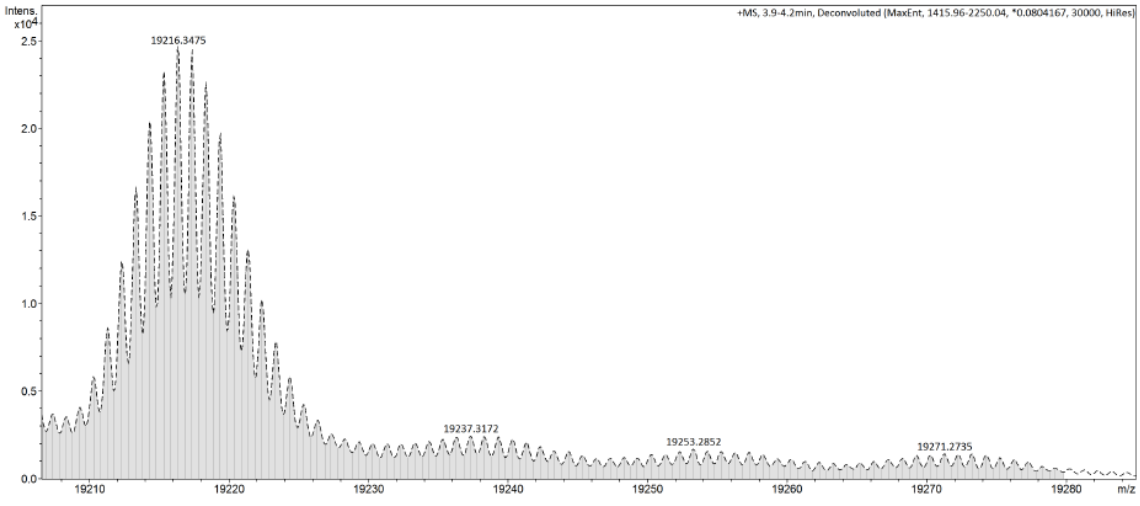

B.3 BCL-2

GST – BCL-2 $^{1-205}$

GST tag + linker with Prescission protease cleavage site leaves GPLGSPEF residues N terminal to protein sequence

Molecular Weights: Fusion protein - 49818.04 Da, tag cleaved - 23405.34 Da

Sequence

MSPILGYWKI KGLVQPTRLL LEYLEEKYEE HLYERDEGDK WRNKKFELGL
EFPNLPYYID GDVKLTQSMA IIRYIADKHN MLGGCPKERA EISMLEGAVL
DIRYGVSRIA YSKDFETLKV DFLSKLPEML KMFEDRLCHK TYLNGDHVTH
PDFMLYDALD VVLYMDPMCL DAFPKLVCFK KRIEAIPQID KYLKSSKYIA
WPLQGWQATF GGGDHPPKSD LEVLFQ/GPLG SPEFMAHAGR TGYDNREIVM
KYIHYKLSQR GYEWDAGDVG AAPPGAAPAP GIFSSQPGHT PHTAASRDPV
ARTSPLQTPA APGAAAGPAL SPVPPVVHLT LRQAGDDFSR RYRRDFAEMS
RQLHLTPFTA RGRFATVVEE LFRDGVNWGR IVAFFEFGGV MCVESVNREM
SPLVDNIALW MTEYLNRHLH TWIQDNGGWD AFVELYGPS

Mass Spectrum

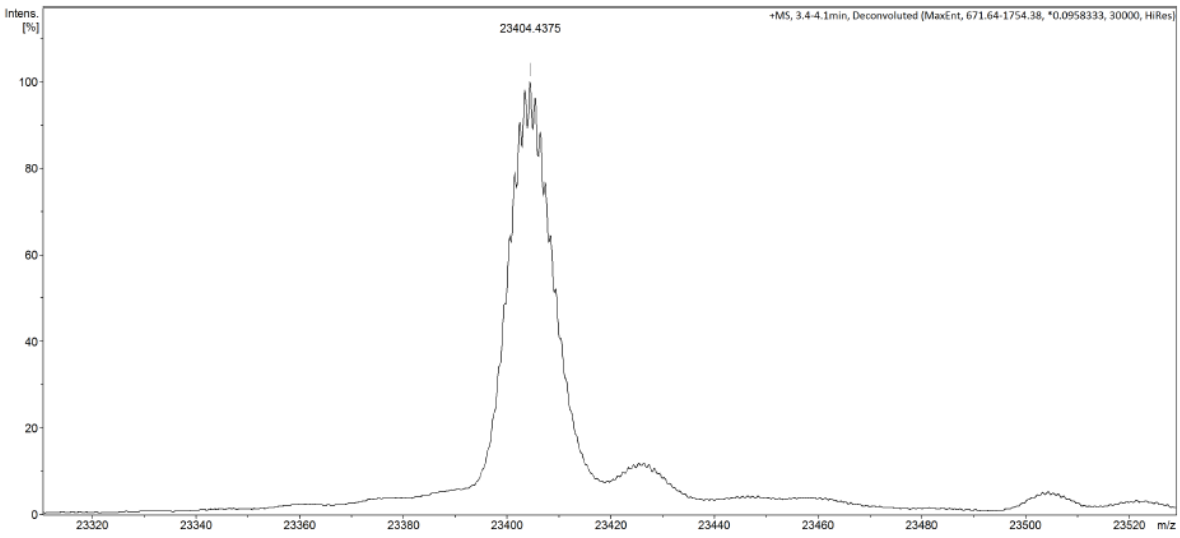

B.4 BCL-X_L

HIS-SUMO-BCL-X_L

SUMO protease recognizes tertiary structure of SUMO, rather than specific sequence of residues. No linker residue attached.

Molecular Weights: Fusion protein – 30896.56 Da, tag cleaved – 17489.57 Da

Sequence

MGSSHHHHHH SSGLVPRGSH MSDSEVNQEA KPEVKPEVKP ETHINLKVSD
GSSEIFFKIK KTTPLRRLME AFAKRQGKEM DSLRFLYDGI RIQADQTPED
LDMEDNDIIE AHREQIGGMS QSNRELVVDF LSYKLSQKGY SWSQMAAVKQ
ALREAGDEFE LRYRRAFSDL TSQLHITPGT AYQSFEQVVN ELFRDGVNWG
RIVAFFSFGG ALCVESVDKE MQVLVSRIAA WMATYLNDHL EPWIQENGGW
DTFVELYGNN AAAESRKGQE R

Mass Spectrum

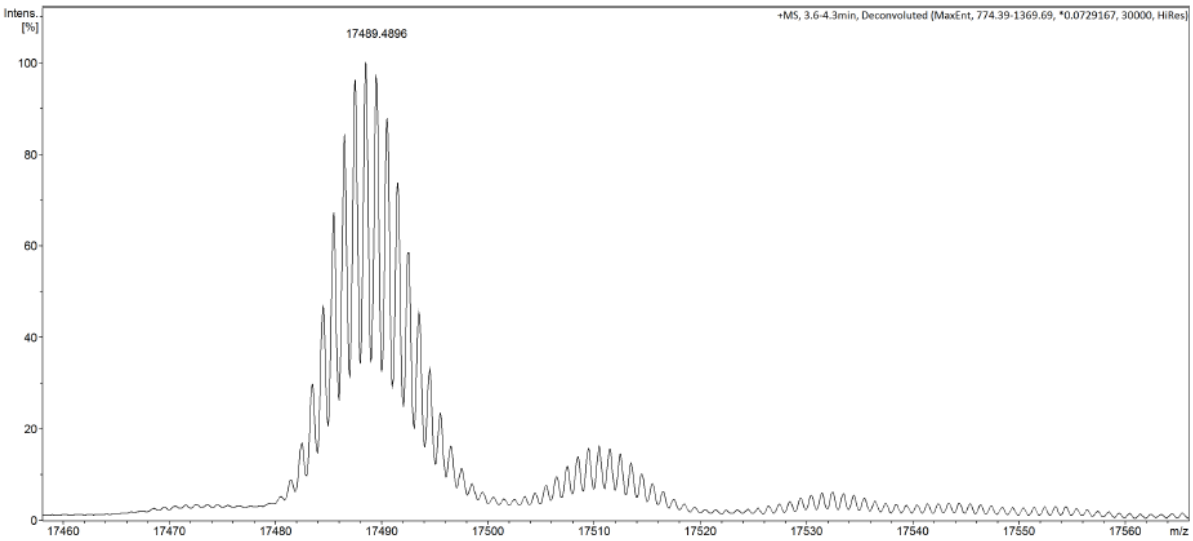

B.5 MCL-1

HIS-SUMO – MCL1
SUMO protease recognizes tertiary structure of SUMO, rather than specific sequence of residues. No linker residue attached.
Molecular Weights: Fusion protein – 31144.19 Da, tag cleaved – 17737.20 Da

Sequence

MGSSHHHHHH SSGLVPRGSH MSDSEVNQEA KPEVKPEVKP ETHINLKVSD
GSSEIFFKIK KTTPLRRLME AFAKRQGKEM DSLRFLYDGI RIQADQTPED
LDMEDNDIIE AHREQIGGSE LYRQSLEIIS RYLREQATGA KDTKPMGRSG
ATSRKALETL RRVGDGVQRN HETAFQGMLR KLDIKNEDDV KSLSRVMIHV
FSDGVTNWGR IVTLISFGAF VAKHLKTINQ ESCIEPLAES ITDVLVRTKR
DWLVKQRGWD GFVEFFHVED LEGG

Mass Spectrum